frontiers | Research Topics

Integration of development, physiology and responses to environmental change in aquatic invertebrates

Edited by
Zhiguo Dong, Vengatesen Thiyagarajan,
Zulin Zhang, Xiaodong Zheng and Tao Zhang

Published in
Frontiers in Marine Science

ISSN 1664-8714
ISBN 978-2-8325-2560-9
DOI 10.3389/978-2-8325-2560-9

About Frontiers

Frontiers is more than just an open access publisher of scholarly articles: it is a pioneering approach to the world of academia, radically improving the way scholarly research is managed. The grand vision of Frontiers is a world where all people have an equal opportunity to seek, share and generate knowledge. Frontiers provides immediate and permanent online open access to all its publications, but this alone is not enough to realize our grand goals.

Frontiers journal series

The Frontiers journal series is a multi-tier and interdisciplinary set of open-access, online journals, promising a paradigm shift from the current review, selection and dissemination processes in academic publishing. All Frontiers journals are driven by researchers for researchers; therefore, they constitute a service to the scholarly community. At the same time, the *Frontiers journal series* operates on a revolutionary invention, the tiered publishing system, initially addressing specific communities of scholars, and gradually climbing up to broader public understanding, thus serving the interests of the lay society, too.

Dedication to quality

Each Frontiers article is a landmark of the highest quality, thanks to genuinely collaborative interactions between authors and review editors, who include some of the world's best academicians. Research must be certified by peers before entering a stream of knowledge that may eventually reach the public - and shape society; therefore, Frontiers only applies the most rigorous and unbiased reviews. Frontiers revolutionizes research publishing by freely delivering the most outstanding research, evaluated with no bias from both the academic and social point of view. By applying the most advanced information technologies, Frontiers is catapulting scholarly publishing into a new generation.

What are Frontiers Research Topics?

Frontiers Research Topics are very popular trademarks of the *Frontiers journals series*: they are collections of at least ten articles, all centered on a particular subject. With their unique mix of varied contributions from Original Research to Review Articles, Frontiers Research Topics unify the most influential researchers, the latest key findings and historical advances in a hot research area.

Find out more on how to host your own Frontiers Research Topic or contribute to one as an author by contacting the Frontiers editorial office: frontiersin.org/about/contact

Integration of development, physiology and responses to environmental change in aquatic invertebrates

Topic editors

Zhiguo Dong — Jiangsu Ocean Universiity, China
Vengatesen Thiyagarajan — The University of Hong Kong, SAR China
Zulin Zhang — The James Hutton Institute, United Kingdom
Xiaodong Zheng — Ocean University of China, China
Tao Zhang — Institute of Oceanology, Chinese Academy of Sciences (CAS), China

Citation

Dong, Z., Thiyagarajan, V., Zhang, Z., Zheng, X., Zhang, T., eds. (2023). *Integration of development, physiology and responses to environmental change in aquatic invertebrates*. Lausanne: Frontiers Media SA.
doi: 10.3389/978-2-8325-2560-9

Table of contents

frontiers | Frontiers in Marine Science

TYPE Editorial
PUBLISHED 15 May 2023
DOI 10.3389/fmars.2023.1206031

OPEN ACCESS

EDITED AND REVIEWED BY
Rachel Collin,
Smithsonian Tropical Research Institute (SI), United States

*CORRESPONDENCE
Zhiguo Dong
dzg7712@163.com

RECEIVED 14 April 2023
ACCEPTED 08 May 2023
PUBLISHED 15 May 2023

CITATION
Dong Z (2023) Editorial: Integration of development, physiology and responses to environmental change in aquatic invertebrates.
Front. Mar. Sci. 10:1206031.
doi: 10.3389/fmars.2023.1206031

Editorial: Integration of development, physiology and responses to environmental change in aquatic invertebrates

Zhiguo Dong[1,2,3]*

[1]Jiangsu Key Laboratory of Marine Bioresources and Environment, Jiangsu Ocean University, Lianyungang, China, [2]Co-Innovation Center of Jiangsu Marine Bio-industry Technology, Jiangsu Institute of Marine Resources Development, Lianyungang, China, [3]Jiangsu Institute of Marine Resources Development, Lianyungang, Jiangsu, China

KEYWORDS

development, physiology, environmental stress, mollusks, crustaceans, farming model

Editorial on the Research Topic
Integration of development, physiology and responses to environmental change in aquatic invertebrates

Aquatic invertebrates, particularly mollusks and crustaceans, are of great economic and food value and are therefore widely farmed throughout the world. However, studies on shellfish and crustaceans are still far from being adequate compared to vertebrates. Specifically, the mechanisms of endocrine regulation of reproduction in shellfish and crustaceans and their response to marine pollution are unknown. In addition, shellfish and crustaceans are experiencing a degradation of germplasm resources and a decline in farmed production. Therefore, in order to encourage more scholars to participate in shellfish and crustacean research, and to promote the development of the shellfish and crustacean industry, the Research Topic is calls for original and novel papers related to shellfish and crustaceans in any of the following Research Topics: (1) Molecular mechanism on reproduction and ovarian development of mollusks and crustaceans; (2) Sex determination and differentiation of mollusks and crustaceans; (3) Aquaculture technology and genetic resources evaluation of mollusks and crustaceans; (4) Environmental response, ecology and taxonomy of mollusks and crustaceans; (5) Nutrition and disease of mollusks and crustaceans.

There three studies (Wang et al., Liu et al., Yan et al.) focused on the reproduction of mollusks by using transcriptomic and molecular biology techniques, *Mytilus coruscus* and *Cyclina sinensis*. The results showed that several key genes involved in the process of sex determination/differentiation and gonadal development of mollusks.

Studies focused on the responses to environmental change of mollusks. Specifically, Zheng et al., conducted starvation experiments on mussels from the perspective of the influence of breeding density on the physiological survival condition of mussels, in order to explore the influence on the secretion of mussels' bursa and further explore the benthic distribution and cultivation of mussels. The results of this study showed that food restrictions may alter the physiology of mussel foot glands, and food shortages have potentially adverse effects on mussel attachment in a variety of habitats may increase

migration risks for mussels in suspension culture. Ge et al., elucidate the effect of ammonia nitrogen stress on the superoxide dismutase (SOD) activity and interferon-induced transmembrane protein 1 (IFITM1) of *C. sinensis*. Liu et al., investigated the effects of acute polychlorinated biphenyls (PCBs) exposure on survival, non-specific immunity, antioxidant capacity and histology of *C. sinensis*. The results showed that acute exposure to PCBS resulted in the loss and shortening of gill filaments and lateral cilia, and increased mortality, oxidative stress, immune dysfunction and energy metabolism disorder *C. sinensis*. Wang et al., conducted a transcriptome study on the immune and antioxidant effects of residual chlorine stress on *C. sinensis*, and the study provides valuable information for understanding the effects of residual chlorine stress on the survival, physiological metabolism, and molecular mechanisms of immune and antioxidant functions of clams. Moreover, Aljbour et al., investigated the metabolic and physiological performance of the upside-down jellyfish in response to UV at the cellular level. The results showed that the jellyfish was able to cope with UV-mediated increased energy requirements in an aerobic state. Zhou et al., studied genome-wide identification, structural and evolutionary characteristics, and expression analysis of aquaporin gene family members in *Mercenaria mercenaria*. This study provides a comprehensive understanding of the AQP gene family in hard clams, and lays a foundation for further exploration of the function of AQP in bivalves.

Another study Yang et al., focused on the mechanism underlying the response of *Rapana venosa* to juvenile oysters through the RNA-seq analysis. Taken together, the results show that competent larvae rapidly respond to the inducing effects of oysters *via* some immediate early genes, such as the transcription factor AP-1, which may further regulate downstream pathways such as the MAPK signaling pathway to cause subsequent changes, including a decrease in HSP90 and an increase in IAPs.

Except for mollusks, He et al., carried out research on technological innovations in swimming crab farming. Specifically, He et al., explored a new off-season breeding of *Portunus trituberculatus* by breeding in autumn in 2022, and compared the embryonic development rate, embryonic antioxidant capacity and hatchability, as well as digestive enzyme activities of newly hatched larvae of *P. trituberculatus* under different water temperatures in the off-season (breeding in early autumn). The results showed that the water temperature of embryonic development should be controlled within 31°C to ensure the quality of embryonic development in the crab. In addition, He et al. used a special plastic basket as an anti-injury shelter on the basis of the existing research to explore the covert behavior and molting growth of *P. trituberculatus* with different initial body weight. Overall, the shelter played a positive role in the overall growth of the crab. Therefore, before the seedlings are put into production, it is necessary to shelters, which helps to increase the yield of the *P. trituberculatus*.

From the above aspects, the study of aquatic vertebrates still needs further strengthening and innovation.

Author contributions

The author confirms being the sole contributor of this work and has approved it for publication.

Funding

ZD is supported by the projects (CARS-49) from Modern Agro-industry Technology Research System; the projects (JBGS[2021] 034) from the 'JBGS' Project of Seed Industry Revitalization in Jiangsu Province.

Acknowledgments

We thank authors of the papers published in this research topic for their valuable contributions and the referees for their rigorous review. We also thank the editorial board of the Marine Biology section, and the Frontiers specialists, for their support.

Conflict of interest

The author declares that the research was conducted in the absence of any commercial or financial relationships that could be construed as a potential conflict of interest.

Publisher's note

frontiers | Frontiers in Marine Science

TYPE Original Research
PUBLISHED 14 September 2022
DOI 10.3389/fmars.2022.1018565

OPEN ACCESS

EDITED BY
Zhiguo Dong,
Jiangsu Ocean University, China

REVIEWED BY
Xinguo Zhao,
Yellow Sea Fisheries Research Institute (CAFS), China
Yunfei Sun,
Shanghai Ocean University, China

*CORRESPONDENCE
Wenjun Xu
wjxu1971@hotmail.com

†These authors have contributed equally to this work

SPECIALTY SECTION
This article was submitted to Marine Biology, a section of the journal Frontiers in Marine Science

RECEIVED 13 August 2022
ACCEPTED 29 August 2022
PUBLISHED 14 September 2022

CITATION
He J, Yu H, Wan L, Zhang D and Xu W (2022) At what size do anti-injury shelters start to play a positive role in the culture of *Portunus trituberculatus*? *Front. Mar. Sci.* 9:1018565. doi: 10.3389/fmars.2022.1018565

At what size do anti-injury shelters start to play a positive role in the culture of *Portunus trituberculatus*?

Jie He[1,2†], Huaihua Yu[1,2†], Litao Wan[1,2], Dongxu Zhang[1,2] and Wenjun Xu[1,2*]

[1]Zhejiang Province Key Laboratory of Mariculture and Enhancement, Zhejiang Marine Fisheries Research Institute, Zhoushan, China, [2]Marine and Fisheries Institute, Zhejiang Ocean University, Zhoushan, China

Based on the existing research, special plastic baskets were used as anti-injury shelters to explore the hidden behavior and molting growth of *Portunus trituberculatus* (Swimming crab) different initial body weights (Group A: 5.74 ± 0.11 g, Group B: 12.06 ± 0.15 g, Group C: 24.82 ± 0.41 g, Group D: 49.55 ± 1.12 g and Group E: 94.32 ± 1.19 g). The results showed that the shelter occupancy rate (SOR) during the daytime with all different body weights were significantly higher than that at night ($P < 0.05$), and the SOR was proportional to the crab's body weight, among them, SOR in group E was as high as 71.52%. Meanwhile, the territorial consciousness of smaller body weight crabs (Groups A, B and C) was poor, and there was a phenomenon in which multiple individuals occupied the same shelter at the same time, while the individuals with the body weight of approximately 50 g and above (Groups D and E) had strong territorial consciousness, and most of them occupied one shelter alone. In all groups, more individuals chose to molt in the shelter on condition that there existed shelter, and the rate of molting in group B was high up to 81.15% and that in other groups was about 60%. Although the existence of shelter had no significant influence on the molting interphase (MI) of swimming crab in each group, the body weight growth rate (WGR) and carapace width growth rate (WGR_C) after molting were increased by shelter compared with those without shelter. In addition, shelter could improve the survival rate (SR) in each group, and the effect of shelter on individuals with large body weight was relatively more obvious, in which the SR in Group D was significantly improved ($P < 0.05$). In general, the shelter can play a positive role in the whole growth of swimming crab. Therefore, it is necessary to set up the shelter in advance before the seedlings are put into production, which is helpful to increase the yield of swimming crab.

KEYWORDS

***Portunus trituberculatus*, cannibalism, different body weights, shelter, behavior, growth**

1 Introduction

Cannibalism refers to the behavioral characteristics of injury or death caused by mutual attacks, struggles and fighting among individuals of the same species (Polis, 1981; Marshall et al., 2005). It can effectively reduce the waste of space and food by the vulnerable individuals and enable the winners obtain more living materials, survival space, mating rights and other benefits, and have positive effects on selecting the best and most preserving seed (Liu, 2002; Li and Sun, 2013). However, cannibalism has also resulted in massive deaths of aquatic organisms, which is an exceedingly severe problem in the aquaculture industry. Many researchers have found that aquatic cannibalism is caused by a variety of complex factors, including individual size differences, feed density, feed species, stock density, neurochemical factors, temperature, light, water turbidity, and so on (Chen, 2006; Chen et al., 2008; Qin and Li, 2014; Wang et al., 2015).

It has been proved that the use of suitable shelters can reduce the incidence of cannibalism of aquatic organisms, thereby improving the survival rate and yield per unit area. For example, the use of halved PVC agricultural drainage pipes can provide a hiding space for the *Salvelinus alpinus*, which is conducive to the growth of the *S. alpinus* and reduces mortality (Benhaïm et al., 2009). The survival rate and growth rate of *Callinectes sapidus* growing in the vegetated environment were significantly higher than those in the non-vegetated group (Perkins-Visser et al., 1996). In the condition of wavy nets, seaweed, plastic threads and bamboo tubes as shelters, *Scylla serrata* survived significantly better (Mann et al., 2007; Mirera and Moksnes, 2013). *Maja squinado* showed a significantly higher growth rate and survival rate in the natural seaweed shelter group than those in the artificial coir fiber shelter group (Gil et al., 2019).

Swimming crab is one of the dominant species of aquaculture in China. Whereas, its aggressive nature, strong territoriality and extremely serious cannibalism lead to low unit yield, which has been hindering the healthy and sustainable development of this species in the aquaculture industry (He et al., 2016). Our previous research found that plastic baskets, as shelters, had an unexpectedly positive effect on reducing cannibalism, improving the survival rate and promoting the growth and development of swimming crab, and the survival rate was up to 68% (He et al., 2017). Moreover, according to this result, a special shelter was developed (Chinese Patent No. ZL2018206226941.X) for swimming crab culture, which is now widely used in China, with an area of 800 ha in Zhejiang Province alone. However, it is uncertain about the confusion at which growth stage of swimming crab the shelter begins to have a better effect, in other words, we are not sure when the best time to place the shelter is. Consequently, this study aims to investigate the hidden behavior and molting growth rule of swimming crab with different body weights, accompanied by the presence of shelters. On the one hand, to understand the hidden habits with different body weights and enrich the theoretical knowledge of the behavioral ecology of swimming crab. On the other hand, to analyze the effect of shelter on the survival and growth at different growth stages. These points will provide a scientific basis for further elucidating the mechanism of shelter in aquaculture production and optimizing the application technology of shelter in aquaculture production of swimming crab.

2 Materials and methods

2.1 Source of experimental crabs

This experiment was conducted at the test site of Zhejiang Marine Fisheries Research Institute in July 2020. The experimental crabs were captured from the same aquaculture pond by the bait trapping method and placed in the indoor cement pool (6 × 1.8 × 0.7 m) for temporary culture. The experimental water was sand filter seawater, the water depth was approximately 0.4 m, and the oxygen was continuously increased for 24 h. Fresh trash fish were fed at 16: 00 every day, and the feed amount was approximately 5%~10% of the crab's weight. The following morning at 7:00, the residual feed and excrement were removed, and two-thirds of the water was exchanged. During the temporary culture period, the water temperature was kept at 26.7 ± 1.4°C, the salinity was at 25.9 ± 0.9, and dissolved oxygen (DO) > 5 mg/L.

2.2 Experimental design

The experiment was carried out in the indoor cement pool (6 × 1.8 × 0.7 m). Each cement pool was divided into three small pools of equal size, and the small pools adjacent to each other were connected, such that the water could flow freely, but the crabs could not pass freely. The total number of small pools was 6 (3 without and 3 with shelters), and 12 shelters were placed in each of the three pools (The shelter is shown in Figure 1), The arrangement was 3 rows×4 columns, with 35 cm between the front and back and 15 cm between the left and right, and the openings were in the same direction. 5 different body weight groups (A, B, C, D and E) were set up in the experiment. They were 5.74 ± 0.11 g, 12.06 ± 0.15 g, 24.82 ± 0.41 g, 49.55 ± 1.12 g and 94.32 ± 1.19 g, respectively. A comparative study on the hidden behavior and growth rule of five groups (A, B, C, D and E) was carried out successively. In the same weight group, a total of 108 juvenile crabs of similar size and sound appendages were selected from each group. 18 juvenile crabs were randomly placed in each small pool, the weight of the crabs was weighed, and their carapace width was measured before placement, and the crabs were numbered on

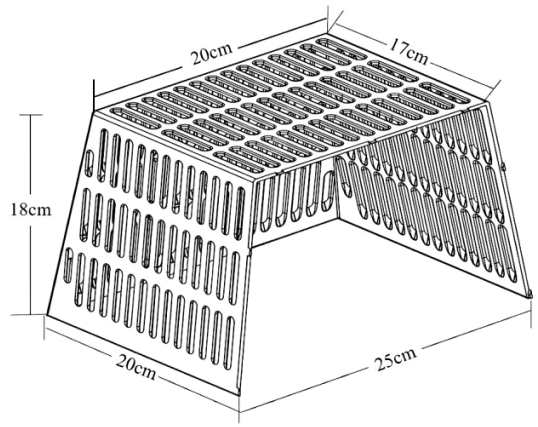

FIGURE 1
Shape and specification of the shelter of swimming crab used in this study.

their carapaces with a marker pen. The mean body weights of the no shelter group (NSG) were 5.67 ± 0.12 g, 12.02 ± 0.07 g, 24.76 ± 0.68 g, 49.59 ± 1.07 g, and 94.09 ± 1.16 g, respectively, while those of the shelter group (SG) were 5.80 ± 0.10 g, 12.10 ± 0.25 g, 24.88 ± 0.08 g, 49.50 ± 1.27 g, and 94.55 ± 1.27 g, respectively.

2.2.1 Culture management

During the experiment, the water depth in the pool was maintained at 0.4 m, and oxygen was continuously provided. Enough fresh wild fish was fed at 16:00 each afternoon, and then the residual feed was removed and the water was changed by 1/2 at 8:00 the next morning. Moreover, the water temperature was 26.9 ± 1.2°C, salinity was 26.1 ± 0.1, pH was 8.3 ± 0.1, DO > 5 mg/L, and light/dark = 12 h:12 h.

2.2.2 Data collection

After the experiment began, the activities and hidden behaviors of crabs were observed continuously, and the hidden situation was recorded every 3 hours. In addition, the molt time and molt position of crabs were observed daily. Molting time divided into daytime (6:00-18:00) and night (18:00-6:00), and molting position divided into inside the shelter and outside the shelter. The newly molted crabs were gently dried with a towel after their carapace hardened and weighed and measured for carapace width. After the measurement, renumber the crabs on their carapace and put back into the original pool for further cultivation until all crabs in that group have completed one molt. Afterwards, the shelters occupancy rate (SOR), hidden rate (HR), molting rate during day or night (MR_D/MR_N), molting rate in the shelter (MR_S), molting interphase (MI), survival rate (SR), weight growth rate (WGR), carapace width growth rate (WGRc), weight specific growth rate (SGRw) and carapace width specific growth rate (SGRc) were calculated according to the following formulas.

SOR = occupied shelters/total shelters × 100%

HR = hiding individuals/real-time survivals × 100%

MR_D = molting individuals in daytime/total molting individuals × 100%

MR_N = molting individuals at night/total molting individuals × 100%

MR_S = molting individuals in shelter/total molting individuals × 100%

MI = molting time − initial time

SR = final survivals/initial individuals × 100%

WGR = (final weight − initial weight)/initial weight × 100%

WGRc = (final carapace width − initial carapace width)/initial carapace width ×100%

SGRw = (ln weight after molting − ln initial weight)/molting interphase × 100%

SGRc = (ln carapace width after molting − ln initial carapace width)/molting interphase × 100%

2.3 Data analysis

All data are expressed as the mean ± standard deviation. SPSS 22.0 software was used to analyze the experimental data. The homogeneity of variance was detected according to Levene's method, and the inverse sine or square root processing was performed when the homogeneity variance was not satisfied. Independent samples T test were used to examine the differences in each index between the same group of swimming crab with and without shelters. Origin 2018 software was used for drawing, and $P < 0.05$ was taken as the significant difference.

3 Results

3.1 Hidden and molting behavior of swimming crab with different body weights

After the beginning of the experiment, most crabs swam around the pond and slowly hided into the shelter in the SG, some individuals would hide in the shelter, with their bodies close to the inner wall of the shelter, some individuals were close to the outer wall of the shelter, while others were located near the pool wall. However, all crabs in the NSG were distributed around the wall of the pool, and few crabs moved in the center of the pool.

Figure 2 shows the SOR in the daytime (58.58%~71.52%) was significantly higher than that at night (26.50%~37.92%). Overall, with the increase in the body weight of the crab, the SOR gradually increased during the daytime, especially in Group E, which was as high as 71.52%, a value that was significantly higher than that in Groups A, B and C ($P < 0.05$). As for the HR, it is also significantly higher in the daytime than at night, but the difference in each group was small, basically between 57.14% and 64.20%, of which Group B had the highest HR in the daytime (64.20%), followed by Group E with 61.40% (Figure 3). In addition, we found that there were different numbers of crabs in a single shelter, including 1 ind/shelter, 2 ind/shelter, 3 ind/shelter, 4 ind/shelter and 5 ind/shelter. In Group B, there were even 6 ind/shelter, while in Groups D and E, there were at most 3 crabs in a shelter, and most individuals occupied one shelter alone. Furthermore, if other crabs try to enter the shelter where crabs were already present, the crab in the shelter will open their chelipeds to deter and drive the invaders away. Therefore, other crabs that fail to occupy the shelter can only be forced to hide around the outer shelter wall or the cement pool wall. By comparison, the proportion of multiple individuals in a shelter in the smaller body weight group (Groups A, B and C) was significantly higher than that in the larger body weight group (Groups D and E), and the probability of 1 ind/shelter in the larger body weight group (Groups D and E) was high up to 77% (Figure 4). As a whole, the proportion of multiple crabs in a shelter decreased as the body weight of crabs increased.

After some intervals, the crabs started to molt. The molting of crabs with different body weights during the day or night was not significantly affected by the shelter on the basis of Figure 5, indicating that the existence of shelter did not change the molting habits of the crab. Additionally, there were some differences in the molting habits of different body weight crabs, especially among Groups A, B, C and D. With the increase of body weight, the MR_D was higher.

Under the condition of the existence of the shelter, most crabs choose to molt inside the shelter. Overall, no matter which body weight group, more than half individuals would choose to molt in the shelter. Among them, Group B had the largest number of individuals molting in the shelter, and the MR_S was high up to 81.15%, followed by Group A with 66.01%, and the lowest was 57.70% in Group E (Figure 6). The MI of all groups was less affected by shelter (Figure 7), but the MI in Groups B, D and E was slightly shortened in the presence of shelter. These results demonstrate that the larger the crab's body weight is, the longer the MI is, regardless of the presence of shelters

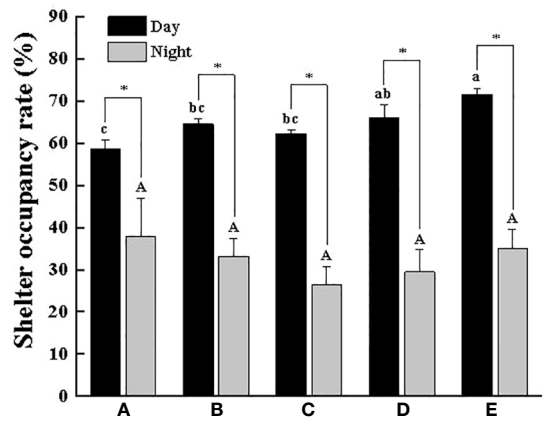

FIGURE 2
Shelter occupancy rate of swimming crab with different body weight groups in the presence of shelters. Different letters indicate significant differences among different body weight groups ($P < 0.05$) and "*" indicates significant differences between day and night ($P < 0.05$).

3.2 Survival and growth of swimming crab with different body weights

No matter whether there were shelter or not, as long as there was no molting crab, all the crabs get along well. There was basically no aggressive behavior except for normal food grabbing, and several crabs gathered in the corner. During the experiment, no crabs died from the diseases and hunger. However, the intra-specific aggression and predation did cause a high mortality during the molting period, especially in the soft-shell phase. The SR with shelter was higher than that without shelter (Figure 8), In particular, the SR of group D in SG was significantly higher than that in NSG ($P < 0.05$), indicating that the shelter showed a better anti-injury effect. Additionally, whether the shelter existed or not, there was a tendency that the larger the crab weight, the more serious the intraspecific cannibalism phenomenon and the lower the SR

After one molting, the body weight and carapace width of all surviving crabs changed evidently. The body weight, carapace width, WGR and WGR_C of all groups in the SG were higher than those in the NSG (Table 1; Figures 9 and 10). In particular, the WGR and WGR_C in Group A in the presence of shelter was significantly higher than that in the absence of shelter ($P < 0.05$), indicating that shelter has a certain promoting effect on the growth performance of different body weights. Regardless of the presence or absence of shelter, the larger the body weight of crab was, the smaller of the WGR and SGR after molting.

4 Discussion

In the groups without shelters, crabs with different body weights all preferred to hide in the corners of the cement pool, but rarely in the middle area of the cement pool, suggesting

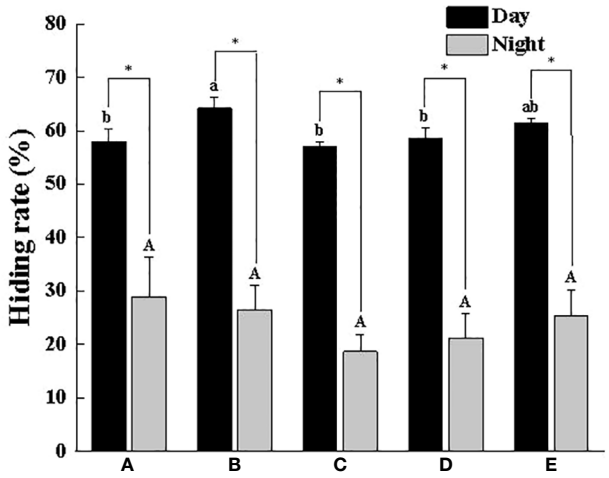

FIGURE 3
Hidden rate of swimming crab with different body weight groups in the presence of shelters. Different letters indicate significant differences among different body weight groups ($P < 0.05$) and "*" indicates significant differences between day and night ($P < 0.05$).

that swimming crab preferred supported and low-light places. Although the preference for shelters varied from group to group in the experiment, most individuals entered the shelters voluntarily and hid under the shelters for an extended, and there was a significant positive correlation between the SOR and body weight, which was consistent with the hidden law of *Neogobius melanostomus* of different body weights (Stammler and Corkum, 2005). It is noteworthy that the phenomenon of crabs hidden in the same shelter was more frequent in the smaller body weight groups and decreased significantly with increasing body weight, especially in Groups D and E where a shelter was usually occupied by only one crab and when other individuals try to enter the occupied shelter, the occupant would take a defensive posture (using walking legs to lift the body and opening two chelipeds). It showed obvious domain defense behavior, which contained a truth that the territorial consciousness of swimming crab gradually increased with increasing body weight. Similar phenomena have been reported in many crustaceans such as *Cancer irroratus*, *Fiddler crab* and *Oratosqilla oratoria* (Matheson and Gagnon, 2012; Dennenmoser and Christy, 2013; Jian, 2016).

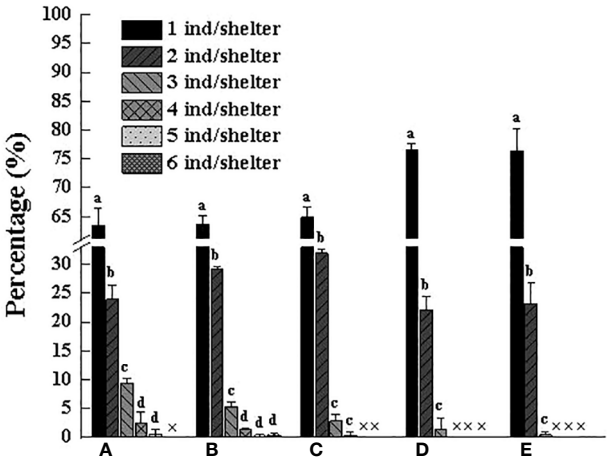

FIGURE 4
The percentage of the number of swimming crabs in each body weight group in the same shelter at the same time to the total number of the group. Different letters indicate significant differences among different numbers of swimming crab under the same shelter ($P < 0.05$).

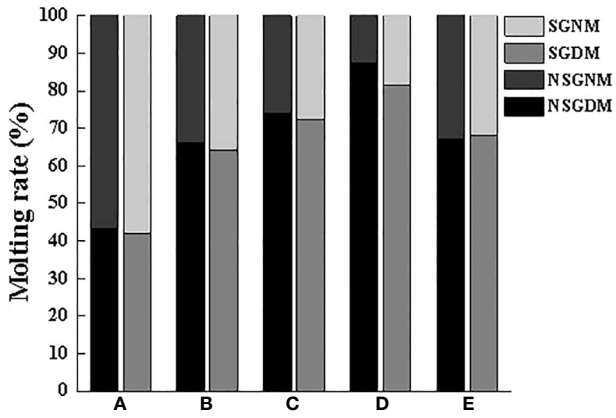

FIGURE 5
Molting rate of swimming crab in daytime and at night with different body weight groups in the presence and absence of shelters. NSGDM, No shelter group molting during the day; NSGNM, No shelter group molting during the night; SGDM, Shelter group molting during the day; SGNM, Shelter group molting during the night.

This study also manifested that the HR and the SOR with different body weights in the SG remained at approximately 60% during the daytime, while at night crabs would take the initiative to leave the shelters for food and swim freely, thus leading to a reduction in the HR and the SOR, which was consistent with the habit of swimming crab hiding during the day and going out at night (Dai et al., 1977).

Crustaceans such as shrimp and crabs rely on molting to grow. Internal mechanisms and external environment jointly regulate the molting time and molting cycle of crustaceans (Luppi et al., 2001; He et al., 2017). Shelters change the three-dimensional spatial structure in the cement pool, especially increased the complexity of the bottom level, thus playing a positive role in keeping the distance between the swimming crab individuals play a positive role. We still found that only the MR_D of the swimming crab with smaller body weight (Group A) was lower than that of MR_N, which was quite the opposite to the other groups. Because molting at night can reduce the probability being preyed and killed by similar species, which also indicates that swimming crab can change molting time through their own regulation. With the presence of shelter, more than 50% of individuals would choose to molt in the shelter, especially in Group B, where the molting rate in the shelter was the highest at 81.15%, while the molting rate

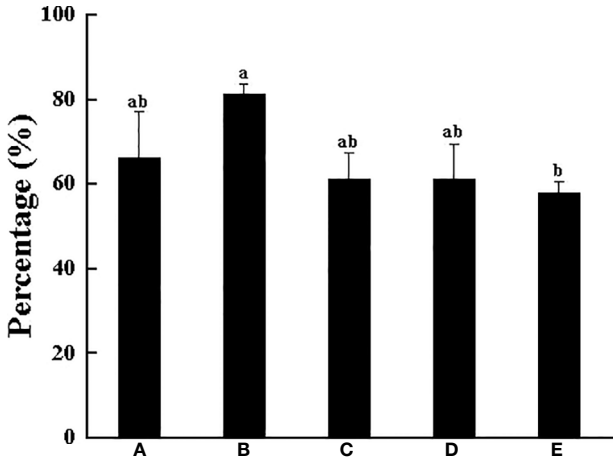

FIGURE 6
The percentage of swimming crab completing molting under the shelter with different body weight groups. Different letters indicate significant differences among different body weight groups ($P < 0.05$).

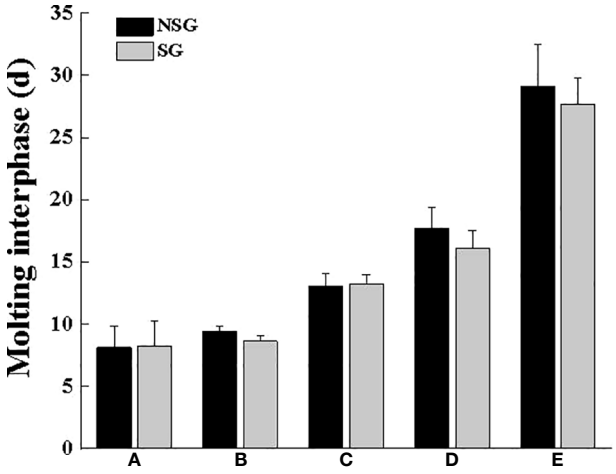

FIGURE 7
Molting interphase of swimming crab with different body weight groups between NSG and SG. Unmarked letters indicate no significant difference ($P > 0.05$).

in the shelter was as low as 57.7% in Group E. This result further illustrates that the setting of shelters has a good attractive effect on all body weights, also confirms that to reduce the visual cues in the population, the numerous crustaceans in the molting process, usually choose relatively hidden spaces to complete molting to avoid the invasion and slaughter of the same species, thereby reducing the risk of cannibalism (Polis, 1981; Moksnes et al., 1997). In addition, the molting interphase in Groups B, D and E was slightly shortened under the condition of the existence of shelter, this means that the setting of shelter accelerated the growth speed of swimming crab.

This study also found that regardless of whether there were shelters or not, when there were no soft-shelled crabs existed, all the crabs were more harmonious with each other, and there would even be multiple crabs gathering in the same corner. Cannibalism mainly occurs in the soft-shell phase. Related studies show that some active chemical factors released by crustaceans during molting are also one of the important factors leading to the intensification of cannibalism, in addition to its soft body, slow swimming speed and poor self-defense ability, leading to the intensification of cannibalism (Bolingbroke and Kass-Simon, 2001). Active chemicals such as amine neurons and

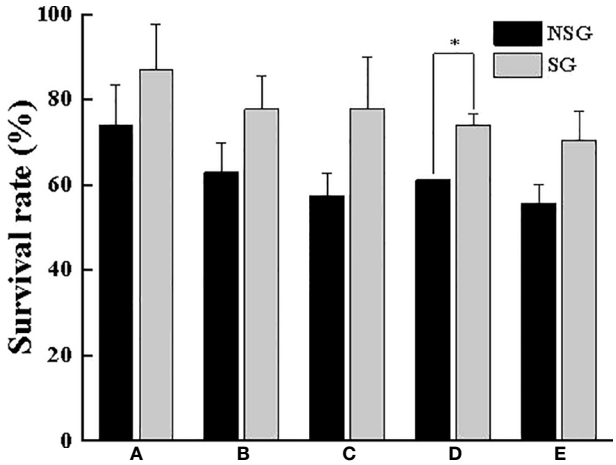

FIGURE 8
Survival rate of swimming crab with different body weight between NSG and SG. "*" indicates significant difference ($P < 0.05$).

TABLE 1 Changes in body weight and carapace width of swimming crab with different body weight in the NSG and SG.

Group		BW_0 (g)	CW_0 (mm)	BW_1 (g)	CW_1 (mm)
A	NSG	5.67 ± 0.12	35.69 ± 0.22	11.47 ± 0.27	45.67 ± 0.82
	SG	5.80 ± 0.10	35.86 ± 0.23	12.17 ± 0.36	46.91 ± 0.26
B	NSG	12.02 ± 0.07	45.76 ± 0.26	23.71 ± 1.13	59.86 ± 1.05
	SG	12.10 ± 0.25	45.87 ± 0.31	24.22 ± 0.56	60.03 ± 0.23
C	NSG	24.76 ± 0.68	59.03 ± 0.57	50.70 ± 2.54	76.59 ± 0.72
	SG	24.88 ± 0.08	59.25 ± 0.06	52.03 ± 0.09	77.66 ± 0.22
D	NSG	49.59 ± 1.07	74.79 ± 0.76	90.62 ± 4.01	94.26 ± 0.93
	SG	49.50 ± 1.27	74.74 ± 0.72	93.31 ± 0.43	95.69 ± 0.32
E	NSG	94.09 ± 1.16	93.25 ± 0.26	167.65 ± 6.09	115.62 ± 1.14
	SG	94.55 ± 1.27	93.39 ± 0.38	170.65 ± 6.52	116.66 ± 0.41

BW_0: initial body weight; CW_0, initial carapace width; BW_1, body weight after molting; CW_1, carapace width after molting. There were no significant differences in body weight and carapace width in the NSG and SG before and after molting ($P > 0.05$).

20-hydroxyecdysone have been demonstrated to be essential for the central and peripheral neurotransmission transmission of aggressive behavior in crustaceans (Ruffner et al., 1999; Kravitz, 2000). Soft-shelled crabs that molted in the period before the beginning of this experiment were less likely to be eaten by conspecifics. When individuals with larger molted shell masses were present, those crabs with smaller body weights in the molting process or the soft-shell stage were extremely vulnerable to attack by hard-shelled larger crabs, which means that the asymmetry between individuals was one of the important factors causing the increase of the dynamic stability of cannibalism. There was no individual mortality during the whole experiment due to fighting among the same species caused by food shortage or hunger, disease and other factors, and all mortality was the result of cannibalism. Point view of final SR, the SR was higher in the presence of shelters, especially Group D, which was significantly higher with shelter than that without shelters, revealing those shelters had better anti-injury properties at this body weight stage. Studies on shrimps and crabs have shown that the presence of shelters not only changes the spatial structure of the water column, but also improves the dispersal of individuals (Mirera and Moksnes, 2014). This contributes to reduce the probability of contact and delay the aggressive behavior between them, thus increasing the final SR (Moksens, 2004; He et al., 2017). What is more, regardless of the presence or absence of shelter, there was a trend that the larger the body weight of the crab was, the more severe the intraspecies fratricide and the lower the SR. This is inevitably related to the fact that territorial and hidden consciousness is gradually strengthened as body weight increases. Similar phenomena of intensified fighting behavior and the establishment of intraspecies dominance with increasing body weight have been reported in crustaceans such as *Oratosqilla oratoria* and *Procambarus* clarkii (Horner et al., 2008; Jian, 2016).

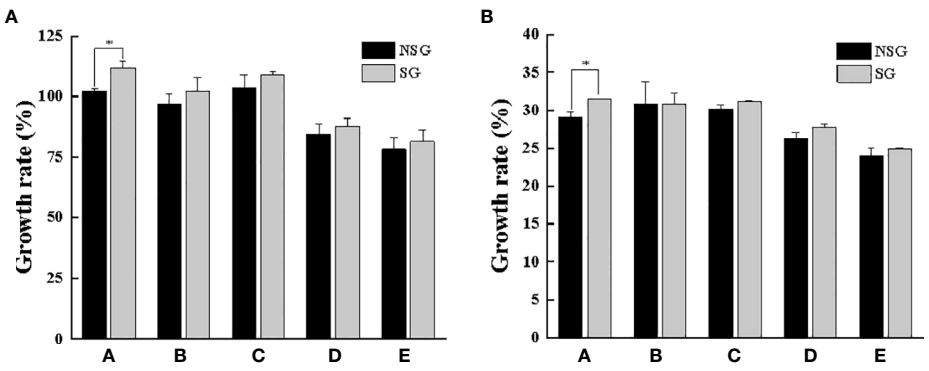

FIGURE 9
Growth rate of body weight **(A)** and carapace width **(B)** of swimming crab with different body weight between NSG and SG. "*" indicates significant differences ($P < 0.05$).

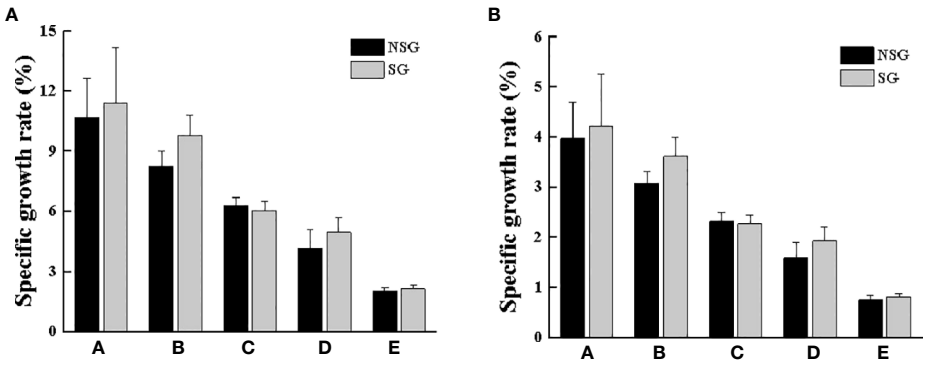

FIGURE 10
Specific growth rates of body weight **(A)** and carapace width **(B)** of swimming crab with different body weight between NSG and SG. Unmarked letters indicate no significant differences ($P > 0.05$).

Of particular note was that at smaller body weights, swimming crabs were able to get along amicably even when multiple individuals were hiding inside the same shelter at the same time, and many individuals could safely molt in the shelter. Our study further elucidates that swimming crab with a smaller body weight is weak in territorial consciousness and low in aggression.

Contrary to the previously mentioned fact that the presence of shelter slightly shortened the MI, shelter increase the body weight, carapace width, WGR and WGR_C of swimming crab after molting. This illustrates the setting of shelters indirectly changed the growth law based on changing the activity behavior. The authors believe that the main reason for this is that the setting of shelters provides a more suitable living environment for swimming crab, which reduces the energy consumption caused by competing for resources and defending against the same species, such that energy intake is more used for growth. The positive effect of shelter settings on promoting the growth of aquatic animals and improving their growth characteristics has been fully confirmed in varieties such as *Salvelinus alpinus* and *Sebastes schlegelii* (Benhaïm et al., 2009; Guo et al., 2015).

5 Conclusion

Our study proved that swimming crab with different body weights exhibited obvious hiding behavior in the presence of shelter, especially in the daytime, the larger the body weight was, the higher the SOR was. In the case of crabs with a smaller body weight (below 50 g), there were poor territorial consciousness, with multiple individual hiding in the same shelter at the same time. Conversely, in the case of individuals with larger body weight (approximately 50 g or above), there were strong territorial consciousness, and in most cases, a shelter was occupied by a single crab. Furthermore, most individuals of all body weights selected to molt in the shelter. The molting survival rate and growth performance of swimming crab were improved under the protection of the shelter. Accordingly, we recommend that in the process of swimming crab breeding and production, the shelter should be set up in advance before the release of seedlings, which can play a positive role in the whole growth process, and thus improve the survival rate and yield of pond culture.

Data availability statement

The original contributions presented in the study are included in the article/supplementary material. Further inquiries can be directed to the corresponding author.

Author contributions

JH and HY: Investigation, Formal analysis, Writing - original draft. LW: Conceptualization, Data curation, Formal analysis. DZ: Visualization, Writing - reviewing and editing. WX: Supervision, Funding acquisition, Writing - reviewing and editing. All authors contributed to manuscript revision, read, and approved the submitted version.

Funding

This work was supported by the Basic Public Welfare Program of Zhejiang Province (Grant No. LGN22C190005); the National Science Foundation of China (Grant No. 32172993); the Major Agricultural Technology Cooperation Plan of Zhejiang Province (Grant No. 2020XTTGSC03); the science and technology project of Zhoushan City and Putuo District (Grant No. 2018C31078, 2020JH131); the planned

project of Zhejiang Marine Fisheries Research institute (HYS-CZ-202105, HYS-CZ-202209).

Conflict of interest

The authors declare that the research was conducted in the absence of any commercial or financial relationships that could be construed as a potential conflict of interest.

Publisher's note

References

Benhaïm, D., Leblancb, C. A., and Lucas, G. (2009). Impact of a new artificial shelter on Arctic charr (*Salvelinus alpinus*, l.) behaviour and culture performance during the endogenous feeding period. *Aquaculture* 295 (1-2), 38–43. doi: 10.1016/j.aquaculture.2009.06.024

Bolingbroke, M., and Kass-Simon, G. (2001). 20-hydroxyecdysone causes increased aggressiveness in female American lobsters. *Homarus americanus. Horm. Behav.* 39 (2), 144–156. doi: 10.1006/hbeh.2001.1642

Chen, X. (2006). "Behavioural ecology study on megalopae and first juvenile of mud crab, Scylla serrata (Forskål)," (Xiamen University). in *Doctoral dissertation*, vol. pp 9-pp. 25.

Chen, X., Li, S., Wang, G., Lin, Q., Ye, H., and Ai, C. (2008). Study on relationship between cannibalism and resource Availability/Starvation of mud crab, *Scylla paramamosain* megalopae. *J. Xiamen Univer. (Natur. Sci).* 47 (1), 99–103. doi: 10.3321/j.issn:0438-0479.2008.01.022

Dai, A., Feng, Z., Song, Y., Huang, Z., and Wu, H. (1977). Fisheries biology of *Portunus trituberculatus* linneis initialing investigatgtion. *Chi. J. Zool.* 2, 30–33. doi: 10.13859/j.cjz.1977.02.015

Dennenmoser, S., and Christy, J. H. (2013). The design of a beautiful weapon: compensation for opposing sexual selection on a trait with two functions. *Evol* 67 (4), 1181–1188. doi: 10.1111/evo.12018

Gil, M. D. M., Pastor, E., and Durán, J. (2019). Survival and growth of hatchery-reared mediterranean spider crab juveniles, *maja squinado*, under different rearing conditions. *Aquacult* 498, 37–43. doi: 10.1016/j.aquaculture.2018.08.001

Guo, H., Zhang, X., and Gao, T. (2015). Effects of artificial shelters and feeding frequency on growth and behavior of juvenile sebastes schlegelii. *J. Fish. Sci. Chi.* 22 (2), 319–331. doi: 10.3724/SP.J.1118.2015.1422

He, J., Gao, Y., Wang, W., Xie, J., Shi, H., Wang, G., et al. (2016). Limb autotomy patterns in the juvenile swimming crab (*Portunus trituberculatus*) in earth ponds. *Aquaculture* 463, 189–192. doi: 10.1016/j.aquaculture.2016.05.043

He, J., Gao, Y., Xu, W., Yu, F., Su, Z., and Xuan, F. (2017). Effects of different shelters on the molting, growth and culture performance of *Portunus trituberculatus*. *Aquaculture* 481, 133–139. doi: 10.1016/j.aquaculture.2017.08.027

Horner, A. J., Schmidt, M., Edwards, D. H., and Derby, C. D. (2008). Role of the olfactory pathway in agonistic behavior of crayfish, *Procambarus clarkii*. *Invertebr. Neurosci.* 8 (1), 11–18. doi: 10.1007/s10158-007-0063-1

Jian, T. (2016). "A preliminary study on the behavior in oratosqilla oratoria," in *Master dissertation* (Dalian Ocean University), pp13–pp15.

Kravitz, E. A. (2000). Serotonin and aggression: insights gained from a lobster model system and speculations on the role of amine neurons in a complex behavior. *J. Comp. Physiol. A.* 186 (3), 221–238. doi: 10.1007/s003590050423

Li, Y., and Sun, X. (2013). Agonistic behaviors of aquatic animals. *Zool. Res.* 34 (3), 214–220. doi: 10.11813/j.issn.0254-5853.2013.3.0214

Liu, H. (2002). Study on cannibalism of carnivorous fish under culture ecological conditions. *Fish. Sci. Tech. Infor.* 29 (6), 261–263. doi: 10.3969/j.issn.1001-1994.2002.06.001

Luppi, T. A., Spivak, E. D., and Anger, K. (2001). Experimental studies on predation and cannibalism of the settlers of *Chasmagnathus granulata* and *Cyrtograpsus angulatus* (Brachyura: Grapsidae). *J. Exp. Mar. Biol. Ecol.* 265 (1), 29–48. doi: 10.1016/s0022-0981(01)00322-7

Mann, D. L., Asakawa, T., Kelly, B., Lindsay, T., and Paterson, B. (2007). Stocking density and artificial habitat influence stock structure and yield from intensive nursery systems for mud crabs *Scylla serrata* (Forsskål 1775). *Aquacult. Res.* 38 (14), 1580–1587. doi: 10.1111/j.1365-2109.2006.01626.x

Marshall, S., Warburton, K., Paterson, B., and Mann, D. (2005). Cannibalism in juvenile blue-swimmer crabs *Portunus pelagicus* (Linnaeus 1766): effects of body size, moult stage and refuge availability. *Appl. Anim. Behav. Sci.* 90 (1), 65–82. doi: 10.1016/j.applanim.2004.07.007

Matheson, K., and Gagnon, P. (2012). Effects of temperature, body size, and chela loss on competition for a limited food resource between indigenous rock crab (*Cancer irroratus say*) and recently introduced green crab (*Carcinus maenas l.*). *J. Exp. Mar. Biol. Ecol.* 428, 49–56. doi: 10.1016/j.jembe.2012.06.003

Mirera, D. O., and Moksnes, P.-O. (2013). Cannibalistic interactions of juvenile mud crabs *Scylla serrata*: the effect of shelter and crab size. *Afr. J. Mar. Sci.* 35 (4), 545–553. doi: 10.2989/1814232X.2013.865677

Mirera, D. O., and Moksnes, P.-O. (2014). Comparative performance of wild juvenile mud crab (*Scylla serrata*) in different culture systems in East Africa: effect of shelter, crab size and stocking density. *Aquacult. Int. 23* 1), 155–173. doi: 10.1007/s10499-014-9805-3

Moksnes, P.-O. (2004). Self-regulating mechanisms in cannibalistic populations of juvenile shore crabs *Carcinus maenas*. *Ecology* 85 (5), 1343–1354. doi: 10.1890/02-0750

Moksnes, P.-O., Lipcius, R. N., Pihl, L., and Montfrans, J. V. (1997). Cannibal prey dynamics in young juveniles and post larvae of the blue crab. *J. Exp. Mar. Biol. Ecol.* 215 (2), 157–187. doi: 10.1016/S0022-0981(97)00052-X

Perkins-Visser, E., Wolcott, T. G., and Wolcott, D. L. (1996). Nursery role of seagrass beds: enhanced growth of juvenile blue crabs (*Callinectes sapidus*, rathbun). *J. Exp. Mar. Biol. Ecol.* 198 (2), 155–173. doi: 10.1016/0022-0981(96)00014-7

Polis, G. A. (1981). The evolution and dynamics of intraspecific predation. *Annu. Rev. Ecol. Syst.* 12 (1), 225–251. doi: 10.1146/annurev.es.12.110181.001301

Qin, H., and Li, Y. (2014). The effects of stocking density and food on agonistic behavior and growth performance in *fenneropenaeus chinensis*. *Ocean. Limn. Sin.* 45 (4), 834–838. doi: 10.11693/hyhz20140400095

Ruffner, M. E., Cromarty, S. I., and Cooper, R. I. (1999). Depression of synaptic efficacy in high- and low-output *Drosophila* neuromuscular junctions by the molting hormone (20-HE). *J. Neurophysiol.* 81 (2), 788–794.

Stammler, K. L., and Corkum, L. D. (2005). Assessment of fish size on shelter choice and intraspecific interactions by round gobies *Neogobius melanostomus*. *Environ. Biol. Fishes.* 73 (2), 117–123. doi: 10.1007/s10641-004-5562-x

Wang, R., Jiang, L., and Li, Y. (2015). Effects of internal and external factors on cannibalismin post-larvae of *Litopenaeus vannamei*. *J. Henan. Agric. Sci.* 44 (2), 142–145. doi: 10.15933/j.cnki.1004-3268.2015.02.032

frontiers | Frontiers in Marine Science

TYPE Original Research
PUBLISHED 20 September 2022
DOI 10.3389/fmars.2022.1013857

OPEN ACCESS

EDITED BY
Zhiguo Dong,
Jiangsu Ocean Universiity, China

REVIEWED BY
Yuehuan Zhang,
Chinese Academy of Sciences (CAS), China
Kaida Xu,
Zhejiang Ocean University, China
Baoying Guo,
Zhejiang Ocean University, China

*CORRESPONDENCE
Jin-Long Yang
jlyang@shou.edu.cn
Mingyou Li
myli@shou.edu.cn

†These authors have contributed equally to this work and share first authorship

SPECIALTY SECTION
This article was submitted to Marine Biology, a section of the journal Frontiers in Marine Science

RECEIVED 07 August 2022
ACCEPTED 05 September 2022
PUBLISHED 20 September 2022

CITATION
Wang M, Xia J, Jawad M, Wei W, Gui L, Liang X, Yang J-L and Li M (2022) Transcriptome sequencing analysis of sex-related genes and miRNAs in the gonads of *Mytilus coruscus*. *Front. Mar. Sci.* 9:1013857. doi: 10.3389/fmars.2022.1013857

Transcriptome sequencing analysis of sex-related genes and miRNAs in the gonads of *Mytilus coruscus*

Min Wang[1,2†], Jiao Xia[1,2†], Muhammad Jawad[1,2], Wenbo Wei[1,2], Lang Gui[1,2], Xiao Liang[2,3], Jin-Long Yang[2,3*] and Mingyou Li[1,2*]

[1]Key Laboratory of Integrated Rice-Fish Farming, Ministry of Agriculture and Rural Affairs, Shanghai Ocean University, Shanghai, China, [2]Key Laboratory of Exploration and Utilization of Aquatic Genetic Resources, Ministry of Education, Shanghai Ocean University, Shanghai, China, [3]Southern Marine Science and Engineering Guangdong Laboratory, Guangzhou, China

Mytilus coruscus is a significant economic species in China's eastern coastal areas. As a dioecious species, it lacks secondary sexual characteristics, which makes it difficult for selective breeding. However, limited research is carried out on the genetic data regarding reproductive development and gender differentiation. In the current study, *de novo* transcriptome sequencing analyses were used to detect gonad-specific genes and miRNAs in *M. coruscus*. By comparing testis and ovary, 159,970 unigenes and 300 miRNAs were obtained totally, of which differentially expressed genes and miRNAs were 9,566 and 25, respectively. Analysis of qRT-PCR showed that *cyp26a*, *dmrt4*, *foxl2*, *gdf9*, *17β-hsd14*, *sc6a9*, *zar1*, and *zp4* were highly expressed in the ovary as compared to the testis, while *sox2* showed lower expression in the ovary. Expression of miR-750-3p, novel 1, and miR-193 was higher in the ovary than that in the testis, whereas the expression of miR-9-5p, miR-9-3p, miR-317, novel 124, miR-2d and miR-263b were lower in the ovary. Furthermore, analysis of miR-317 by Targetscan and MiRanda predicted to target *dmrt4* and the luciferase reporter was performed to confirm it. Our research provides a molecular basis for understanding sexual development and reproductive regulation. Further research is needed on the mechanism of gonadal maturation and differentiation in *M. coruscus*.

KEYWORDS

***mytilus coruscus*, transcriptome, gonad, mRNA, miRNA, miRNA-mRNA interaction, DMRT4, miR-317**

Highlights:

- Transcriptome sequencing was used to analyze the mRNA and miRNA in gonads of *Mytilus coruscus*.
- In total, 9,566 DEGs and 25 DEMs were identified from the gonad of *Mytilus coruscus*.
- Dual-luciferase reporter assay proved that a testis biased expressed miRNA-133 targeting *5-HT1*.

Introduction

In the field of life science, the concept of sex is among the most intriguing. In most animals, once the sex is established, it is typically retained for life. The gonad, which includes the testis and ovary, is a necessary reproductive organ. Gonadal development and sex determination are regulated by several genes that express themselves differently in testes and ovaries (Li et al., 2022a). The process of sex determination involves different sex-determining genes, and several conserved sex-determining genes have been identified and systematically studied in vertebrates. Previous study showed that sex-related genes *DMY* (Matsuda et al., 2002), HMG box (*SOX*) (Sutton et al., 2011), and forkhead box L3 (*FOXL3*) (Nishimura et al., 2015) are identified. These genes were also found as sex-determining genes in invertebrates, especially in economically important bivalve mollusks (Zhang et al., 2014; Ning et al., 2021). Recent studies have identified *vg* as a gonadal-associated gene and highly expressed in the ovary in the Pacific White Shrimp *Litopenaeus vannamei* (Li et al., 2022b). The genes *foxl2, dmrt, soxE, soxH*, and *wnt4* all have been recently reported in shellfish (Naimi et al., 2009; Shi et al., 2015; Li et al., 2016; Shi et al., 2018), which are identified to be associated with gonadal development and gender differentiation.

MicroRNA is a non-coding single-stranded RNA molecule in eukaryotes, consisting of approximately 22 nucleotides. It is generally believed that miRNA binds to specific sequences of a target gene, the so-called "seed sequences", which can cause degradation of target mRNA or inhibit its translation (Ambros, 2004; Bartel, 2007). Previous studies found that miRNAs participated in regulating many biogenesis processes, such as cell growth, cell proliferation, cell apoptosis, tissue differentiation, and embryo development (Mitchell et al., 2008; Miao et al., 2017; Saliminejad et al., 2019). The research on the expression of miRNA has been intensively studied in gonads of different aquatic species such as yellow catfish (Jing et al., 2014), *Eriocheir sinensis* (He et al., 2015) and *Oryzias latipes* (Qiu et al., 2018), *Macrobrachium rosenbergii* (Xia et al., 2022).

As a dioecious species, *Mytilus coruscus* (*M. coruscus*) is one of the most popular economic shellfish in China's eastern coastal areas (Ye et al., 2012; Yang et al., 2021), which has the advantage of fast growth, immense reproductive ability, strong disease resistance, strong adaptability and easy artificial breeding. So far, studies have been conducted on pharmacological (Yang et al., 2013a) and molecular microbiology levels (Yang et al., 2013b; Yang et al., 2014). However, little research is conducted on genes and miRNAs related to gonadal development and differentiation. A comprehensive study of the mussel developmental mechanisms, including gonad-related genes and miRNAs, is currently required.

This study aims to identify important differentially expressed genes and miRNAs controlling sex determination and gonadal development in mussels and their potential biological functions. This research might help us to understand the mechanism of sex differentiation of mussels at the molecular level and provide data for the follow-up study of sexual dimorphism of economic shellfish.

Materials and methods

Sample collection

Three healthy male mussels and three healthy female mussels were collected from Gouqi Island in Zhejiang province. At the time of sampling, *M. coruscus* were one year old and had reached the stage of sexual differentiation. After dissection, samples of the ovary, testis, mantle, muscle, labial flap, and foot from mussels were obtained and frozen in liquid nitrogen at once and stored at −80°C. All the experiments about *M. coruscus* were conducted under the Declaration of Helsinki and approved by the Shanghai Ocean University Animal Care and Use Committee with approval number SHOU-2021-118.2.2.

Gonadal histology

To investigate the gonadal developmental stages of mussels, histological analysis was performed. The tissues were fixed in 4% polyformaldehyde (PFA) for 24 hours, and the fixed tissues were dehydrated in a gradient of 70-100% ethanol gradient, embedded in paraffin, sectioned, and stained with hematoxylin-eosin (H.E). Gender and period of gonadal development were determined by mounting sections of each sample on glass slides and examining them under a microscope.

Construction of mRNA and small RNA library

By using Trizol® (Invitrogen, Carlsbad, CA), the total gonadal RNA was extracted. The RNA integrity was evaluated by Agilent 2100 Bioanalyzer (Agilent Technologies, Santa Clara, CA, USA). To obtain cDNA, 1 μg of the above RNA was taken, and then reversed transcribed. The cDNA was further amplified

by the PCR method. After that, cDNA constructs were purified. Following the instructions of the TruSeq Small RNA Sample Preparation Kit (Illumina, San Diego, USA), the libraries were conducted using 1 μg total RNA. Then the RNA-seq was conducted on the Illumina sequencing platform (HiSeq 2500) at OE Biotech. Co., Ltd. (Shanghai, China).

Bioinformatics analysis of mRNA and miRNA

Trimmomatic was used to process raw data (raw reads). To get clean reads, the ploy-N-containing reads and the poor-quality sequences were removed. Then the clean reads were assembled into expressed sequence tag clusters (contigs). And *de novo* assembled into the transcript *via* the usage of Trinity (version 2.4) within the paired-end strategy. Based on the size and similarity of sequences, the longest transcript was selected as a unigene for subsequent investigation.

For the miRNA transcriptome, cutadapt was used to remove the linker sequence. The sequence was subjected to Q20 quality control using a fast toolkit (version 0.0.13), and those sequences with Q20 of at least 80% were retained. Afterward, using NGSQCToolkit to filter out reads containing N bases (version 2.3.2) Finally, high-quality clean reads were evaluated to analyze the subsequent study. Novel miRNAs were predicted by analyzing the unannotated small RNAs using mirdeep2. The corresponding miRNA star sequences were also determined by analyzing the hairpin structure of pre-miRNAs and aligning with the miRBase database.

The DEG difference algorithm in the R package was used to evaluate the p-value, and the miRNA and mRNA were screened out. TargetScan and MiRanda were used for targeting the prediction of differentially expressed mRNAs (DEGs) and miRNAs (DEMs). TargetScan and MiRanda were used for targeting the prediction of differentially expressed mRNAs and miRNAs.

mRNA/miRNA extraction and QRT-PCR

To validate the DEGs and DEMs in mussels, 9 mRNAs and 9 miRNAs were randomly selected. Total RNA extracted from 7 different tissues of mussel (ovary, testis, mantle, muscle, labial flap, foot) were collected and extracted into total RNA using TRizol® reagent. Then 1 μg total RNA was taken out and reverse transcribed into cDNA with M-MLV reverse transcriptase (Takara, Japan). miRNAs were obtained using TruSeq Small RNA Sample Preparation Kit (Illumina, San Diego, USA). miRNA primers were designed by the stem-loop method and verified by qRT-PCR. miRNA extraction kit was used to extract miRNA from the above 7 tissues. Then miRNAs were transcribed into cDNA using PrimerScript® RT reagent kit with gDNA Eraser kit (Takara, Japan). qRT-PCR was conducted using ABI 7500 real-time fluorescent PCR system and SYBR® premix Ex Taq™ II (Tli RNaseH Plus), and ROX plus (Takara, Japan). The procedure followed the guidelines described in the previous study (Zhang et al., 2021). Using the $2^{-\Delta\Delta Ct}$ method to determine the relative expression of genes, the samples were normalized with 18S rRNA. Three parallel experiments were performed for each reaction. Using Student's t-test to perform the comparative analysis of ovary and testis. $P < 0.05$ was considered significant difference. The specific primers for each mRNA and miRNA are shown in Table S1.

Molecular cloning of *Dmrt4* gene and plasmid construction

Using the above cDNA, according to the database sequence obtained by sequencing, The primer *dmrt4*-F/R amplified the *dmrt4* coding region by PCR, and the amino acid sequence was compared with the Vector NTI. Bioinformatics analysis showed that miR-317 has a binding site on *dmrt4*. To validate the targeting relationship between miR-317 and the 3'-UTR of *dmrt4*, the 3'-UTR of *dmrt4* consisting of the miR-317 binding site was cloned into the pmirGLO vector to construct a non-mutant plasmid (WT-pGLO). The seed region where miR-317 binds to the 3'-UTR of *dmrt4* was mutated by the primer mutation method and inserted into the pmirGLO vector to complete the mutant plasmid construction (MT-pGLO). For MT-pGLO, the binding sequence (TATACATCACAAAATGTGTGTTCC) was replaced by TATACATCACAAAATGACCAGAGC using the primers, which were conducted into the pmirGLO vector through XbaI and SalI sites. All recombinant plasmids have been sequenced by Sanger to confirm their accuracy. All primers mentioned in this part can be found in Table S1.

Dual-luciferase reporter assay

The culture and transfection methods of human embryonic kidney 293 (HEK293) cells used in the experiment were as previously described (Sun et al., 2020). Using FuGENE@HD (Promega, USA), WT-pGLO and MT-pGLO were co-transfected with miR-317 mimics to HEK293 cells respectively. After 36 hours of transfection, a luciferase activity reporter was conducted using the Dual-Glo® Luciferase Assay System, Promega, USA. To ensure the credibility of the results, each of the experiments was conducted at least three times.

Results

M. coruscus sex and gonad developmental stages

After dissection, gonadal sections of *M. coruscus* were examined under the microscope. The structure of the ovary

and testis could be easily distinguished (Figure 1).oogonia and mature oocytes can be visible in the ovary section of *M. coruscus* (Figures 1A, B). In the mussel nest sections, spermatogonia and spermatocytes could be seen (Figures 1C, D). According to the histological results, the testicles and ovaries of *M. coruscus* were at stage III of gonadal maturation. These tissues were then used for RNA sequencing and qRT-PCR.

Assembly, annotation, and bioinformatical analysis

Six gonadal tissues (3 ovaries and 3 testes) were sequenced by Illumina HiSeq 2500. In this analysis, 159,970 unigenes were assembled with a length of 150,935,287 bp totally and an average length of 943 bp. Annotating the Unigene database, there were 32,460 (20.29%) annotated genes in the NR library, 17,903 (11.19%) annotated genes in the Swissprot library, and 14,631 (9.15%) annotated genes in the KOG library, 20,651 (12.91%) annotated genes in the eggNOG library, 11293 (7.06%) annotated genes in the KEGG library, and 16,359 (10.23%) annotated genes in the GO library. These reads were aligned to unigenes with an alignment rate of 79.11-81.46% (Table 1).

DEGs and DEMs in gonad

In this research, 9,566 DEGs were found when comparing the transcriptional data of the ovary and testis. As compared to the ovary, 2,575 DEGs were in higher expression and 6991 DEGs were in lower expression (Figure 2A). A total of 300 miRNAs between 15-26 nt in length were screened from miRNA sequencing data of 6 gonad tissues (3 ovaries and 3 testes), of which 206 were novel and 94 were known miRNAs. After further comparing the miRNA expression of the ovary and testis, 25 DEMs were obtained. As compared to the ovary, 11 DEMs were expressed highly and 14 DEMs were expressed lowly (Figure 2C). Clear differences in miRNAs expression between the male and female were shown in the volcano plot (Figures 2B, D).

GO and KEGG analysis of DEMs

According to Gene Ontology (Mitchell et al., 2008) analysis, the functions of DEGs were described, and a total of 3,138 terms were enriched, including 2,076 biological processes, 390 cellular components, and 672 molecular functions. The most prevalent ones in the three comparison groups were the innate immune response, defense response to the virus, collagen trimer, and nuclear RNA-directed RNA polymerase complex. cysteine-type endopeptidase inhibitor activity (Figure 3A). In the KEGG database, all controls had 262 enriched pathways. The bubble chart stated the top 20 enrichment pathways of the KEGG analysis (Figure 3B). The main enrichment pathways of these differentially expressed genes were Apoptosis–multiple species, Toxoplasmosis, TNF signaling pathway, NF–kappa B signaling pathway, and Ubiquitin mediated proteolysis.

Validation of DEGs and DEMs by qRT-PCR

To evaluate the accuracy of transcriptomics data, qRT-PCR was further used to validate the expression levels of the

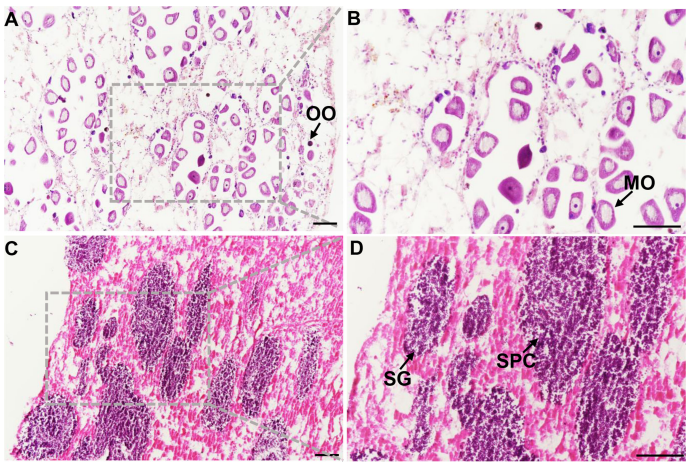

FIGURE 1
Mytilus coruscus gonad sections. **(A)** and **(B)** ovary tissue at stage III, **(C)** and **(D)** testis tissue at stage III. OO, oogonia; MO, mature oocyte; SG, spermatogonia; SPC, spermatocytes. Scale bars, 100 μm.

TABLE 1 Annotation statistics of the *Mytilus coruscus*.

Gene_number	NR	Swissprot	KEGG	KOG	eggNOG	GO	Pfam
159970	32460	17903	11293	14631	20651	16359	19086
100%	20.29%	11.19%	7.06%	9.15%	12.91%	10.23%	11.93%

randomly selected 9 mRNAs (*cyp26a*, *dmrt4*, *foxl2*, *gdf9*,*17β-hsd14*, *sc6a9*, *sox2*, *zar1*, *zp4*) and 9 miRNAs (miR-193, miR-317, miR-750-3p, miR-2d, miR-9-5p, miR-9-3p, miR-263b, novel 1, novel 124). The qRT-PCR results of the above genes and miRNAs were consistent with the results of RNA-seq. Meanwhile, their expressions in different tissues were detected.

Among the differentially expressed genes selected above, the expression levels of *cyp26a*, *dmrt4*, *foxl2*, *gdf9*, *17β-hsd14*, *sc6a9*, *zar1*, and *zp4* in the ovary were remarkably higher than those in the testis. However, *sox2* was in high expression in the testis (Figure 4). Among the above-mentioned DEMs, the expression level of miR-193, novel 1, and miR-750-3p in the ovary was significantly higher than in the testis, whereas miR-9-5p, miR-9-3p, miR-317, novel 124, miR-2d, and miR-263b expressed lowly in the ovary. (Figure 5).

Analysis of the miRNA–mRNA interaction

The interaction between miRNA and mRNA is one of the important regulatory roles of miRNA in biological processes. To understand the miRNA-mRNA interaction, we explored differentially expressed genes and their miRNAs with targeting relationships. A DEM could target one or more DEGs, which could also be predicted by one or more DEMs. This means that a complex

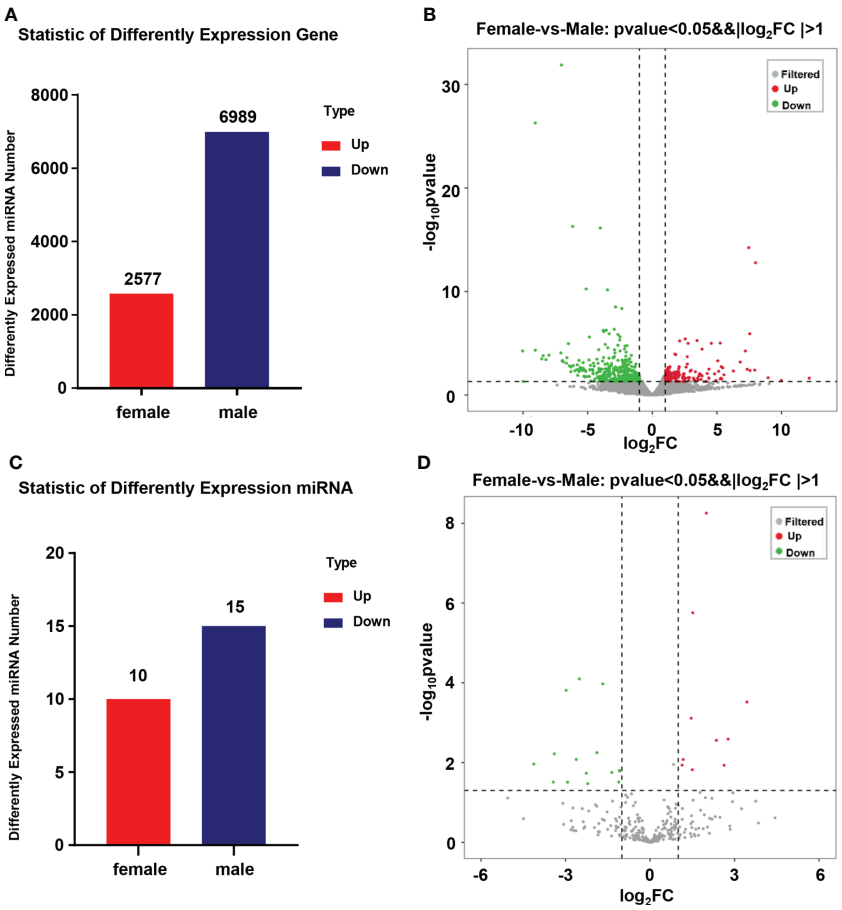

FIGURE 2
Statistics of DEGs and DEMs in the gonad of *Mytilus coruscus*. **(A)** and **(C)** Statistic of differently expressed mRNA and miRNA. **(B)** and **(D)** Volcanic map of male and female *Mytilus coruscus* differently expressed mRNA and miRNA in the gonad.

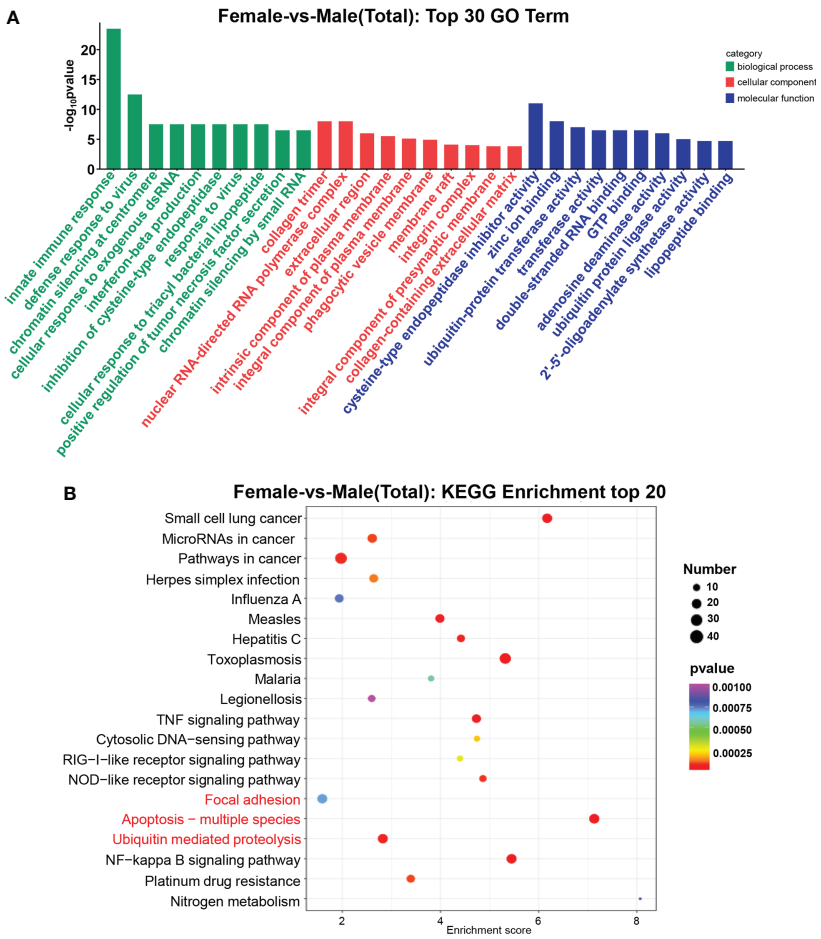

FIGURE 3
GO terms and KEGG pathway enrichments in DEGs. **(A)** Distribution of DE miRNAs among the top 30 GO terms. The GO terms are related to sex determination. **(B)** The top 20 enriched pathways in the gonad. Gonadal-related pathways are marked in red.

regulatory network exists in miRNAs and mRNAs (Figure 6). For example, lgi-miR-92 and mle-miR-92b-3p can target *dmrt4* and *vasa*.

Cloning and characterization of *Dmrt4*

The *dmrt4* sequence contains a 1050 bp open reading frame (ORF) encoding 349 amino acids (Figure S1). The results of multiple sequence alignment validated that *dmrt4* had high homology with other organisms, among which *Crassostrea gigas* was 63.9%, *Pinctada fucata* was 62.1%, and *Azumapecten farreri* was 60.1% (Figure S2).

Dmrt4 is regulated by miR-317

By screening the target genes with Targetscgan threshold > 50 and Miranda energy value < -10, it was found that the miR-317 of the differentially expressed gene completely matched the 3'UTR of *dmrt4*. Sequence analysis revealed that the binding site miR-317 predicted on 3'UTR of *dmrt4* was highly conserved in mussels (Figure 7A). To verify whether miR-317 and *dmrt4* had a targeting relationship, two vectors (miR-*dmrt4* 3'-UTR WT and miR-*dmrt4* 3'-UTR MT) were co-transfected with miR-317 mimics into HEK293 cells respectively. The results indicated that miR-317 significantly reduced luciferase activity reported by *dmrt4*-3'-UTR-WT while there have no significance in the negative control (pmirGLO+ miR-317 mimics) and blank control (pmirGLO+ NC). Furthermore, there has no inhibitory effect on the luciferase activity reported by miR-*dmrt4* RT 3'UTR MT (Figure 7B). The results strongly suggest that *dmrt4* is regulated by miR-317 in the gonad and potentially involves in the gonadal development of mussel.

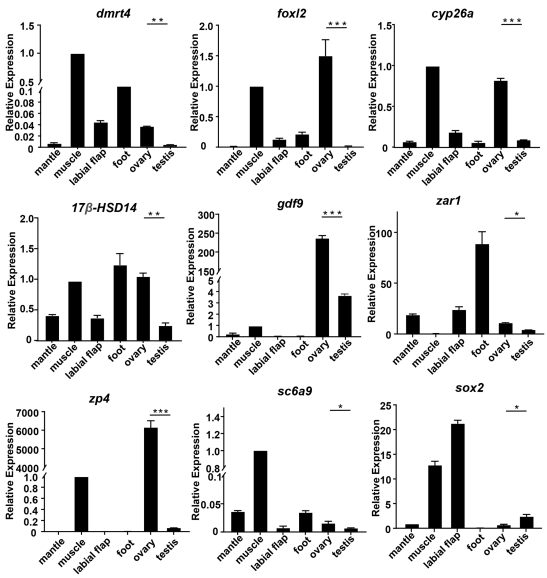

FIGURE 4
The relative expression of DEGs in mussels. The relative expression of each DEGs was determined by comparative CT (ΔΔCT) methods using 18s rRNA as the internal reference gene. *0.01 < p < 0.05; **0.001 < p < 0.01; ***p < 0.001.

Discussion

In the current investigation, high-throughput sequencing was performed in the gonad of mussels. After data was analyzed, the DEGs and DEMs were investigated in the ovary and testis of mussels. Additionally, the cloned *dmrt4*, which is differentially expressed in the gonad was predicted to be the target of miRNA-317. By luciferase reporter gene analysis, it

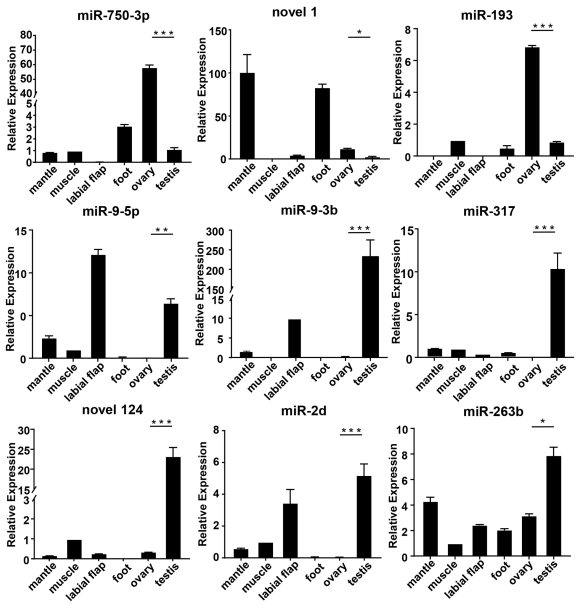

FIGURE 5
The relative expression of DEMs in mussels. The relative expression of each DEMs was determined by comparative CT (ΔΔCT) methods using 18s rRNA as the internal reference gene. *0.01 < p < 0.05; **0.001 < p < 0.01; ***p < 0.001.

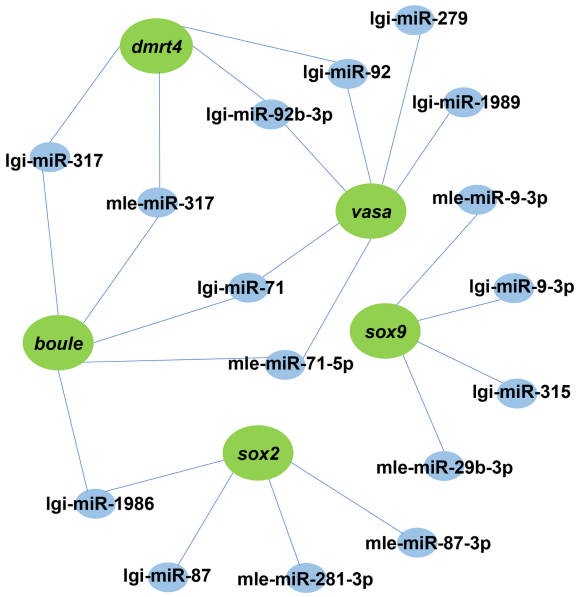

FIGURE 6
A proposed network of interactions between miRNAs and mRNAs. DEMs and DEGs regulatory networks are illustrated by Cytoscape. Blue indicates miRNA, green represents its target gene.

was confirmed that miRNA-317 indeed inhibited the expression of *dmrt4*.

In this study, specific genes and miRNAs of mussel gonad were identified by transcriptome sequencing analysis. 159,970 unigenes were identified, of which 9,566 were expressed differently in the gonad. Compare to these DEGs in the ovary, of which 2,575 DEGs were highly expressed, while 6,991 DEGs were in low expression. *Cyp26a* is an important gene in the cytochrome P450 family, which is expressed highly in the ovary of Yellow catfish (Xiong et al., 2015). *Foxl2*, a central player in the ovary, elaborates on the functional divergence in gibel carp. Furthermore, *Foxl2a-b* deficiency led to ovary development arrest or complete sex reversal, while complete disruption of *foxl2b-A* and *foxl2b-B* result in the depletion of germ cells in gibel carp (Gan et al., 2021). *Gdf9*, as the transforming growth factor beta (TGF-β) superfamily, regulates steroidogenesis in granulosa cells (Yu et al., 2020). *Sc6a9b* is a glycine transporter gene whose expression is higher in the ovary and affects ovarian development by affecting neurotransmitters (Li et al., 2016). Using *de novo* transcriptome analysis, it is revealed that *zp4* was differentially expressed in *Opsariichthys bidens* (Tang et al., 2022). *Zar1* plays a role in the early zebrafish ovary by inhibiting *ZP* gene translation (Miao et al., 2017). The above DEGs have similar biological roles during sex gonadal development in diverse species, implying that these DEGs might involve in the gonadal development of mussels.

The method of studying the mechanism of sex determination by DEMs has been widely used as the high-throughput sequencing technology develops. In this research, compared with the ovary and testis, a total of 25 DEMs were found, of which 11 DEMs were expressed highly and 14 DEMs were in low expression. A great number of miRNAs have been studied that involve gonadal development and other biological processes. Studies have shown that miR-9 is expressed highly in the ovary of Mud Crab (*Scylla paramamosain*) (Meng et al., 2018) and swimming crab (*Portunus trituberculatus)* (Waiho et al., 2019). Furthermore, miR-9 can negatively regulate the expression of the ERK pathway genes *Rap-1b* in the ovary of Mud Crab (*Scylla paramamosain*) (Zhou et al., 2020). In *Monopterus albus*, the relationship between *Foxl3* and miR-9 has been found, which could promote ovarian apoptosis and spermatogenesis (Gao et al., 2016). In Drosophila, miR-317 is one of the DEMs which are involved in early embryonic development and larval ovarian morphogenesis (Pushpavalli et al., 2014; Yang et al., 2016; Li et al., 2019). However, in our research, the results of qRT-PCR indicated that miR-9-3p, miR-9-5p, and miR-317 expressed highly in the testis. miR-193 involves the downregulation of c-kit protein, which regulates the development of ovarian follicles in Wistar rats. This is consistent with the expression pattern of miR-193 studied in *M. coruscus*.

By analyzing multiple amino acid sequences, we identified the *dmrt4* and identify the DM domain of this gene. It is a cysteine-rich DNA-binding domain shared by the *dmrt* gene family, characterized by the intertwining of CCHC and HCCC which is the binding site for Zn^{2+} (Naimi et al., 2009). In the *dmrt* gene family, genes with different names have different expression patterns in different species (Hong et al., 2007). Currently, members of the *dmrt* gene family *dmrt1* to *dmrt5*

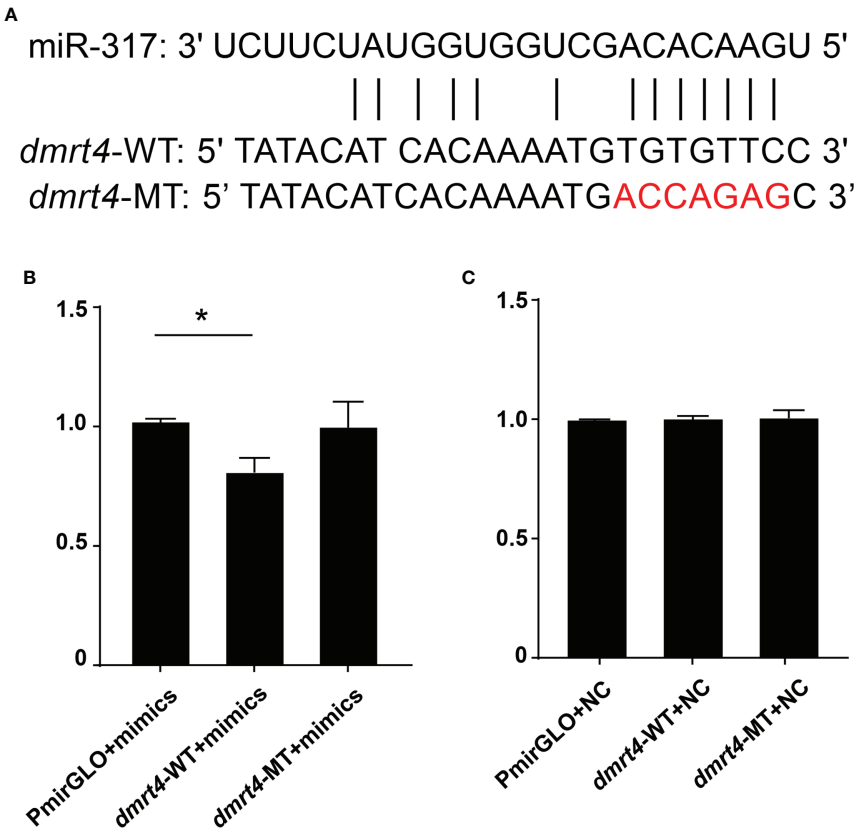

FIGURE 7
Dual-luciferase reporter assay of miR-317 and *dmrt4*. **(A)** Targeted sites of miR-317 and *dmrt4* 3'UTR, and mutated bases. **(B)** and **(C)** The relative luciferase activity in HEK293 cells. GraphPad Prism 7 draws a histogram. The means ± standard deviations of the three independent experiments are shown in the data. *p < 0.05.

have been cloned in a variety of fish particularly zebrafish, medaka, and tilapia (Winkler et al., 2004; Cao et al., 2007; Webster et al., 2017). A member of the *dmrt* gene family, specifically *dmrt4*, has expressed differently in various species, and these variations may be related to gonad developmental and other processes. In tilapia, the expression level of *dmo* (*dmrt4* in other species) is substantially higher in the ovary than in the testes, thus suggesting that *dmo* may be a key regulator of gonadal development (Cao et al., 2007).In *Oryzias latipes*, *dmrt4* is identified as maternal transcripts and expressed in gonads until the early larval stages (Kondo et al., 2002; Winkler et al., 2004). By conducting the qRT-PCR experiment, the pattern of the *dmrt4* was verified in different tissues of mussels. The result showed that *dmrt4* may participate in mussels' gonadal differentiation. Furthermore, the high expression of *dmrt4* in adductor and foot suggests that the gene has other biological functions besides gonadal differentiation. With the in-depth study of miRNAs, more and more miRNAs have been found to participate in regulation through the miRNA-mRNA regulatory network (Jing et al., 2014; Zhang et al., 2016). In this study, we focused on the relationship between miR-317 and *dmrt4*. The results of qRT-PCR indicated the opposite expression pattern of miR-317 and *dmrt4* in the ovary and testis and the results of bioinformatics analysis indicated that *dmrt4* may be the target gene of miR-317. Then, the targeting relationship between *dmrt4* and miR-317 was confirmed by a luciferase reporter assay. The above experimental results indicate that miR-317-*dmrt4* is essential for the gonadal development of mussels.

In conclusion, mRNA and miRNA from the ovary and testis of mussels were sequenced by transcriptome sequencing and then analyzed using bioinformatics. A total of 159,970 unigenes and 300 miRNAs were identified. qRT-PCR technology was performed to validate the accuracy of RNA-seq results, and also explore the expression patterns of DEGs and DEMs. Then, the structural network of mRNA-miRNA interaction was constructed. Moreover, Bioinformatics analysis and luciferase reporter analysis confirmed a targeting relationship between miR-317 and *dmrt4*. These results are of great significance to our further study of the gonad-related mechanism of mussels

and provide valuable data for future research on mussel gonadal development.

Data availability statement

The datasets presented in this study can be found in online repositories. The names of the repository/repositories and accession number(s) can be found below: https://figshare.com/, https://doi.org/10.6084/m9.figshare.20424369.v2.

Ethics statement

The animal study was reviewed and approved by Shanghai Ocean University Animal Care and Use Committee.

Author contributions

Methodology, Investigation Data Curation, Analysis, Writing: MW and JX. Visualization: LG and XL. Review and Editing: MJ and WW. Funding, Writing - Review and Editing: ML and JY. All authors have read and agreed to the published version of the manuscript.

Funding

This work was supported by the National Key R&D Program of China (2018YFD0901205), Program of Shanghai Academic Research Leader (20XD1421800), Key Special Project for Introduced Talents Team of Southern Marine Science and Engineering Guangdong Laboratory (Guangzhou) (GML2019 ZD0402) and Program for study on genetic resources, environment and strategy of mussel culture in coast of Gouqi Island offshore.

Conflict of interest

The authors declare that the research was conducted in the absence of any commercial or financial relationships that could be construed as a potential conflict of interest.

Publisher's note

All claims expressed in this article are solely those of the authors and do not necessarily represent those of their affiliated organizations, or those of the publisher, the editors and the reviewers. Any product that may be evaluated in this article, or claim that may be made by its manufacturer, is not guaranteed or endorsed by the publisher.

Supplementary material

The Supplementary Material for this article can be found online at: https://www.frontiersin.org/articles/10.3389/fmars.2022.1013857/full#supplementary-material

References

Ambros, V. (2004). The functions of animal microRNAs. *Nature*. 431(7006), 350–355. doi: 10.1038/nature02871

Bartel, D. P. (2007). MicroRNAs: Genomics, biogenesis, mechanism, and function. *Cell* 131 (4), 11–29. doi: 10.1016/s0092-8674(04)00045-5

Cao, J., Cao, Z., and Wu, T. (2007). Generation of antibodies against DMRT1 and DMRT4 of oreochromis aurea and analysis of their expression profile in *Oreochromis aurea* tissues. *J. Genet. Genomics* 34 (6), 497–509. doi: 10.1016/S1673-8527(07)60055-1

Gan, R. H., Wang, Y., Li, Z., Yu, Z. X., Li, X. Y., Tong, J. F., et al. (2021). Functional divergence of multiple duplicated Foxl2 homeologs and alleles in a recurrent polyploid fish. *Mol. Biol. Evol.* 38 (5), 1995–2013. doi: 10.1093/molbev/msab002

Gao, Y., Jia, D., Hu, Q., and Li, D. (2016). Foxl3, a target of miR-9, stimulates spermatogenesis in spermatogonia during natural sex change in *Monopterus albus*. *Endocrinology* 157 (11), 4388–4399. doi: 10.1210/en.2016-1256

He, L., Wang, Y. L., Li, Q., Yang, H. D., Duan, Z. L., and Wang, Q. (2015). Profiling microRNAs in the testis during sexual maturation stages in *Eriocheir sinensis*. *Anim. Reprod. Sci.* 162, 52–61. doi: 10.1016/j.anireprosci.2015.09.008

Hong, C.-S., Park, B.-Y., and Saint-Jeannet, J.-P. (2007). The function of dmrt genes in vertebrate development: It is not just about sex. *Dev. Biol.* 310 (1), 1–9. doi: 10.1016/j.ydbio.2007.07.035

Jing, J., Wu, J., Liu, W., Xiong, S., Ma, W., Zhang, J., et al. (2014). Sex-biased miRNAs in gonad and their potential roles for testis development in yellow catfish. *PloS One* 9 (9), e107946. doi: 10.1371/journal.pone.0107946

Kondo, M., Froschauer, A., Kitano, A., Nanda, I., Hornung, U., Volff, J. N., et al. (2002). Molecular cloning and characterization of DMRT genes from the medaka oryzias latipes and the platyfish xiphophorus maculatus. *Gene* 295 (2), 213–222. doi: 10.1016/S0378-1119(02)00692-3

Li, R., Huang, Y., Zhang, Q., Zhou, H., Jin, P., and Ma, F. (2019). The miR-317 functions as a negative regulator of toll immune response and influences drosophila survival. *Dev. Comp. Immunol.* 95, 19–27. doi: 10.1016/j.dci.2019.01.012

Li, X. Y., Mei, J., Ge, C. T., Liu, X. L., and Gui, J. F. (2022a). Sex determination mechanisms and sex control approaches in aquaculture animals. *Sci. China Life Sci.* 65 (6), 1091–1122. doi: 10.1007/s11427-021-2075-x

Li, Y., Zhang, L., Sun, Y., Ma, X., Wang, J., Li, R., et al. (2016). Transcriptome sequencing and comparative analysis of ovary and testis identifies potential key sex-related genes and pathways in scallop *Patinopecten yessoensis*. *Mar. Biotechnol. (NY)* 18 (4), 453–465. doi: 10.1007/s10126-016-9706-8

Li, Z., Zhou, M., Ruan, Y., Chen, X., Ren, C., Yang, H., et al. (2022b). Transcriptomic analysis reveals yolk accumulation mechanism from the hepatopancreas to ovary in the pacific white shrimp *Litopenaeus vannamei*. *Front. Mar. Sci.* 9. doi: 10.3389/fmars.2022.948105

Matsuda, M., Nagahama, Y., Shinomiya, A., Sato, T., Matsuda, C., Kobayashi, T., et al. (2002). DMY is a y-specific DM-domain gene required for male development in the medaka fish. *Nature* 417 (6888), 559–563. doi: 10.1038/nature751

Meng, X., Zhang, X., Li, J., and Liu, P. (2018). Identification and comparative profiling of ovarian and testicular microRNAs in the swimming crab *Portunus trituberculatus*. *Gene* 640, 6–13. doi: 10.1016/j.gene.2017.10.026

Miao, L., Yuan, Y., Cheng, F., Fang, J., Zhou, F., Ma, W., et al. (2017). Translation repression by maternal RNA binding protein Zar1 is essential for early oogenesis in zebrafish. *Development* 144 (1), 128–138. doi: 10.1242/dev.144642

Mitchell, P. S., Parkin, R. K., Kroh, E. M., Fritz, B. R., Wyman, S. K., Pogosova-Agadjanyan, E. L., et al. (2008). Circulating microRNAs as stable blood-based markers for cancer detection. *Proc. Natl. Acad. Sci. United States America* 105 (30), 10513–10518. doi: 10.1073/pnas.0804549105

Naimi, A., Martinez, A. S., Specq, M. L., Mrac, A., Diss, B., Mathieu, M., et al. (2009). Identification and expression of a factor of the DM family in the oyster *Crassostrea gigas*. *Comp. Biochem. Physiol. A Mol. Integr. Physiol.* 152 (2), 189–196. doi: 10.1016/j.cbpa.2008.09.019

Ning, J., Cao, W., Lu, X., Chen, M., Liu, B., and Wang, C. (2021). Identification and functional analysis of a sex-biased transcriptional factor Foxl2 in the bay scallop argopecten irradians irradians. *Comp. Biochem. Physiol. B Biochem. Mol. Biol.* 256, 110638. doi: 10.1016/j.cbpb.2021.110638

Nishimura, T., Sato, T., Yamamoto, Y., Watakabe, I., Ohkawa, Y., Suyama, M., et al. (2015). Sex determination. foxl3 is a germ cell-intrinsic factor involved in sperm-egg fate decision in medaka. *Science* 349 (6245), 328–331. doi: 10.1126/science.aaa2657

Pushpavalli, S. N., Sarkar, A., Bag, I., Hunt, C. R., Ramaiah, M. J., Pandita, T. K., et al. (2014). Argonaute-1 functions as a mitotic regulator by controlling cyclin b during drosophila early embryogenesis. *FASEB J.* 28 (2), 655–666. doi: 10.1096/fj.13-231167

Qiu, W., Zhu, Y., Wu, Y., Yuan, C., Chen, K., and Li, M. (2018). Identification and expression analysis of microRNAs in medaka gonads. *Gene* 646, 210–216. doi: 10.1016/j.gene.2017.12.062

Saliminejad, K., Khorram Khorshid, H. R., Soleymani Fard, S., and Ghaffari, S. H. (2019). An overview of microRNAs: Biology, functions, therapeutics, and analysis methods. *J. Cell Physiol.* 234 (5), 5451–5465. doi: 10.1002/jcp.27486

Shi, J., Hong, Y., Sheng, J., Peng, K., and Wang, J. (2015). *De novo* transcriptome sequencing to identify the sex-determination genes in *Hyriopsis schlegelii*. *Biosci. Biotechnol. Biochem.* 79 (8), 1257–1265. doi: 10.1080/09168451.2015.1025690

Shi, Y., Liu, W., and He, M. (2018). Proteome and transcriptome analysis of ovary, intersex gonads, and testis reveals potential key sex Reversal/Differentiation genes and mechanism in scallop chlamys nobilis. *Mar. Biotechnol. (NY)* 20 (2), 220–245. doi: 10.1007/s10126-018-9800-1

Sun, L. L., Zhong, Y., Qiu, W. W., Guo, J., Gui, L., and Li, M. Y. (2020). MiR-26 regulates *ddx3x* expression in medaka (Oryzias latipes) gonads. *Comp. Biochem. Physiol. B-Biochemistry Mol. Biol.* 246-247, 110456. doi: 10.1016/j.cbpb.2020.110456

Sutton, E., Hughes, J., White, S., Sekido, R., Tan, J., Arboleda, V., et al. (2011). Identification of SOX3 as an XX male sex reversal gene in mice and humans. *J. Clin. Invest.* 121 (1), 328–341. doi: 10.1172/JCI42580

Tang, R., Zhu, Y., Gan, W., Zhang, Y., Yao, Z., Ren, J., et al. (2022). *De novo* transcriptome analysis of gonads reveals the sex-associated genes in Chinese hook snout carp *Opsariichthys bidens*. *Aquaculture Rep.* 23, 101068. doi: 10.1016/j.aqrep.2022.101068

Waiho, K., Fazhan, H., Zhang, Y., Zhang, Y., Li, S., Zheng, H., et al. (2019). Gonadal microRNA expression profiles and their potential role in sex differentiation and gonadal maturation of mud crab *Scylla paramamosain*. *Mar. Biotechnol. (NY)* 21 (3), 320–334. doi: 10.1007/s10126-019-09882-1

Webster, K. A., Schach, U., Ordaz, A., Steinfeld, J. S., Draper, B. W., and Siegfried, K. R. (2017). *Dmrt1* is necessary for male sexual development in zebrafish. *Dev. Biol.* 422 (1), 33–46. doi: 10.1016/j.ydbio.2016.12.008

Winkler, C., Hornung, U., Kondo, M., Neuner, C., Duschl, J., Shima, A., et al. (2004). Developmentally regulated and non-sex-specific expression of autosomal dmrt genes in embryos of the medaka fish (*Oryzias latipes*). *Mech. Dev.* 121 (7-8), 997–1005. doi: 10.1016/j.mod.2004.03.018

Xia, J., Liu, D., Zhou, W. Z., Yi, S. K., Wang, X. H., Li, B. L., et al. (2022). Comparative transcriptome analysis of brain and gonad reveals reproduction-related miRNAs in the giant prawn, *Macrobrachium rosenbergii*. *Front. Genet.* 2331. doi: 10.3389/fgene.2022.990677

Xiong, S., Jing, J., Wu, J., Ma, W., Dawar, F. U., Mei, J., et al. (2015). Characterization and sexual dimorphic expression of cytochrome P450 genes in the hypothalamic-pituitary-gonad axis of yellow catfish. *Gen. Comp. Endocrinol.* 216, 90–97. doi: 10.1016/j.ygcen.2015.04.015

Yang, J. L., Feng, D. D., Liu, J., Xu, J. K., Chen, K., Li, Y. F., et al. (2021). Chromosome-level genome assembly of the hard-shelled mussel *Mytilus coruscus*, a widely distributed species from the temperate areas of East Asia. *Gigascience* 10 (4), giab024. doi: 10.1093/gigascience/giab024

Yang, H., Li, M., Hu, X., Xin, T., Zhang, S., Zhao, G., et al. (2016). MicroRNA-dependent roles of drosha and pasha in the drosophila larval ovary morphogenesis. *Dev. Biol.* 416 (2), 312–323. doi: 10.1016/j.ydbio.2016.06.026

Yang, J. L., Li, X., Liang, X., Bao, W. Y., Shen, H. D., and Li, J. L. (2014). Effects of natural biofilms on settlement of plantigrades of the mussel *Mytilus coruscus*. *Aquaculture* 424, 228–233. doi: 10.1016/j.aquaculture.2014.01.007

Yang, J. L., Li, S. H., Li, Y. F., Liu, Z. W., Liang, X., Bao, W. Y., et al. (2013a). Effects of neuroactive compounds, ions and organic solvents on larval metamorphosis of the mussel *Mytilus coruscus*. *Aquaculture* 396, 106–112. doi: 10.1016/j.aquaculture.2013.02.039

Yang, J. L., Shen, P. J., Liang, X., Li, Y. F., Bao, W. Y., and Li, J. L. (2013b). Larval settlement and metamorphosis of the mussel *Mytilus coruscus* in response to monospecific bacterial biofilms. *Biofouling* 29 (3), 247–259. doi: 10.1080/08927014.2013.764412

Ye, Y. Y., Li, J. J., Wu, C. W., Xu, M. Y., and Guo, B. Y. (2012). Genetic analysis of mussel (*Mytilus coruscus*) populations on the coast of East China Sea revealed by ISSR-PCR markers. *Biochem. Systematics Ecol.* 45, 1–6. doi: 10.1016/j.bse.2012.07.022

Yu, H., Wang, Y., Wang, M., Liu, Y., Cheng, J., and Zhang, Q. (2020). Growth differentiation factor 9 (gdf9) and bone morphogenetic protein 15 (bmp15) are potential intraovarian regulators of steroidogenesis in Japanese flounder (*Paralichthys olivaceus*). *Gen. Comp. Endocrinol.* 297, 113547. doi: 10.1016/j.ygcen.2020.113547

Zhang, N., Xu, F., and Guo, X. (2014). Genomic analysis of the pacific oyster (*Crassostrea gigas*) reveals possible conservation of vertebrate sex determination in a mollusc. *G3 (Bethesda)* 4 (11), 2207–2217. doi: 10.1534/g3.114.013904

Zhang, X., Yuan, L., Li, L., Jiang, H., and Chen, J. (2016). Conservation, sex-biased expression and functional annotation of microRNAs in the gonad of amur sturgeon (*Acipenser schrenckii*). *Comp. Biochem. Physiol. Part D Genomics Proteomics* 18, 54–61. doi: 10.1016/j.cbd.2016.04.001

Zhang, Y., Zhong, Y., Guo, S. Y., Zhu, Y. F., Guo, J., Fu, Y. S., et al. (2021). CircRNA profiling reveals circ880 functions as miR-375-3p sponge in medaka gonads. *Comp. Biochem. Physiol. D-Genomics Proteomics* 38, 100797. doi: 10.1016/j.cbd.2021.100797

Zhou, M., Jia, X., Wan, H., Wang, S., Zhang, X., Zhang, Z., et al. (2020). miR-9 and miR-263 regulate the key genes of the ERK pathway in the ovary of mud crab *Scylla paramamosain*. *Mar. Biotechnol. (NY)* 22 (4), 594–606. doi: 10.1007/s10126-020-09981-4

frontiers | Frontiers in Marine Science

TYPE Original Research
PUBLISHED 10 October 2022
DOI 10.3389/fmars.2022.1040466

OPEN ACCESS

EDITED BY
Zhiguo Dong,
Jiangsu Ocean University, China

REVIEWED BY
Liqiang Zhao,
Guangdong Ocean University, China
Pengzhi Qi,
Zhejiang Ocean University, China

*CORRESPONDENCE
Gao-Hai Zheng
yixiaolou@163.com
Yi-Feng Li
yifengli@shou.edu.cn

†These authors have contributed equally to this work

SPECIALTY SECTION
This article was submitted to Marine Biology, a section of the journal Frontiers in Marine Science

RECEIVED 09 September 2022
ACCEPTED 27 September 2022
PUBLISHED 10 October 2022

CITATION
Zheng Y, Yang Y-M, Xu Y-F, Wang Y-Q, Shi X, Zheng G-H and Li Y-F (2022) Starvation shrinks the mussel foot secretory glands and impairs the byssal attachment.
Front. Mar. Sci. 9:1040466.
doi: 10.3389/fmars.2022.1040466

Starvation shrinks the mussel foot secretory glands and impairs the byssal attachment

Yi Zheng[1,2†], Yue-Ming Yang[1,2†], Yue-Feng Xu[1,2†], Yu-Qing Wang[1,2], Xue Shi[1,2], Gao-Hai Zheng[3*] and Yi-Feng Li[1,2*]

[1]International Research Center for Marine Biosciences, Ministry of Science and Technology, Shanghai Ocean University, Shanghai, China, [2]Key Laboratory of Exploration and Utilization of Aquatic Genetic Resources, Ministry of Education, Shanghai Ocean University, Shanghai, China, [3]Bureau of Agriculture and Rural Affairs of Sanmen County, Taizhou, China

Mussel is an economically and ecologically important species widely distributed throughout the world. The mussel adheres to the attachment substrate by secreting byssus external to the body. Various environmental and biological factors influence the process of byssus secretion, and the present study investigated the effect of starvation on byssal secretion in the hard-shelled mussel *Mytilus coruscus*. Histological changes in mussel foot secretory glands and gene expression of mussel foot proteins were also determined. The experimental setup consisted of starvation treatments for 7, 14 and 21 days, and the control groups. The results showed that the number of produced byssus was higher in the starvation group compared to the control (CTR) group, and the starvation group had a significantly higher of byssal shedding number from 6 days of starvation treatment onwards ($p < 0.05$). The byssal thread diameter was significantly reduced in all starvation treatment groups ($p < 0.05$). However, starvation treatment had no effect on the length of the byssal thread ($p > 0.05$). After 21 days of starvation treatment, the byssal thread volume was significantly lower than that of the CTR group ($p < 0.05$). A significant decrease in the breaking force of the byssal thread was observed after 14 and 21 days of starvation treatment ($p < 0.05$), along with an upward shift in the breakpoints. Starvation treatment significantly reduced the percentage of foot secretory glands area to total tissue ($p < 0.05$). The expression of the mussel foot protein genes (*Mcfp-1P* and *Mcfp-1T*) was significantly up-regulated at 7 days of starvation treatment ($p < 0.05$). These findings reveal that starvation weakens byssal thread performance by influencing mussel foot secretory glands, which increases the dislodgment risks of suspended-cultured mussels.

KEYWORDS

starvation, byssal threads, mussel foot secretory glands, mussel foot protein, *Mytilus coruscus*

Introduction

As benthic organisms, mytilid mussels are ecologically and economically important species in the coastal marine food webs (Fitzgerald-Dehoog et al., 2012). Mussels generally aggregate on the sea floor and rocky shore mussel beds, forming dense mussel beds, and are thought to support a diverse community structure. (Buschbaum et al., 2009). Mussels are intermediate between primary producers and higher consumers in the marine ecosystem, transferring energy and nutrients to higher levels of the food web (Harris and Carrington, 2020). In addition, mussels have been extensively farmed and represent a key economic species, providing high-quality protein and a wide range of vitamins and minerals (Buck et al., 2010; Suplicy, 2020). According to data from FAO, world aquaculture production of mussels reached 2.1 million tons (worth $4.5 billion) in 2018 (FAO, 2020).

Marine mussels produce the byssal threads that act as anchors, allowing them to be firmly attached to ropes or other natural substrates (O'Donnell et al., 2013). The mussel foot is comprised of secretory glands in which the thread proteins are stored (Demartini et al., 2017). Foot glands secrete a variety of mussel foot proteins (mfps) into the foot groove by exocrine secretion and solidify *in vitro* after a series of reactions to form stiff, stretchable threads (Pujol, 1967; Priemel et al., 2017). Generally, a byssal thread can be subdivided into four distinct regions: the stem, the plaque, and the proximal and distal portions of the thread (Harrington and Waite, 2007). The stem attaches the thread to the mussel tissue, with a corrugated proximal portion near the stem and a smoother distal portion (Lucas et al., 2002; Harrington and Waite, 2007). The plaque contains a series of adhesive foot proteins enriched in 3,4-dihydroxyphenyl-L-alanine (DOPA) that ensure the ability to attach to the substrate (Lin et al., 2007).

The adhesion strength of mussels depends on the number and the mechanical performance of the byssal threads (Newcomb et al., 2019). The physiological condition of mussels is influenced by biological and environmental factors that can alter the production of byssal threads and the strength of attachment to the substratum (Lachance et al., 2008; Carrington et al., 2015). Previous studies have demonstrated that changes in seawater temperature, pH, current, food availability and hypoxia can affect the secretion of byssus (Babarro et al., 2008; Fitzgerald-Dehoog et al., 2012; Garner and Litvaitis, 2013; O'Donnell et al., 2013; Sui et al., 2015; Clements et al., 2018; George and Carrington, 2018). The production of byssal threads costs 2-8%, or even up to 47% of the daily mussel's energy budget (Roberts et al., 2021). Food supply determines the amount of energy budget available to organisms, reflecting the partitioning energy among reproduction, growth and maintenance functions (Sarà et al., 2014). Food availability plays an important role in buffering the energy expenditure caused by byssus secretion (Carrington et al., 2015). Energy balance can be disturbed when less food is available, which may result in less energy being allocated to mussel byssus secretion (Clarke, 1999; Babarro et al., 2008; Shang et al., 2021). Reduced feeding or starvation can compromise the energy balance, resulting in less energy allocation to mussel byssus secretion (Clarke, 1999; Babarro et al., 2008). Mussels located close to the rope are within the mussel aggregation layer and may not have access to enough food or endure starvation during periods when algae levels are low.

The hard-shelled mussel (*Mytilus coruscus*) is a major cultured bivalve in China. In recent years, the sea area dedicated to the aquaculture of *M. coruscus* has expanded rapidly on the coast of Shengsi Island. Increased cultured mussel density impedes the food available to mussels. It leads to a reduction in the somatic mass of individual mussels and elevated mussel dislodgment risk. The present study aims to explore the effects of starvation on the byssus secretion of the mussel *M. coruscus*. We observed byssus secretion and shedding number and measured byssal breaking force, byssal thread length, and diameter. Changes in foot glands area and expression levels of byssus protein genes were determined. The evidence obtained in this study can reveal the effect of starvation stress on mussel byssus secretion, providing a theoretical basis and data support for the study of mussel aquaculture and benthic ecology.

Material and methods

Experimental animals

Adult mussels (*M. coruscus*) (shell length: 9.1 ± 0.4 cm) were obtained in November 2020 from Gouqi Island (30°73′N; 122°77′ E), Zhoushan, Zhejiang Province, China. Upon arrival in the laboratory, the mussels' surface attachments were removed, and the byssus was cut off along the edge of the shell, and then the mussels were acclimated in a polycarbonate tank with 10 L of seawater at a salinity of 30 for two weeks at 21°C. The seawater was changed every day. The mussels were fed with a mixture of microalgae *Platymonas helgolandica* var. *tsingtaoensis* and *Isochrysis zhanjiangensis* twice a day at concentrations of 5×10^6 cells/mL and 1.5×10^6 cells/mL, respectively. All procedures for mussel acclimation and experimentation were authorized by the Animal Ethics committee of Shanghai Ocean University with the registration number of SHOU-DW-2021-011.

Experimental design

The experimental setup consisted of a starvation treatment for 21 days and a control group (CTR). Additional starvation treatment groups for 7 and 14 days were carried out, which were

only for mussel foot sampling. The starvation-treated mussels were kept without feeding. The control mussels were fed as described above. Twenty-eight mussels from each treatment were evenly distributed in four polycarbonate tanks containing 10 L of seawater, with seven mussels in each tank. The seawater was changed daily during the experiment. The numbers of byssus secretion and shedding were recorded daily. At the end of the experiment, byssus and foot samples were collected.

Measurement of byssal threads parameters

The parameters of byssal threads were determined as previously described (Li et al., 2020). Briefly, the diameter of the byssal thread was measured with an ocular micrometer under a stereo microscope (SZX2, Olympus, Japan). The proximal, intermediate, and distal plaques (near the adhesive plaque) of the byssus were used to calculate the mean diameter of a byssal thread. Byssal thread length was determined from the proximal region of the thread to the adhesive plaque with a vernier caliper. The volume of the byssal thread was calculated on the assumption that the byssal thread is a cylindrical tube using the formula: $V = \pi r^2 \times l$, where r = byssal thread radius and l = byssal thread length. A digital force gauge installed on a testing frame (HLB, Handpi, China) was used to measure the byssal breaking force. The thread was expanded at a rate of 10 mm min^{-1} until it broke, and the breaking force were recorded. The breaking point of each thread was also determined based on measuring the length of two threads that came from a whole thread after the breaking force measurement. The value of the byssal breaking force was calculated based on a total of 405, 512 and 509 measurements from 7, 14 and 21 days of treatment groups and presented in Newton (N).

Histology of the mussel foot

The foot samples of *M. coruscus* were fixed in Bouin's Fixative (Phygene Biotechnology Co., Ltd, Fuzhou, China) for 12 h at 4°C. The fixed samples were then cleaned with 30%, 50% and 70% ethanol for 30, 20 and 20 minutes, respectively. Samples were dehydrated in a graduated series of ethanol (50%, 70%, 90% and 100% for 45 min, respectively). After dehydration, the samples were cleaned and waxed with the steps of alcohol and xylene (1:1) for 40 min, xylene twice for 15 min each, xylene and paraffin wax (1:1) for 50 min at 60°C and paraffin wax for 3 h at 60°C, followed by embedding in paraffin blocks. Paraffin-embedded samples were cut at a thickness of 5 μm on a microtome (Leica, RM2245, Germany). For the histological analysis, the sections were stained with Harris hematoxylin and eosin (BBI, Shanghai, China), dipped for 5 min in 95% ethanol, two times 5 min in 100% ethanol, and two times 5 min in xylene. Finally, the sections were covered with neutral balsam (Solarbio, Beijing, China), and photographed using the Axio Imager M2 microscope (Zeiss, Germany). The foot glands area was determined using FIJI software. For each treatment group, nine replicates were performed.

Quantitative real-time PCR analysis

Total RNA was extracted from the mussel foot samples using RNAiso Plus reagent and following the manufacturer's instructions (Takara, Japan). The concentration of the extracted total RNA was assessed using a NanoDrop spectrophotometer (ND-2000, NanoDrop Technologies, USA). A 1% agarose gel was used to assess the quality of total RNA by electrophoresis. A volume of 10 μL of the mixture containing 1 μL gDNA Eraser, 500 ng total RNA, 2 μL 5× gDNA Eraser buffer and RNase-free dH2O was used to eliminate genomic DNA with the PrimeScript™ RT kit (Takara, China). For cDNA synthesis, 10 μL volume of the mixture was added to a final volume of 20 μL containing 4 μL 5× PrimeScript Buffer 2, 1 μL RT Primer Mix, 1 μL PrimeScript RT Enzyme Mix I, and 4 μL RNase Free dH_2O. The reactions were performed at 37°C for 15 min and followed by 5 sec at 87°C.

Three genes (*Mcfp-1P*, *Mcfp-1T* and *Mccol2*) implicated in byssus formation were analyzed by qPCR. The elongation factor 1α (*EF-1α*) of *M. coruscus* was used as the reference gene for normalization. Primer 6.0 software was utilized to design specific primers (Table 1). qPCR analysis was performed with four biological replicates/treatment in 96 multi-well plates using a LightCycler 960 (Roche). PCR amplicons were sequenced to confirm their identity and were used as standards ranging from 10^7 - 10^1 DNA copies of the target amplicon for absolute quantification. qPCR reaction contained 1 μL cDNA, 0.3 μL of each of the primers (10 μM), 5 μL of 2 × FastStart Essential DNA Green Master (Roche) and sigma water to reach a final reaction volume of 10 μL with the following amplification protocol: 10 min at 95°C followed by 45 cycles of 10 s at 95°C and 10 s at 57°C. Melting curve analysis verified a single reaction peak and the standard curve confirmed the amplification efficiency of the primers (90%-110%). As previously mentioned, absolute quantification was used to calculate the relative mRNA expression (Li et al., 2019a).

Statistical analysis

JMP™ software (Version 10.0.0) was used to analyze the data. The Shapiro-Wilk and O'Brien tests were first used to determine the normality and homogeneity of all data. The Student's *t*-test was performed when data conformed to normal distribution and homogeneity. Alternatively, the data were analyzed by the Wilcoxon test when data do not meet the requirements of normality and homogeneity. Differences were considered significant at $p < 0.05$.

10.3389/fmars.2022.1040466

TABLE 1 Primers used to qRT-PCR expression analysis of 3 selected genes and EF-1α.

Target	Primer	Sequence (5'-3')	Amplicon size (bp)	Efficiency (%)	r^2
Mcfp-1P	FW	CAAATTAAATCTGTGCCTCCTG	134	90	1.00
	RV	GTGAACCGGGTAATGTCTTGTA			
Mcfp-1T	FW	ACAGAGCAAATGCTGAGAGCA	155	90	1.00
	RV	GCCAGAGAAGGATGAGAACGA			
Mccol2	FW	TAGTATATCCGCGAACCACG	148	91	0.99
	RV	TAATTTTATCAGCGCCCCCT			
EF-1α	FW	CACCACGAGTCTCTCCCTGA	105	90	1.00
	RV	GCTGTCACCACAGACCATTCC			

Results

Byssal threads secretion and byssal shedding

The results of the secretion and shedding of byssal threads for 21 days of starvation are shown in Figure 1. A significantly higher number of byssal threads secretion was observed in the starvation group than in the control group from day 3 to day 8 ($p < 0.05$, Figure 1A). The shedding number of byssal threads significantly increased in the starvation group compared to the CTR group after six days of treatment ($p < 0.05$, Figure 1B).

Byssal thread's mechanical performance

After 7, 14 and 21 days of starvation treatment, byssal thread diameter was significantly reduced in the starvation group compared to the CTR group ($p < 0.05$, Figure 2A). However, starvation treatment had no effect on byssal thread length ($p > 0.05$, Figure 2B). The volume of the byssal thread was significantly lower than the CTR group after 21 days of starvation treatment ($p < 0.05$, Figure 2C).

The breaking force of the byssal thread significantly decreased in 14 and 21 days of treatment groups compared to the CTR group ($p < 0.05$, Figure 3A). The failure location of threads was identified to understand the weakest part in the byssal threads (Figure 3B). The breakpoints of the byssal threads mainly occurred in the middle of the thread, representing 54.4% (7d, CTR), 54.11% (7d, starvation), 40.13% (14d, CTR), 41.04% (14d, starvation), 45.53% (21d, CTR) and 50.41% (21d, starvation) (Figure 3B). Increased breakpoints in the upper part of the thread were observed on 14 and 21 days of starvation treatment compared to the CTR group (Figure 3B).

Histology of the mussel foot secretory glands

The effect of starvation on the foot tissues of *M. coruscus* is shown in Figure 4. The foot was oval in the transverse section. A foot groove (fg) was situated in the middle of the ventral surface (Figure 4). The epidermis of the foot had "creases" that were depressed inward (Figure 4). The foot glands were located close to the foot groove with purplish red color (Figure 4). The muscles of the mussel foot were located at the periphery of the glands, away from the foot groove side, and the whole muscles were pink in color (Figure 4). The proportion of foot glands area versus total foot tissue was analyzed and the results show that starvation treatment for 7, 14 and 21 days significantly reduced the percentage of foot secretory glands area relative to CTR groups ($p < 0.05$, Figure 4H).

Mfps gene expression profile

As shown in Figure 5, the gene expression of *Mcfp-1P* and *Mcfp-1T* in foot tissue was affected by starvation stress. The transcript abundance of *Mcfp-1P* and *Mcfp-1T* was only significantly up-regulated after 7 days of starvation ($p < 0.05$, Figures 5A, B), while no effect was observed on 14 and 21 days ($p > 0.05$, Figures 5A, B). There was no significant difference in *Mccol2* transcript abundance in the starvation group relative to the CTR group ($p > 0.05$, Figure 5C).

Discussion

The secretion of the byssus is a biologically and chemically process by which the mussel anchors itself to the substrate to resist the impact of enormous waves and predators (Carrington, 2002; Li et al., 2020). Food limitation constrains the energy available to mussels, which may increase the risk of promoting mussel detachment (Carrington et al., 2015). The results of this study show that starvation affects byssal production (including byssus number, diameter, and the cumulative byssal thread volume), the number of byssus shedding number, and the mechanical performance of byssal threads (breaking force and failure location). Furthermore, we showed that starvation alters the mussel foot secretory glands area and the expression level of foot protein genes.

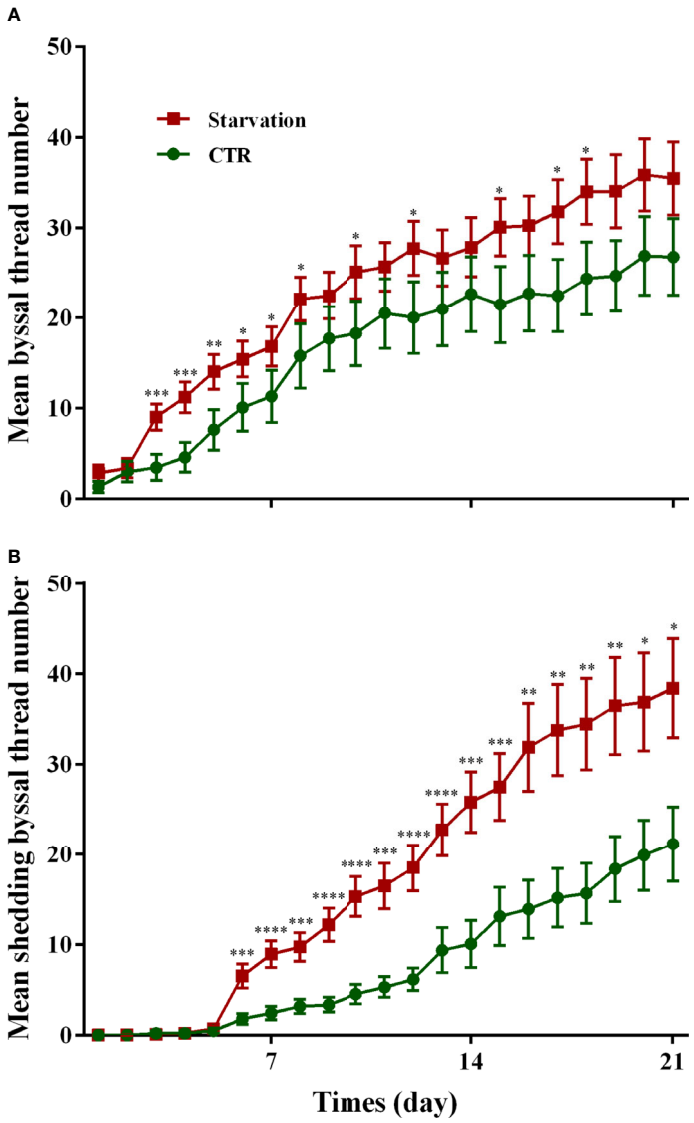

FIGURE 1
Effects of 21 days of starvation on the **(A)** secreted byssal thread number and **(B)** byssal shedding number in *M. coruscus*. CTR: control group. Asterisks indicate significant differences between starvation groups and CTR groups. *$p < 0.05$; **$p < 0.01$; ***$p < 0.001$; ****$p < 0.0001$.

Byssal threads are the fibrous holdfast for mussel attachment, and unfavorable conditions such as reduced wind-driven water movement in summer restrict food delivery to the innermost layers of mussel aggregations, resulting in weaker attachment and promoting detachment (Carrington et al., 2015). In the present study, we found that starvation-treated mussels at 21°C did not show a reduction of byssus secretion number, and even the number of byssus was observed to exceed that of the CTR group. This result is contrary to previous results showing that hard-shelled mussels (*M. coruscus*) starved for 21 days at 26°C reduced byssus production (Shang et al., 2021). This discrepancy in byssus secretion might be attributed to the variation of temperature and the experimental body size of mussels. Temperature is one of the most critical environmental factors affecting mussel physiology, controlling many biological and chemical processes (Zippay and Helmuth, 2012). Moreover, high temperatures inhibited mussel byssus production (Young, 1985; Newcomb et al., 2019; Li et al., 2020). In addition, the experimental body size of mussels could be another reason for the contrary results. The mussels with a shell length of 9.1 ± 0.4 cm were used in this study, which was larger than the mussels (shell length of 7.5 ± 0.2 cm) used in a previous study (Shang et al., 2021). Larger mussels may have more energy reserves to ensure their byssus production under starvation (Babarro et al., 2008).

10.3389/fmars.2022.1040466

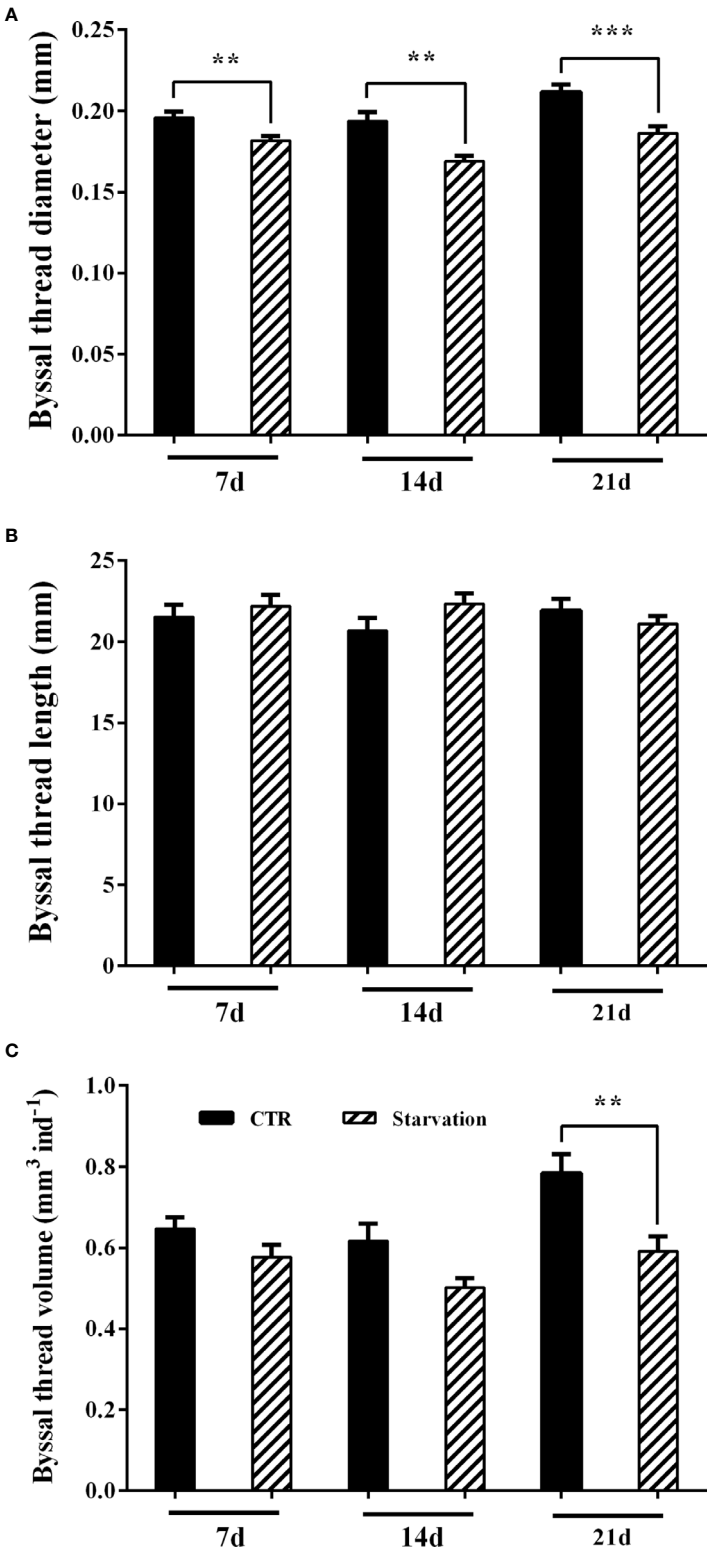

FIGURE 2
Effects of 21 days of starvation on **(A)** byssal thread diameter, **(B)** byssal thread length and **(C)** the cumulative byssal thread volume in *M. coruscus*. Asterisks indicate significant differences between starvation groups and CTR groups. $^{**}p < 0.01$; $^{***}p < 0.001$.

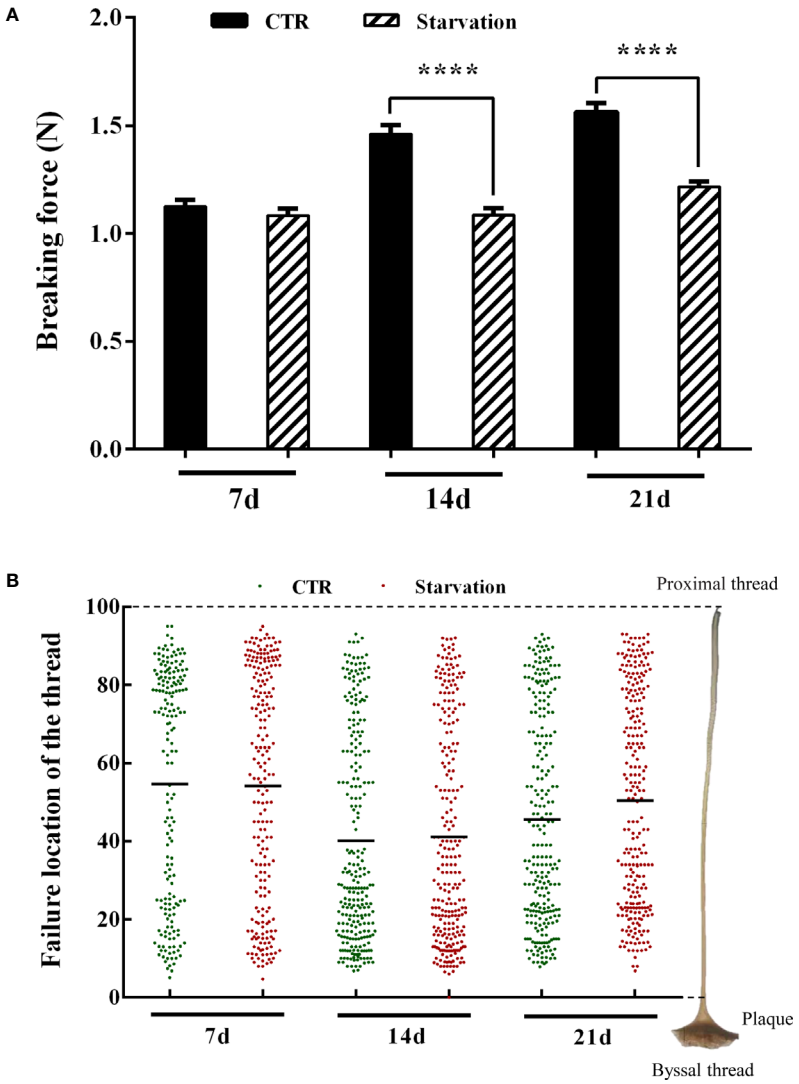

FIGURE 3
Effects of 21 days of starvation on **(A)** breaking force of the byssal thread and **(B)** failure location in the mussel *M. coruscus*. Each green dot and the red dot represent a thread breaking force test measurement. Each green dot and the red dot on the Y-axis corresponds to the breakpoints of a single byssal thread on the right side of the diagram. The value 100 on the Y-axis represents the proximal region of the thread, and the value 0 on Y-axis represents the distal region of the thread (close to the plaque). The amount of byssal breaking force measurements was as follows: 184 (7d, CTR), 221 (7d, starvation), 256 (14d, CTR), 256 (14d, starvation), 253 (21d, CTR) and 256 (21d, starvation). Asterisks indicate significant differences between starvation groups and CTR groups. ****$p < 0.0001$.

Mussels undergo migration under unfavorable conditions, which can be reflected in the secretion and shedding of byssus (Côté and Jelnikar, 1999; Carrington et al., 2015; Li et al., 2015). Passive migration can be seen as a form of self-protection for mussels when they encounter unfavorable environments, dislodging themselves from the substrate to find suitable habitats (Hunt and Scheibling, 2001; Duchini et al., 2015; Iwasaki, 2015). Hard-shelled mussels (*M. coruscus*) are more prone to shedding byssus under high temperatures, low pH, and predator presence (Li et al., 2015; Li et al., 2020). In the present study, we found that starvation led to a significant increase in the number of byssus shedding. This could be an adaptive response to passive migration in a hostile environment (food scarcity), where mussels may release themselves from attachments and move.

Unfavorable environmental stresses may compromise the integrity of the byssal thread structure and ultimately weaken the attachment (Carrington et al., 2015; Li et al., 2017; Clements et al., 2018; Li et al., 2020). In this study, the starvation treatment decreased the byssal thread diameter and byssal breaking force, which undermined the byssal attachment strength in starved mussels. These results were consistent with a previous study

10.3389/fmars.2022.1040466

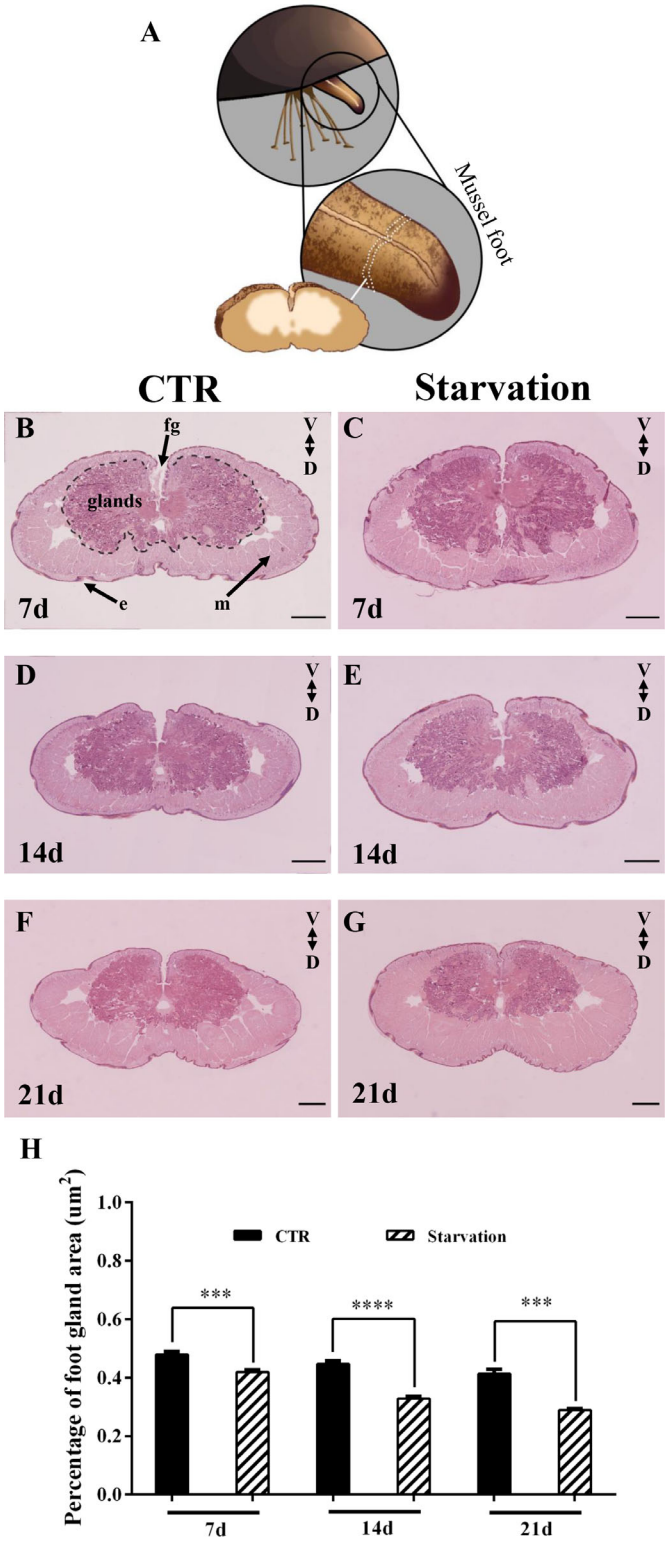

FIGURE 4
The foot of *M. coruscus* stained with hematoxylin and eosin (H&E). **(A)** A schematic depiction of foot section sampling. **(B)** 7d CTR, **(C)** 7d starvation, **(D)** 14d CTR, **(E)** 14d starvation, **(F)** 21d CTR, **(G)** 21d starvation. **(H)** The percentage of foot gland area versus total foot tissue. CTR: control group; fg: foot groove; m: muscle; e: epidermis; V: ventral; D: dorsal. Scale bar = 500 μm. Asterisks indicate significant differences between starvation groups and CTR groups. ***$p < 0.001$; ****$p < 0.0001$.

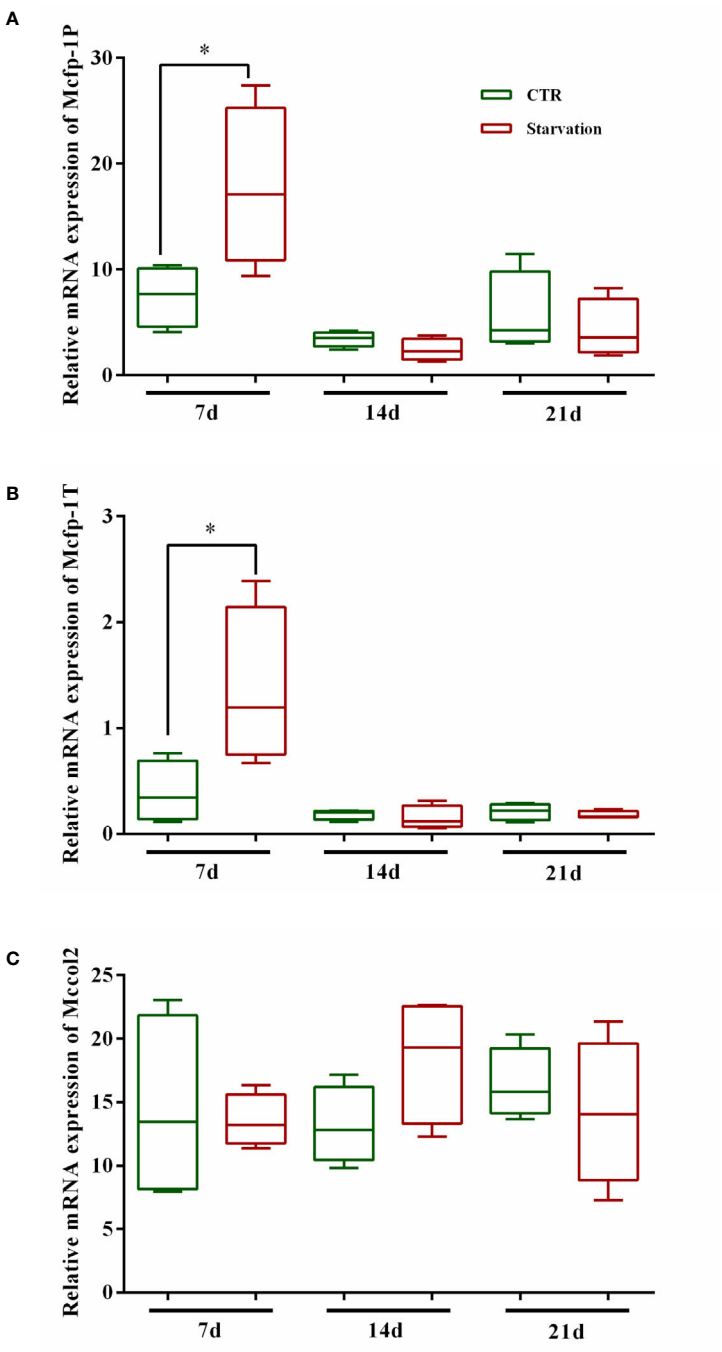

FIGURE 5
Effects of 21 days of starvation on gene expressions of mfps in foot tissue of *M. coruscus*. *Mcfp-1P*: adhesive plaque matrix protein; *Mccol2*: byssus collagen protein 2; *Mcfp-1T*: thread protein. CTR: control group. The results of statistical significance of the starvation groups compared to the control group were marked with asterisks above the columns. *$p < 0.05$.

showing decreased byssal attachment strength in non-feeding *M. galloprovincialis* (Babarro et al., 2008). The process of byssus formation may consume a large portion of the mussel's energy budget (Li et al., 2017). Under starvation stress, insufficient energy intake may negatively affect protein synthesis in mussels, leading to thinner byssal thread and reduced breaking force, and these directly lead to weakened attachment strength, increasing the risk of mussels detaching from the attachment substrate. The

weakest part of the thread might be an important factor that determines the strength of mussel attachment. We found that the mean value of the failure location on day 7 was mainly found in the upper part of the thread, while the breakpoints mainly occurred in the lower part of the thread due to increased breakpoints after 14 and 21 days of starvation treatment. However, after 14 and 21 days of starvation treatment, the mean value of the failure location increased due to the increase of break points in the upper part of the threads. Reduced byssal breaking force and shifted failure location both lead to reduced adhesion (Li et al., 2020). Similar results suggest that changes in the location of byssal thread breakage are also an indication of environmental stress in mussels (O'Donnell et al., 2013; Li et al., 2019b; Li et al., 2020). Considering that byssus is formed by proteins that secrete proteins, it can be hypothesized that starvation may regulate byssus performance by affecting the synthesis and secretion of proteins in the mussel foot.

Many animals suffer from stress due to food scarcity in their natural environment, and though some can tolerate such conditions, they still respond physiologically (Sánchez-Paz et al., 2008; Watts et al., 2014). For example, chronic starvation led to changes in the activity of some key enzymes in the digestive glands of redclaw crayfish (*Cherax quadricarinatus*), and histological analysis showed structural alterations (Sacristán et al., 2016). There was a significant difference in the size of the digestive glands between mussels (*M. galloprovincialis*) fed more food per day and those fed less food per day (Albentosa et al., 2012). Pacific oysters (*Crassostrea gigas*) differed significantly in the wet weight of digestive glands when fed low and high rations (Huvet et al., 2003). In this study, we found that starvation resulted in a decrease in the percentage of foot secretory glands area to total foot tissue. Therefore, the reduction in the foot secretory glands area observed in this study might be due to the atrophy of mussel foot secretory glands caused by starvation. The mussel foot tissue consists mainly of muscles and secretory glands (collagen, enzyme and phenolic glands) that are responsible for the synthesis and storage of the molecular components of the byssus (Waite, 1992; Waite, 2017). The mussel foot secretory glands contain large amounts of endoplasmic reticulum, ribosomes and secretory vesicles containing proteins essential for byssus production (Tamarin and Keller, 1972; Priemel et al., 2017). Given the close association between byssus production and foot secretory glands, it is hypothesized that foot secretory glands atrophy leads to abnormal gland function, further impacting the structure and strength of the byssus.

Various molecular precursor proteins that form the byssus are assembled in the foot, and the increased expression of the mussel foot protein genes promotes the accumulation of mussel foot proteins, which is essential for byssus production (Waite, 2017; Li et al., 2020). Mcfp-1P and Mcfp-1T are located in the plaque and thread of the byssus, respectively (Inoue et al., 1996; Liao et al., 2012). In this study, we found that starvation treatment for 7 days increased *Mcfp-1P* and *Mcfp-1T* mRNA expression levels. The up-regulation of *Mcfp-1P* and *Mcfp-1T* mRNA expression corresponded with the increase in the number of byssuses reflected the involvement of mussel foot proteins in byssus synthesis. However, after 14 days, the mRNA expression of *Mcfp-1P* and *Mcfp-1T* in control and starvation mussels showed no difference, although the number of byssuses was higher in the starved group than in the control group. Thus, suggesting that *Mcfp-1P* and *Mcfp-1T* are not the most critical element in the production of byssus.

Conclusion

The present study shows that starvation increases the number of byssus secretions in mussels, but also increases the number of shed byssus and weakens byssus performance. Furthermore, starvation treatment reduced the percentage of mussel foot glands area to total foot tissue which might be a cause for the weakened byssal thread strength. Food limitation might alter the mussel foot gland's physiology, which needs further investigation. Food scarcity has potentially adverse effects on the byssus production of mussels in a variety of habitats, which can increase the dislodgment risks of suspended-cultured mussels.

Data availability statement

The original contributions presented in the study are included in the article/supplementary materials. Further inquiries can be directed to the corresponding authors.

Author contributions

YZ: Investigation, Data curation, Formal analysis, Writing – original draft review and editing. Y-MY: Investigation, Data curation, Formal analysis, Writing – original draft. Y-FX: Investigation, Writing – original draft. Y-QW: Investigation, Data curation. XS: Investigation. G-HZ: Investigation, Conceptualization, Writing - review and editing. Y-FL: Conceptualization, Supervision, Writing – original draft, Writing – review and editing, Funding acquisition. All authors contributed to the article and approved the submitted version.

Funding

The authors acknowledge grants from the National Natural Science Foundation of China (No. 32172992) and Science and technology innovation action plan (19590750500).

Conflict of interest

The authors declare that the research was conducted in the absence of any commercial or financial relationships that could be construed as a potential conflict of interest.

Publisher's note

References

Albentosa, M., Sánchez-Hernández, M., Campillo, J. A., and Moyano, F. J. (2012). Relationship between physiological measurements (SFG-scope for growth-) and the functionality of the digestive gland in *Mytilus galloprovincialis*. *Comp. Biochem. Physiol. Mol. Integr. Physiol.* 163 (3-4), 286–295. doi: 10.1016/j.cbpa.2012.07.019

Babarro, J. M. F., Reiriz, M. J. F., and Labarta, U. (2008). Secretion of byssal threads and attachment strength of mytilus galloprovincialis: The influence of size and food availability. *J. Mar. Biol. Assco UK.* 88, 783–791. doi: 10.1017/S0025315408001367

Buck, B. H., Ebeling, M. W., and Michler-Cieluch, T. (2010). Mussel cultivation as a co-use in offshore wind farms: Potential and economic feasibility. *Aquacult. Econ. Manage.* 14 (4), 255–281. doi: 10.1080/13657305.2010.526018

Buschbaum, C., Dittmann, S., Hong, J. S., Hwang, I. S., Strasser, M., Thiel, M., et al. (2009). Mytilid mussels: Global habitat engineers in coastal sediments. *Helgoland Mar. Re.* 63 (1), 47–58. doi: 10.1007/s10152-008-0139-2

Carrington, E. (2002). Seasonal variation in the attachment strength of blue mussels: Causes and consequences. *Limnol. Oceanogr.* 47 (6), 1723–1733. doi: 10.4319/lo.2002.47.6.1723

Carrington, E., Waite, J. H., Sarà, G., and Sebens, K. P. (2015). Mussels as a model system for integrative ecomechanics. *Annu. Rev. Mar. Sci.* 7, 443–469. doi: 10.1146/annurev-marine-010213-135049

Clarke, M. (1999). The effect of food availability on byssogenesis by the zebra mussel (Dreissena polymorpha pallas). *J. Mollus.* Stu. 65 (3), 327–333. doi: 10.1093/mollus/65.3.327

Clements, J. C., Hicks, C., Tremblay, R., and Comeau, L. A. (2018). Elevated seawater temperature, not pCO2, negatively affects post-spawning adult mussels (Mytilus edulis) under food limitation. *Conserv. Physiol.* 6 (1), cox078. doi: 10.1093/conphys/cox078

Côté, I. M., and Jelnikar, E. (1999). Predator-induced clumping behaviour in mussels (Mytilus edulis Linnaeus). *J. Exp. Mar. Biol. Ecol.* 235 (2), 201–211. doi: 10.1016/S0022-0981(98)00155-5

Demartini, D. G., Errico, J. M., Sjoestroem, S., Fenster, A., and Waite, J. H. (2017). A cohort of new adhesive proteins identified from transcriptomic analysis of mussel foot glands. *J. R. Soc Interface.* 14 (131), 20170151. doi: 10.1098/rsif.2017.0151

Duchini, D., Boltovskoy, D., and Sylvester, F. (2015). Detachment, displacement and reattachment activity in a freshwater byssate mussel (Limnoperna fortunei): the effects of light, temperature and substratum orientation. *Biofouling* 31 (7), 599–611. doi: 10.1080/08927014.2015.1080251

FAO (2020). "Fishery and aquaculture statistics," in *FAO yearbook*.

Fitzgerald-Dehoog, L., Browning, J., and Allen, B. J. (2012). Food and heat stress in the California mussel: Evidence for an energetic trade-off between survival and growth. *Biol. Bull-US.* 223 (2), 205–216. doi: 10.1086/BBLv223n2p205

Garner, Y. L., and Litvaitis, M. K. (2013). Effects of wave exposure, temperature and epibiont fouling on byssal thread production and growth in the blue mussel, mytilus edulis, in the gulf of Maine. *J. Exp. Mar. Biol. Ecol.* 446, 52–56. doi: 10.1016/j.jembe.2013.05.001

George, M. N., and Carrington, E. (2018). Environmental post-processing increases the adhesion strength of mussel byssus adhesive. *Biofouling* 34, 388–397. doi: 10.1080/08927014.2018.1453927

Harrington, M. J., and Waite, J. H. (2007). Holdfast heroics: comparing the molecular and mechanical properties of mytilus californianus byssal threads. *J. Exp. Biol.* 210 (24), 4307–4318. doi: 10.1242/jeb.009753

Harris, L. S., and Carrington, E. (2020). Impacts of microplastic vs. natural abiotic particles on the clearance rate of a marine mussel. *Limnol. Oceanogr. Lett.* 5 (1), 66–73. doi: 10.1002/lol2.10120

Hunt, H. L., and Scheibling, R. E. (2001). Patch dynamics of mussels on rocky shores: integrating process to understand pattern. *Ecology* 82 (11), 3213–3231. doi: 10.1890/0012-9658(2001)082[3213:PDOMOR]2.0.CO;2

Huvet, A., Daniel, J. Y., Quéré, C., Dubois, S., Prudence, M., Van Wormhoudt, A., et al. (2003). Tissue expression of two α-amylase genes in the pacific oyster *Crassostrea gigas*. effects of two different food rations. *Aquaculture* 228 (1-4), 321–333. doi: 10.1016/S0044-8486(03)00323-5

Inoue, K., Takeuchi, Y., Takeyama, S., Yamaha, E., Yamazaki, F., Odo, S., et al. (1996). Adhesive protein cDNA sequence of the mussel mytilus coruscus and its evolutionary implications. *J. Mol. Evol.* 43, 348–356. doi: 10.1007/BF02339009

Iwasaki, K. (2015). Behavior and taxis of young and adult limnoperna fortunei. *Springer Cham.* 2015, 249–260. doi: 10.1007/978-3-319-13494-9_14

Lachance, A., Myrand, B., Tremblay, R., Koutitonsky, V., and Carrington, E. (2008). Biotic and abiotic factors influencing attachment strength of blue mussels mytilus edulis in suspended culture. *Aquat. Biol.* 2, 119–129. doi: 10.3354/ab00041

Liao, Z., Li, N. N., Wang, X. C., Sun, J. J., Shen, W., Fan, M. H., et al. (2012). Identification of novel foot proteins from mytilus coruscus byssus through proteomic analysis. *Chin. J. Biochem. Mol. Biol.* 28, 870–878. doi: 10.13865/j.cnki.cjbmb.2012.09.016

Li, Y. F., Canário, A. V. M., Power, D. M., and Campinho, M. A. (2019a). Ioxynil and diethylstilbestrol disrupt vascular and heart development in zebrafish. *Environ. Int.* 124, 511–520. doi: 10.1016/j.envint.2019.01.009

Li, S. G., Chen, Y. Y., Gao, Y. C., Xia, Z. Q., and Zhan, A. B. (2019b). Chemical oxidants affect byssus adhesion in the highly invasive fouling mussel Limnoperna fortunei. *Sci. Total Environ.* 646, 1367–1375. doi: 10.1016/j.scitotenv.2018.07.434

Li, S. G., Liu, C., Zhan, A. B., Xie, L. P., and Zhang, R. Q. (2017). Influencing mechanism of ocean acidification on byssus performance in the pearl oyster pinctada fucata. *Environ. Sci. Technol.* 51 (13), 7696–7706. doi: 10.1021/acs.est.7b02132

Li, L. S., Lu, W. Q., Sui, Y. M., Wang, Y. J., Gul, Y., and Dupont, S. (2015). Conflicting effects of predator cue and ocean acidification on the mussel mytilus coruscus byssus production. *J. Shellfish Res.* 34 (2), 393–400. doi: 10.2983/035.034.0222

Li, Y. F., Yang, X. Y., Cheng, Z. Y., Wang, L. Y., Wang, W. X., Liang, X., et al. (2020). Near-future levels of ocean temperature weaken the byssus production and performance of the mussel mytilus coruscus. *Sci. Total Environ.* 733, 139347. doi: 10.1016/j.scitotenv.2020.139347

Lin, Q., Gourdon, D., Sun, C., Holten-Andersen, N., Anderson, T. H., Waite, J. H., et al. (2007). Adhesion mechanisms of the mussel foot proteins mfp-1 and mfp-3. *PNAS* 104 (10), 3782–3786. doi: 10.1073/pnas.0607852104

Lucas, J. M., Vaccaro, E., and Waite, J. H. (2002). A molecular, morphometric and mechanical comparison of the structural elements of byssus from mytilus edulis and mytilus galloprovincialis. *J. Exp. Biol.* 205 (12), 1807–1817. doi: 10.1242/jeb.205.12.1807

Newcomb, L. A., George, M. N., O'Donnell, M. J., and Carrington, E. (2019). Only as strong as the weakest link: Structural analysis of the combined effects of elevated temperature and pCO2 on mussel attachment. *Conserv. Physiol.* 7 (1), coz068. doi: 10.1093/conphys/coz068

O'Donnell, M. J., George, M. N., and Carrington, E. (2013). Mussel byssus attachment weakened by ocean acidification. *Nat. Clim. Change* 3, 587–590. doi: 10.1038/NCLIMATE1846

Priemel, T., Degtyar, E., Dean, M. N., and Harrington, M. J. (2017). Rapid self-assembly of complex biomolecular architectures during mussel byssus biofabrication. *Nat. Commun.* 8 (1), 1–12. doi: 10.1038/ncomms14539

Pujol, J. P. (1967). Formation of the byssus in the common mussel (Mytilus edulis l.). *Nature* 214 (5084), 204–205. doi: 10.1038/214204a0

Roberts, E. A., Newcomb, L. A., McCartha, M. M., Harrington, K. J., LaFramboise, S. A., Carrington, E., et al. (2021). Resource allocation to a structural biomaterial: Induced production of byssal threads decreases growth of a marine mussel. *Funct. Ecol.* 35 (6), 1222–1239. doi: 10.1111/1365-2435.13788

Sacristán, H. J., Ansaldo, M., Franco-Tadic, L. M., Fernández Gimenez, A. V., and López Greco, L. S. (2016). Long-term starvation and posterior feeding effects on biochemical and physiological responses of midgut gland of *Cherax quadricarinatus* juveniles (Parastacidae). *PloS One* 11 (3), e0150854. doi: 10.1371/journal.pone.0150854

Sánchez-Paz, A., Soñanez-Organis, J. G., Peregrino-Uriarte, A. B., Muhlia-Almazán, A., and Yepiz-Plascencia, G. (2008). Response of the phosphofructokinase and pyruvate kinase genes expressed in the midgut gland of the pacific white shrimp *Litopenaeus vannamei* during short-term starvation. *J. Exp. Mar. Biol. Ecol.* 362 (2), 79–89. doi: 10.1016/j.jembe.2008.06.002

Sarà, G., Rinaldi, A., and Montalto, V. (2014). Thinking beyond organism energy use: a trait-based bioenergetic mechanistic approach for predictions of life history traits in marine organisms. *Mar. Ecol.* 35, 506–515. doi: 10.1111/MAEC.12106

Shang, Y., Gu, H., Li, S., Chang, X., Sokolova, I., Fang, J. K., et al. (2021). Microplastics and food shortage impair the byssal attachment of thick-shelled mussel mytilus coruscus. *Mar. Environ. Res.* 171, 105455. doi: 10.1016/j.marenvres.2021.105455

Sui, Y., Hu, M., Huang, X., Wang, Y., and Lu, W. (2015). Anti-predatory responses of the thick shell mussel mytilus coruscus exposed to seawater acidification and hypoxia. *Mar. Environ. Res.* 109, 159–167. doi: 10.1016/j.marenvres.2015.07.008

Suplicy, F. M. (2020). A review of the multiple benefits of mussel farming. *Rev. Aquacult.* 12 (1), 204–223. doi: 10.1111/raq.12313

Tamarin, A., and Keller, P. J. (1972). An ultrastructutal study of the byssal thread forming system in mytilus. *J. Ultrastruct. Res.* 40 (3-4), 401–416. doi: 10.1016/S0022-5320(72)90110-4

Waite, J. H. (1992). "The formation of mussel byssus: anatomy of a natural manufacturing process," in *Structure, cellular synthesis and assembly of biopolymers. results and problems in cell differentiation*. Ed. S. T. Case (Berlin, Heidelberg: Springer), 27–54. doi: 10.1007/978-3-540-47207-0_2

Waite, J. H. (2017). Mussel adhesion–essential footwork. *J. Exp. Biol.* 220 (4), 517–530. doi: 10.1242/jeb.134056

Watts, A. J. R., McGill, R. A. R., Albalat, A., and Neil, D. M. (2014). Biophysical and biochemical changes occur in *Nephrops norvegicus* during starvation. *J. Exp. Mar. Biol. Ecol.* 457, 81–89. doi: 10.1016/j.jembe.2014.03.020

Young, G. A. (1985). Byssus-thread formation by the mussel mytilus edulis: effects of environmental factors. *Mar. Ecol. Prog. Ser.* 24, 261–271. doi: 10.3354/meps024261

Zippay, M. L., and Helmuth, B. (2012). Effects of temperature change on mussel, mytilus. *Integr. Zool.* 7, 312–327. doi: 10.1111/j.1749-4877.2012.00310

frontiers | Frontiers in Marine Science

TYPE Original Research
PUBLISHED 16 November 2022
DOI 10.3389/fmars.2022.1066151

OPEN ACCESS

EDITED BY
Zhiguo Dong,
Jiangsu Ocean University, China

REVIEWED BY
Rantao Zuo,
Dalian Ocean University, China
Ioannis A. Giantsis,
University of Western Macedonia, Greece

*CORRESPONDENCE
Wenjun Xu
wjxu1971@hotmail.com

†These authors have contributed equally to this work

SPECIALTY SECTION
This article was submitted to Marine Biology, a section of the journal Frontiers in Marine Science

RECEIVED 10 October 2022
ACCEPTED 01 November 2022
PUBLISHED 16 November 2022

CITATION
He J, Wan L, Yu H, Peng Y, Zhang D and Xu W (2022) Effect of water temperature on embryonic development of *Protunus trituberculatus* in an off-season breeding mode. *Front. Mar. Sci.* 9:1066151. doi: 10.3389/fmars.2022.1066151

Effect of water temperature on embryonic development of *Protunus trituberculatus* in an off-season breeding mode

Jie He[1,2†], Litao Wan[1,2†], Huaihua Yu[1,2], Yingying Peng[2], Dongxu Zhang[1] and Wenjun Xu[1,2*]

[1]Zhejiang Province Key Laboratory of Mariculture and Enhancement, Zhejiang Marine Fisheries Research Institute, Zhoushan, China, [2]Marine and Fisheries Institute, Zhejiang Ocean University, Zhoushan, China

Portunus trituberculatus (swimming crab) is an important breeding crab in China. The current breeding mode of swimming crab is still the traditional "spring seedling and winter harvest" breeding mode. In recent years, researchers have begun to explore a new off-season breeding mode through autumn seedling. In this study, the rate of embryonic development, embryo antioxidant ability and hatching rate of swimming crab in different water temperatures in an off-season breeding mode (breeding in early autumn) and digestive enzyme activity of newly hatched larvae were compared. The results showed that the duration of each development stage of swimming crab embryos was gradually reduced with increasing water temperature. The total development time was 9.43 d at 27°C and only 6.88 d at 33°C. These effects were accompanied by an increase in the development rate from 0.11 d^{-1} to 0.15 d^{-1}. The total effective accumulated temperature under the 4 temperature conditions was basically maintained at about 150°C·d (147.08 ~ 153.62°C·d), and there was no significant difference between different groups. The development of embryos at 27°C and 29°C was very synchronous, and no abnormal embryos were observed. Conversely, at 31°C, the later stage of development exhibited asynchrony, and diapause and death were noted in some embryos. At 33°C, more embryos died. The embryo hatching rate was approximately 70% at 27°C and 29°C, and the rate was significantly reduced at 31°C and 33°C. Specifically, the rate was only 13.89% at 33°C. As the water temperature increased, the activities of superoxide dismutase (SOD) and glutathione peroxidase (GSH-PX) as well as the total antioxidant capacity (T-AOC) and malondialdehyde (MDA) levels of embryos increased first and then decreased, reaching the highest value at 31°C. Catalase (CAT) activity exhibited the opposite trend which was the lowest at 29 °C with a value of only 0.17 U/mg prot and the highest at 33°C with a value of up to 0.51 U/mg prot. At temperatures of 27°C, 29°C and 31°C, the differences in various digestive enzymes of newly hatched larvae primarily manifested as the high activities of pepsin (PEP) and α-amylase (AMS) at 31°C, and other differences were not obvious. At 33°C during embryonic development, the activities of various digestive enzymes were relatively low, especially the activities of trypsin (TPS) and cellulase (CL), which were significantly lower than those of the other three temperature groups. Therefore, judging from

the antioxidant index of embryos and the digestive enzyme activity of newly hatched larvae, the embryonic development was still good when the water temperature was 31°C, accompanied by water temperatures above 31°C that seriously affected enzyme activity. Overall, a temperature below 31°C represents the appropriate temperature for embryonic development in autumn in swimming crabs.

KEYWORDS

Protunus trituberculatus, off-season breeding, water temperature, embryonic development, enzyme activity

Introduction

Protunus trituberculatus (swimming crab), an economic marine crab with the advantages of delicious meat and rich nutrition, is popular among consumers in China and represents a valuable exported aquatic product (He et al., 2017). Due to the implementation of a forbidden fishing period in the natural sea area, the proliferation and release of swimming crabs and the protection of the water ecological environment in the past decade, the wild population of swimming crabs along the coast of China has increased yearly with the annual catch amount of the whole country stabilizing at approximately 500,000 tons from 2015 to 2020 (China Fisheries Statistical Yearbook, 2015-2021). However, the establishment of the forbidden fishing system has also resulted in a lack of crabs available on the market during the forbidden fishing period. Especially in 2017, the Ministry of Agriculture of the People's Republic of China clearly stipulated that the annual forbidden fishing period for swimming crabs is from May 1 to August 1, leading to a three-month gap in the market for swimming crabs.

Since the 1990s, China has conducted more systematic research on swimming crabs in seedling breeding (Fan et al., 2008), breeding of fine varieties (Gao et al., 2015), efficient pond culture (He et al., 2017), prevention and control of common diseases (Wan et al., 2011), and development of compound feed (Han et al., 2018). The results have promoted the rapid development of artificial cultivation of swimming crabs. In 2020, the cultivation area of swimming crabs in China was approximately 20,671 ha, and the production also reached 100,895 tons (data from China Fisheries Statistical Yearbook, 2021). However, the current cultivation mode remains the traditional "spring seedling and winter harvest". Under this model, the seedlings are raised in spring (April to May), cultured until winter, harvested, and marketed in winter. Thus, the current cultivation mode cannot meet the market demands of cultured swimming crabs from May to August.

Off-season marketing through off-season breeding is an effective method to accelerate the transformation and upgrading of the fisheries industry, ensure a balanced supply of aquatic products and achieve sustained and rapid growth of fishermen's income. To fill the market gap of swimming crabs during the forbidden fishing period, researchers began to explore a new off-season breeding and cultivation model to meet the demands of the next year's off-season market by breeding in autumn (Yu et al., 2021). The weather in early autumn in South China is still relatively hot, and the water temperature of the culture pond is approximately 30°C with temperatures occasionally reaching up to 33°C. As an important element in the study of aquatic animal reproductive biology, embryonic development is the basis of larval development. Numerous studies have demonstrated that aquatic animals respond more rapidly to changes in the water environment during embryonic development, and unsuitable environments will seriously affect embryonic development. Specifically, high temperature often leads to embryonic deformity or diapause and cause severe embryonic death (Zhong, 2014; Güralp et al., 2017; Ashaf-Ud-Doulah et al., 2021). Therefore, it is of great significance to determine the appropriate temperature and temperature limits of embryonic development for the breeding and cultivation of swimming crabs in autumn.

The morphology and rate of embryonic development as well as the final hatching rate are important indicators for evaluating the quality of embryonic development. In addition, antioxidant enzyme activity can reflect the physiological condition of embryos to a certain extent (Fan et al., 2019). In addition, digestive enzyme activity can reflect the feeding and digestive capacity of the newly hatched larvae of swimming crabs (Pan and Wang, 1997). Thus, this study compares the rate of embryonic development, embryo antioxidant ability and hatching rate of swimming crab in different water temperatures in an off-season breeding mode (breeding in early autumn) and digestive enzyme activity of newly hatched larvae. The study goal is to identify the temperature limits of swimming crab embryonic development, providing a crucial theoretical basis and practical reference for the selection of off-season breeding time and regulation of water temperature.

Materials and methods

Source of experimental crabs and temporary rearing conditions

In mid-August 2021, 80 wild female swimming crabs with well-developed gonads, sound limbs, an average body weight of 155.48 ± 12.63 g and a carapace length of 68.13 ± 3.27 mm were purchased from a fishing vessel in Daishan County, Zhoushan City, Zhejiang Province. The selection of female crabs with well- developed ovaries was carried out by adopting a non-intrusivemethod of shining a bright light through the underside of the crab carapace (Wu et al., 2010). Crabs were transported to the test site of Zhejiang Marine Fisheries Research Institute and temporarily reared in an indoor culture pond (2.0 × 6.0 × 1.0 m) with 10-cm thick mud and sand at the bottom. The following pool conditions were maintained: 0.4 m water depth, 29.1 ± 0.1°C water temperature, 26.5 ± 0.5 salinity, and DO ≥ 5 mg/ml. During the temporary rearing period, oxygen was continuously increased for 24 hours. Fresh *Sinonovacula constricta* were fed at 5:00 pm daily at approximately 10% of the crab's body weight, and the feeding amount was flexibly adjusted depending on the feeding condition. In addition, isothermal seawater (seawater filtered by screen and dark precipitated) was changed at 7:00 am daily with a renewed seawater volume of 1/2.

Establishment of different water temperatures

Experiments were conducted in 12 culture buckets with four temperature gradients (27°C, 29°C, 31°C and 33°C). Here, 27°C was controlled by a refrigerating machine, and temperatures of 29°C, 31°C and 33°C were controlled by heating rods. Three replicates were performed for each temperature group. Forty-eight crabs with good vitality were selected from the culture pond, numbered individually with a white paint pen on their backs, and randomly divided equally into 12 culture buckets. Thus, there were 12 crabs in 3 buckets of each temperature group. The spawning status of each crab was observed every 8 hours, and the time when the crab began to spawn was recorded.

Observation of embryonic development and calculation of effective accumulated temperature

Once a berried female was found, embryonic development was continuously observed as described by Yu et al. (2021). Observations were made every 1 hour before the blastocyst stage and every 6 hours after the blastocyst stage.), and fixed with Bouin's solution. The embryonic development of each crab was observed using a biological microscope (model: BELONA-XSZ 07), and the development time of each stage of embryonic development was recorded. Regarding the determination of development stage, the criterion was that 60% of the embryos showed developmental characteristics of a certain period. The effective accumulated temperature during embryonic development was calculated based on the following formula (Zhang et al., 2011; Liu et al., 2021):

$$C = \frac{\sum v^2 \sum T - \sum v \sum vT}{n\sum v^2 - (\sum v)^2}$$

$$K = N(T - C)$$

Where C is the biological zero of embryonic development of swimming crab; T is the habitat water temperature (°C); V is developmental rate (1/N); n is the temperature gradient number. K is the effective accumulated temperature (°C·d) for embryonic development of swimming crab; N is the time required for the development of embryos (d).

Determination of embryo hatching rate

The embryo hatching rate was measured in beakers containing 500 ml seawater. The water temperature in the beakers was controlled by a thermostat water bath with four temperature gradients of 27°C, 29°C, 31°C and 33°C, and three beakers were used for each temperature group. When the embryos in each temperature group developed to the prehatching stage and the heartbeat reached greater than 200 beats/min, 30 embryos were removed from the abdomen of broodstock crabs with a pipette (4 crabs were selected from each temperature group only to measure embryo hatching rate) and then divided equally into 3 corresponding beakers for hatching. The next day, the hatching of embryos in beakers was observed. The hatching rate was calculated as follows:

Hatching rate = n2/n1 × 100%

where n2 indicates the number of embryos hatched in the beaker, and n1 indicates the total number of selected embryos in the beaker.

Determination of the embryo antioxidant index and digestive enzyme activity of newly hatched larvae

4 crabs were selected from each temperature group only to determine the embryo antioxidant index and digestive enzyme activity of newly hatched larvae. When the embryos developed to the prehatching stage (heartbeat was approximately 200 beats/min), approximately 5.0 g embryos were obtained from the abdomen of broodstock crabs. After these embryos were quickly dried by absorbent paper, they were placed in centrifuge tubes and stored at -80°C. These embryos were used for subsequent determination of antioxidant enzyme activity. Embryo samples were rinsed with preprepared physiological saline (4°C, 0.9%), and then 10% homogenate was made by adding prechilled physiological saline

in the mass-volume ratio (1 g:10 ml) and mechanical homogenization under ice bath conditions. Subsequently, the supernatant was centrifuged at 4°C for 10 min at 2,500 r/min and stored in a -80°C refrigerator for the determination of antioxidant enzyme activity. Notably, for the determination of the total antioxidant ability, the mass-volume ratio was 1 g:4 ml, and the centrifugation conditions were 12,000 r/min to sufficiently break the cells to release the antioxidants. The enzyme solutions were prepared in different concentrations in accordance with the specific needs. Finally, the index was determined.

When the embryo developed to the prehatching stage, broodstock crabs of all temperature groups were moved to 24 hatching buckets of the same water temperature (30°C), and 500 L volume was prepared in advance for hatching (1 crab was put in each hatching bucket). After hatching, all larvae were removed immediately with a 200-mesh sieve. Similarly, excess water was absorbed with absorbent paper, packed in centrifuge tubes and store it in a -80°C refrigerator. The supernatant was obtained from the newly hatched larvae samples in the same manner as described above and used for digestion enzyme determination (cellulase should be determined by centrifugation at 4000 r/min).

The activities of superoxide dismutase (SOD), catalase (CAT), glutathione peroxidase (GSH-Px), total antioxidant capacity (T-AOC) and the levels of malondialdehyde (MDA)of the embryos were measured using kits produced by Nanjing Jiancheng Bioengineering Institute. Similarly, the activities of pepsin (PEP), trypsin (TPS), lipase (LPS), α-amylase (AMS) and cellulase (CL) of the newly hatched larvae were determined using commercially available kits (produced by Nanjing Jiancheng Bioengineering Institute).

Analysis of data

Excel 2019 was used to collect the experimental data, and all results are expressed as the mean ± standard deviation (mean ± SD). The data were subjected to one-way analysis of variance (one-way ANOVA) using SPSS 22.0 software. Multiple comparisons were performed by LDS, and significant differences were indicated when $P< 0.05$.

Results

Embryonic development characteristics of swimming crabs

During the experiment, there was no natural death of the broodstock crabs under the four water temperatures.The cleavage mode during the embryonic development of swimming crabs is typical superficial cleavage. The embryonic development of swimming crabs was divided into seven stages of embryonic development, namely, zygote, cleavage, blastocyst, gastrula, nauplius, protozoea, and prehatching stages, based on the morphological characteristics of each stage. When round or oval zygotes were closely distributed on the outside of the setae of the pleopods, the zygotes were dark in color, and the colorless transparent egg membrane was tightly adhered to the surface of the zygotes (Figure 1A). The surface of the embryo at cleavage was covered by a transparent egg membrane, and clear cleavage grooves were visible (Figure 1B). Multiplicative growth was

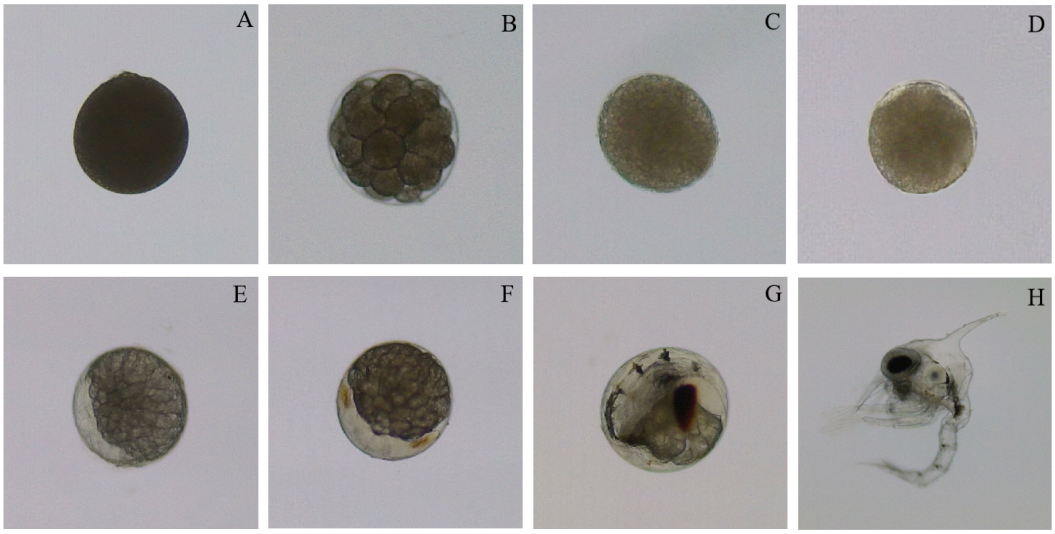

FIGURE 1
Embryonic development characteristics of swimming crab **(A)**: Zygote; **(B)**: Cleavage; **(C)**: Blastocyst; **(D)** Gastrula; **(E)**: Nauplius; **(F)**: Protozoea; **(G)**: Prehatching stage; **(H)**: Newly hatched larvae.

noted throughout this development period with the zygotes eventually entering the 256-cell stage after eight cleavages. At the blastocyst stage, the cleavage grooves disappeared, and the surface of the embryo exhibited a uniform and dense state without any massive structure. In addition, a mass of blastomeres were arranged on the surface of the embryo and wrapped by a thin blastoderm (Figure 1C). In addition, the yolk granules filled all the blastocoel under the blastoderm, forming the yolk sac. At the gastrula, one end of the yolk inside the embryo invaginated from the outside to the inside, and a small crescent-shaped transparent area appeared, forming the archenteron and protostoma (Figure 1D). During this period, the cells achieved the recombination of blastocyst cells by movement. Given constant cell proliferation and differentiation, cells and tissues gradually underwent morphological self-organization. The transparent area at the nauplius gradually increased while the yolk color faded step by step, and the yolk mass was also vaguely visible (Figure 1E). In addition, with the continuous cell division and differentiation, the optic lobe rudiment, antenna rudiment and mandible rudiment were gradually formed, and the number of appendages also increased until seven pairs formed. At the protozoea stage, the transparent area further expanded. In addition, the yolk area decreased, and stripes of jacinth eyespots began to appear on both sides of the transparent area (Figure 1F). Subsequently, the compound eye pigment area expanded and became darker. The cardiac rudiment appeared on the back of the yolk sac, and a heartbeat was soon identified. However, the heart rate was low and irregular. Until the prehatching stage, the yolk was gradually absorbed, and only a small amount remained beside the compound eye. The color deepened while the area of compound eye pigment became larger, and the telson appeared at this stage with obvious abdominal somites (Figure 1G). Moreover, the heartbeat was rhythmic with a speed of up to 200 beats/min. This stage was followed by the larvae exiting the membrane (Figure 1H).

Effect of water temperature on embryonic development rate and total effective accumulated temperature of swimming crabs

As shown in Table 1, the duration of each development stage gradually shortened with increasing water temperature, especially the total development time. The total development time was 9.43 d at 27°C and only 6.88 d at 33°C, representing an approximately one-quarter reduction. Correspondingly, the development rate increased from 0.11 h^{-1} to 0.15 h^{-1}. Regression analysis of total development time and development rate with water temperature was used to obtain the following regression equation of total embryonic development time and water temperature: N=-0.4174T+20.448 (R^2 = 0.9414, Figure 2). In addition, the regression equation of embryonic development rate and water temperature was V=0.0065T-0.0667 (R^2 = 0.9766, Figure 3). A highly significant linear correlation was observed. Additionally, the highest total effective accumulated temperature was 153.62°C·d at 27°C, and compared with the other three groups, these values were not significantly different (P>0.05).

Effect of water temperature on the embryonic development synchronization and hatching rate of swimming crabs

For the same broodstock crab, embryonic development was very synchronous at 27°C and 29°C, and no abnormal embryos were observed (Figure 4A, B). However, at 31°C, the embryos were not synchronous at the later stage of development. For example, when most of the embryos entered protozoea, some were still in the nauplius, and some embryos exhibited diapause and death (Figure 4C). The situation was more serious at 33°C; in particular, many embryos with darker color and their internal

TABLE 1 The embryonic development time and effective accumulated temperature of swimming crab at four water temperatures.

Development stage	27°C	29°C	31°C	33°C
Zygote	0.28 ± 0.10	0.17 ± 0.03	0.18 ± 0.07	0.14 ± 0.05
Cleavage	0.58 ± 0.22	0.47 ± 0.24	0.44 ± 0.12	0.44 ± 0.08
Blastula	1.11 ± 0.04	1.09 ± 0.26	0.96 ± 0.06	0.92 ± 0.06
Gastrula	0.90 ± 0.09	0.74 ± 0.27	0.67 ± 0.27	0.61 ± 0.02
Nauplius	2.71 ± 0.41 ^{a}	2.03 ± 0.36 ^{b}	1.89 ± 0.10 ^{b}	1.72 ± 0.26 ^{b}
Protozoea	1.60 ± 0.10	1.31 ± 0.16	1.33 ± 0.34	1.38 ± 0.14
Prehatching stage	2.25 ± 0.12	2.23 ± 0.43	1.89 ± 0.24	1.67 ± 0.22
Total time	9.43 ± 0.29 ^{a}	8.04 ± 0.66 ^{b}	7.36 ± 0.49 $^{b\ c}$	6.88 ± 0.09 ^{c}
Development rate (d^{-1})	0.11 ± 0.00 ^{c}	0.13 ± 0.01 ^{b}	0.14 ± 0.01 a ^{b}	0.15 ± 0.00 ^{a}
Total effective accumulated temperature (°C·d)	153.62 ± 4.71	147.08 ± 12.16	149.36 ± 9.99	153.24 ± 2.01

Different lowercase letters in the same row indicate significant differences (P< 0.05).

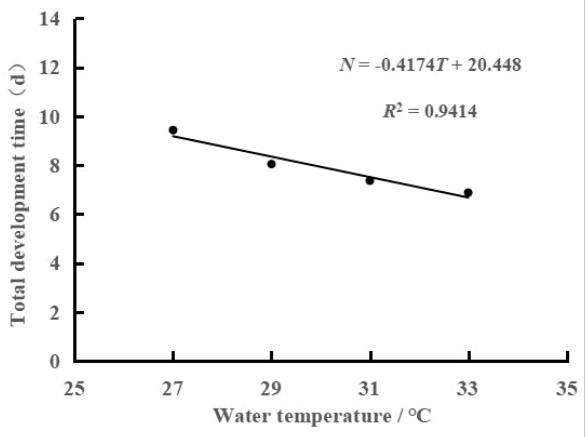

FIGURE 2
Relationship between time (*N*) and water temperature (*T*) for embryonic development of swimming crab.

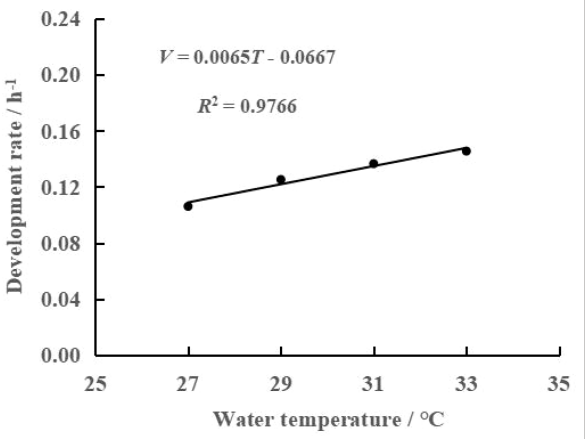

FIGURE 3
Relationship between rate (*V*) and water temperature (*T*) for embryonic development of swimming crab.

structures were not visible (Figure 4D). Notably, there were no dead eggs remaining in the abdomen of the broodstock crabs after the embryos hatched at 27°C and 29°C, and no dead embryos that sank to the bottom of the water were visible in the hatching bucket. However, at 31°C and 33°C, the abdomen of the broodstock crabs was not so clean, especially at 33°C, when more dead eggs were left in the abdomen, and many dead embryos and dead newly hatched larvae could be observed at the bottom of the hatching bucket. To obtain a clearer understanding of the final hatching rate of embryos at the four water temperatures, the hatching rate of embryos was observed individually in beakers. The results revealed that the higher hatching rates of approximately 70% at 27°C and 29°C, and the rate significantly decreased to only 13.89% at 33°C (Figure 5).

Effect of water temperature on the embryo antioxidant index of swimming crabs

With increasing water temperature, the activities of SOD, GSH-PX and T-AOC as well as the MDA content showed a trend of first increasing and then decreasing and was the highest at 31°C (Figure 6). Among them, the SOD activity at 31°C reached 188.42 U/mg prot, which was significantly higher than that noted in the other groups ($P<0.05$), whereas GSH-PX activity and MDA content were not significantly different compared with values obtained from the other groups. The trend of CAT activity was opposite to the above four indicators. Specifically, with increasing water temperature, the enzyme activity first decreased and then increased. CAT activity was the lowest at 29°C (0.17 U/mg prot), and the highest at 33°C (0.51 U/mg prot). In addition, significantly greater CAT activity was noted at 31°C compared with that at 27°C and 29°C ($P<0.05$). In general, the water temperatures tested in this study had minimal effects on the embryo antioxidant index of swimming crabs. Relatively high values were obtained at 31°C.

Effect of water temperature during embryonic development on digestive enzyme activity of newly hatched larvae of swimming crab

The digestive enzyme activities differed among the newly hatched larvae of swimming crabs subject to different water temperatures during embryonic development, even under the same rearing conditions. PEP, TPS, LPS, AMS and CL activities all increased and then decreased with increasing water temperature during embryonic development (Figure 7). At 29°C, TPS, LPS and CL exhibited the highest activities, reaching 6529.77 U/mg prot, 2.68 U/mg prot and 76.10 U/mg prot, respectively. Similar values were obtained at 27°C and 31°C. However, once the temperature reached 33°C, TPS, LPS and CL activities declined rapidly with values of only 1767.19 U/mg prot, 1.47 U/mg prot and 37.88 U/mg prot, respectively. In addition, TPS and CL activities at 33°C were significantly lower than those obtained at 27°C, 29°C and 31°C. In addition, the activities of PEP and AMS at 31°C were the highest at 4.33 U/mg prot and 4.95 U/mg prot, respectively. These values decreased significantly at 33°C to 2.30 U/mg prot and 3.01 U/mg prot, respectively.

Discussion

The embryonic development of aquatic animals is crucial in the study of evolutionary biology, and the stage of embryonic development in crustaceans, shrimps and crabs is typically

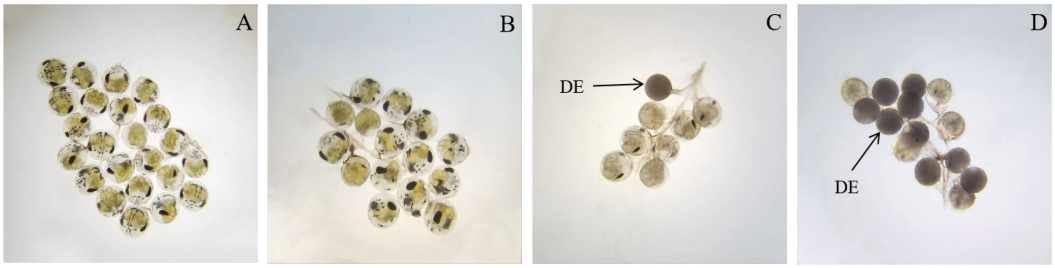

FIGURE 4
Embryonic development synchronization of swimming crab at four water temperatures (**A**: 27°C; **B**: 29°C; **C**: 31°C; **D**: 33°C; DE: Dead embryos).

classified based on different external morphological features, such as the proportion of yolk during embryonic development, the presence of rudiment, changes in the number of appendages, the pigment degree of compound eyes, and the appearance of heartbeat (Nagao et al., 1999). In our study, based on the method of Yu et al. (2021) in combination with the changes in important external characteristics during the embryonic development of swimming crabs, embryonic development was divided into seven stages, zygote, cleavage, blastocyst, gastrula, nauplius, protozoea, and prehatching stages. The duration of each developmental stage was shorter in autumn, and the whole embryonic development process lasted less than 10 d. In contrast, Xue et al. (2001) reported that the whole embryonic development process in spring took approximately 28 d when the water temperature was 12~19.8°C. It was evident that the high temperature in autumn significantly shortened embryonic development time. Moreover, this study demonstrated that the duration of each development stage was gradually reduced as the water temperature increased from 27 to 33°C. The total development time was 9.43 d at 27°C and only 6.88 d at 33°C.

It has been confirmed in other shrimp and crab species that the protein within the yolk is the main energy source and structural material for embryonic development. As the temperature increased under suitable conditions, the activity of protein degrading enzymes in the embryo increases, which contributes to enhancing the relevant metabolic activities and formation of structural material in the egg. These findings imply that the accelerated rate of yolk consumption promotes the rate

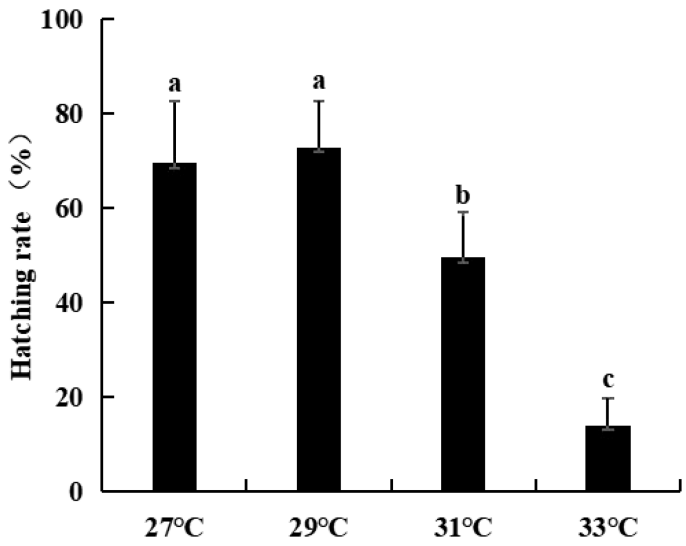

FIGURE 5
Embryo hatching rate of swimming crab at four water temperature. Different lowercase letters above the figure column indicate that there are significant differences between different temperature groups ($P < 0.05$).

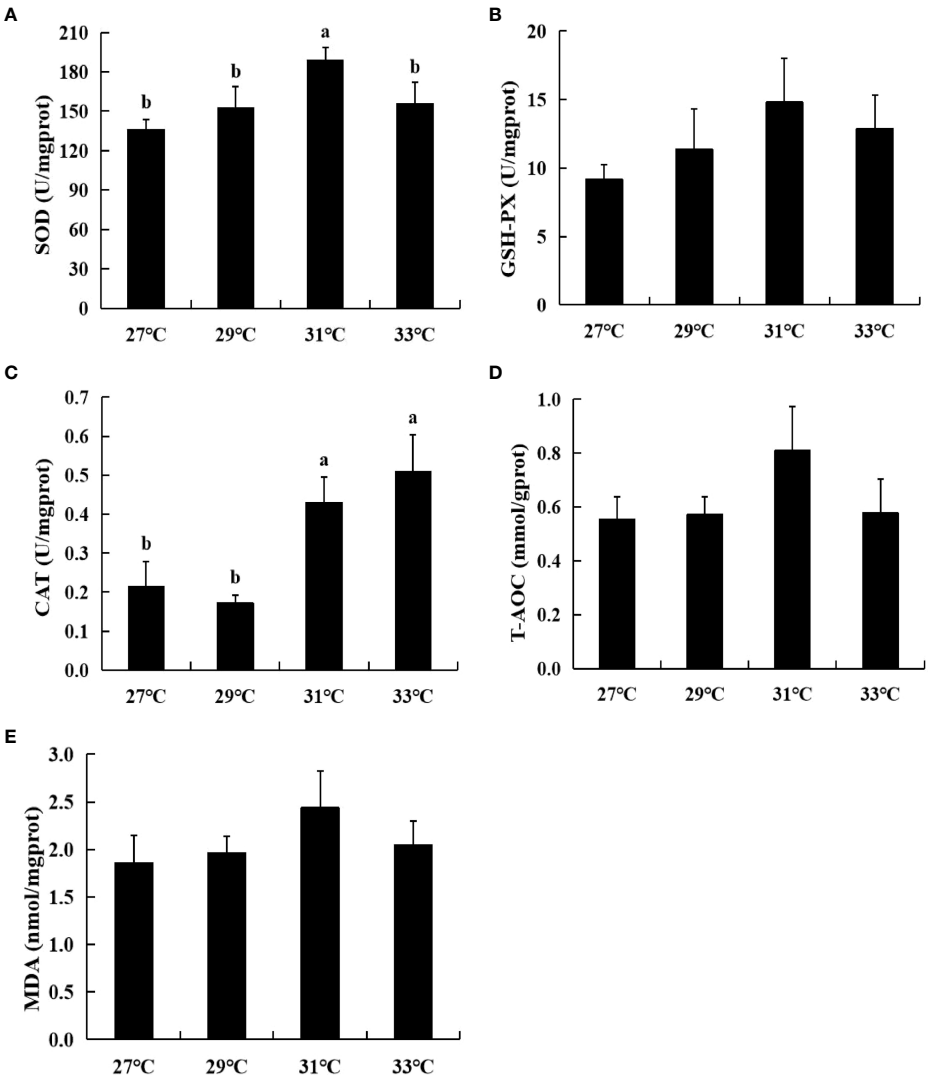

FIGURE 6
Embryo antioxidant index of swimming crab at four water temperatures. **(A)** Superoxide dismutase (SOD); **(B)** Glutathione peroxidase (GSH-Px); **(C)** Catalase (CAT); **(D)** Total antioxidant capacity (T-AOC); **(E)** Malondialdehyde (MDA). Different lowercase letters above the figure column indicate that there are significant differences between different temperature groups ($P< 0.05$).

of embryonic development (Babu, 1987; Huang et al., 2011; Liu et al., 2021). The concept of effective accumulated temperature represents the total amount of heat accumulated necessary for embryonic development; this constant is referred to as the thermal constant (Ito et al., 1980). In *Cynoglossus semilaevis* (Du et al., 2004), *Pelteobagrus vachelli* (Yuan et al., 2005) and *Pomoxis nigromaculatus* (Zhong, 2014), different embryonic development stages were found to have different sensitivities to the hatching temperature, resulting in deviations in the effective accumulated temperature of embryonic development at different water temperatures. Swimming crabs in this study had very similar effective accumulated temperatures of embryonic development at the four temperatures, which were almost unaffected by water temperature.

Different species of crustaceans exhibit differences in temperature tolerance during embryonic development. Embryos can develop normally at suitable water temperatures. Once the water temperature exceeds the tolerance range, development desynchrony, diapause or even death occur (Ashaf-Ud-Doulah et al., 2021). Related studies found that the embryos of Scylla serrata at cleavage were uneven and irregular at 35 °C water temperature. After 18 hours of cleavage to the 132-cell stage, the cleavage stopped, and the embryos gradually died (Zeng et al., 1991). In Eriocheir sinensis, approximately 50% of

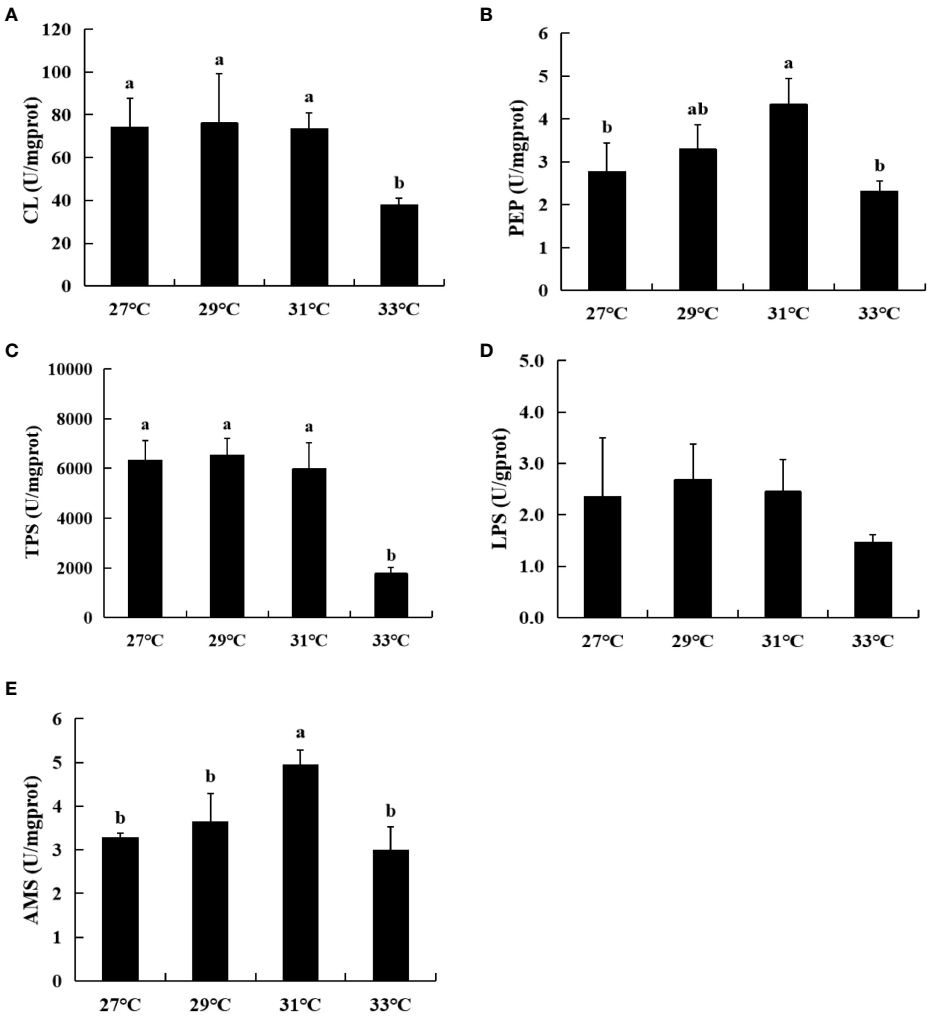

FIGURE 7
Digestive enzyme activity of newly hatched larvae of swimming crab at four water temperatures during embryonic development. **(A)** Cellulase (CL); **(B)** Pepsin (PEP); **(C)** Trypsin (TPS); **(D)** Lipase (LPS); **(E)** α-amylase (AMS). Different lowercase letters above the figure column indicate that there are significant differences between different temperature groups ($P < 0.05$).

the embryo developed asynchrony when cleavage reached the 128-cell stage at a water temperature of 26°C (Zhao et al., 1993). The embryos of Macrobrachium nipponense could not hatch normally at water temperatures greater than 36°C (Xing and Liu, 1996). Procambarus clarkii is grown at water temperatures greater than 28°C, the embryo cannot develop normally, and deformities and even death occur (Liu et al., 2021). The present study had similar findings. At a water temperature of 31°C, the embryos of swimming crabs began to develop asynchronously accompanied by partial embryo mortality. When the water temperature reached 33°C, many embryos died. A related study by Aritaki and Seikai, (2004) suggested that this phenomenon may be caused by the inhibition of yolk degrading enzyme activity under high temperature conditions, resulting in changes in the permeability of embryonic cell membranes, disruption in the process of embryonic organ differentiation and formation, and a significant increase in the embryo deformity and diapause rate. Furthermore, the hatching rate of *in vitro* embryos of swimming crabs was higher (approximately 70% at 27°C and 29°C) and decreased significantly with increasing water temperature (31°C and 33°C), especially the hatching rate, which was only 13.89% at 33°C. On the one hand, massive embryos exhibit diapause and death; on the other hand, excessive water temperature may reduce the activity of hatching enzymes or even cause irreversible inactivation, thereby reducing the embryonic hatching rate.

With the continuous deepening of research, it is recognized that the ability of aquatic organisms to adapt and resist adverse

external factors in early development stages is importantly linked to their self-protection systems in metabolic processes. The most important of these systems is the antioxidant system, which maintains the dynamic balance of free radicals in the body (Livingstone, 2001). Numerous studies have revealed that when aquatic animals are exposed to external high- or low-temperature stress, they will produce excessive harmful reactive oxygen species, and the organism will eliminate these reactive oxygen species by producing more antioxidant enzymes to maintain the normal physiological activities of cells and the organism (Gieseg et al., 2000; Martínez-Álvarez et al., 2005). As important antioxidant enzymes, SOD, CAT and GSH-Px play pivotal roles in the self-protection system during embryonic development and represent the key enzymes involved in the intraembryonic antioxidant process (Huang et al., 2010). SOD and GSH-Px activities as well as the T-AOC level of swimming crab embryos were proportional to the water temperature in the range of 27°C to 31°C. It is hypothesized that the increase in water temperature can induce an increase in embryo activity and mobilize SOD, GSH-Px and other related enzymes to resist the stress response generated by high temperature. However, the regulatory capacity of the embryo is limited, and the enzyme activity cannot increase indefinitely. Thus, when the water temperature is too high, the enzymes and their synthesis in the embryo will be altered, and the enzyme activity will be significantly reduced. This phenomenon explains why the SOD and GSH-Px activities decrease significantly at 33°C. CAT activity is the highest at 33°C, which may be that CAT is not sensitive to temperature and has a higher tolerance, or it can activate the activity of CAT only at high temperature.As the final product of the oxidation of unsaturated fatty acids in the organism, the level of MDA indirectly reflects the severity of the condition of cells attacked by free radicals (Parihar et al., 1997). The ability of swimming crab embryos to eliminate harmful free radicals is weakened at high temperatures (31°C and 33°C), leading to increased peroxidation of lipids, such as MDA.

Given that a single index of antioxidant enzyme activity was not able to explain the developmental response of swimming crab embryos under high temperature conditions, this study was conducted to evaluate the quality of embryos by combining various digestive enzymes (CL, PEP, TPS, LPS and AMS) of the newly hatched larvae to better assess the quality of embryonic development at high temperatures. Numerous studies believe that the level of digestive enzyme activity of aquatic poikilothermic animals determines their ability to digest and absorb nutrients, thus determining their growth and development speed. The nutrients required by swimming crabs during embryonic development are directly supplied by endogenous nutrients, whereas the nutrients for the development of newly hatched larvae are provided by residual yolk and gradually change to exogenous nutrients at a later stage. In addition, the differences in the activity of different digestive enzymes can directly reflect the ability of larvae to absorb and utilize different nutrients (Pan and Wang, 1997). In our study, the differences in digestive enzymes of the newly hatched larvae at 27°C, 29°C and 31°C during embryonic development were mainly demonstrated by the increased activities of PEP and AMS at 31°C along with other insignificant differences. The activities of digestive enzymes of the newly hatched larvae at 33°C during embryonic development were relatively low; in particular, the activities of TPS and CL were significantly lower than those of the other three temperature groups, further indicating that the newly hatched larvae at 33°C during embryonic development were of poor quality. The influencing mechanism needs further study.

Conclusion

Overall, the embryonic development of swimming crabs occurs faster and in a shorter timeframe (generally less than 10 d)under higher water temperatures (27~33°C) in autumn. Here, a temperature of approximately 29°C represented a suitable water temperature for embryonic development of swimming crabs in autumn. At this temperature, the embryo antioxidant ability and digestive enzyme activity of newly hatched larvae are increased, and the embryo hatching rate and quality of larvae are excellent. Although the embryo hatching rate is more affected at 31°C, the surviving embryos and newly hatched larvae are still of better quality. The most serious limitation is that at 33°C, asynchronous embryonic development is noted. In addition, an extremely low hatching rate and poor quality of surviving embryos and newly hatched larvae were observed. Therefore, we suggest that under the off-season breeding mode of swimming crab, the water temperature for embryo development should be controlled within 31°C to ensure the quality of embryo development.

Data availability statement

The original contributions presented in the study are included in the article/supplementary material. Further inquiries can be directed to the corresponding author.

Author contributions

JH and LW: Investigation, Formal analysis, Writing -original draft. HY: Conceptualization, Data curation, Formal analysis. YP

and DZ: Visualization, Writing - reviewing and editing. WX: Supervision, Funding acquisition, Writing - reviewing and editing. All authors contributed to the article and approved the submitted version.

Funding

This work was supported by the Basic Public Welfare Program of Zhejiang Province (Grant No. LGN22C190005); the National Science Foundation of China (Grant No.32172993); the Major Agricultural Technology Cooperation Plan of Zhejiang Province (Grant No. 2022XTTGSC04); the planned project of Zhejiang Marine Fisheries Research institute (HYSCZ-202105, HYS-CZ-202209).

Conflict of interest

The authors declare that the research was conducted in the absence of any commercial or financial relationships that could be construed as a potential conflict of interest.

Publisher's note

References

Aritaki, M., and Seikai, T. (2004). Temperature effects on early development and occurrence of metamorphosis-related morphological abnormalities in hatchery-reared brown sole *Pseudopleuronectes herzensteini*. *Aquac* 240 (1-4), 517–530. doi: 10.1016/j.aquaculture.2004.06.033

Ashaf-Ud-Doulah, M., Islam, S. M. M., Zahangir, M. M., Islam, M. S., Brown, C., and Shahjahan, M. (2021). Increased water temperature interrupts embryonic and larval development of Indian major carp rohu *Labeo rohita*. *Aquacult Int.* 29, 711–722. doi: 10.1007/s10499-021-00649-x

Babu, D. E. (1987). Observation on the embryonic development and energy source in the crab *Xantho bidentatus*. *Mar. Biol.* 95 (1), 123–127. doi: 10.1007/BF00447493

Du, W., Meng, Z., Xue, Z., Jiang, Y., Zhuang, Z., and Wan, R. (2004). Embryonic development of *Cynoglossus semilaevis* and its relationship with incubation temperature. *J. Fisher Sci. China* 11 (1), 48–53. doi: 10.3321/j.issn:1005-8737.2004.01.009

Fan, Y., Shao, P., Jia, X., Gao, J., Dou, Y., Shi, X., et al. (2019). Effects of temperature stress on partial antioxidant and non-specific immunity indices of *Paramisgurnus dabryanus*. *Progr Fisher Sci.* 40 (2), 58–64. doi: 10.19663/j.issn2095-9869.20180306001

Fan, X., Wang, C., Zhu, D., Cui, Z., Song, W., Shao, Y., et al. (2008). A research on feminization breeding of. *Portunus trituberculatus*. *Mar. Fisher Res.* 29 (5), 89–94. doi: 10.3969/j.issn.1000-7075.2008.05.014

Gao, B., Liu, P., Li, J., Wang, Q., and Han, Z. (2015). Effect of inbreeding on growth and genetic diversity of *Portunus trituberculatus* based on the full-sibling inbreeding families. *Aquacult Int.* 23 (6), 1401–1410. doi: 10.1007/s10499-015-9892-9

Gieseg, S. P., Cuddihy, S., Hill, J. V., and Davison, W. (2000). A comparison of plasma vitamin c and e levels in two Antarctic and two temperate water fish species. *Comp. Biochem. Phys. B.* 125 (3), 371–378. doi: 10.1016/s0305-0491(99)00186-8

Güralp, H., Pocherniaieva, K., Blecha, M., Policar, T., Pšenička, M., and Saito, T. (2017). Development, and effect of water temperature on development rate,of pikeperch *Sander lucioperca* embryos. *Theriogenology* 104, 94–104. doi: 10.1016/j.theriogenology.2017.07.050

Han, T., Li, X., Wang, J., Wang, C., Yang, M., and Zheng, P. (2018). Effects of dietary astaxanthin (AX) supplementation on pigmentation, antioxidant capacity and nutritional value of swimming crab, *Portunus trituberculatus*. *Aquac* 490, 169–177. doi: 10.1016/j.aquaculture.2018.02.030

He, J., Gao, Y., Xu, W., Yu, F., Su, Z., and Xuan, F. (2017). Effects of different shelters on the molting, growth and culture performance of *Portunus trituberculatus*. *Aquac* 481, 133–139. doi: 10.1016/j.aquaculture.2017.08.027

Huang, X., Zhang, L., Zhuang, P., Jiang, Q., Yao, Z., Liu, J., et al. (2010). Effect of cryopreservation on enzyme activity in embryo of macrobrachium rosenbergii. *Mar. Fisher* 32 (2), 166–171. doi: 10.13233/j.cnki.mar.fish.2010.02.009

Huang, X., Zhuang, P., Zhang, L., Qu, L., Yao, Z., Liu., T., et al. (2011). Embryonic development and the variation of some metabolism enzyme activity during embryonic development of Chinese mitten crab (*Eriocheir sinensis*). *J. Fisher China* 35 (2), 192–199. doi: 10.3724/SP.J.1231.2011.17130

Ito, Y., Hokyo, N., and Fujisaki, K. (1980). *Animal population and community* (Tokyo: Tokai University Press).

Liu, Y., Zhang, D., Tao, Z., Fu, F., and Gu, Z. (2021). Effects of temperature on embryonic and larval development of *Procambarus clarkia*. *J. Huazhong Agricu Univer* 40 (5), 146–153. doi: 10.13300/j.cnki.hnlkxb.2021.05.018

Livingstone, D. R. (2001). Contaminant-stimulated reactive oxygen species production and oxidative damage in aquatic organisms. *Mar. pollut. Bull.* 42 (8), 656–666. doi: 10.1016/s0025-326x(01)00060-1

Martínez-Álvarez, R. M., Morales, A. E., and Sanz, A. (2005). Antioxidant defenses in fish: biotic and abiotic factors. *Rev. Fish Biol. Fisher* 15 (1-2), 75–88. doi: 10.1007/s11160-005-7846-4

Nagao, J., Munehara, H., and Shimazaki, K. (1999). Embryonic development of the hair crab *Erimacrus isenbeckii*. *J. Crustacean Biol.* 19 (1), 77–83. jstor.org/stable/1549549 doi: 10.2307/1549549

Pan, L., and Wang, K. (1997). Studies on digestive enzyme activities and amino acid in the larvae of *Portunus trituberculatus*. *J. Fisher China* 21 (3), 246–251. cnki:sun:sckx.0.1997-03-003

Parihar, M. S., Javeri, T., Hemnani, T., Dubey, A. K., and Prakash, P. (1997). Response of superoxide dismutase, glutathione peroxidase and reduced glutathione antioxidant defenses in gills of the freshwater catfish (*Heteropneustes fossilis*) to short-term elevated temperature. *J. Therm Biol.* 22 (2), 151–156. doi: 10.1016/S0306-4565(97)00006-5

Wan, X., Shen, H., Wang, L., and Cheng, Y. (2011). Isolation and characterization of *Vibrio metschnikovii* causing infection in farmed *Portunus trituberculatus* in China. *Aquacult Int.* 19 (2), 351–359. doi: 10.1007/s10499-011-9422-3

Wu, X., Cheng, Y., Zeng, C., Wang, C., and Yang, X. (2010). Reproductive performance and offspring quality of wild-caught and pond-reared swimming crab *Portunus trituberculatus* broodstock. *Aquac* 301, 78–84. doi: 10.1016/j.aquaculture.2010.01.016

Xing, K., and Liu, M. (1996). The effect of temperature on embryonic development of *Macrobrachium nipponense*. *J. Hebei Univer* 16 (5), 22–26. cnki:sun:hbdd.0.1996-S1-006

Xue, J., Du, N., and Lai, W. (2001). Morphology of egg-larvae of swimming crab (*Portunus trituberculatus)* during embryonic development. *Acta Zool. Sin.* 47 (4), 447–452. doi: 10.3969/j.issn.1674-5507.2001.04.016

Yuan, L., Xie, X., Cao, Z., and Luo, Y. (2005). Effects of temperature on embryonic development of the darkbarbel catfish *Pelteobagrus vachelli*. *Act Zool. Sin.* 51 (4), 753–757. doi: 10.3969/j.issn.1674-5507.2005.04.028

Yu, H., Xu, W., Zhang, D., Cheng, H., Wu, K., and He, J. (2021). Development of embryos and larvae of *Portunus trituberculatus* (Decapoda, brachyura) in off-season breeding mode. *Crustaceana* 94 (6), 679–695. doi: 10.1163/15685403-bja10126

Zeng, C., Wang, G., and Li, S. (1991). Observation on embryonic development of *Scylla serrata* and study on the effect of temperature on embryonic development. *Fujian Fisher* 1, 45–50. doi: 10.14012/j.cnki.fjsc.1991.01.011

Zhang, J., Chi, C., and Wu, C. (2011). Biological zero temperature and effective accumulated temperature for embryonic development of *Sepiella maindroni*. *South China Fisher Sci.* 7 (3), 45–49. doi: 10.3969/j.issn.2095-0780·2011.03.008

Zhao, Y., Du, N., and Lai, W. (1993). Effects of different gradient temperature on embryonic development of the Chinese mitten-handed crab *Eriocheir sinensis* (Crustacea, decapoda). *Zool Res.* 14 (1), 49–53. doi: cnki:sun:sckx.0.1997-03-003

Zhong, Q. (2014). Observation on the embryonic development of *Pomoxis nigromaculatus* and the effect of the water temperature on the embryonic development. *J. Fujian Fisher* 36 (5), 333–343. doi: 10.14012/j.cnki.fjsc.2014.05.001

frontiers | Frontiers in Marine Science

TYPE Original Research
PUBLISHED 18 November 2022
DOI 10.3389/fmars.2022.1034152

OPEN ACCESS

EDITED BY
Yafei Duan,
South China Sea Fisheries Research Institute, China

REVIEWED BY
Hu Beijuan,
Nanchang University, China
Yi-Feng Li,
Shanghai Ocean University, China

*CORRESPONDENCE
Zhiguo Dong
dzg7712@163.com

SPECIALTY SECTION
This article was submitted to Marine Biology, a section of the journal Frontiers in Marine Science

RECEIVED 01 September 2022
ACCEPTED 27 September 2022
PUBLISHED 18 November 2022

CITATION
Ge H, Ni Q, Liu J, Dong Z and Chen S (2022) Effect of chronic ammonia nitrogen stress on the SOD activity and interferon-induced transmembrane protein 1 expression in the clam *Cyclina sinensis*. *Front. Mar. Sci.* 9:1034152. doi: 10.3389/fmars.2022.1034152

Effect of chronic ammonia nitrogen stress on the SOD activity and interferon-induced transmembrane protein 1 expression in the clam *Cyclina sinensis*

Hongxing Ge[1,2,3], Qian Ni[1], Jialing Liu[1], Zhiguo Dong[1,2,3]* and Shibo Chen[1]

[1]Jiangsu Key Laboratory of Marine Bioresources and Environment, Jiangsu Ocean University, Lianyungang, China, [2]Co- Innovation Center of Jiangsu Marine Bio-Industry Technology, Jiangsu Institute of Marine Resources Development, Lianyungang, China, [3]Jiangsu Key Laboratory of Marine Biotechnology, Jiangsu Ocean University, Lianyungang, China

Ammonia nitrogen plays a crucial part in oxidative stress in aquatic animals. To elucidate the effect of ammonia nitrogen stress on the superoxide dismutase (SOD) activity and interferon-induced transmembrane protein 1 (*IFITM1*) expression in the clam *Cyclina sinensis*, clams were exposed to ammonia nitrogen (8.07 mg/L) for 768 h (32 days) and then challenged with *Vibrio parahaemolyticus*. The results showed that the SOD activity in the hepatopancreas of *C. sinensis* exposed to ammonia nitrogen first increased and then decreased with time, returning to the control group's normal level at 768 h. Following infection with *V. parahaemolyticus*, the SOD activity in the hepatopancreas fluctuated over time. The SOD activity in clams infected with *V. parahaemolyticus* at 144 h did not return to the control group's normal level. The full-length cDNA of *CsIFITM1* was 2,434 bases in length, including a 2,301-bp open reading frame (ORF) encoding 714 amino acids, with a putative molecular weight of 83.86 kDa. *CsIFITM1* contains an RNA helicase domain (DEXHc_RLR, DR) and a Helicase_C (HC) domain. The transcriptional levels of *CsIFITM1* were upregulated by exposure to ammonia nitrogen and were significantly higher from 6 to 768 h compared to the control (0 h) ($p < 0.05$). Following infection with *V. parahaemolyticus*, the transcript levels of *CsIFITM1* in the hepatopancreas were upregulated and were significantly higher from 6 to 144 h, in contrast to those of the control (0 h) ($p < 0.05$). The present data provide the first evidence of the SOD activity and *CsIFITM1* transcript levels being able to reflect the effect of ammonia on the clam *C. sinensis*.

KEYWORDS

cyclina sinensis, ammonia nitrogen exposure, vibrio challenge, SOD activity, IFITM1 gene

Introduction

As an unavoidable factor, ammonia nitrogen easily accumulates in the aquaculture system (Barbieri and Bondioli, 2013; Egnew et al., 2019). The accumulation of total ammonia nitrogen (TAN) in the water environment can ultimately lead to severe problems such as oxidative stress (Ge et al., 2022a), gill hyperplasia (Zuffo et al., 2021), inefficient feed utilization (Silva et al., 2018), and poor immune response of aquatic animals (Mangang and Pandey, 2021). As a result, some opportunistic bacteria such as *Vibrio parahaemolyticus* may cause serious vibriosis (Ni et al., 2020). In some cases, it could even lead to death in aquatic animals (Barbieri et al., 2019). Aquatic animals suffer from oxidative stress, which causes the accumulation of reactive oxygen species (ROS) (Ge et al., 2022a), and the scavenging capacity induces lipid peroxidation (Debbarma et al., 2021). To protect organisms from such oxidative stress, antioxidant enzymes are likely to be activated. Therefore, a change in the antioxidant enzyme activities is one of the reliable and sensitive tools for the evaluation of oxidation resistance in aquatic animals (Ni et al., 2020; Debbarma et al., 2021). Superoxide dismutase (SOD) is one of the key antioxidant enzymes (Ge et al., 2021). It can reduce oxidative damage by eliminating ROS and enhancing the antioxidant capacity (Sinha et al., 2015). Ammonia nitrogen exposure may activate the antioxidant system and alter the activities of antioxidant enzymes (Ghelichpour et al., 2019).

Interferon (IFN) is one of the major multifunctional cytokines that play vital roles in the innate immune response in aquatic animals (Wan and Chen, 2008; Zhang et al., 2020). Among the IFN-responsive genes that collectively regulate the multifunctional effects of IFNs is the interferon-induced transmembrane (IFITM) protein family (Johnson et al., 2006; Wan and Chen, 2008). Members of the IFITM family are likely to be expressed basally in various tissues and cells. They may play a crucial part in the promotion and maintenance of the pluripotent state of an organism's cells (Johnson et al., 2006). All of the IFITM proteins share a conserved short topology, two transmembrane (TM) domains, and highly variable amino and carboxy termini (Zhang et al., 2020). Thus far, in aquatic animals, *IFITM1*, *IFITM2*, *IFITM3*, and *IFITM5* have been annotated in the fish genome (Johnson et al., 2006). The *IFITM* family comprises the known innate immune effectors involved in the regulation of immunoreaction, such as endocytosis, immune cell signaling, cell physiology, and antioxidative damage (Baird et al., 2001; Zhu et al., 2013). When organisms are under oxidative stress, they may synthesize some proteins, such as IFNs, interleukins, heat shock proteins, and the IFITM proteins (Ghelichpour et al., 2019). In humoral immunity, the transcriptional levels of members of the IFITM family can reflect the current immune status of aquatic animals (Johnson et al., 2006).

As one of the most important economic bivalves, the clam *Cyclina sinensis* is widely distributed in the coastal areas of East Asia, and the clam industry is growing rapidly (Ge et al., 2022b). The clam grows fast, tastes delicious, and has great market demand (Ge et al., 2021; Liao et al., 2022). The clam is highly adaptable to ammonia nitrogen (Ni et al., 2022). However, when the accumulation of ammonia nitrogen reaches the threshold level, this can have serious effects on the clam, including oxidative stress and poor immune response (Ni et al., 2021; Ge et al., 2022a). Therefore, it is essential to evaluate the effects of ammonia nitrogen on antioxidant enzymes and immunoreaction (Chai et al., 2022). Because a change in the SOD activity and *IFITM1* expression level can reflect the current immune status of aquatic animals, we assessed the SOD activity and the *IFITM1* transcription response in clams exposed to chronic ammonia nitrogen and following infection with *V. parahaemolyticus*. The present study provides a theoretical basis for the research on the detoxification mechanisms in marine animals.

Materials and methods

Experimental animal

C. sinensis (2.99 ± 0.45 g each) from Lianyungang Zhongchuang Aquaculture Company were transported to the experimental base of Jiangsu Ocean University. To acclimate the clams to laboratory conditions, they were stored in concrete tanks (0.8 m × 0.8 m × 0.5 m) with 200 L aerated seawater for 10 days. During the acclimation and the experiment, the seawater temperature was maintained at 24 ± 0.5°C, with pH at 8.0 ± 0.4, dissolved oxygen (DO) ≥ 4.9 mg/L, and TAN < 0.09 mg/L (Chen et al., 2021). Clams were fed twice daily with a mixture of alive microalgae (*Isochrysis zhangjiangensis* and *Nannochloropsis oceanica*) at a density of 2×10^4 cells/ml.

Six clams were dissected and various tissues collected, which were then frozen in liquid nitrogen for RNA extraction (Ni et al., 2022).

Long-term chronic ammonia nitrogen stress

Seven hundred and twenty selected clams were randomly stored in six concrete tanks (200 L water) at a density of 120 clams per tank, with three replicates for each treatment. According to the 96-h median lethal concentration (LC_{50}-96 h) TAN for *C. sinensis* (Ni et al., 2022), the TAN level in the experimental group was set at 8.07 mg/L. To achieve the designed level of TAN, a stock solution of NH_4Cl (1.0 g/L) was used. The control group was natural seawater. The other management conditions were the same as those used during the temporary rearing period, and the stress experiment was carried

out for 768 h. During the test, the seawater was changed twice daily to maintain the concentration of TAN.

Three individuals in each treatment were randomly selected at different time points after the clams were exposed to ammonia nitrogen (0, 3, 6, 12, 24, 48, 96, 192, 384, and 768 h). The hepatopancreas was collected and then frozen in liquid nitrogen for the SOD activity analysis and total RNA isolation. The SOD activity was determined using kits purchased from Nanjing Jiancheng Bioengineering Institute (Ge et al., 2022a).

Vibrio challenge

To determine the effect of ammonia nitrogen stress on the disease resistance of the clam, *Vibrio* challenge tests were further performed. After the ammonia nitrogen stress experiment, clams in the experimental group were transferred into the normal seawater tank with three replicates and challenged with *V. parahaemolyticus*. The clams were immersed and infected with *V. parahaemolyticus* at a level of 1×10^7 CFU/ml for 1 week (Ni et al., 2020). During the infection experiment, to achieve the level of *V. parahaemolyticus* (1×10^7 CFU/ml), all of the seawater was replaced twice daily. The control group was natural seawater without the addition of *V. parahaemolyticus*.

Three individuals in each treatment were randomly selected at different time points during the infection experiment (0, 3, 6, 12, 24, 48, 96, 120, and 144 h). The hepatopancreas was collected and then frozen in liquid nitrogen for the SOD activity analysis and total RNA isolation.

IFITM1 gene cloning and sequence analysis

The CDS sequence of the *IFITM1* gene was derived from the clam whole-genome sequencing complementary DNA (cDNA) library (Wei et al., 2020). To clone the full-length cDNAs, rapid amplification of cDNA ends PCR (RACE-PCR) was conducted (Ni et al., 2022). The primers required for *IFITM1* gene cloning are shown in Table 1. The *IFITM1* sequence was verified by DNA sequencing and analyzed using the BLAST program (Zhang et al., 2020). The NCBI database was used to predict the ORF of the *IFITM1* gene. Sequence homology retrieval and alignment were also performed. The ExPASy ProtParam program was utilized to predict the molecular weight and isoelectric points of the IFITM1 protein. According to a previous report, multiple sequence alignments were generated and a phylogenetic tree was constructed (Ni et al., 2022).

TABLE 1 Primers used for the cloning of *IFITM1* in *Cyclina sinensis*.

Primer	Sequence (5′–3′)	Sequence information
IFITM1-5GSP	CTTCCGTCTTACGCATACATTCTTC	5′RACE outer amplification primer
IFITM1-5GSP	ACAAGTCTTCCGTCTTACGCATACA	5′RACE outer amplification primer
IFITM1-5NGSP	TCGGCATCATGTCGCTTAATAGTGT	5′RACE inner amplification primer
IFITM1-3GSP	CAACAGGAAGGCAAACGGATAACG	3′RACE outer amplification primer
IFITM1-3GSP	GGCTTCAAATGTTCCTCTTTCACTG	3′RACE outer amplification primer
IFITM1-3NGSP	TTCAAAGACAACAAGGGACAAAGGT	3′RACE inner amplification primer
M13F	GTTGTAAAACGACGGCCAG	Positive clone verification
M13R	CAGGAAACAGCTATGAC	Positive clone verification
UPM-long	CTAATACGACTCACTATAGGGCAAGCAGT GGTATCAACGCAGAGT	RACE-PCR outer layer amplification
NUP	AAGCAGTGGTAACAACGCAGAGT	RACE-PCR inner layer amplification

RACE, rapid amplification of cDNA ends.

Quantitative real-time PCR analysis

To analyze the transcriptional level of *IFITM1* messenger RNA (mRNA), quantitative real-time PCR (qRT-PCR) was carried out with the SYBR method (Ge et al., 2022b). The primers required for qRT-PCR are shown in Table 2. Each sample was in triplicate. The $2^{-\Delta\Delta Ct}$ method was applied to calculate the mRNA transcriptional level with β-actin as the internal control (Ge et al., 2022b).

TABLE 2 Specific primers for the quantitative real-time PCR (qRT-PCR) of *IFITM1* from *Cyclina sinensis*.

Primer	Sequence (5′–3′)	Sequence information
IFITM1—upstream	AAACGCTCATCTTGTCCTTGG	qRT-PCR
IFITM1—downstream	GTCTTCTTCCAGTGGCGGTAT	qRT-PCR
β-actin—upstream	CACCACAACTGCCGAGAG	Reference gene
β-actin—downstream	CCGATAGTGATGACCTGACC	Reference gene

Statistical analysis

Data were analyzed with one-way ANOVA using SPSS. 18 (Ge et al., 2019). Duncan's multiple comparison tests were performed when significant differences were detected in the ANOVA. Difierences were considered statistically significant when $p < 0.05$ (Zhang et al., 2020).

Results

Activity of SOD in the clam exposed to long-term ammonia nitrogen

The SOD activity in the hepatopancreas of *C. sinensis* exposed to ammonia nitrogen first increased and then

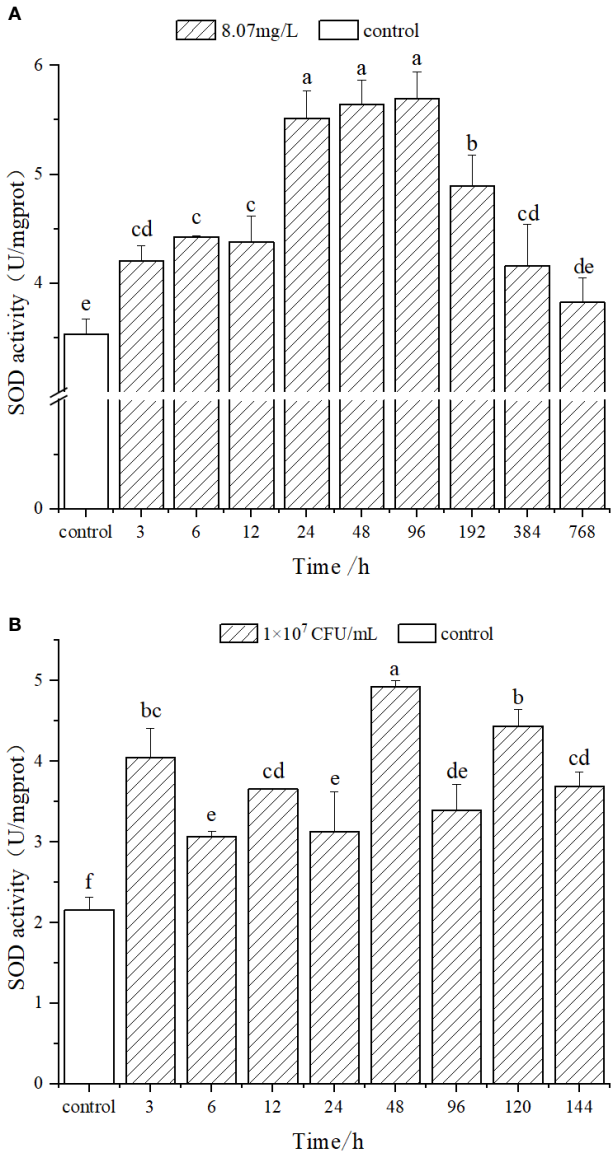

FIGURE 1
Superoxide dismutase (SOD) activity in the hepatopancreas tissue of *Cyclina sinensis* under long-term ammonia. **(A)** SOD activity in *C sinensis* exposed to long-term ammonia. **(B)** SOD activity in *C sinensis* infected with *Vibrio parahaemolyticus*. The control group in **(A)** comprised clams raised in natural seawater. The control group in **(B)** included clams raised in natural seawater without the addition of *V. parahaemolyticus*. The *same lowercase letters* indicate non-significant differences between the different stress time points ($p > 0.05$); otherwise, the difference is significant ($p < 0.05$).

decreased with time (Figure 1A). The SOD activity in the experimental group increased to the maximum value at 96 h. No significant difference was found at 24 and 48 h ($p > 0.05$), whereas the SOD activity was significantly higher than that at other time points ($p < 0.05$). At 768 h, the SOD activity returned to the control group's normal level. Following infection with *V. parahaemolyticus*, the SOD activity fluctuated with time (Figure 1B). The SOD activity from 3 to 144 h in the clams infected with *V. parahaemolyticus* was significantly higher than that in the control group ($p < 0.05$).

Identification of *CsIFITM1*

As shown in Figure 2, the full-length cDNA of *CsIFITM1* was 2,434 bases in length, including a 5′ untranslated region (UTR) of 34 bp and a 3′-UTR of 99 bp with a poly(A) sequence. It contained a 2,301-bp ORF encoding 714 amino acids, with a putative molecular weight of 83.86 kDa and a theoretical isoelectric point of 11.18. The *CsIFITM1* protein contained putative transmembrane domains, but did not contain a signal peptide (Figure 3). Multiple sequence alignment showed that it contained an RNA helicase domain (DEXHc_RLR, DR) located at amino acid residues 70–265 and a Helicase_C (HC) domain located at amino acid residues 468–564 (Figure 4). Phylogenetic analysis showed that *CsIFITM1* formed a cluster with the *IFITM1* of *Mercenaria mercenaria*, *Crassostrea gigas*, *Crassostrea virginica*, *Dreissena polymorpha*, and *Mytilus edulis*, but not with the *IFITM1* of *Haliotis rufescens*, *Haliotis rubra*, and *Pomacea canaliculata* (Figure 5). Expression analysis revealed that the *CsIFITM1* mRNA was constitutively expressed in the adductor muscle, mantle, gill, axon foot, hepatopancreas, and gonad, with higher levels of mRNA detected in the hepatopancreas and the adductor muscle (Figure 6).

CsIFITM1 transcript levels in the hepatopancreas of clams exposed to ammonia nitrogen and *Vibrio* challenge

The transcript levels of *CsIFITM1* in the hepatopancreas of the clams exposed to ammonia nitrogen were determined at different time points after exposure using qRT-PCR (Figure 7A). Exposure to ammonia nitrogen upregulated the transcriptional levels of *CsIFITM1*, which reached the peak at 192 h post-exposure. The expression levels of *CsIFITM1* were significantly higher from 6 to 768 h in clams exposed to ammonia nitrogen than those of the control (0 h) ($p < 0.05$).

Following infection with *V. parahaemolyticus*, the transcript levels of *CsIFITM1* in the hepatopancreas were upregulated (Figure 7B). The transcriptional levels of *CsIFITM1* were also upregulated by *V. parahaemolyticus* infection, which reached the peak at 48 h post-infection. The transcript levels of *CsIFITM1* in clams infected with *V. parahaemolyticus* from 6

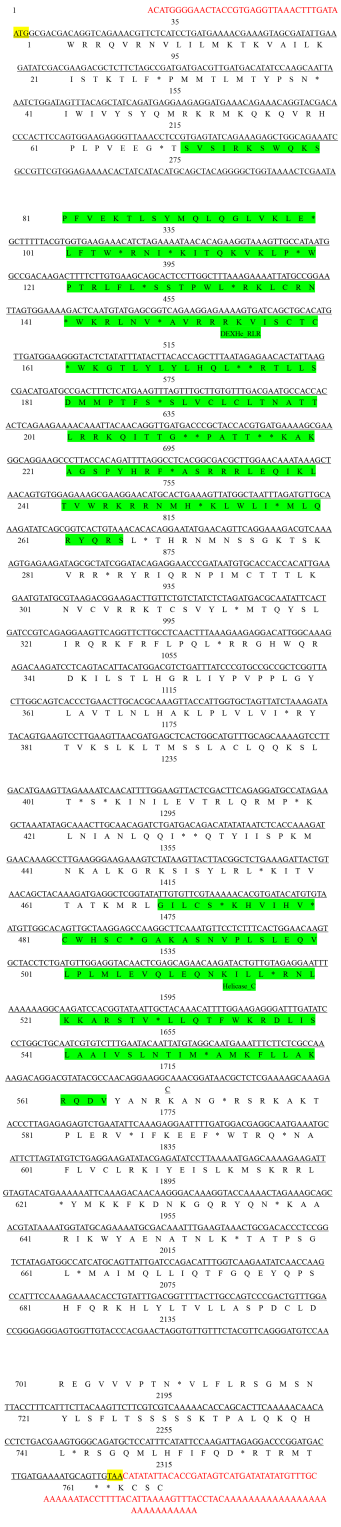

FIGURE 2
The cDNA of *IFITM1* and the deduced amino acid sequence of *Cyclina sinensis*. The *yellow part* indicates the start codon ATG and the stop codon TAA, the *underlined area* indicates the open reading frame (ORF), and the *green part* indicates the conserved domain of *IFITM1*.

FIGURE 3
Prediction of the protein model of *IFITM1*.

to 144 h were significantly higher, in contrast to those of the control (0 h) ($p < 0.05$).

Discussion

The accumulation of ammonia nitrogen in water can ultimately lead to serious oxidative stress (Barbieri and Bondioli, 2013). As one of the key antioxidant enzymes, SOD can reduce oxidative damage (Ge et al., 2021). In the current study, the SOD activity in the hepatopancreas of *C. sinensis* exposed to ammonia nitrogen first increased and then decreased with time. This may be because aquatic animals have to activate antioxidant enzymes in order to deal with oxidative stress (Ni et al., 2022). This result showed that exposure to ammonia nitrogen could activate the SOD in the clam, and activating SOD can reduce the oxidative damage induced by ammonia nitrogen stress. At 768 h, the SOD activity returned to the control group's normal level, which is probably due to the toxicity of the low level of ammonia nitrogen (8.07 mg/L) being low. On the other hand, the 768-h recovery period may have been adequate to compensate for the SOD activity in clams exposed to ammonia nitrogen (Ni et al., 2022). This indicated that the SOD activity in clams exposed to ammonia nitrogen (8.07 mg/L) for 768h could return to normal levels. Bacterial infection can cause serious oxidative stress (Kumar, 2021). In the current study, the SOD activity from 3 to 144 h in the clams infected with *V. parahaemolyticus* was significantly higher than that in the control. This showed that SOD can be activated in clams infected with *V. parahaemolyticus*. The SOD activity in clams infected with *V. parahaemolyticus* for 144 h did not return to the control group's normal level. The reason may be that the bacterial infection may have caused irreparable damage to the antioxidant system, or it could be due to the 144-h recovery time being too short for the recovery of the SOD activity (Ge et al., 2022a).

In the current study, we cloned the *IFITM1* gene from the clam *C. sinensis*. The full-length cDNA of *CsIFITM1* was 2,434 bp in length, including a 2,301-bp ORF encoding 714 amino acids, with a putative molecular weight of 83.86 kDa. The *CsIFITM1* protein possessed putative transmembrane domains, which showed that the protein contained the typical structural features of IFITMs (Wan and Chen, 2008). This indicated that *CsIFITM1* may be a cell surface molecule (Tanaka et al., 2005). As is well known, members of the IFITM family are expressed in various cells in mammals (Bailey et al., 2014). In the present study, the expression analysis showed that, although at a different level, the *CsIFITM1* mRNA was constitutively broadly expressed in all the selected tissues, indicating that the *IFITM1* gene may be widely distributed among tissues and is expressed in various cells in *C. sinensis*. This is probably because immune cells (including leukocytes and lymphocytes) are widely distributed in various tissues (Desai et al., 2017).

The *IFITM1* gene in mammals is induced by IFNs, and the mRNA transcript level of this gene can increase as much as 100-fold upon induction by IFNs (Wan and Chen, 2008). In the present study, the transcript levels of *CsIFITM1* were upregulated by exposure to ammonia nitrogen and were

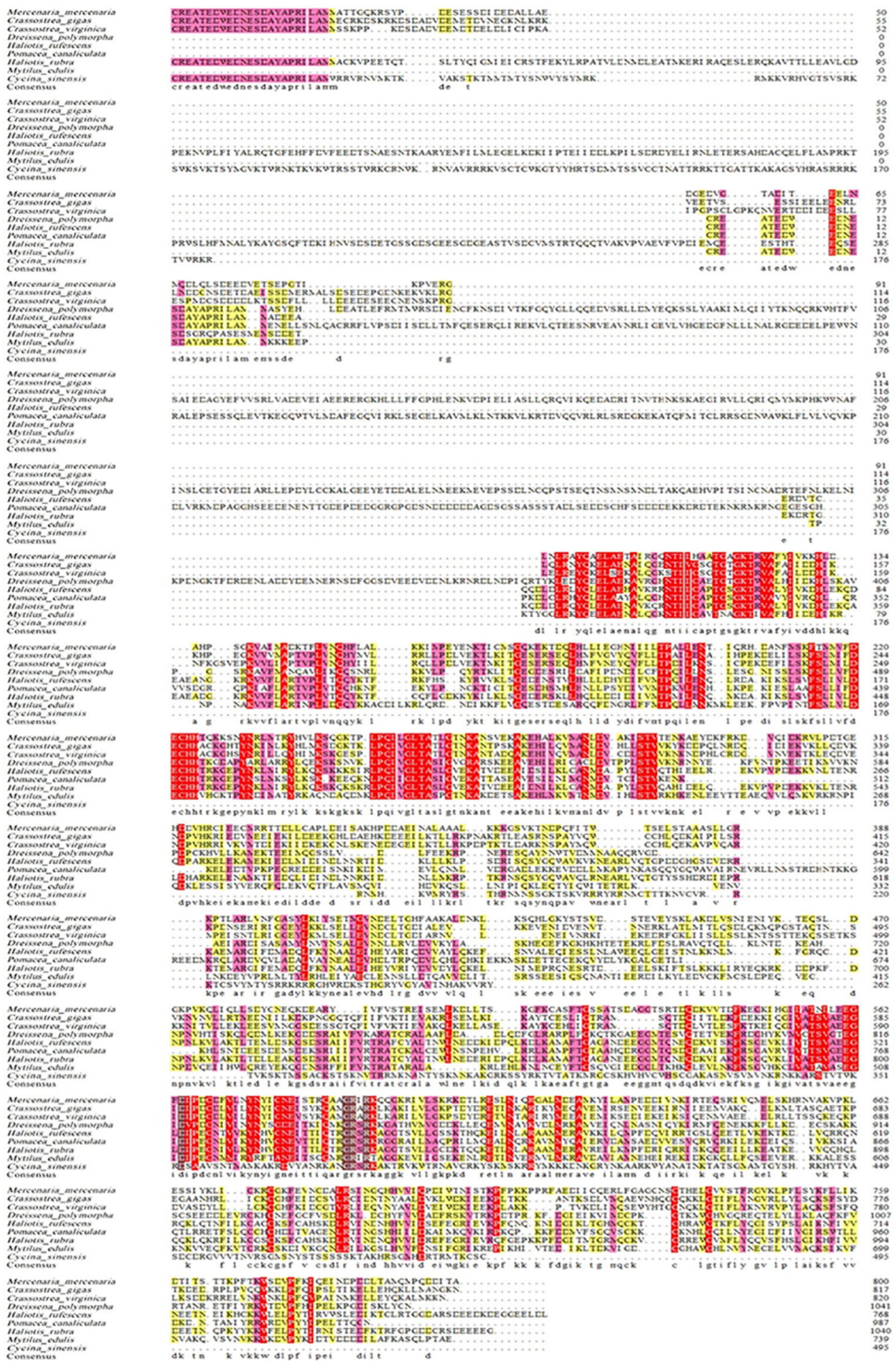

FIGURE 4
Alignment of the *IFITM1* amino acids from *Cyclina sinensis* and other species. All *shaded regions* represent residues sharing homology. The *light red regions* represent homology above 75%, while the *dark red regions* represent 100% homology. *Dots* denote amino acid deletion.

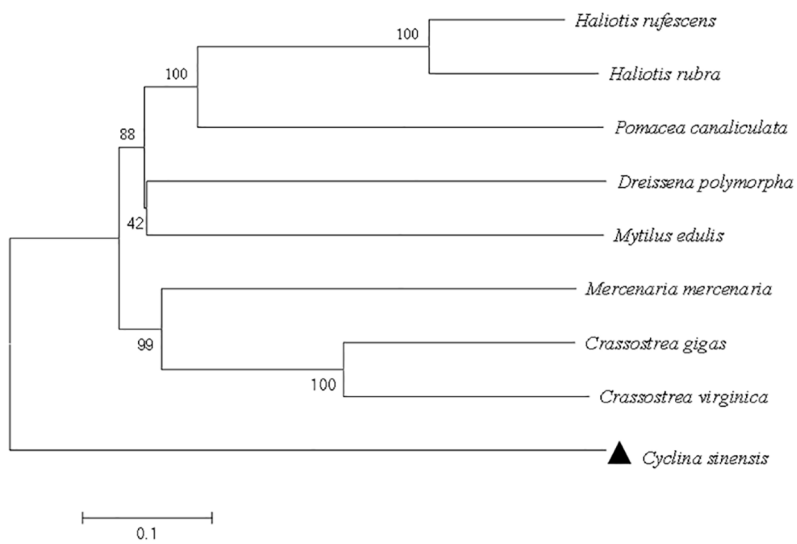

FIGURE 5
Phylogenetic tree derived from multiple alignment of the *IFITM1* amino acids from *Cyclina sinensis* and other species.

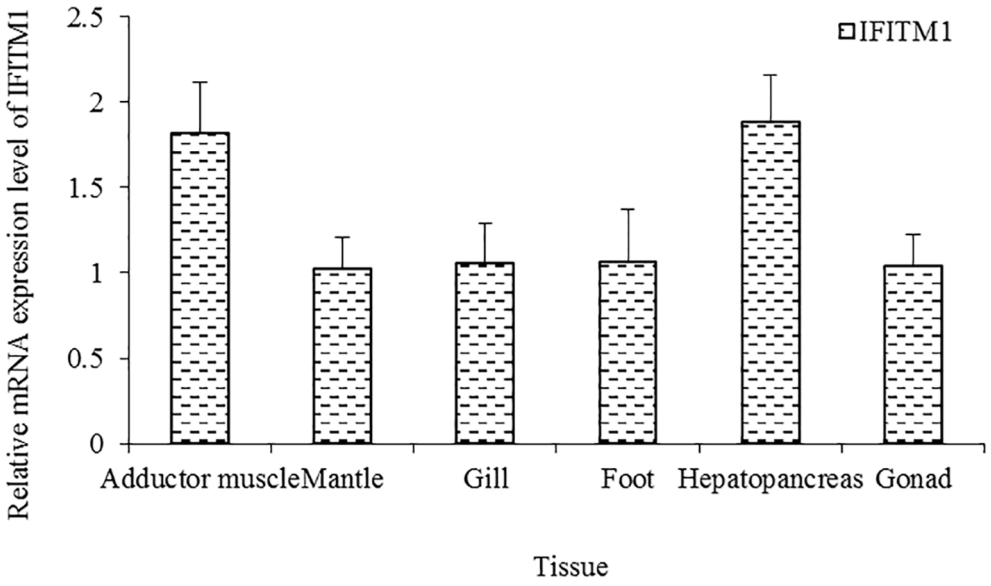

FIGURE 6
Expression of the *IFITM1* gene in various tissues of *Cyclina sinensis*.

significantly higher from 6 to 768 h in the clams exposed to ammonia nitrogen compared to the control. This result indicated that the gene expression of *CsIFITM1* could be induced by ammonia nitrogen stress. This is probably because ammonia nitrogen exposure can stimulate the *CsIFITM1* gene (Tanaka et al., 2005) or induce IFNs (Zou et al., 2005). Following infection with *V. parahaemolyticus*, the transcript levels of *CsIFITM1* in hepatopancreas were upregulated, indicating that the gene expression of *CsIFITM1* can be induced by infection with *V. parahaemolyticus*, suggesting that the *CsIFITM1* gene may be involved in the immune response of *C. sinensis*. This observation is consistent with the reported role of *IFITM* in the large yellow croaker (*Larimichthys crocea*), which can be stimulated by *Vibrio alginolyticus* (Zhang et al., 2021).

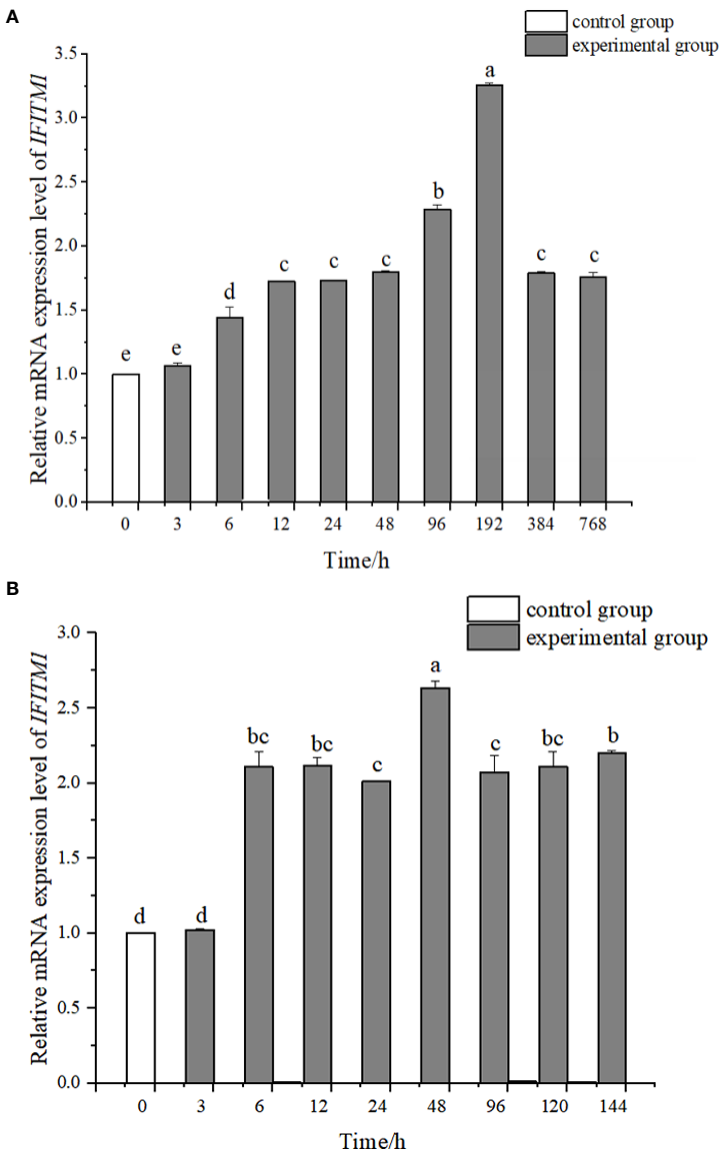

FIGURE 7
Expression of the *IFITM1* gene in the hepatopancreas tissue of *Cyclina sinensis*. **(A)** Gene expression in *C sinensis* exposed to long-term ammonia. **(B)** Gene expression in *C sinensis* infected with *Vibrio parahaemolyticus*. *Different letters in the column* indicate significant difference ($p < 0.05$).

In summary, exposure to ammonia nitrogen can activate the SOD in the clam, and activating SOD can reduce the oxidative damage induced by ammonia nitrogen stress. Furthermore, infection with *V. parahaemolyticus* may cause irreparable damage to the antioxidant system. The *IFITM1* gene from *C. sinensis* was cloned, and the *CsIFITM1* mRNA was broadly expressed in all the tissues selected. The *CsIFITM1* protein possessed the typical structural features of members of the IFITM family. The gene expression of *CsIFITM1* can be induced by ammonia nitrogen stress and *V. parahaemolyticus* infection.

Data availability statement

The original contributions presented in the study are included in the article/supplementary material. Further inquiries can be directed to the corresponding authors.

Author contributions

HG: Conceptualization, methodology, and writing—review and editing. QN: Formal analysis and writing—original draft. JL: Software, validation, and investigation. ZD: Project administration, conceptualization, and funding acquisition. SC: Investigation. All authors contributed to the article and approved the submitted version.

Funding

This research was supported by the earmarked fund for CARS (CARS-49); The "JBGS" Project of Seed Industry Revitalization in Jiangsu Province (JBGS[2021]034); China's National Key Research and Development Projects (2019YFD0900403); Open-End Funds of Jiangsu Key Laboratory of Marine Bioresources and Environment (SH20211209); Jiangsu Agricultural Science and technology Independent Fund (CX(20)3150); and the Priority Academic Program Development of Jiangsu. The funding bodies played a key role in the design of the study, the collection, analysis, and interpretation of data, and in the writing of the manuscript.

Conflict of interest

The authors declare that the research was conducted in the absence of any commercial or financial relationships that could be construed as a potential conflict of interest.

Publisher's note

All claims expressed in this article are solely those of the authors and do not necessarily represent those of their affiliated organizations, or those of the publisher, the editors and the reviewers. Any product that may be evaluated in this article, or claim that may be made by its manufacturer, is not guaranteed or endorsed by the publisher.

References

Bailey, C., Zhong, G., Huang, I. C., and Farzan, M. (2014). IFITM-family proteins: the cell's first line of antiviral defense. *Annu. Rev. Virol.* 1, 261–283. doi: 10.1146/annurev-virology-03141-085537

Baird, J., Ryan, K., Hayes, I., Hampson, L., Heyworth, C., Clark, A., et al. (2001). Differentiating embryonal stem cells are a rich source of haemopoietic gene products and suggest erythroid preconditioning of primitive haemopoietic stem cells. *J. Biol. Chem.* 276, 9189–9198. doi: 10.1074/jbc.M008354200

Barbieri, E., and Bondioli, A. C. V. (2013). Acute toxicity of ammonia in pacu fish (*Piaractus mesopotamicus*, holmberg 1887) at different temperatures levels. *Aquac. Res.* 46, 565–571. doi: 10.1111/are.12203

Barbieri, E., Lenz, R. M., de Nascimento, A. A., de Almeida, G. L., Roselli, L. Y., and Henriques, M. B. (2019). Lethal and sublethal effects of ammonia in *Deuterodon iguape* (Eigenmann 1907), potential species for brazilian aquaculture. *Bol. Inst. Pesca* 45, 1–7. doi: 10.20950/1678-2305.2019.45.1.440

Chai, Y., Peng, R., Jiang, M., Jiang, X., Han, Q., and Han, Z. (2022). Effects of ammonia nitrogen stress on the blood cell immunity and liver antioxidant function of *Sepia pharaonic*. *Aquaculture* 546, 737417. doi: 10.1016/j.aquaculture.2021.737417

Chen, Y., Li, H., Ding, H., Dong, Z., and Li, J. (2021). Heritability estimation and path analysis for growth traits of the razor clam sinonovacula constricta under high salinity. *Aquaculture* 545, 737175. doi: 10.1016/j.aquaculture.2021.737175

Debbarma, R., Biswas, P., and Singh, S. (2021). An integrated biomarker approach to assess the welfare status of *Ompok bimaculatus* (Pabda) in biofloc system with altered C/N ratio and subjected to acute ammonia stress. *Aquaculture* 545, 737184. doi: 10.1016/j.aquaculture.2021.737184

Desai, T., Marin, M., Mason, C., and Melikyan, G. (2017). pH regulation in early endosomes and interferon-inducible transmembrane proteins control avian retrovirus fusion. *J. Biol. Chem.* 292 (19), 7817–7827. doi: 10.1074/jbc.M117.783878

Egnew, N., Renukdas, N., Ramena, Y., Yadav, A. K., Kelly, A. M., Lochmann, R. T., et al. (2019). Physiological insights into largemouth bass (*Micropterus salmoides*) survival during long-term exposure to high environmental ammonia. *Aquat. Toxicol.* 207, 72–82. doi: 10.1016/j.aquatox.2018.11.027

Ge, H., Liang, X., Liu, J., Cui, Z., Guo, L., Li, L, et al. (2021). Effects of acute ammonia exposure on antioxidant and detoxification metabolism in clam *Cyclina sinensis*. ecotox. *Environ. Safe.* 211, 111895. doi: 10.1016/j.ecoenv.2021.111895

Ge, H., Liu, J., Ni, Q., Wang, F., and Dong, Z. (2022a). Effects of acute ammonia exposure and post-exposure recovery on nonspecific immunity in clam *Cyclina sinensis*. isr. *J. Aquacul. Bamid.* 74, 1552688. doi: 10.46989/001c.32647

Ge, H., Ni, Q., Li, J., Li, J., Chen, Z., and Zhao, F. (2019). Integration of white shrimp (*Litopenaeus vannamei*) and green seaweed (*Ulva prolifera*) in minimum-water exchange aquaculture system. *J. Appl. Phycol.* 31 (1), 1425–1432. doi: 10.1007/s10811-018-1601-4

Ge, H., Shi, J., Liu, J., Guo, L., and Dong, Z. (2022b). Combined analysis of mRNA-miRNA reveals the regulatory roles of miRNAs in the metabolism of clam *Cyclina sinensis* hepatopancreas during acute ammonia nitrogen stress. *Aquacul. Res.* 53 (4), 1492–1506. doi: 10.1111/are.15683

Ghelichpour, M., Mirghaed, A., Hoseinifar, S., Khalili, M., Yousefid, M., Doan, H., et al. (2019). Expression of immune, antioxidant and stress related genes in different organs of common carp exposed to indoxacarb. *Aquat. Toxicol.* 208, 208–216. doi: 10.1016/j.aquatox.2019.01.011

Johnson, M., Sangrador-Vegas, A., Smith, T., and Cairns, M. (2006). Cloning and characterization of two genes encoding rainbow trout homologues of the IFITM protein family. *Vet. Immunol. Immunop.* 110, 357–362. doi: 10.1016/j.vetimm.2005.12.007

Kumar, N. (2021). Dietary riboflavin enhances immunity and anti-oxidative status against arsenic and high temperature in *Pangasianodon hypophthalmus*. *Aquaculture* 533, 736209. doi: 10.1016/j.aquaculture.2020.736209

Liao, X., Sun, Z., Cui, Z., Yan, S., Fan, S., Xia, Q., et al. (2022). Effects of different sources of diet on the growth, survival, biochemical composition and physiological metabolism of clam (*Cyclina sinensis*). *Aquacul. Res.* 53 (10), 3797–3806. doi: 10.1111/are.15886

Mangang, Y., and Pandey, P. (2021). Hemato-biochemical responses and histopathological alterations in the gill and kidney tissues of *Osteobrama belangeri* (Valencienne) exposed to different sub-lethal unionized ammonia. *Aquaculture* 542, 736887. doi: 10.1016/j.aquaculture.2021.736887

Ni, Q., Li, W., Jia, X., Dong, Z., and Ge, H. (2020). Effect of salinity on growth performance and resistance of the clam *Cyclina sinensis* against *Vibrio parahaemolyticus* infection. *Isr. J. Aquacul. Bamid.* 72, 1124924. doi: 10.46989/IJA.72.2020.1124924

Ni, Q., Li, W., Liang, X., Liu, J., Ge, H., and Dong, Z. (2021). Gill transcriptome analysis reveals the molecular response to the acute low-salinity stress in *Cyclina sinensis*. *Aquaculture Rep.* 19, 100564. doi: 10.1016/j.aqrep.2020.100564

Ni, Q., Wang, D., Xie, L., Ge, H., and Dong, Z. (2022). Unraveling the characterization of hypoxia-inducible factor-1α (*HIF-1α*) and antioxidant enzymes in clam *Cyclina sinensis* in response to hypoxia. *Aquaculture Res.* 16062. doi: 10.1111/are.16062

Silva, M. J., Dos, S., Da Costa, F. F. B., Leme, F. P., Takata, R., Costa, D. C., et al. (2018). Biological responses of neotropical freshwater fish lophiosilurus alexandri exposed to ammonia and nitrite. *Sci. Total Environ.*, 616-617, 1566–1575. doi: 10.1016/j.scitotenv.2017.10.157

Sinha, A. K., Zinta, G., AbdElgawad, H., Asard, H., Blust, R., and De Boeck, G. (2015). High environmental ammonia elicits differential oxidative stress and antioxidant responses in five different organs of a model estuarine teleost (*Dicentrarchus labrax*). *Comp. Biochem. Physiol. C* 174, 21–31. doi: 10.1016/j.cbpc.2015.06.002

Tanaka, S. S., Yamaguchi, L., Tsoi, B., Lickert, H., and Tam, P. P. L. (2005). IFITM/Mil/Fragilis family proteins IFITM1 and IFITM3 play distinct roles in mouse primordial germ cell homing and repulsion. *Dev. Cell* 9, 745–756. doi: 10.1016/j.devcel.2005.10.010

Wan, X., and Chen, X. (2008). Molecular cloning and expression analysis of interferon-inducible transmembrane protein 1 in large yellow croaker *Pseudosciaena crocea*. vet. *Immunol. Immunop.* 124, 99–106. doi: 10.1016/j.vetimm.2008.01.004

Wei, M., Ge, H., Shao, C., Yan, X., Nie, H., Duan, H., et al. (2020). Chromosome-level genome assembly of the Venus clam, *Cyclina sinensis*, helps to elucidate the molecular basis of the adaptation of buried life. *iScience* 23 (6), 101148. doi: 10.1016/j.isci.2020.101148

Zhang, Y., Huang, Y., Wang, L., Huang, L., Zheng, J., Huang, X., et al. (2020). Grouper interferon-induced transmembrane protein 3 (IFITM3) inhibits the infectivity of iridovirus and nodavirus by restricting viral entry. *Fish Shellfish Immun.* 104, 172–181. doi: 10.1016/j.fsi.2020.06.001

Zhang, W., Zhu, C., Chi, H., Liu, X., Gong, H., Xie, A., et al. (2021). Early immune response in large yellow croaker (*Larimichthys crocea*) after immunization with oral vaccine. *Mol. Cell. Prob.* 56, 101708. doi: 10.1016/j.mcp.2021.101708

Zhu, R., Wang, J., Lei, X., Gui, J., and Zhang, Q. (2013). Evidence for *Paralichthys olivaceus* IFITM1 antiviral effect by impeding viral entry into target cells. *Fish Shellfish Immun.* 35, 918–926. doi: 10.1016/j.fsi.2013.07.002

Zou, J., Carrington, A., Collet, B., Dijkstra, J. M., Yoshiura, Y., Bols, N., et al. (2005). Identification and bioactivities of IFN-gamma in rainbow trout (*Oncorhynchus mykiss*): the first Th1-type cytokine characterized functionally in fish. *J. Immunol.* 175 (4), 2484–2494. doi: 10.4049/jimmunol.175.4.2484

Zuffo, T., Durigon, E., Morselli, M., Picoli, F., Folmannd, S., Kinas, J., et al. (2021). Lethal temperature and toxicity of ammonia in juveniles of curimbatá (*Prochilodus lineatus*). *Aquaculture* 545, 737138. doi: 10.1016/j.aquaculture.2021.737138

frontiers | Frontiers in Marine Science

TYPE Original Research
PUBLISHED 10 January 2023
DOI 10.3389/fmars.2022.1031977

OPEN ACCESS

EDITED BY
Zulin Zhang,
The James Hutton Institute,
United Kingdom

REVIEWED BY
Tania Islas-Flores,
National Autonomous University of Mexico, Mexico
William Fitt,
University of Georgia, United States

*CORRESPONDENCE
Samir M. Aljbour
Samir.aljbour@kaust.edu.sa

SPECIALTY SECTION
This article was submitted to Marine Biology, a section of the journal Frontiers in Marine Science

RECEIVED 30 August 2022
ACCEPTED 14 December 2022
PUBLISHED 10 January 2023

CITATION
Aljbour SM, Alves RN and Agustí S (2023) Aerobic respiration, biochemical composition, and glycolytic responses to ultraviolet radiation in jellyfish *Cassiopea* sp. *Front. Mar. Sci.* 9:1031977. doi: 10.3389/fmars.2022.1031977

Aerobic respiration, biochemical composition, and glycolytic responses to ultraviolet radiation in jellyfish *Cassiopea* sp

Samir M. Aljbour*, Ricardo N. Alves and Susana Agustí

Red Sea Research Center (RSRC), King Abdullah University of Science and Technology (KAUST), Thuwal, Saudi Arabia

The light-dependent zooxanthellate jellyfish *Cassiopea* sp. (the upside-down jellyfish) is invasive/exotic in many shallow and clear marine habitats, where the jellyfish might be exposed to high levels of ultraviolet radiation (UVR). Compared to other reef organisms, the sensitivity/resilience of the semi-transparent jellyfish to UVR exposure is overlooked. Therefore, we experimentally investigated the metabolic and physiological responses of *Cassiopea* sp. from the Red Sea to natural levels of underwater UVR following 16 days of exposure to three light treatments: 1) control group with only photosynthetically active radiation (PAR), 2) PAR+UV-B, and 3) PAR+UV-B +UV-A. While jellyfish body mass increased (by 40%) significantly in the control group, it did not increase in either of the UV treatments. However, both UV-exposed jellyfish had higher (98% to 120%) mitochondrial electron transport system (ETS) activity than the control group. Therefore, the results indicate elevated aerobic respiration rates in UV-exposed jellyfish (i.e., reflecting a higher energy cost of UVR exposure). Neither the lactate dehydrogenase (LDH) activity nor the available energy (*Ea*) exhibited different levels among UVR treatments compared to the control group. In contrast, pyruvate kinase activity was significantly lower (by 46%) in all UV-exposed jellyfish compared to the control group. Unchanged *Ea* and LDH activity combined with higher ETS activity indicates a high aerobic capacity of jellyfish, which might explain their ability to cope with UVR exposure-induced higher energy demands without inducing the onset of anaerobiosis. The results indicated that UV-A does not amplify or modulate jellyfish physiology and growth under UV-B exposure. In conclusion, the findings suggest that the jellyfish is more resilient (i.e., in terms of survival) to UVR than other cnidarians. This study on *Cassiopea* is the first to address its metabolic and physiological responses to UVR. Therefore, it could be used as a framework for further studies aiming to better understand jellyfish physiology.

KEYWORDS

jellyfish, *Cassiopea* sp., mitochondrial respiration, pyruvate kinase, lactate dehydrogenase, energy allocation, medusae, anaerobic respiration

1 Introduction

The upside-down jellyfish (genus *Cassiopea*) has displayed signs of being exotic/invasive in many shallow marine coastal systems (Nabipour et al., 2015; Özbek and Oztürk, 2015; Thé et al., 2021). Unlike many other jellyfish, *Cassiopea* sp. is epibenthic and has symbiotic dinoflagellates (endosymbiont algae). This peculiarity (i.e., association with photosynthetic dinoflagellates) is shared with few other jellyfish (e.g. *Linuche unguiculata* and *Mastigias* sp.; Kremer et al., 1990; McCloskey et al., 1994). Therefore, it is a photosynthetic mixotrophic cnidarian, analogous to coral. Thus, *Cassiopea* sp. requires sufficient doses of photosynthetically active radiation (PAR) to grow optimally. Depending on light availability, the jellyfish might act as a functional photoautotroph (Cates, 1975; Verde and McCloskey, 1998), where it gains most of energy needs from photosynthesis. In *Cassiopea*, the symbiotic dinoflagellates live in oral arm and the bell, and can reach high densities (i.e., 1.52×10^6 to 2.68×10^6 cells mg^{-1} protein; Verde and McCloskey, 1998). These symbionts synthesize mycosporine-like amino acids (MAAs) and transport them to the host, protecting the holobiont from excessive ultraviolet radiation (UVR) in shallow water habitats (Banaszak and Trench, 1995). Furthermore, *Cassiopea* has a special photoprotective dimeric protein pigment known as Cassio Blue (Blanquet and Phelan, 1987; Phelan et al., 2005). While this pigment allows the passage of PAR, it shields against the damaging solar radiation (Blanquet and Phelan, 1987; Phelan et al., 2005). In coral reefs, the jellyfish plays critical roles in food web and nutrient cycling and the food web (Jantzen et al., 2010; Niggl et al., 2010; Zarnoch et al., 2020). Furthermore, *Cassiopea* medusae are mass-cultured as food for medusivores in captivity in aquaculture industry (Pierce, 2005). The jellyfish usually prefers calm and shallow marine habitat such as mangrove forest and lagoons, however, it is also common in shallow seagrass beds and coral reefs (Fleck and Fitt, 1999; Arai, 2001; Todd et al., 2006; Niggl and Wild, 2009; Jantzen et al., 2010). *Cassiopea*, temporarily, fixes its bell to the substrate (i.e., in an upside-down orientation) with help of its beating motion and mucus (Gohar and Eisawy, 1960). This unusual orientation maximizes the exposure of the symbiotic dinoflagellates to light for proper photosynthesis.

In general, scyphozoans grow rapidly and die en masse (Pitt et al., 2009). Therefore, jellyfish blooms are usually associated with the rapid release of massive amounts of organic matter, which could, temporally and spatially, change the physical and biological properties of confined water bodies (Pitt et al., 2009; Tinta et al., 2016). Jellyfish's feeding menu varies, ranging from zooplankton to fish and their larvae (Breitburg et al., 1997; Mills, 2001). Scyphozoans are generally known to be robust and tolerate wild range of environmental stresses, such as temperature and pollutants (Aljbour et al., 2018; Aljbour et al., 2019). Furthermore, global warming and anthropogenic activities (e.g. eutrophication and coastal constructions) are proposed as the main drivers of jellyfish blooms (Arai, 2001; Mills, 2001; Purcell, 2005; Aljbour et al., 2018; Aljbour et al., 2019).

The subtropical Red Sea marine ecosystem, like most subtropical and tropical ecosystems, is oligotrophic and characterized by highly transparent waters due to low concentrations of ultraviolet radiation (UVR)-absorbing substances in the water column (Kheireddine et al., 2017; Overmans and Agustí, 2019). Furthermore, this ecosystem receives intense incident solar and UVR (Khogali and Al-Bar, 1992). Moreover, Overmans and Agustí (2020) demonstrated that UVR deeply penetrates the Red Sea water in moderately high doses, even at depths of 3 to 5 m. Therefore, marine organisms living in the shallow waters of this area are usually overexposed to harmful doses of UVR (Overmans and Agustí, 2019).

The UVR reaching the sea surface may represent, depending on the location, about the 6% of the incident solar radiation and is distributed in ~95% and ~5% in the UVR A (UV-A, 315 to 400 nm) and UVR B (UV-B, 280 to 315 nm) bands, respectively (Moan, 2001). Furthermore, UV-B and UV-A differ markedly in biological activity, water penetration, abundance in solar radiation, energy content, and damaging effects. While UV-B has significantly less penetration underwater, it has more damaging effects due to the higher energy content of its shorter wavelengths compared to UV-A. Moreover, UV-B is one of the most potent agents that adversely affect cellular homeostasis and genomic stability by inducing a variety of cytotoxic DNA lesions (Rastogi et al., 2010) and triggering reactive oxygen species (ROS) formation (Lesser, 1996; Lesser and Farrell, 2004; Lu and Wu, 2005). In contrast, UV-A, which is less damaging but more abundant than UV-B (i.e., 10 to 100 times more; Moan, 2001), contributes in activating the photoreactivation enzymes to repair UVR-damaged DNA (Hearst, 1995; Sancar, 1996; Rastogi et al., 2010).

Therefore, organisms have developed a variety of highly conserved defensive repair mechanisms to counteract the deleterious DNA-damaging effects of UVR. For example, the synthesis or acquisition of photoprotective UV-B-absorbing pigments (e.g., carotenoid, melanin, and mycosporine-like amino acids; Roy, 2000; Rossbach et al., 2020), and the evolution of DNA repair mechanisms such as base excision repair, and photoreactivation (using photolyases "alternatively called photoenzymes"; Sinha and Häder, 2002; Rastogi et al., 2010). In DNA, cyclobutane pyrimidine dimers (CPDs) and pyrimidine (6–4) pyrimidone photoproducts (6–4PPs) are the two major classes of UVR induced DNA helix distorting lesions (Sancar, 1996). DNA photoreactivating phosphorylases contain chromophores (i.e., as light harvesting antenna) and flavin adenine dinucleotide (FAD) molecule as a catalytic cofactor (Thoma, 1999). Interestingly, photolyases binds to UVR-

damaged DNA and make use of light in the range of 350-450 nm (i.e., near UV-A and blue light) as an energy source to split the cyclobutane ring of CPDs, restoring the altered nucleotides to their native form (Hearst, 1995; Sancar, 1996). In nature, organisms exposed to UV-B are also exposed to UV-A and blue light. Thus while UVR (mainly UV-B) could cause DNA damage, the co-exposure to UV-A and blue light activate photoreactivating enzymes, alleviating the harmful impacts of shorter UVR to certain extent (Hearst, 1995; Sancar, 1996). Nevertheless, the ability of organisms to tolerate UVR varies considerably across various life stages, taxonomic groups, and prevailing environmental conditions (Alves et al., 2021; Alves et al., 2020; Leech and Williamson, 2000; Bancroft et al., 2007).

Compared to UV-A, UV-B has received more attention and is recognized to be harmful to the majority of marine animals, including fish and benthic invertebrates (Lesser, 1996; Häder et al., 2011; Torres-Pérez and Armstrong, 2012; Häder et al., 2015; Donner et al., 2017; Nordborg et al., 2021). Furthermore, the detrimental effects of UV-B are usually dose-dependent (Alves and Agustí, 2020). For example, *Stylophora pistillata* coral exhibited photoinhibition (Winters et al., 2003) and DNA breakages (Baruch et al., 2005) following UV-B exposure at levels comparable to those received at <5 m depths in the Red Sea. Furthermore, UV-B induced oxidative stress and cell death in the host tissue of shallow water coral while impairing the photosynthesis in symbiotic dinoflagellates and resulting in reduced fecundity of the holobiont (Lesser, 1996; Lesser and Farrell, 2004; Torres-Pérez and Armstrong, 2012). In sea urchins, 30 min of exposure to UV-A negatively affected sperm motility and fertilization and induced ROS production (Lu and Wu, 2005). According to Rijstenbil (2001), 4 h of daily exposure to UV-A for 4 weeks significantly increased superoxide dismutase and caused lipid peroxidation in *Ditylum brightwellii* diatoms. In *Caenorhabditis elegans* nematodes, UV-A triggered photoaging in DAF-16 dependent pathway (Prasanth et al., 2016). In contrast, in coral larvae and *Symbiodiniaceae*, UV-A alleviated the adverse effects of UV-B on photosynthesis (Zhou et al., 2016). The variation in UV sensitivity/tolerance in organisms could imply important consequences for community and ecosystem responses to the present and future predicted levels of UVR (associated with climate change and the stratospheric ozone depletion; Anderson et al., 2012).

In animal physiology, the onset of anaerobic metabolism indicates energy stress (i.e., elevated energy demand beyond organismal aerobic capacity; Bagwe et al., 2015). Therefore, transition to anaerobiosis is crucial to cope with accelerated energy demands under stressful conditions (Pörtner, 2002). Under normal physiological conditions (i.e., sufficient oxygen supply and undisturbed homeostasis), aerobic mitochondrial ATP production is sufficient to meet cellular energy requirements. Aerobic respiration is the primary and most efficient pathway of ATP synthesis in the animal kingdom. The maximum aerobic respiration potential (i.e., that supported by the existing enzymatic machinery) is estimated by measuring the activity of the mitochondrial electron transport system (ETS) in organisms carrying out aerobic respiration (Packard, 1971; Owens and King, 1975).

In contrast, anaerobic metabolism could be estimated by measuring the activity of pyruvate kinase (PK) and lactate dehydrogenase (LDH; Hochachka et al., 1983). In most animals, PK and LDH are the two primary enzymes controlling the glycolysis rate. In addition, PK mediates the conversion of phosphoenolpyruvate and ADP to pyruvate and ATP. Therefore, it sits at the crossroads between anabolism and catabolism of glucose carbons (Mazurek et al., 2002). In contrast, LDH channels pyruvate into anaerobic metabolism to maintain a sustained supply of ATP under anoxic/hypoxic conditions. Furthermore, the enzyme is a universally used biomarker of anaerobiosis because it correlates well with cellular anaerobic capacity (Hochachka et al., 1983).

There is little information on the effect of UV-B and UV-A radiation on the metabolic rate and biochemical composition of *Cassiopea* jellyfish. However, few studies investigated the effect of UVR on MAA synthesis by symbiotic dinoflagellates in *Cassiopea* (Banaszak and Trench, 1995), and scyphistomae proliferation and survival (Klein et al., 2016). While Banaszak and Trench (1995) demonstrated an elevated synthesis of MAA in symbiotic *Cassiopea* in response to UVR, Klein et al. (2016) found that UV-B adversely affected the scyphistomae health and survival. Nevertheless, both studies did not address differential effects of UV-A and UV-B on the metabolic rate and biochemical composition of *Cassiopea* medusae. In general, some jellyfish are robust and tolerant of many environmental disturbances. For example, the jellyfish acclimated well under high temperatures (32°C) incubations (Aljbour et al., 2017; Aljbour et al., 2018). Furthermore, the jellyfish were abundant in polluted areas with no signs of oxidative stress (Aljbour et al., 2018).

This study aims to develop a better understanding of the metabolic and physiological performance of *Cassiopea* at the cellular level in response to UVR. Therefore, we asked the following questions: Does UVR (i.e., UV-B alone and UV-B +UV-A combined) affect aerobic respiration and glycolytic potential in jellyfish? Do the defined conditions of UVR in this experiment affect the survival and growth of jellyfish? Do the UVR doses used in this experiment induce changes in available energy (*Ea*) resources (i.e., carbohydrates, lipids, and proteins)? Finally, does UV-A affect or modulate the jellyfish response to UV-B under the defined conditions in this experiment?

To answer these questions, we measured the activity of PK and LDH (i.e., the key regulatory enzymes of glycolysis), ETS activity (i.e., a proxy to evaluate the aerobic cellular respiration), and the total content of carbohydrates, lipids, and proteins to evaluate the available energy (*Ea*) in jellyfish. Therefore, we exposed *Cassiopea* sp. Medusae to three different light scenarios (i.e., PAR only as a control treatment, PAR + UV-B treatment,

and PAR +UV-B and UV-A treatment) to investigate the differential effects of UV-B and UV-A on jellyfish. Overall, this is the first study on *Cassiopea* of its kind that rigorously addresses the metabolic and physiological performance of *Cassiopea* at the cellular level in response to UVR.

2 Materials and methods

2.1 Experimental animals

Medusae of *Cassiopea* sp. jellyfish were collected by gently scooping them (using a bucket) from shallow water at King Abdullah University of Science and Technology (KAUST) in August and September 2021. We immediately transferred the jellyfish to the aquarium facilities in the Coastal and Marine Resources Core Lab (CMR, in KAUST). In CMR, we maintained the jellyfish in a 300 L temperature-controlled (27.5 ± 0.7°C) aquarium tank supplied with filtered seawater (20 µm, salinity: 40.5 ± 0.5‰) until the commencement of the experiment in November 2021. The aquarium was lighted with PAR using radion light-emitting diodes (EcoTech Marine, USA) on a 12 h/12 h light/dark cycle. The PAR intensity ranged from 500 µmol·m^{-2}·s^{-1} (high PAR) at the water surface to 171 µmol·m^{-2}·s^{-1} (low PAR) at the aquarium bottom (water depth = 0.40 m). Three days before starting the experiment, we carefully selected 20 jellyfish and kept them at a depth of 0.10 m in a perforated tray in the same aquarium (i.e., receiving an average of 370 µmol·m^{-2}·s^{-1}; refer to Figure 1). We applied the selection criteria used by (Aljbour et al., 2017; Aljbour et al., 2019) to ensure that the selected jellyfish were morphologically healthy (i.e., no lost arms, pitched umbrella, or perforated bells). One day before the experiment (Day 0), we measured jellyfish size parameters (i.e., bell diameter = 3.5 ± 0.3 cm, wet body mass (WM) = 5.0 ± 0.5 g) to avoid putting extra stress on the organism on Day 1 of the experiment. The jellyfish bell diameter and body mass were measured according to the protocol used by (Aljbour et al., 2017; Aljbour et al., 2019).

2.2 UVR exposure

To investigate jellyfish responses to UV-B alone and highlight the role of UV-A in jellyfish responses to UV-B, we ran three UV-exposure treatments (refer to Figure 1). Treatment 1 was the control, alternatively called the PAR treatment. In this treatment (N = 8), jellyfish were only exposed to PAR (average intensity of 460 µmol·m^{-2}·s^{-1}; ca. 25% of natural PAR at sea surface) for 12 h a day on a 12 h/12 h light/dark cycle using radion light-emitting diodes (EcoTech Marine, USA). The PAR lights were automatically switched on at 6:00 am and off at 6:00 pm. Treatment 2 was the UV-AB treatment (i.e., UVA+UVB). In this treatment (N = 6), in addition to PAR exposure, the jellyfish were exposed to UV-A using Philips TL20W/12RS UV-B and UV-A broadband lamps (average intensity = 4.0 ± 0.5 W·m^{-2}; dose = 143 ± 19 kJ·m^{-2}·d^{-1}) on a 10 h/14 h light/dark photoperiod and to UV-B (average intensity = 0.18 ± 0.03 W·m^{-2}; dose = 3.9 ± 0.6 kJ·m^{-2}·d^{-1}) on a 6 h/16 h light/

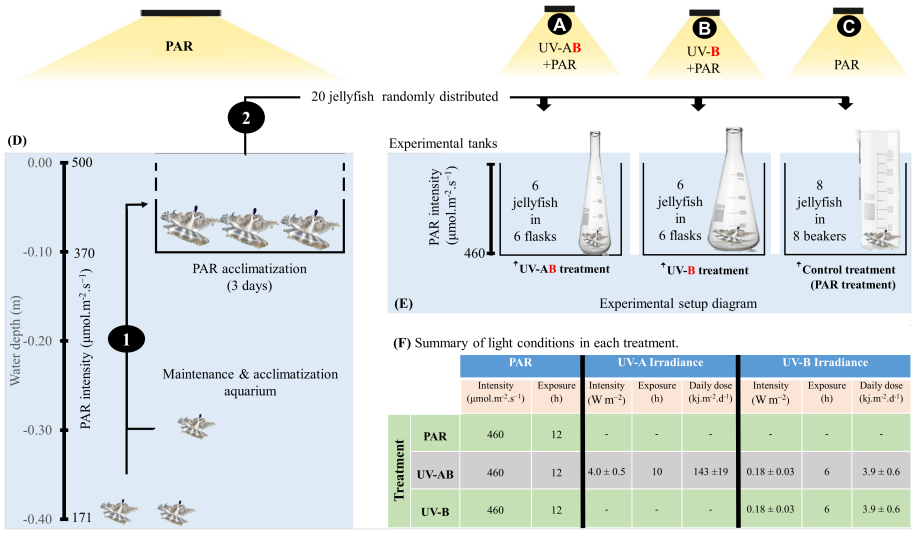

FIGURE 1
Diagram illustrating the jellyfish rearing and experimental design **(D, E)**. (1) Jellyfish were transferred to an elevated tray at 0.10 m depth for 3 days to acclimatize them for higher photosynthetically active radiation (PAR) values. (2) Jellyfish were randomly distributed into three treatments (i.e., indicated by the letters **A–C**. Each organism represented a biological replica and was kept in a separate incubation chamber. **(F)** summarizes the light exposure conditions in each treatment. Refer to the materials and methods section for more detailed explanations.

dark photoperiod. We switched UV−A lamps on and off at 8:00 am and 6:00 pm, respectively. In contrast, UV-B lamps were switched on and off at 10:00 am and 4:00 pm, respectively. Therefore, jellyfish were exposed to a combination of UV-A and UV-B light for 6 h a day (in addition to PAR). Furthermore, the delay in switching on the UV-B light might partially mimic the fact that UV-B reaches the earth at later hours than UV-A. Treatment 3 was the UV-B treatment ($N = 6$), where in addition to PAR exposure, the jellyfish were only exposed to UV-B (average intensity = 0.18 ± 0.03 $W \cdot m^{-2}$; dose = 3.9 ± 0.6 $kJ \cdot m^{-2} \cdot d^{-1}$) on a 6 h/16 h light/dark photoperiod only (refer to Figure 1F). Undetectable underwater UV-C levels were confirmed before the start of the experiment using the PMA2100 radiometer fitted with a UV Germicidal PMA2122-WP sensor (Solar LightTM, USA). When considering the averaged doses measured by Overmans and Agustí (2020) in the coastal Red Sea (34.6 and 1270 KJ m-2 d-1, for UVB and UVA respectively), the UVA and UVB doses provided in the experiment represented ~11.5% of the doses received at the surface.

All physical factors were held constant in all treatments (i.e., temperature, 27.5 ± 0.5°C, salinity, 40.5 ± 0.5‰). In addition, 0.8 L glass beakers were used as incubation chambers for jellyfish in PAR treatment, whereas 2.0 L wide mouth (7 cm) quartz flasks were used in both UV treatments. The quartz flasks were used because quartz allows UVR penetration, whereas glass does not allow UVR penetration. Jellyfish were fed (to repletion) every second day during the morning with freshly hatched Artemia nauplii. Water exchange (i.e., after 12 h of feeding) was achieved by removing about 90% of the incubation water and replacing it with filtered seawater at the same incubation temperature. To avoid stressing the jellyfish, we did not feed jellyfish on Days 1 and 16 (i.e., 24 h before sampling). Body mass was measured (according to the protocol from Aljbour et al., 2019) on Days 0 and 16 (i.e., 24 h before sampling).

2.3 Tissue sampling and homogenization

From each jellyfish (i.e., on day 17), the oral arms (four per tube) and the bell (i.e., devoid of gonadal tissue) were sampled in preweighed tubes and immediately snap-frozen in liquid nitrogen. Then, they were stored at -80°C until analyzed.

Oral samples were solely used for enzymatic assays and protein quantification (i.e., for enzyme activity normalization). For both ETS and glycolytic enzyme (PK and LDH) assays, we used the following common homogenization practice except for the type of the homogenization buffer specific for each enzyme set (buffer ingredients were described in detail by Aljbour et al., 2019). Oral arms (assigned for different enzymes) were double homogenized using the MicroDisTecTM MDT125 homogenizer (Thermo Fisher Scientific, USA) for <40 s and QIAGEN TissueLyser II (i.e., using about 0.5-g glass bead mixture; 0.4 and 1.0 mm diameter) and applying the following program (TN: 12×15, for 15 s) and immediately kept on ice to avoid heat build-up. Afterward, the resulting homogenates were centrifuged (5,000 x *g* for 5 min at 4°C), and the supernatants were distributed into different tubes for enzymatic activity measurement. All aliquots were snap-frozen in liquid nitrogen and kept at -80°C until analyzed.

Bell samples were double homogenized (without buffers) using the approach mentioned above. Therefore, the resultant homogenates (called crude homogenate hence after) were divided into aliquots (in preweighed tubes) and immediately snap-frozen in liquid nitrogen and stored at -80°C until analyzed. Bell crude homogenates were exclusively used for *Ea* estimation.

All enzymatic assays were performed at 28°C using a microplate spectrometer (SpectraMax, USA). Moreover, when we mention the word "supernatant" in the subsequent sections, we mean the above-described supernatant aliquots collected from the oral arms following the homogenization process. Similarly, the word "crude homogenate" refers to the nonbuffered bell homogenate aliquots described in the bell homogenization section.

2.4 Metabolic Enzyme Activity Assays

2.4.1 Electron transport system activity

We measured ETS activity using the common iodonitrotetrazolium (INT) reduction assay (Packard, 1971; Owens and King, 1975), following the methodology described in detail by Aljbour et al. (2019). This assay assumes that the INT reduction rate reflects the oxygen consumption rate. Technically, ETS enzymes mediate the reduction of INT to INT-formazan in the reaction mixture containing electron donors (i.e., nicotinamide adenine dinucleotide or NADH). We estimated the ETS-mediated oxygen consumption using the theoretical stoichiometric relationship that the formation of 2.0 µmol INT-formazan is equivalent to 1.0 µmol of O_2 consumed. The increase in absorbance at 490 nm was followed spectrophotometrically. Then, the results were calculated based on the corrected slopes and presented in milligrams of O_2 per hour per milligram of protein. Protein concentration was determined spectrophotometrically at 595 nm following the Bradford (1976) method, using the bovine serum albumin to build the standard curve.

2.4.2 Glycolytic Enzyme Activity

We measured the activity of PK (EC 2.7.1.40) according to Hickey and Clements (2003), following the methodology described in detail by Aljbour et al. (2018). Technically, pyruvate conversion to lactate is associated with NADH oxidation, which changes the absorbance at 340 nm. The results were calculated based on the corrected slopes and

presented as milliunits per milligram of protein (mU·mg protein^{-1}.) In addition, LDH (EC 1.1.1.27) activity was measured according to (Lushchak et al., 1998; Lushchak et al., 2001), following the methodology described in detail by Aljbour et al. (2018).

2.5 Biochemical composition quantification (available energy resources)

We measured the total soluble protein and carbohydrate content of the bell tissue following the methods described by De Coen and Janssen (1997). Bell crude homogenates were deproteinated with 12% Trichloroacetic acid (0.2 mL per ca. 0.08 g of bell tissue) aided by incubation at -20°C for 10 min. Following centrifugation (1000 x *g* for 10 min), supernatants were recovered in new tubes, and the carbohydrates were quantified with anthrone (Van Handel, 1965), using glucose as a standard with absorbance at 630 nm. The anthrone reagent was prepared fresh right before analysis. The results are presented as milligrams of glucose per gram of WM. The pellets were resuspended in 1.0 N of NaOH and incubated at 60°C for 30 min. Finally, they were neutralized with 2.0 M of HCl, and the protein concentration was determined spectrophotometrically at 595 nm following the Bradford (1976) method, using the bovine serum albumin to build the standard curve. Results are presented as milligrams of protein per gram of WM.

Total lipids were extracted following Bligh and Dyer (1959), following the methods outlined by De Coen and Janssen (1997). Bell crude homogenates were mixed with a 2.0 volume of chloroform and methanol and a 0.85 volume of H_2O. Following centrifugation (1000 x *g* for 5 min), 0.13 mL of the organic phase was transferred to a capped glass vial containing 0.65 mL of H_2SO_4 and was charred at 200°C for 15 min. Then, 0.5 mL of the charred mixture was mixed with 1.13 mL of H_2O and centrifuged at 15,000 x *g* for 15 min. The total lipid was determined by measuring the absorbance at 375 nm. Tripalmitin was used as a standard to build the standard curve. The results are presented as milligrams of tripalmitin per gram of WM.

2.6 Statistical analysis

Before conducting the analysis, all data were tested for compliance with the statistical test assumptions, normality, and homoscedasticity. Nonparametric tests were applied when assumptions were violated. The Kruskal–Wallis test and Dunn's Kruskal–Wallis multiple comparisons were applied to test for significant variation between groups. Spearman's rank correlation test was applied to test for the correlation between variables. We used the R software (R Foundation for Statistical Computing) to conduct the statistical analysis. A p-value <.05 was used as the borderline of statistical significance to reject the null hypothesis for each test, and the word "significant" was used only if the p-value of the test was <.05.

3 Results

3.1 Changes in jellyfish body mass

While the jellyfish in the control treatment significantly increased their WM by about 40% (Wilcoxon signed-rank test with continuity correction: $V = 0$, $p = .01$), neither the UV-B-exposed nor UV-AB-exposed jellyfish demonstrated any significant change in body mass (Figure 2A). However, we did not notice any abnormal behavioural or morphological changes (i.e., bell perforation or oral arm complex separation) during the experiment in either treatment.

3.2 Enzymatic activity responses

The ANOVA using the Kruskal–Wallis test revealed that UVR exposure significantly affected ETS activity in jellyfish in at least one treatment ($\chi^2 = 9.9$ $df = 2$, p <.01; Figure 2B). The results of the *post hoc* analysis using the Dunn (1964) Kruskal–Wallis multiple comparisons indicated that the ETS activity was significantly higher (i.e., 98% to 120%) in UV-B and UV-AB-exposed jellyfish when compared pairwise to the control group (p <.01; Figure 2B). However, the ETS activity in the UV-B and UV-AB-exposed jellyfish was not significantly different when compared pairwise to each other (Dunn (1964) Kruskal–Wallis multiple comparison test: $Z = 0.2398773$, $p = .81$; Figure 2B).

Moreover, UV exposure significantly affected the activity of PK in jellyfish in at least one treatment (Kruskal–Wallis test: $\chi^2 = 10.517$, $df = 2$, p <.01). The PK activity was significantly lower (by 46%) in both UV-B and UV-AB-exposed jellyfish when compared pairwise to the control group (Dunn's (1964) Kruskal–Wallis multiple comparison test: p <.01; Figure 3A). However, pairwise comparison of PK activity between UV-exposed jellyfish did not detect any significant differences between UV-B and UV-AB-treated jellyfish when compared pairwise to each other (Dunn's Kruskal–Wallis multiple comparison test: $Z = 0.098$, $p = .92$; Figure 3A). In contrast, UV exposure did not have any significant effect on LDH activity in either treatment (Kruskal–Wallis rank sum test: $\chi^2 = 3.137$, $df = 2$, p >.05; Figure 3B).

Using the enzymatic ratio analysis, we found that the PK/LDH ratio was significantly different in at least one treatment (one-way ANOVA: $df = 2$, $F = 9.05$, $p = .002$). The ratio was significantly lower in both UV-B and UV-AB-exposed jellyfish when compared pairwise to the control group (Tukey's HSD test for multiple comparison test: p <.05; Figure 4A). However, the ratio did not differ between UV-B and UV-AB-exposed jellyfish when compared

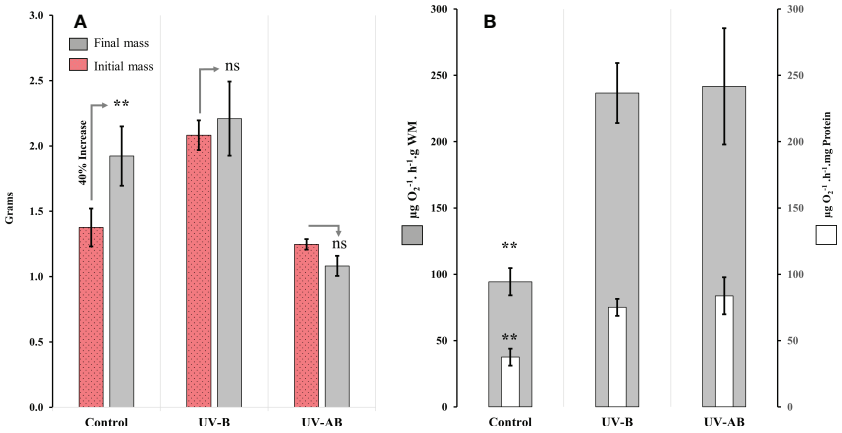

FIGURE 2
Body mass and aerobic respiration response of *Cassiopea* to UVR. **(A)** Wet body mass at the beginning and the end of the experiment; *N* = 8 (control), 6 (UV-B), and 6 (UV-AB). Statistical significance was calculated using Wilcoxon signed-rank test. **(B)** Mitochondrial electron transport system (ETS) activity in oral arms at the end of the experiment; *N* = 8 (control), 6 (UV-B), and 5 (UV-AB). Bars present the data in two normalization methods: 1- activity per wet body mass (i.e., external bars), 2- activity per total protein content (internal bars). Statistical significance was tested using Dunn (1964) Kruskal–Wallis multiple comparison test. In both panels, Data represent the mean ± SE. An asterisk above bars means statistical significance (*$p \leq 0.05$, **$p \leq 0.01$). An "ns" above the bars indicates nonsignificant differences.

pairwise to each other (Tukey's HSD test for multiple comparison test: 95% confidence interval [0.032, 0.132], $p = .70$). We did not find any correlation between PK and LDH. In contrast, when the data from all treatments were combined, the PK was inversely correlated to the ETS activity (Spearman's rank correlation rho: $p < .002$, rho = -0.66). However, at the treatment levels, PK did not correlate with ETS. The ETS activity was negatively correlated with the PK/LDH ratio when data from all treatments were combined (Spearman's rank correlation rho: -0.58, $p = .002$; Figure 4B).

3.3 Energy allocation parameters (carbohydrates, lipids, and total protein content)

The ANOVA using the Kruskal–Wallis test did not reveal any significant effect of UVR on the jellyfish *Ea* parameters in any treatment (Kruskal–Wallis rank sum test: $p > .2$ for all parameters; Figure 5). When we performed the correlation analysis, the correlation type (if present) between enzymatic

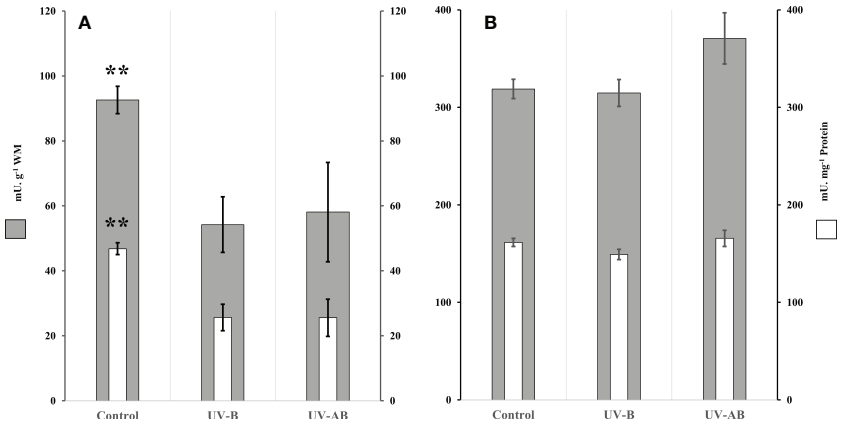

FIGURE 3
Glycolytic enzymes activity in *Cassiopea* oral arms in response to UVR. **(A)** Pyruvate kinase activity (PK); *N* = 8 (control), 6 (UV-B), and 6 (UV-AB). **(B)** Lactate dehydrogenase (LDH) activity; *N* = 8 (control), 5 (UV-B), and 6 (UV-AB). Data represent the mean ± SE; an asterisk above bars means statistical significance (*$p \leq 0.05$, **$p \leq 0.01$). Statistical significance was tested using Dunn (1964) Kruskal–Wallis multiple comparison test. Bars present the data in two normalization methods: 1- activity per wet body mass (i.e., external bars), 2- activity per total protein content (internal bars).

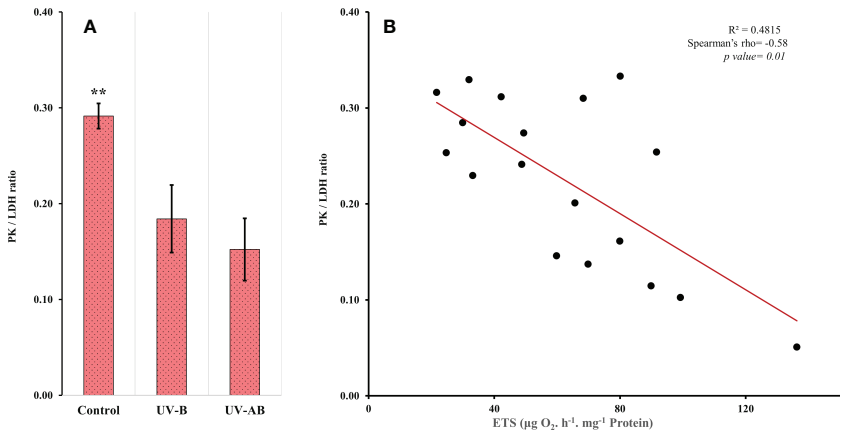

FIGURE 4
(A) Pyruvate kinase (PK)/lactate dehydrogenase (LDH) activity ratio. *N* = 8 (control), 5 (UV-B), and 6 (UV-AB). Data represent the mean ± SE; an asterisk above bars means statistical significance (∗$p \leq 0.05$, ∗∗$p \leq 0.01$). Statistical significance was tested using Tukey HSD test for multiple comparisons. **(B)** Scatter plot showing the correlation between the ETS and PK/LDH ratio. Spearman's test.

activity and *Ea* parameters was always a negative correlation. For example, LDH negatively correlated with the lipid content in UV-B-exposed jellyfish (Spearman's test: rho = -1, p = .017), and PK negatively correlated with carbohydrates content in the same treatment (Spearman's test: rho = -0.93, p = .008). The ETS, LDH, and PK did not correlate with any *Ea* parameter in any other treatment except for the mentioned cases. We measured *Ea* and enzymatic activities in different tissue types (umbrella (bell) vs. oral arms).

4 Discussion

In this study, while aerobic metabolism increased significantly in terms of ETS activity in UV-exposed jellyfish compared to the control group, we did not detect signs of anaerobiosis (e.g., unchanged LDH) in any treatment. We discuss the findings considering the effect of UVR on other organisms due to the lack of research on jellyfish addressing this topic.

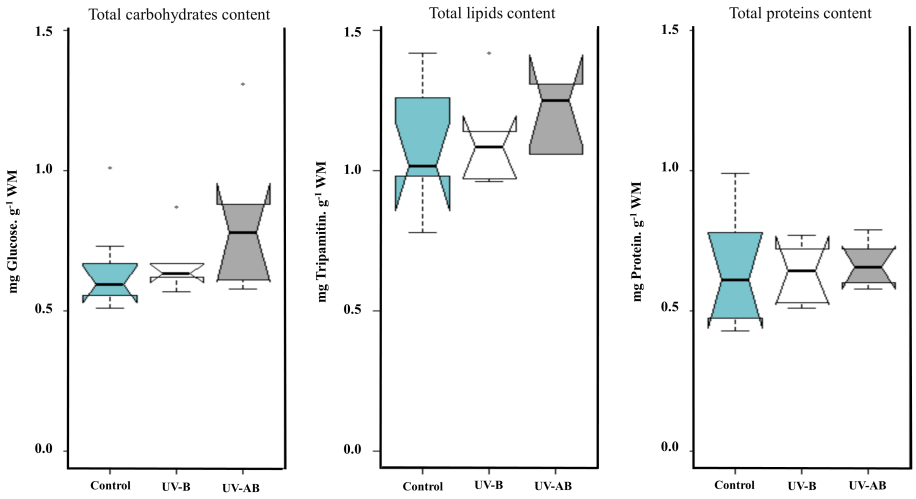

FIGURE 5
Cellular available energy (*Ea*) content in *Cassiopea* umbrella (bell) in response to UVR. Treatments were pairwise-compared to test for any significant differences in *Ea* (i.e., carbohydrates, lipids, and soluble protein). *N* = 8 (control), 6 (UV-B), and 6 (UV-AB). Statistical significance was tested using Kruskal–Wallis rank sum test.

In general, organisms vary greatly in their response to UVR. For example, while a 2-h exposure to high PAR supplemented with UV-A + UV-B significantly stimulated the aerobic respiration rate in the green alga *Selenastrum capricornutum*, it significantly inhibited the respiration rate in the cyanobacterium *Aphanizomenon flos-aquae* (Beardall et al., 1997). According to Chuang et al. (2006), UV-A or UV-B significantly decreased the respiration rate in the earthworm *Amynthas gracilis*. In contrast to earthworms, in the present study, the ETS activity was significantly higher (98% to 120%) in all UV-treated jellyfish compared to the control group, which indicates a higher aerobic cellular respiration rate and oxygen uptake. However, these highly respiring jellyfish did not display equivalent increases in body mass (i.e., compared to about a 40% increase in body mass of the control group). Therefore, this mismatch between a high respiration rate and a reduced growth rate might indicate an elevated energy demand associated with UVR exposure (i.e., more energy is allocated to maintain cellular homeostasis due to ROS and DNA repair, for example). According to Aljbour et al. (2019), the ETS activity was significantly high in *Cassiopea* medusae incubated at a cold temperature (20°C) for two weeks. Moreover, high ETS activity was associated with oxidative stress-mediated cellular damage and significant body mass losses. Furthermore, the medusae were morphologically unhealthy, with shrunk oral arms and perforated bells (Aljbour et al., 2019). In the present study, however, the survival rate of jellyfish was 100%, and they appeared morphologically healthy, suggesting that the jellyfish is more resilient to UVR than to temperature drops.

Many scyphozoan jellyfish might thrive/bloom in response to climate change-driven changing environmental factors (e.g., a rising seawater temperature and eutrophication; Graham, 2001; Purcell et al., 2007; Gambill and Peck, 2014). According to (Aljbour et al., 2017; Aljbour et al., 2019), *Cassiopea* sp. attained larger sizes and enhanced performance when incubated at 32°C for 2 weeks. In the oligotrophic subtropical/tropical marine reef ecosystem (the Red Sea), a high SWT is usually associated with high doses of UVR, even at depths of 3 to 5 m (Overmans and Agustí, 2020). Therefore, marine organisms living in shallow waters of this area might be overexposed to harmful doses of UVR (Overmans and Agustí, 2019). According to Zhou et al. (2016), a high seawater temperature exacerbated the effect of UVR exposure on coral. Furthermore, UVR decreased the concentration of chlorophyll only at higher SWTs or higher UVR doses/intensities (Zhou et al., 2016). Compared to the findings of (Aljbour et al., 2017; Aljbour et al., 2019), the results from the present study might indicate that *Cassiopea* sp. is more sensitive to UVR than to rising seawater temperature. However, this conclusion is beyond the goals of this study and requires further investigation.

Under normal physiological conditions, aerobic respiration generates enough ATP to suffice the cellular energy demands. However, when the aerobic scope declines severely and the Krebs cycle is about to shut down due to an insufficient O_2 supply, the onset of anaerobiosis becomes essential to sustain cellular energy demands (Pörtner). When the Krebs cycle shuts down, NADH builds up and exerts negative feedback inhibitory actions on glycolysis. However, the LDH-mediated re-oxidation of NADH to NAD^+ frees glycolysis from the inhibitory action of NADH. Therefore, energy production from glycolysis can continue.

In invertebrate toxicological studies, LDH is commonly used as a proxy for anaerobiosis (Hochachka et al., 1983). For example, in adductor muscles of the green mussel *Perna viridis*, copper treatment caused higher activity and the onset of anaerobiosis (Aanand et al., 2010). In the present study, UV-treated *Cassiopea* sp. did not exhibit changes in LDH activity or *Ea* (carbohydrates, lipids, and protein content) compared to the control group, which might rule out the onset of anaerobic metabolism under the defined experimental conditions. In a recent study, Enrique-Navarro et al. (2022) demonstrated that the umbrella tissue of *Cotylorhiza tuberculate* jellyfish could effectively absorb light in the UV region and attenuate the light intensity inside the jellyfish. Furthermore, they suggested a protective role of the jellyfish tissue itself, demonstrating an added reason to explain the success of the *Cotylorhiza tuberculata* population (Enrique-Navarro et al., 2022). The jellyfish seems to have high resilience (i.e., compared to coral) to UV and a higher ability to aerobically cope with elevated energy demands without switching their metabolism into anaerobic mode.

Interestingly, PK activity unexpectedly decreased in UV-exposed jellyfish. According to Aljbour et al. (2018), PK activity was significantly higher in jellyfish from heavy-metal polluted aquatic habitats. The authors related this increase to the enhanced anaerobic metabolism of the jellyfish. Furthermore, Dailianis and Kaloyianni (2004) observed the same pattern of PK activity change in Cd-treated mollusks. While a low PK/LDH ratio usually indicates enhanced anaerobic glycolysis, the unchanged LDH activities combined with the decreased PK activities in UV-exposed jellyfish rule out this possibility in the present study.

Furthermore, we found that ETS activity is inversely correlated to PK and the PK/LDH ratio when data from all treatments were combined. However, at the treatment levels, PK did not correlate with the ETS. However, these data do not imply causality and require more experiments with a higher number of organisms to decipher the correlation at treatment levels.

The UVR (mainly UV-B) could initiate oxidative stress (Lesser, 1996; Lesser and Farrell, 2004; Lu and Wu, 2005) and

induce DNA damage (Rastogi et al., 2010) in marine organisms. Therefore, it adversely affects genomic stability and cellular homeostasis. In coral, UV-B impaired photosynthesis initiated DNA damage and triggered ROS formation (Lesser, 1996; Torres-Pérez and Armstrong, 2012; Donner et al., 2017; Nordborg et al., 2021). In contrast, UV-A might induce varying effects in different organisms. For example, UV-A adversely affected sea urchin productivity (Lu and Wu, 2005). Furthermore, UV-A increased superoxide dismutase activity and lipid peroxidation rate in the *Distyle brightwellii* diatom. In contrast, UV-A minimizes the adverse effects of UV-B on photosynthesis in coral larvae and *Symbiodinium* (Zhou et al., 2016). In *Cassiopea* sp., all UV-B and (UV-B+UV-A)-treated jellyfish responded similarly (i.e., in terms of all response parameters tested in this study). Therefore, it seems that the presence of UV-A did not synergize or hinder the effects of UV-B in jellyfish under the defined conditions in this experiment.

5 Conclusion

The results demonstrate that *Cassiopea* sp. was aerobically poised to deal with UVR-mediated elevated energy demands. Furthermore, the jellyfish did not switch to anaerobic metabolism, as *Ea* and LDH activity remained unchanged in UVR-treated jellyfish. The UVR did not affect jellyfish survival while reducing their growth rate. Although UV-A might exacerbate/modulate the effect of UV-B on different marine organisms, the results indicate that UV-A did not seem to amplify or modulate UV-B effects on jellyfish physiology and growth. However, the findings suggest that the jellyfish is more resilient (i.e., concerning unaffected survival) to UVR than other cnidarians.

Data availability statement

The raw data supporting the conclusions of this article will be made available by the authors, without undue reservation.

Author contributions

SMA, RA, and SA conceived and designed the study. SMA conducted the jellyfish sampling from the field and performed enzymatic and biochemical analyses. All authors contributed to the writing of the manuscript and critically read and approved the final version. All authors contributed to the article and approved the submitted version.

Funding

This work was supported by the King Abdullah University of Science and Technology through baseline funding to Prof. SA.

Acknowledgments

We would like to acknowledge the effort of the CMR team at KAUST. I would like to extend my sincere thanks to Aussama Alzeem for his excellent assistance in the field.

Conflict of interest

The authors declare that the research was conducted in the absence of any commercial or financial relationships that could be construed as a potential conflict of interest.

Publisher's note

References

Aanand, S., Purushothaman, C. S., Pal, A. K., and Rajendran, K. V. (2010). Toxicological studies on the effect of copper lead and zinc on selected enzymes in the adductor muscle and intestinal diverticula of the green mussel perna viridis. *Indian J. Mar. Sci.* 39 (2), 299–302.

Aljbour, S. M., Al-Horani, F., and Kunzmann, A. (2018) Metabolic and oxidative stress responses of the jellyfish cassiopea to pollution in the gulf of aqaba Jordan. *Mar. pollut. Bull* 130, 271–278. doi: 10.1016/j.marpolbul.2018.03.044

Aljbour, S. M., Zimmer, M., Al-Horani, F., and Kunzmann, A. (2019). Metabolic and oxidative stress responses of the jellyfish cassiopea sp. to changes in seawater temperature. *J. Sea. Res.* 145, 1–7. doi: 10.1016/j.seares.2018.12.002

Aljbour, S. M., Zimmer, M., and Kunzmann, A. (2017). Cellular respiration oxygen consumption and trade-offs of the jellyfish cassiopea sp. in response to temperature change. *J. Sea. Res.* 128, 92–97. doi: 10.1016/j.seares.2017.08.006

Alves, R., and Agustí, S. (2020). Effect of ultraviolet radiation (UVR) on the life stages of fish. *Rev. Fish. Biol. Fisher.* 30 (2), 335–372. doi: 10.1007/s11160-020-09603-1

Alves, R. N., Mahamed, A. H., Alarcon, J. F., Al Suwailem, A., and Agustí, S. (2020). Adverse effects of ultraviolet radiation on growth, behavior, skin condition, physiology, and immune function in gilthead seabream (sparus aurata). *Front. Mar. Sci.* 7:306. doi: 10.3389/fmars.2020.00306

Alves, R. N., Justo, M. S. S., Laranja, J. L. Q., Alarcon, J. F., Al Suwailem, A., and Agustí, S. (2021). Exposure to natural ultraviolet b radiation levels has adverse effects on growth behavior physiology and innate immune response in juvenile European seabass (*Dicentrarchus labrax*). *Aquaculture* 533, 736215. doi: 10.1016/j.aquaculture.2020.736215

Anderson, J. G., Wilmouth, D. M., Smith, J. B., and Sayres, D. S. (2012). UV Dosage levels in summer: Increased risk of ozone loss from convectively injected water vapor. *Science* 337 (6096), 835–839. doi: 10.1126/science.1222978

Arai, M. N. (2001). Pelagic coelenterates and eutrophication: a review. *Hydrobiologia* 451, 69–87. doi: 10.1023/A:1011840123140

Bagwe, R., Beniash, E., and Sokolova, I. M. (2015). Effects of cadmium exposure on critical temperatures of aerobic metabolism in eastern oysters crassostrea virginica (Gmelin 1791). *Aquat. Toxicol.* 167, 77–89. doi: 10.1016/j.aquatox.2015.07.012

Banaszak, A. T., and Trench, R. K. (1995). Effects of ultraviolet (UV) radiation on marine microalgal-invertebrate symbioses. II. the synthesis of mycosporine-like amino acids in response to exposure to UV in anthopleura elegantissima and cassiopea xamachana. *J. Exp. Biol. Ecol.* 194, 233–250. doi: 10.1016/0022-0981(95)00073-9

Bancroft, B., Baker, N., and Blaustein, A. (2007). Effects of UVB radiation on marine and freshwater organisms: a synthesis through meta-analysis. *Ecol. Lett.* 10 (4), 332–345. doi: 10.1111/j.1461-0248.2007.01022.x

Baruch, R., Avishai, N., and Rabinowitz, C. (2005). UV Incites diverse levels of DNA breaks in different cellular compartments of a branching coral species. *J. Exp. Biol.* 208 (5), 843–848. doi: 10.1242/jeb.01496

Beardall, J., Berman, T., Markager, S., Martinez, R., and Montecino, V. (1997). The effects of ultraviolet radiation on respiration and photosynthesis in two species of microalgae. *Can. J. Fisher. Aquat. Sci.* 54 (3), 687–696. doi: 10.1139/f96-320

Blanquet, R. S., and Phelan, M. A. (1987). An unusual blue mesogleal protein from the mangrove jellyfish cassiopea xamachana. *Mar. Biol.* 94, 423–430. doi: 10.1007/BF00428249

Bligh, E. G., and Dyer, W. J. (1959). A rapid method of total lipid extraction and purification. *Can. J. Biochem. Physiol.* 37 (8), 911–917. doi: 10.1139/y59-099

Bradford, M. M. (1976). A rapid and sensitive method for the quantitation of microgram quantities of protein utilizing the principle of protein-dye binding. *Analytical. Biochem.* 72 (1-2), 248–254. doi: 10.1016/0003-2697(76)90527-3

Breitburg, D. L., Loher, T., Pacey, C. A., and Gerstein, A. (1997). Varying effects of low dissolved oxygen on trophic interactions in an estuarine food web. *Ecol. Monogr.* 67 (4), 489–507. doi: 10.1890/0012-9615(1997)067[0489:VEOLDO]2.0.CO;2

Cates, N. (1975). Productivity and organic consumption in cassiopea and conductylus. *J. Exp. Biol. Ecol.* 18, 55–59. doi: 10.1016/0022-0981(75)90016-7

Chuang, S. C., Lai, W. S., and Chen, J. H. (2006). Influence of ultraviolet radiation on selected physiological responses of earthworms. *J. Exp. Biol.* 209 (21), 4304–4312. doi: 10.1242/jeb.02521

Dailianis, S., and Kaloyianni, M. (2004). Cadmium induces both pyruvate kinase and Na+/H+ exchanger activity through protein kinase c mediated signal transduction in isolated digestive gland cells of mytilus galloprovincialis (L.). *J. Exp. Biol.* 207 (10), 1665–1674. doi: 10.1242/jeb.00925

De Coen, W., and Janssen, C. (1997). The use of biomarkers in *Daphnia magna* toxicity testing. IV. cellular energy allocation: a new methodology to assess the energy budget of toxicant-stressed daphnia populations. *J. Aquat. Ecosyst. Stress Recovery.* 6, 43–55. doi: 10.1023/A:1008228517955

Donner, S., Rickbeil, G., and Heron, S. (2017). A new high-resolution global mass coral bleaching database. *PloS One* 12 (4), e0175490. doi: 10.1371/journal.pone.0175490

Dunn, O. J. (1964). Multiple comparisons using rank sums. *Technometrics* 6(3), 241–252. doi: 10.1080/00401706.1964.10490181

Enrique-Navarro, A., Huertas, E., Flander-Putrle, V., Bartual, A., Navarro, G., Ruiz, J., et al. (2022). Living inside a jellyfish: The symbiosis case study of host-specialized dinoflagellates "Zooxanthellae" and the scyphozoan cotylorhiza tuberculata*Front. Mar. Sci.*9, 817312. doi: 10.3389/fmars.2022.817312

Fleck, J., and Fitt, W. K. (1999). Degrading mangrove leaves of rhizophora mangle linne provide a natural cue for settlement and metamorphosis of the upside-down jellyfish *Cassiopea xamachana* Bigelow. *J. Exp. Biol. Ecol.* 234, 83–94. doi: 10.1016/S0022-0981(98)00140-3

Gambill, M., and Peck, M. (2014). Respiration rates of the polyps of four jellyfish species: Potential thermal triggers and limits. *J. Exp. Mar. Biol. Ecol.* 459, 17–22. doi: 10.1016/j.jembe.2014.05.005

Gohar, H. A. F., and Eisawy, A. M. (1960). The development of Cassiopea andromeda. *Publ. Mar. Biol. Stat.* 11, 148–190.

Graham, W. M. (2001). Numerical increases and distributional shifts of chrysaora quinquecirrha (Desor) and aurelia aurita (Linnè) (Cnidaria: Scyphozoa) in the northern gulf of Mexico. *Hydrobiologia* 451, 97–111. doi: 10.1023/A:1011844208119

Häder, D., Helbling, E., Williamson, C., and Worrest, R. (2011). Effects of UV radiation on aquatic ecosystems and interactions with climate change. *Photochem. Photobiolog. Sci.* 10 (2), 242–260. doi: 10.1039/c0pp90036b

Häder, D., Williamson, C., Wängberg, S., Rautio, M., Rose, K., Gao, K., et al. (2015). Effects of UV radiation on aquatic ecosystems and interactions with other environmental factors. *Photochem. Photobiolog. Sci.* 14 (1), 108–126. doi: 10.1039/c4pp90035a

Hearst, J. (1995). The structure of photolyase: Using photon energy for DNA repair. *Science* 268 (5219), 1858–1859. doi: 10.1126/science.7604259

Hickey, A. J. R., and Clements, K. D. (2003). Key metabolic enzymes and muscle structure in triplefin fishes (Tripterygiidae): a phylogenetic comparison. *J. Comp. Physiol. B.* 173 (2), 113–123. doi: 10.1007/s00360-002-0313-9

Hochachka, P. W., Stanley, C., Merkt, J., and Sumar-Kalinowski, J. (1983). Metabolic meaning of elevated levels of oxidative enzymes in high altitude adapted animals: an interpretive hypothesis. *Respir. Physiol.* 52 (3), 303–313. doi: 10.1016/0034-5687(83)90087-7

Jantzen, C., Wild, C., Rasheed, M., El-Zibdah, M., and Richter, C. (2010). Enhanced pore-water nutrient fluxes by the upside-down jellyfish cassiopea sp. in a red Sea coral reef. *Mar. Ecol. Prog. Ser.* 411, 117–125. doi: 10.3354/meps08623

Kheireddine, M., Ouhssain, M., Claustre, H., Uitz, J., Gentili, B., and Jones, B. (2017). Assessing pigment-based phytoplankton community distributions in the red Sea. *Front. Mar. Sci.* 4. doi: 10.3389/fmars.2017.00132

Khogali, A., and Al-Bar, O. F. (1992). A study of solar ultraviolet-radiation at makkah solar station. *Solar. Energy* 48, 79–87. doi: 10.1016/0038-092X(92)90036-A

Klein, S. G., Pitt, K. A., and Carroll, A. R. (2016). Surviving but not thriving: inconsistent responses of zooxanthellate jellyfish polyps to ocean warming and future UV-b scenarios. *Sci. Rep.* 6 (1), e28859. doi: 10.1038/srep28859

Kremer, P., Costello, J., Kremer, J., and Canino, M. (1990). Significance of photosynthetic endosymbionts to the carbon budget of the scyphomedus linuche unguiculata. *Limnol. Oceanogr.* 35, 609–624. doi: 10.4319/lo.1990.35.3.0609

Leech, D., and Williamson, C. (2000). Is tolerance to uv radiation in zooplankton related to body size taxon or lake transparency? *Ecol. Appl.* 10 (5), 1530–1540. doi: 10.1890/1051-0761(2000)010[1530:itturi]2.0.co;2

Lesser, M. P. (1996). Elevated temperatures and ultraviolet radiation cause oxidative stress and inhibit photosynthesis in symbiotic dinoflagellates. *Limnol. Oceanogr.* 41 (2), 271–283. doi: 10.4319/lo.1996.41.2.0271

Lesser, M. P., and Farrell, J. H. (2004). Exposure to solar radiation increases damage to both host tissues and algal symbionts of corals during thermal stress. *Coral. Reefs.* 23 (3), 367–377. doi: 10.1007/s00338-004-0392-z

Lushchak, V. I., Bagnyukova, T. V., Storey, J. M., and Storey, K. B. (2001). Influence of exercise on the activity and the distribution between free and bound forms of glycolytic and associated enzymes in tissues of horse mackerel. *Braz. J. Med. Biol. Res.* 34 (8), 1055–1064. doi: 10.1590/S0100-879X2001000800013

Lushchak, V. I., Bahnjukova, T. V., and Storey, K. B. (1998). Effect of hypoxia on the activity and binding of glycolytic and associated enzymes in sea scorpion tissues. *Braz. J. Med. Biol. Res.* 31 (8), 1059–1067. doi: 10.1590/S0100-879X1998000800005

Lu, X. Y., and Wu, R. S. S. (2005). UV Induces reactive oxygen species damages sperm and impairs fertilisation in the sea urchin anthocidaris crassispina. *Mar. Biol.* 148 (1), 51–57. doi: 10.1007/s00227-005-0049-7

Mazurek, S., Grimm, H., Boschek, C. B., Vaupel, P., and Eigenbrodt, E. (2002). Pyruvate kinase type M2: a crossroad in the tumor metabolome. *Br. J. Nutr.* 87 (1), 23–29. doi: 10.1079/BJN2001454

McCloskey, L. R., Muscatine, L., and Wilkerson, F. P. (1994). Daily photosynthesis, respiration, and carbon budgets in a tropical marine jellyfish (mastigias sp..). *Marine Biology* 119 (1), 3–22. doi: 10.1007/bf00350101

Mills, C. E. (2001). Jellyfish blooms: are populations increasing globally in response to changing ocean conditions? *Hydrobiologia* 451, 55–68. doi: 10.1007/978-94-010-0722-1_6

Moan, J. (2001). "Visible light and UV radiation," in *Radiation at home outdoors and in the workplace*. Eds. A. Brune, R. Hellborg, B. R. R. Persson and R. Pääkkönen (Oslo: Scandinavian Science Publisher), p 69–p 85.

Nabipour, I., Moradi, M., and Mohebbi, G. H. (2015). A first record on population of the alien venomous jellyfish *Cassiopea andromeda* (Forsskål 1775) (Cnidaria: Scyphozoa: Rhizostomea) in the nayband lagoon from bushehr-Iran (Persian gulf). *J. Chem. Pharm. Res.* 7, 1710–1713.

Niggl, W., Naumann, M. S., Struck, U., Manasrah, R., and Wild, C. (2010). Organic matter release by the benthic upside-down jellyfish cassiopea sp. fuels pelagic food webs in coral reefs. *J. Exp. Mar. Biol. Ecology.* 384, 99–106. doi: 10.1016/j.jembe.2010.01.011

Niggl, W., and Wild, C. (2009). Spatial distribution of the upsidedown jellyfish cassiopea sp. within fringing coral reef environments of the northern red Sea: implications for its life cycle. *Helgoland. Mar. Res.* 64, 281–287. doi: 10.1007/s10152-009-0181-8

Nordborg, F., Brinkman, D., Ricardo, G., Agustí, S., and Negri, A. (2021). Comparative sensitivity of the early life stages of a coral to heavy fuel oil and UV radiation. *Sci. Total. Environ.* 781, e146676. doi: 10.1016/j.scitotenv.2021.146676

Overmans, S., and Agustí, S. (2019). Latitudinal gradient of UV attenuation along the highly transparent red Sea basin. *Photochem. Photobiol.* 95 (5), 1267–1279. doi: 10.1111/php.13112

Overmans, S., and Agustí, S. (2020). Unraveling the seasonality of UV exposure in reef waters of a rapidly warming (Sub-)tropical Sea. *Front. Mar. Sci.* 7. doi: 10.3389/fmars.2020.00111

Owens, T. G., and King, F. D. (1975). The measurement of respiratory electron-transport-system activity in marine zooplankton. *Mar. Biol.* 30 (1), 27–36. doi: 10.1007/BF00393750

Özbek, E.Ö., and Oztürk, B. (2015). The new location record of *Cassiopea andromeda* (Forsskå) from asin bay gulf of güllük muğla Aegean coast of Turkey. *J. Black. Sea. /. Mediterr. Environ.* 21 (1), 96–101.

Packard, T. T. (1971). The measurement of respiratory electron transport activity in marine plankton. *J. Mar. Res.* 29, 235–244.

Phelan, M., Matta, J., Reyes, Y., Fernando, R., Boykins, R., and Blanquet, R. (2005). Associations between metals and the blue mesogleal protein of cassiopea xamachana. *Mar. Biol.* 149 (2), 307–312. doi: 10.1007/s00227-005-0189-9

Pierce, J. (2005). A system for mass culture of upside-down jellyfish *Cassiopea* spp as a potential food item for medusivores in captivity. *Int. Zoo Yearbook* 39, 62–69. doi: 10.1111/j.1748-1090.2005.tb00005.x

Pitt, K. A., Welsh, D. T., and Condon, R. H. (2009) Influence of jellyfish blooms on carbon nitrogen and phosphorus cycling and plankton production*Hydrobiolog* 616, 133–149 doi: 10.1007/s10750-008-9584-9

Pörtner, H. O. (2002). Climate variations and the physiological basis of temperature dependent biogeography: systemic to molecular hierarchy of thermal tolerance in animals. *Comp. Biochem. Physiol. Part A.: Mol. Integr. Physiol.* 132 (4), 739–761. doi: 10.1016/S1095-6433(02)00045-4

Prasanth, M. I., Santoshram, G. S., Bhaskar, J. P., and Balamurugan, K. (2016). Ultraviolet-a triggers photoaging in model nematode *Caenorhabditis elegans* in a DAF-16 dependent pathway. *Age. (Dordr).* 38 (1), 27. doi: 10.1007/s11357-016-9889-y

Purcell, J. (2005). Climate effects on formation of jellyfish and ctenophore blooms: a review. *J. Mar. Biol. Assoc. United. Kingdom.* 85 (3), 461–476. doi: 10.1017/S0025315405011409

Purcell, J., Uye, S., and Lo, W. (2007). Anthropogenic causes of jellyfish blooms and their direct consequences for humans: a review. *Mar. Ecol. Prog. Ser.* 350, 153–174. doi: 10.3354/meps07093

Rastogi, R., Richa,, Kumar, A., Tyagi, M., and Sinha, R. (2010). Molecular mechanisms of ultraviolet radiation-induced DNA damage and repair. *J. Nucleic Acids*. 2010, 1–32. doi: 10.4061/2010/592980

Rijstenbil, J. (2001). Effects of periodic low UVA radiation on cell characteristics and oxidative stress in the marine planktonic diatom ditylum brightwellii. *Eur. J. Phycology.* 36 (1), 1–8. doi: 10.1080/09670260110001735138

Rossbach, S., Overmans, S., Kaidarova, A., Kosel, J., Agustí, S., and Duarte, C. M. (2020). Giant clams in shallow reefs: UV-resistance mechanisms of Tridacninae in the Red Sea. *Coral Reefs.* 39 (5), 1345–1360. doi: 10.1007/s00338-020-01968-w.

Roy, S. (2000). "Strategies for the minimization of UV-induced damage," in *The effects of UV radiation in the marine environment*, vol. 10 . Eds. S. De Mora, S. Demers and M. Vernet (Cambridge: Cambridge University Press), 177–205.

Sancar, A. (1996). No "End of history" for photolyases. *Science* 272 (5258), 48–49. doi: 10.1126/science.272.5258.48

Sinha, R., and Häder, D. (2002). UV-Induced DNA damage and repair: a review. *Photochem. Photobiolog. Sci.* 1 (4), 225–236. doi: 10.1039/b201230h

Thé, J., Gamero-Mora, E., Chagas da Silva, M. V., Morandini, A. C., Rossi, S., and d Soares, M. O. (2021). Non-indigenous upside-down jellyfish cassiopea andromeda in shrimp farms (Brazil). *Aquaculture.* 532, 735999. doi: 10.1016/j.aquaculture.2020.735999

Thoma, F. (1999). Light and dark in chromatin repair: repair of UV-induced DNA lesions by photolyase and nucleotide excision repair. *EMBO J.* 18 (23), 6585–6598. doi: 10.1093/emboj/18.23.6585

Tinta, T., Kogovšek, T., Turk, V., Shiganova, T. A., Mikaelyan, A. S., and Malej, A. (2016). Microbial transformation of jellyfish organic matter affects the nitrogen cycle in the marine water column-a black Sea case study. *J. Exp. Mar. Biol. Ecol.* 475, 19–30. doi: 10.1016/j.jembe.2015.10.018

Todd, B. D., Thornhill, D. J., and Fitt, W. K. (2006). Patterns of inorganic phosphate uptake in *Cassiopea xamachana*: a bioindicator species. *Mar. pollut. Bull.* 52, 515–552. doi: 10.1016/j.marpolbul.2005.09.044

Torres-Pérez, J., and Armstrong, R. (2012). Effects of UV radiation on the growth photosynthetic and photoprotective components and reproduction of the Caribbean shallow-water coral porites furcata. *Coral. Reefs.* 31, 1077–1091. doi: 10.1007/s00338-012-0927-7

Van Handel, E. (1965). Microseparation of glycogen sugars and lipids. *Analytical. Biochem.* 11 (2), 266–271. doi: 10.1016/0003-2697(65)90014-X

Verde, E. A., and McCloskey, L. R. (1998). Production respiration and photophysiology of the mangrove jellyfish cassiopea xamachana symbiotic with zooxanthellae: effect of jellyfish size and season. *Mar. Ecol. Prog. Ser.* 168, 147–162. doi: 10.3354/meps168147

Winters, G., Loya, Y., Röttgers, R., and Beer, S. (2003) Photoinhibition in shallow-water colonies of the coral stylophora pistillata as measured in situ. *Limnol. Oceanogr.* 48 (4), 1388–1393. doi: 10.4319/lo.2003.48.4.1388

Zarnoch, C. B., Hossain, N., Fusco, E., Alldred, M., Hoellein, T. J., and Perdikaris, S. (2020). Size and density of upside-down jellyfish cassiopea sp. and their impact on benthic fluxes in a Caribbean lagoon. *Mar. Environ. Res.* 154, 104845. doi: 10.1016/j.marenvres.2019.104845

Zhou, J., Fan, T.-Y., Beardall, J., and Gao, K. (2016). Incident ultraviolet irradiances influence physiology development and settlement of larva in the coral pocillopora damicornis. *Photochem. Photobiol.* 92 (2), 293–300. doi: 10.1111/php.12567

frontiers | Frontiers in Marine Science

TYPE Original Research
PUBLISHED 16 January 2023
DOI 10.3389/fmars.2022.1110587

OPEN ACCESS

EDITED BY
Bo Liu,
Qingdao Agricultural University, China

REVIEWED BY
Ping Liu,
Yellow Sea Fisheries Research Institute (CAFS), China
Zhi Liao,
Zhejiang Ocean University, China

*CORRESPONDENCE
Zhiguo Dong
dzg7712@163.com

SPECIALTY SECTION
This article was submitted to Marine Biology, a section of the journal Frontiers in Marine Science

RECEIVED 29 November 2022
ACCEPTED 29 December 2022
PUBLISHED 16 January 2023

CITATION
Liu M, Ni H, Rong Z, Wang Z, Yan S, Liao X and Dong Z (2023) Gonad transcriptome analysis reveals the differences in gene expression related to sex-biased and reproduction of clam *Cyclina sinensis*. *Front. Mar. Sci.* 9:1110587. doi: 10.3389/fmars.2022.1110587

Gonad transcriptome analysis reveals the differences in gene expression related to sex-biased and reproduction of clam *Cyclina sinensis*

Meimei Liu[1,2,3], Hongwei Ni[1], Zichao Rong[1], Zi Wang[1], Susu Yan[1], Xiaoting Liao[1] and Zhiguo Dong[1,2,3]*

[1]Jiangsu Key Laboratory of Marine Bioresources and Environment, Jiangsu Ocean University, Lianyungang, China, [2]Co-Innovation Center of Jiangsu Marine Bio-industry Technology, Jiangsu Institute of Marine Resources Development, Lianyungang, China, [3]Key Laboratory of Marine Biotechnology of Jiangsu Province, Jiangsu Ocean University, Lianyungang, China

Sexual differentiation and gonad development are important biological processes for bivalve species. The clam *Cyclina sinensis* is an important cultured marine bivalve widely distributed along with the coastal areas of China. However, the information related to sexual determination/differentiation and gonadal development of *C. sinensis* almost has no reported. To study the molecular mechanisms of its sexual determination/differentiation and gonadal development, transcriptome analysis was performed in the gonad of *C. sinensis*, and the potential biological functions of reproduction-related gene were also investigated in this study. The results showed that 1 013 and 427 genes were differentially expressed in the ovary and testis, respectively. KEGG enrichment analysis showed that the DEGs in the gonad were significantly clustered in progesterone-mediated oocyte maturation, cell cycle and oocyte meiosis. Further analysis showed that 23 genes were mainly involved in sex determination/differentiation, including *Dmrt1*, *Sox2/4/9*, *Foxl2*, *β-catenin* and *GATA-type zinc finger protein 1-like*. Twenty key genes were mainly involved in the process of spermatogenesis, and five genes encode steroid biosynthesis and metabolism. Fifteen genes related to ovarian development were also identified in this study, such as *Vitellogenin*, *MAM and LDL-receptor class A domain-containing protein 1* and *Cell division cycle protein 20 homolog*. Moreover, 50μg/L estradiol treatment significantly up-regulated the expression levels of *CsVg* in the ovary and hepatopancreas. These results highlight the genes involved in sexual determination/differentiation and gonadal development, which enhance our understanding for further studies of reproduction and breeding of *C. sinensis* and other marine bivalves.

KEYWORDS

Cyclina sinensis, sex-differentially expressed genes, spermatogenesis, ovarian development, vitellogenin

Highlights

- 23 genes involved in sex determination/differentiation of *C. sinensis* were identified.
- Twenty key genes played important role in the process of spermatogenesis of *C. sinensis*.
- 15 key genes played important role in the ovarian development of *C. sinensis*.
- 50μg/L estradiol treatment significantly up-regulated the expression levels of *CsVg*.

1 Introduction

Sexual reproduction is one of the most universal phenomena in the animal kingdom, and it includes sexual determination/differentiation and gonadal development (Li et al., 2016a; Liu et al., 2016). Sexual determination/differentiation refers to the event that triggers the bipotential primordia to make the fate decision to become testes or ovaries, and it is very flexible in fish, with several species showing a chromosomal basis and others with influencing environmental factors (Devlin and Nagahama, 2002; Sandra and Norma, 2010). Previous studies showed that sex-determining/–differentiating pathways share common genes such as *SRY-related HMG box 9* (*SOX9*), *wingless-type MMTV integration site family member-4* (*WNT4*), *R-spondin1* (*R-SPO1*) and *transcription factor forkhead box L subfamily member 2* (*FOXL2*), among vertebrates and invertebrates, (Bertho et al., 2016; Major et al., 2019; Estermann et al., 2020; Broquard et al., 2021). Among those genes, Sox9 has been identified and proved its crucial roles in male sex determination, male gonad development, and Sertoli cell development and differentiation (Vidal et al., 2002; Chaboissier et al., 2004; Barrionuevo et al., 2009).

WNT4 is a key regulator of ovarian development in mammals, and R-spondin1 tips the balance in sex determination (Capel, 2006; Farhadi et al., 2021). Ning et al. (2021) reported that the transcription factor FoxL2 is an evolutionarily conserved gene playing pivotal roles in regulation of early ovarian differentiation and maintenance in animals. Similarly, as the primary reproductive organs, the ovary and testis play keys role in gametogenesis and steroid regulation of vertebrates and invertebrates (Nagaraju, 2011; Senthilkumaran and Kar, 2021).

As the second largest phylum of invertebrates, mollusks exhibit different reproductive strategies: they are dioecious, hermaphrodites or exhibit sex reversal (Li et al., 2018). Therefore, the studies on reproduction of mollusk, especially commercial mollusk species has received significant research attention in recent years (Wang et al., 2020; Broquard et al., 2021; Shangguan et al., 2022). For example, Santerre et al. (2014) reported that *SoxE* and *β-catenin* are involved in early gonadic differentiation of Pacific oyster *Crassostrea gigas*. Shangguan et al. (2022) reported that *17-alpha-hydroxylase/17,20 lyase* (*cyp17a1*) plays an important role in gonadal development of *Hyriopsis cumingii*. Meanwhile, several gonadal transcriptome analyses identified candidate genes (*SoxH*, *Sox9*, *Foxl2*, *Doublesex-and mab-3-related transcription factor 1* (*Dmrt1*), *sex determining protein Fem-1* (*Fem-1*), *Beta-catenin*, *wnt4*, *cyp17a1*, *Estradiol 17-beta-dehydrogenase 2* (*17β-hsd2*) and *Vitellogenin* (*Vg*)) that participate in gender determination/differentiation and gonadal maturation pathway of mollusks, including *Crassostrea hongkongensis*, *C. gigas*, *Patinopecten yessoensis*, *Sinonovacula constricta*, *Pinctada margaritifera*, *Tegillarca granosa*, *Chlamys nobilis* and *Hyriopsis schlegelii* (Teaniniuraitemoana et al., 2014; Zhang et al., 2014; Tong et al., 2015; Li et al., 2016a; Chen et al., 2017; Yue et al., 2018; Broquard et al., 2021; Yao et al., 2021; Zeng et al., 2022). Despites the identification of some candidate genes, studies on sex determination/differentiation and gonadal maturation genes in bivalves and other molluscs were still limited, and more sex and gonad related genes and their functions need to be studied.

The clam, *Cyclina sinensis*, is one of the important cultured marine bivalves found widely along the coastal areas of China, Korea, Japan, and Southeast Asia (Wei et al., 2020; Ge et al., 2021; Liao et al., 2022). To date, the research on *C. sinensis* mainly focuses on genetic evaluation, breeding techniques, nutritional value and physiological responses (Wei et al., 2020; Dong et al., 2021; Ge et al., 2021; Liao et al., 2022). However, the information related to sexual determination/differentiation and gonadal development of *C. sinensis* is limited. Transcriptome sequencing provides an effective way to obtain large amounts of sequence data, has been widely applied to model and non-model species (Qian et al., 2014). The availability of the *C. sinensis* genome and the reduced cost of next-generation sequencing provide the opportunity for enhance our understanding of the complex regulation mechanisms of reproduction (Wei et al., 2020; Dong et al., 2021; Ge et al., 2021; Liao et al., 2022). Therefore, the present study sequenced *C. sinensis* gonad transcriptomes and investigated the potential biological functions of reproduction-related genes. The results of this study will help us understand the general underlying molecular mechanisms of bivalve reproduction and provide a scientific basis for the sexual control and breeding of shellfish.

2 Materials and methods

2.1 Ethics statement

All the study design and animal experiments were conducted in accordance with guidelines of Jiangsu Ocean University's Animal Care and Use Committee.

2.2 Sample collection

The female and male *C. sinensis* used in this experiment were purchased from a commercial farmer in Qinzhou, Guangxi, China. After being transferred to the laboratory, the clams were acclimated in cement tanks (length×width× depth=100cm×100cm×80cm) filled with natural seawater (salinity 24 ± 1 ppt). All clams were fed daily

at 17:00 with a mixture of *Nannochloropsis oceanica* and *Chaetoceros mulleri* quantitatively. After acclimation for seven days, the clams were placed in an ice bath for anesthetisation, and the ovary or testis was dissected. The sampled ovary or testis was divided into two pieces: one piece was immediately frozen in liquid nitrogen for total RNA extraction, and the other piece was fixed in 4% paraformaldehyde for histological examination. Based on the histological features of previously reported by Yan (2009), the gonadal development was classified into five stages: proliferation stage (stage I), growing stage (stage II), maturation stage (stage III), spawning stage (stage IV), and spent stage (stage V). Based on the staging results, the ovary or testis tissues from three individuals at growing stage were selected for transcriptome analysis.

2.3 RNA extraction and transcriptomic sequencing

Total RNA was extracted from each sample using TRIzol reagent (Invitrogen, USA) according the manufacturer's instructions (Invitrogen) and genomic DNA was removed using DNase I (TaKara). The integrity and purity of the total RNA quality were determined by 2100 Bioanalyser (Agilent Technologies) and quantified using the ND-2000 (NanoDrop Technologies).

RNA purification, reverse transcription, library construction and sequencing were performed at Shanghai Majorbio Bio-pharm Biotechnology Co., Ltd. (Shanghai, China) according to the manufacturer's instructions (Illumina, San Diego, CA). The transcriptome library was prepared following TruSeqTM RNA sample preparation kit from Illumina (San Diego, CA) using 1μg total RNA. Then, the synthesized cDNA was subjected to end-repair, phosphorylation and 'A' base addition following Illumina's library construction protocol. After quantification by TBS380, paired-end RNA sequencing library was sequenced with the Illumina NovaSeq 6000 sequencer (2 × 150 bp read length).

2.4 Transcriptome assembly and differential expression analysis

The raw paired-end reads were trimmed and quality controlled by fastp with default parameters (Chen et al., 2018). Then, clean data from the samples were used to perform *de-novo* assembly with Trinity (Grabherr et al., 2011). The assembled transcripts were assessed and optimized with BUSCO (Manni et al., 2021), TransRate (Smith-Unna et al., 2016) and CD-HIT (Fu et al., 2012). All the assembled transcripts were searched against the National Center for Biotechnology Information (NCBI) protein non-redundant (Nr), Swiss-Prot, Pfam, Clusters of Orthologous Groups of proteins, Gene Ontology (GO) and Kyoto Encyclopedia of Genes and Genomes (KEGG) databases using BLASTX to identify proteins that had the highest sequence similarity with the given transcripts to retrieve their function annotations, and a typical cut-off E-values less than 1.0×10^{-5} was set.

The expression level of each transcript was calculated using the fragments per kilobase of exon per million mapped reads (FPKM) method (Trapnell et al., 2010). To identify differentially expressed genes (DEGs) across samples, we considered DEGs with $|\log2(\text{foldchange})| \geq 1$ and P-value ≤ 0.05 to be significantly different expressed genes. To identify DEGs that were significantly enriched in GO terms and metabolic pathways at P-value ≤0.05, we applied Goatools and KOBAS were applied for GO functional enrichment and KEGG pathway analysis, respectively (Xie et al., 2011).

2.5 Quantitative real-time PCR

Eight genes involved in gonadal development and sexual determination/differentiation were randomly selected for validation using qPCR. A reverse first-strand cDNA synthesis kit (RR036A, Takara Bio, Japan) was used to synthesize first-strand cDNA. Primer pairs were designed using Primer 6.0, and all the primer sequences are listed in Table 1. *β-actin* was used as the internal control to normalize

TABLE 1 Specific primers used to in qPCR.

Primer name	Sequence (5′→3′)	Tm (°C)
Testis-specific serine/threonine-protein kinase 1	F: *TGAAATGCGAGAATCTGCTGT* R: *CATGAAGGGGTAGATGGTAAGG*	60.2
Sperm-associated antigen 6	F: *TGGCAATGGCTGTCATAGTCT* R: *TGAGGCATCTGCTCTGAGGTA*	60.2
Doublesex and mab-3-related transcription factor 1 (Dmrt1)	F: *TGTATCCGTCAAACCCTTCCT* R: *CCCACTGCACCATAGCCAAA*	60
MAM and LDL-receptor class A domain-containing protein 1	F: *TCCAGCAGCCATGTTTGAGA* R: *ACTTGTTGGTTGCCCCGTTA*	60
Cell division cycle protein 20 homolog	F: *GGTGTCATAGCAACGGGTGG* R: *AGGGGCTCAAACTGAAACTTCT*	60
Vitellogenin	F: *TTGCTTGGAAGGATTATGGATG* R: *GGCTTTACAGGATTTCTGGGTTT*	60
Prostaglandin reductase 1	F: *GACAATGTGGGAGGCGAGTT* R: *CTGCCCAGCCTATGAACCCT*	60

(Continued)

TABLE 1 Continued

Primer name	Sequence (5′→3′)	Tm (°C)
Forkhead box protein L2 (Foxl2)	F: *ACTTGCTTCCTGTGGATACGG* R: *TAAATGGCTCGCTCTGTTGC*	60
β-actin	F: *CCTGGTATTGCCGACCGTAT* R: *TTGGAAGGTGGACAGTGAAGC*	60

target gene expression. qPCR was carried out with a StepOnePlus™ real-time PCR system using SYBR1 Green I (TakaRa, Japan) according to the manufacturer's instructions. The volume of qPCR reaction system was 20 μl containing 2 μl of cDNA template, 0.4 μl of each primer (10 mM), 10 μl of SYBR premix, 0.4 μl of ROX Reference Dye (50×) and 6.8 μl of water. PCR conditions were as follows: 95°C for 30s; 40 cycles of 95°C for 5s, 60/60.2°C for 30 s, and 72°C for 30 s. The relative expression level of each gene was calculated using the $2^{-\Delta\Delta Ct}$ method (Livak and Schmittgen, 2001).

2.6 Phylogenetic and sequence analysis of *C. sinensis* vitellogenin

Based on the results of transcriptome sequencing, the higher expression level of *CsVg* was found in the ovary of *C. sinensis*, the *CsVg* was selected for the further analysis in this study. The amino acid sequence and open reading frame (ORF) of *CsVg* were predicted by the ORF finder program (http://www.ncbi.nlm.nih.gov/gorf/gorf.html). The conserved domains of *CsVg* and other species were analyzed using the online software Simple Modular Architecture Research Tool (http://smart.embl-heidelberg.de/smart/set_mode.cgi?NORMAL=1). Subsequently, ClustalX and MEGA 5.0 software were used to carry out multiple sequence alignment and phylogenetic tree construction of neighbor-joining (NJ) system. The amino acid sequences of other species used in these analyses were obtained from GenBank, including *Xenopus laevis* (AB092605.1), *Oryzias latipes* (AB092605.1), *Caenorhabditis elegans* (X56213.1), *Portunus trituberculatus* (DQ000638.1), *Scylla paramamosain* (KU987908.1), *Litopenaeus vannamei* (AY321153.2), *Haliotis discus hannai* (AB360714.1), *Scapharca broughtonii* (MG580782.1), *Tegillarca granosa* (JQ266265.2), *Crassostrea angulate* (JX218047.2), *Crassostrea gigas* (AB084783.1), *Saccostrea glomerata* (KU194475.1) and *Ostrea edulis* (XM_048903027.1).

2.7 Expression pattern analysis of *C. sinensis* vitellogenin

To assay the gene expression of *CsVg* in different tissues, several tissues (ovary, hepatopancreas, adductor, pipe, gill, foot, mantle) were dissected from the clams in the gonadal growing stage. In this experiment, different tissues from three individual *C. sinensis* were used for tissue-specific expression analysis. Meanwhile, the ovary from female clams at each gonadal developmental stage were also collected to determine the abundance of *CsVg* transcripts. A total of 6-8 clams were used for sampling in each stage. Total RNA isolation, cDNA synthesis and PCR reactions were all performed as described above.

2.8 Estradiol treatment experiment

To analyze the transcriptional response of *CsVg* to estradiol, we performed an *in vivo* exposure experiment using *C. sinensis* at the gonadal growing stage was performed. Specifically, 120 healthy clams were randomly divided into three groups of 30. The clams were exposed for 21 days to various nominal estradiol concentration (0+ethanol μg/L, 5 μg/L and 50 μg/L) in accordance with previous literature (Wu et al., 2019). During exposure, the clams were maintained in a 20 L plastic container, and uneaten food and feces were removed before water renewal. Throughout the experiment, the seawater with estradiol was changed daily to ensure that the concentration of estradiol in each group remained invariable during the experiment. At the end of the estradiol exposure, the ovary and hepatopancreas were dissected and stored at -80°C for RNA extraction.

2.9 Statistical analysis

Data are presented as the mean ± standard error (SE). Statistical analyses were performed using SPSS Statistics V22.0. P value of < 0.05 was considered statistically significant. When normal distribution and/or homogeneity of variances were not achieved, data were subjected to the Kruskal-Wallis H nonparametric test, followed by the Games-Howell nonparametric multiple comparison test.

3 Result

3.1 Gonad developmental stages of *C. sinensis*

After dissection, the structure of the ovary and testis can be easily distinguished by microscopic observation of gonadal sections. Histological results showed that the ovaries and testes of *C. sinensis* used for RNA sequencing were at growing stage (stage II) of gonadal maturation (Figure 1).

3.2 Sequencing and *de novo* assembly

Two cDNA libraries were constructed from the ovary and testis of *C. sinensis*. After adaptor sequences and low-quality reads were

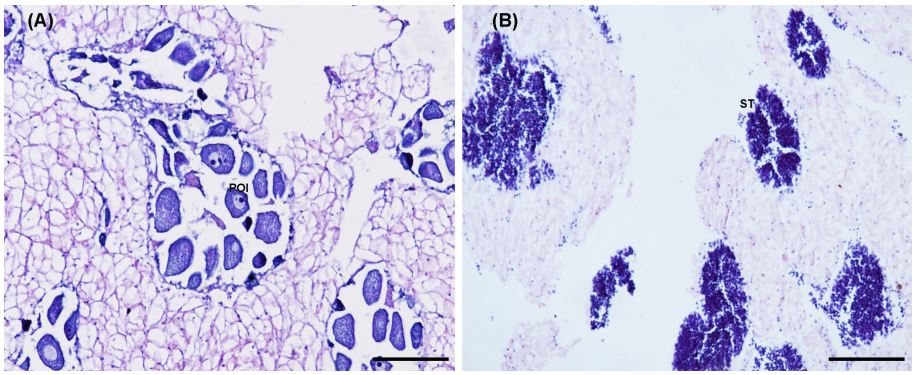

FIGURE 1
Histological characteristics of the ovary **(A)** and testis **(B)** of the *C sinensis* for transcriptome sequencing. POI, pre-vitellogenesis oocyte; ST: spermatid. Scale bars, 100 μm.

removed, 278 million clean reads, including 140 109 554 reads from the ovary libraries and 137 762 234 reads from the testis libraries, were obtained from the ovary and testis of the *C. sinensis* transcriptome (Table 2). Among these clean reads, the Q30 in each sample was above 90%. All reads were submitted to the website of NCBI (PRJNA906186).

All clean reads were assembled into 134 124 unigenes, and the minimum, longest, and average lengths of unigenes were 201, 29 212 and 1 095 bp, respectively. Among the unigenes, 77 305 unigenes (57.64%) were successfully annotated by searching against the Nr, Swissport, Pfam, COG, GO and KEGG databases. Especially, 22 095 (28.59%) unigenes were annotated to the Nr database, whereas 15 142 (19.59%) unigenes can be fully annotated to the SwissProt database (Figure 2). In addition, the species most represented in BLASTx searches included *Pecten maximus* (18.5%), *Mizuhopecten yessoensis* (17.23%) and *Crassostrea gigas* (4%) (Figure 3).

3.3 Analysis of differentially expressed genes

By comparing the databases of ovary and testis, 1 440 DEGs were detected in the transcriptome, of which 1 013 and 427 DEGs were upregulated and downregulated, respectively. To analyze the functions of these DGEs, we conducted GO and KEGG analyses. GO annotation analysis indicated that these DEGs were annotated to three functional ontologies, i.e. molecular function (399 transcripts), cellular component (504 transcripts), and biological process (493 transcripts) (Figure 4). In the biological process category, the metabolic process (GO:0008152) and cellular process (GO:0009987) level 2 terms were the most abundant terms. In the cellular component category, the membrane part (GO:0044425) and cell part (GO:0044464) level 2 terms were the most abundant terms. In the cellular component category, the binding (GO:0005488) and catalytic activity (GO:0003824) level 2 terms were the most abundant terms. KEGG enrichment analysis showed that these DEGs were enriched in 220 specific KEGG metabolic pathways. Several DEGs were mapped to several pathways related with reproduction, such as progesterone-mediated oocyte maturation, cell cycle, cAMP signaling pathway and oocyte meiosis. The top 20 most significantly enriched metabolic pathways are represented in Figure 5.

TABLE 2 Raw reads and quality control of reads for cDNA libraries of *C. sinensis* transcriptome.

Type	Ovary	Testis
Raw reads	140 937 740	138 575 290
Clean reads	140 109 554	137 762 234
Q20 (%)	97.87	97.91
Q30 (%)	93.57	93.71
GC content (%)	39.81	39.55

3.4 Key genes involved in sexual determination/differentiation and gonadal development

Through the analysis of the overall gene expression profiles of gonads, several candidate genes involved in various processes of sex determination/differentiation and gonadal development were identified (Table 3). Among the candidate genes, twenty-three key genes were mainly involved in sexual determination/differentiation. Specifically, the transcript levels of *Foxl2* and *GATA-type zinc finger protein 1-like* in the ovary were significantly higher than those in the testis. The expression levels of *Dmrt1*, *Sox9, Fem-1, Follistatin, Transformer-2 protein homolog alpha isoform X5, Zinc finger Y-chromosomal protein 1-like, E3 ubiquitin-protein ligase MARCHF3 isoform X1, Synaptonemal complex protein 1 isoform X2, Transcription factor Runt* and *Protein dpy-30* in the testis were higher than those in the ovary. Twenty key genes were mainly involved in the process of spermatogenesis, and the higher expression levels of *Spermatogenesis-associated protein 17-like isoform X1, Meiotic recombination protein SPO11-like isoform X1, Meiotic recombination protein REC8 homolog isoform X2, Ropporin-*

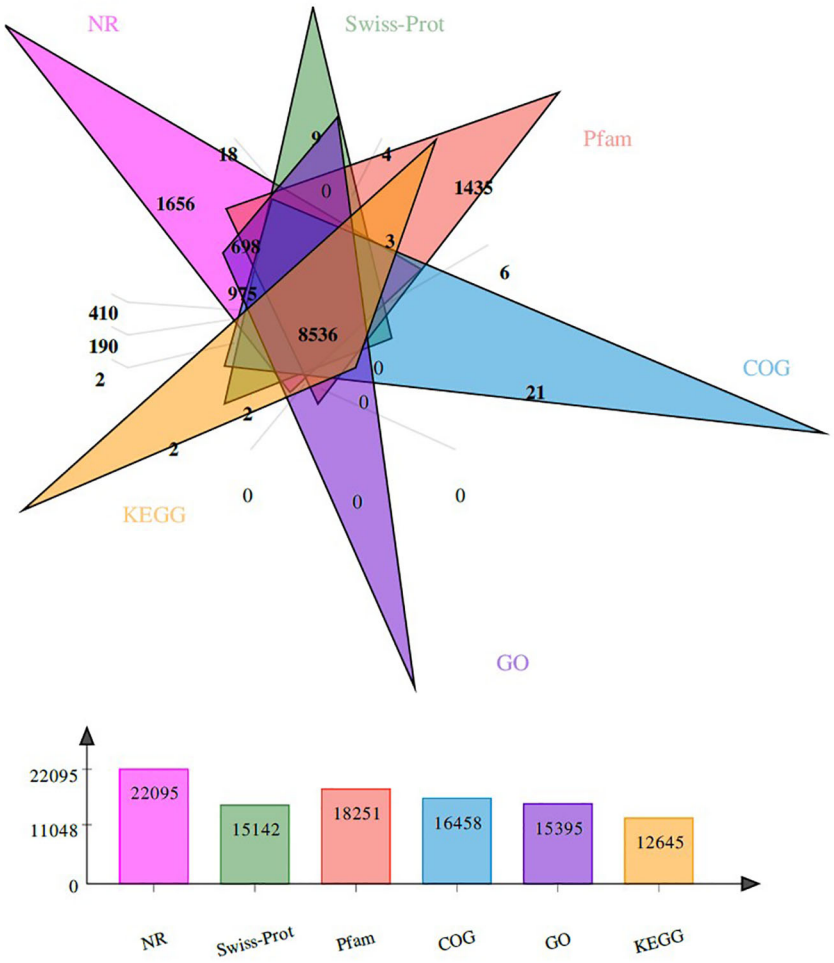

FIGURE 2
The distribution of unigenes in six databases. The colors show different databases. The number represents the total number of unigenes.

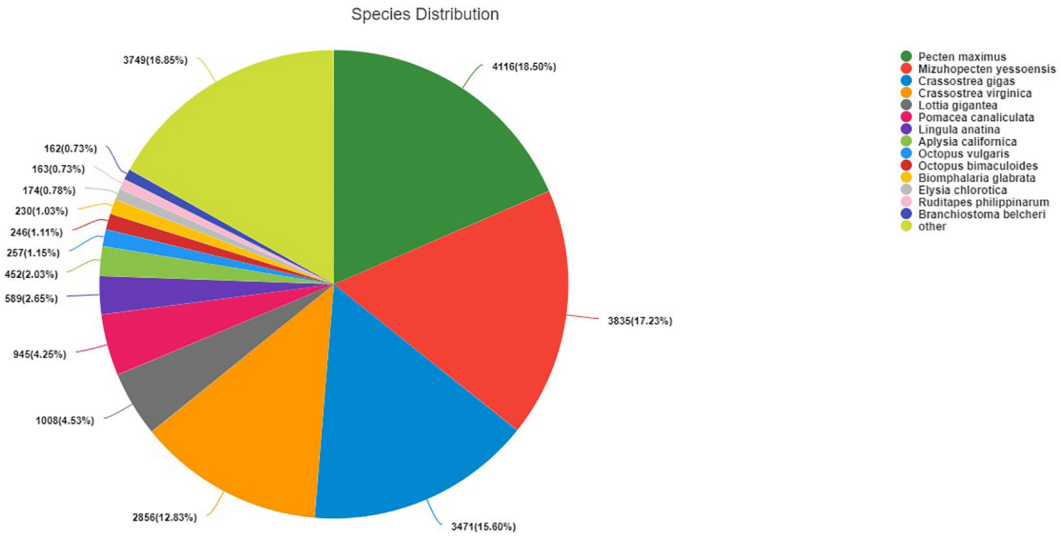

FIGURE 3
Species distribution of BLASTx hits.

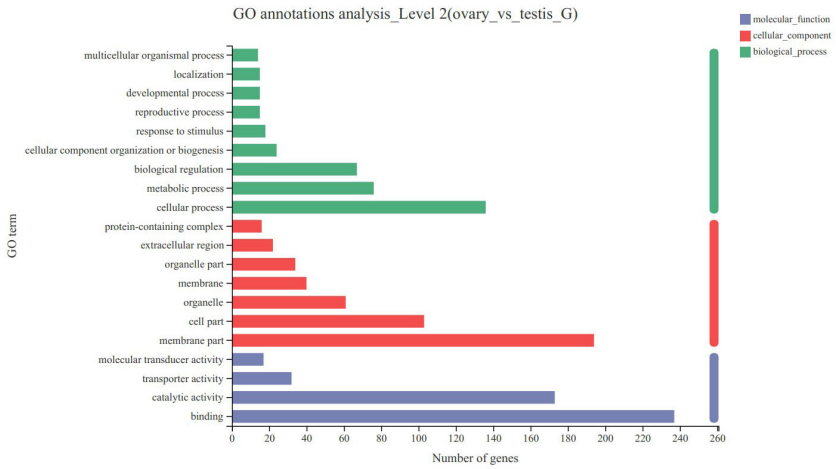

FIGURE 4
GO annotation analyses of differentially expressed genes (DEGs) in *C. sinensis* transcriptome. The left vertical coordinate indicates the second level of GO classification. The horizontal coordinate indicates the number of unigene/transcript included in this secondary classification, and the three colors on the right indicate the three major branches of GO.

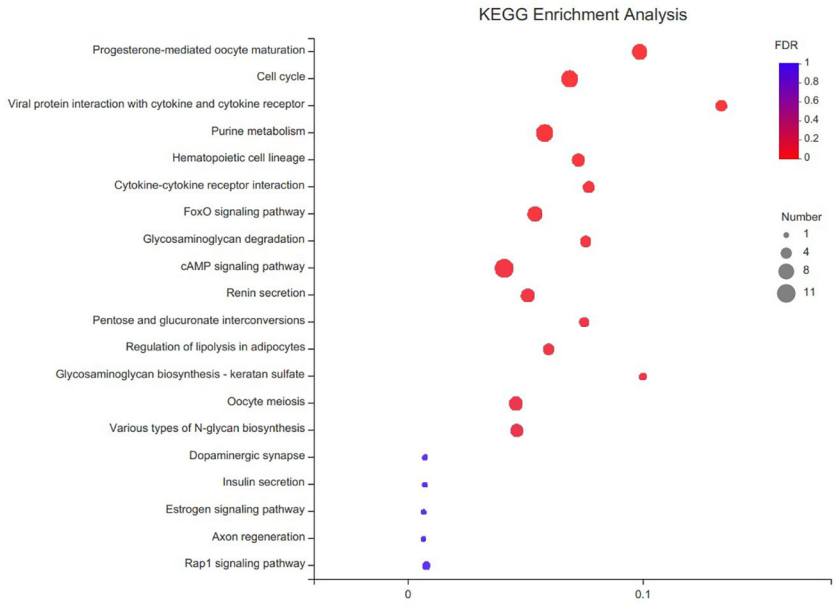

FIGURE 5
KEGG enrichment analyses of differentially expressed genes (DEGs) in *C. sinensis* transcriptome. The vertical coordinate is the name of the KEGG metabolic pathway and the horizontal coordinate is the number of transcript/unigene annotated to the pathway.

1-like protein, Sperm-tail PG-rich repeat-containing protein 2-like (*STPG1*), *Testis-specific serine/threonine-protein kinase 1, Testis-specific serine/threonine-protein kinase 3-like, Sperm-associated antigen 6, Kelch-like protein 10, Armadillo repeat-containing protein 4-like isoform X1* and *G2/mitotic-specific cyclin-B3-like* were found in the testis. Moreover, fifteen genes related to ovarian development and five genes encoding steroid biosynthesis/metabolism were identified in the ovary and testis.

3.5 Validation of gene expression by qPCR

Eight selected important genes related to sexual determination/differentiation and gonadal development of *C. sinensis* were determined using qPCR to validate the RNA-seq results. qPCR results showed that *Dmrt1*, *Testis-specific serine/threonine-protein kinase 1* and *Sperm-associated antigen 6* had significantly higher expression levels in male gonads (Figure 6), whereas *Foxl2*, *Vg*,

10.3389/fmars.2022.1110587

TABLE 3 Summary of differential and non-differentially expressed genes related to sex determination/differentiation and gonadal development in the transcriptome of *C. sinensis*.

Functional category	Gene id	Gene name	log2 Fold changes (testis/ovary)	*P-value*
Sex determination/differentiation				
	TRINITY_DN20554_c0_g1	*Doublesex and mab-3-related transcription factor 1* (*Dmrt1*)	2.10	3.77E-03
	TRINITY_DN32439_c0_g1	*Transcription factor SOXC*(*Sox4*)	-0.20	7.24E-01
	TRINITY_DN12181_c0_g1	*Transcription factor SOXB1*(*Sox2*)	-0.75	3.33E-01
	TRINITY_DN5766_c0_g1	*Transcription factor SOXE*(*Sox9*)	0.63	2.84E-01
	TRINITY_DN17013_c0_g1	*Forkhead box protein L2* (*Foxl2*)	-4.47	1.27E-05
	TRINITY_DN18205_c0_g2	*Wnt-4a*	-0.79	4.91E-01
	TRINITY_DN7453_c0_g2	*GATA-type zinc finger protein 1-like*	-4.21	8.97E-04
	TRINITY_DN1084_c0_g1	*Growth arrest and DNA damage-inducible protein GADD45 alpha*	-0.43	5.04E-01
	TRINITY_DN4959_c0_g1	*β-catenin*	0.03	9.60E-01
	TRINITY_DN3871_c0_g1	*Fem-1*	1.32	1.05E-01
	TRINITY_DN26641_c0_g1	*Follistatin*	1.19	8.01E-01
	TRINITY_DN14753_c0_g1	*Transformer-2 protein homolog alpha isoform X5*	0.64	2.90E-01
	TRINITY_DN7640_c0_g1	*Structural maintenance of chromosomes protein 5-like*	1.25	8.71E-02
	TRINITY_DN4319_c0_g1	*Serine/threonine-protein kinase PLK1-like*	1.17	8.71E-02
	TRINITY_DN11738_c2_g2	*Zinc finger Y-chromosomal protein 1-like*	2.45	5.13E-02
	TRINITY_DN11833_c0_g2	*E3 ubiquitin-protein ligase MARCHF3 isoform X1*	11.8	1.24E-08
	TRINITY_DN12272_c0_g2	*Synaptonemal complex protein 1 isoform X2*	4.48	1.40E-05
	TRINITY_DN5752_c0_g1	*Core histone macro-H2A.1-like isoform X1*	0.47	4.76E-01
	TRINITY_DN11990_c0_g1	*Platelet-derived growth factor subunit A-like*	0.30	6.89E-01
	TRINITY_DN5555_c0_g1	*Transcription factor Runt*	1.09	5.33E-02
	TRINITY_DN27415_c0_g1	*Protein dpy-30*	0.68	2.11E-01
	TRINITY_DN16278_c0_g1	*Elongation factor 1 alpha*	-0.90	1.08E-01
	TRINITY_DN28419_c0_g1	*Paramyosin*	-0.78	1.86E-01
Spermatogenesis				
	TRINITY_DN8046_c2_g1	*Spermatogenesis-associated protein 17-like isoform X1*	2.57	1.44E-04
	TRINITY_DN122_c0_g1	*Meiotic recombination protein SPO11-like isoform X1*	4.52	1.37E-05
	TRINITY_DN7476_c0_g1	*Meiotic recombination protein REC8 homolog isoform X2*	5.11	7.41E-05
	TRINITY_DN3408_c0_g1	*Ropporin-1-like protein*	3.84	4.27E-06
	TRINITY_DN16340_c0_g1	*Sperm flagellar protein 2-like isoform X4*	0.29	6.28E-01
	TRINITY_DN7095_c0_g1	*Sperm-tail PG-rich repeat-containing protein 2-like*	5.35	1.73E-07
	TRINITY_DN46387_c0_g1	*Testis-specific serine/threonine-protein kinase 1(Tssk1)*	10.8	5.73E-10
	TRINITY_DN1043_c0_g1	*Testis-specific serine/threonine-protein kinase 3-like (Tssk3)*	7.78	1.19E-08
	TRINITY_DN2241_c0_g1	*Armadillo repeat-containing protein 4-like isoform X1*	3.53	1.28E-05
	TRINITY_DN5793_c0_g1	*Motile sperm domain-containing protein 1 isoform X1*	1.17	5.66E-02
	TRINITY_DN33601_c0_g1	*Nucleoside diphosphate kinase homolog 5-like*	1.41	2.03E-02
	TRINITY_DN7758_c0_g1	*SH3 domain-containing YSC84-like protein 1*	0.15	7.81E-01
	TRINITY_DN6087_c0_g1	*Axonemal dynein light chain p33*	1.24	4.24E-02
	TRINITY_DN10017_c0_g1	*Sperm-associated antigen 6*	2.96	4.56E-05

(Continued)

TABLE 3 Continued

Functional category	Gene id	Gene name	log2 Fold changes (testis/ovary)	*P-value*
	TRINITY_DN10999_c0_g1	*Kelch-like protein 10*	10.9	1.87E-10
	TRINITY_DN6562_c0_g1	*LIM homeobox 9*	0.27	6.77E-01
	TRINITY_DN5365_c0_g1	*Small ubiquitin-related modifier 2-like*	0.35	5.10E-01
	TRINITY_DN386_c0_g1	*Ubiquitin conjugating enzyme isoform 1*	0.26	6.56E-01
	TRINITY_DN2167_c0_g1	*Mitotic checkpoint protein BUB3*	0.16	8.11E-01
	TRINITY_DN2008_c0_g1	*G2/mitotic-specific cyclin-B3-like*	3.49	1.73E-04
Ovarian development				
	TRINITY_DN1182_c0_g1	*Vitellogenin*	-6.60	5.42E-09
	TRINITY_DN5981_c0_g2	*Estrogen receptor gamma-like isoform X1*	-0.59	4.11E-01
	TRINITY_DN1678_c0_g1	*Estrogen-related receptor*	0.06	9.23E-01
	TRINITY_DN3450_c0_g1	*Vitellogenin receptor-like isoform X2*	0.52	5.21E-01
	TRINITY_DN38987_c0_g4	*MAM and LDL-receptor class A domain-containing protein 1*	-6.00	7.38E-04
	TRINITY_DN9377_c0_g1	*Melatonin receptor type 1B-B-like*	-1.40	3.48E-02
	TRINITY_DN744_c0_g1	*E3 ubiquitin-protein ligase HUWE1-like isoform X4*	-0.40	4.58E-01
	TRINITY_DN2483_c0_g1	*Ubiquitin thioesterase OTUB1-like*	1.05	8.96E-02
	TRINITY_DN2249_c0_g1	*26S proteasome regulatory subunit 7*	0.63	2.37E-01
	TRINITY_DN8661_c0_g1	*Cell division cycle protein 20 homolog*	-9.43	4.41E-12
	TRINITY_DN42248_c0_g1	*Receptor-type guanylate cyclase Gyc76C-like*	-2.53	2.50E-01
	TRINITY_DN5631_c0_g1	*Prostaglandin reductase 1*	-1.58	3.95E-02
	TRINITY_DN26216_c0_g1	*Transcription factor GATA-4 isoform X1*	-1.22	3.18E-02
	TRINITY_DN3852_c0_g2	*Wilms tumor protein 1-interacting protein homolog*	-0.11	8.60E-01
	TRINITY_DN19696_c0_g1	*Fascin-like*	-0.92	1.08E-01
Steroid biosynthesis/metabolism				
	TRINITY_DN982_c0_g1	*Steroid 17-alpha-hydroxylase/17,20 lyase-like (CYP17A)*	-0.73	2.02E-01
	TRINITY_DN25278_c0_g2	*17-beta-hydroxysteroid dehydrogenase 14-like*	-0.12	8.40E-01
	TRINITY_DN18332_c0_g3	*Estradiol 17-beta-dehydrogenase 2-like*	-0.20	8.97E-01
	TRINITY_DN13675_c0_g1	*Hydroxysteroid dehydrogenase-like protein 2*	0.25	6.94E-01
	TRINITY_DN27506_c0_g1	*Estrogen sulfotransferase-like isoform X2*	-1.73	2.61E-01

Fold changes (Log2 ratio) in gene expression.

MAM and LDL-receptor class A domain-containing protein 1, *Cell division cycle protein 20 homolog* and *Prostaglandin reductase 1* had significantly higher expression levels in female gonads (Figure 6). The qPCR results showed that the relative expression patterns of these eight genes were consistent with the RNA-seq results (Figure 6).

3.6 Sequences analysis of *CsVg*

The *CsVg* sequence contains a 5584 bp open reading frame encoding 1860 amino acids. Comparison of the amino acid sequence encoded by the *CsVg* with the homologues from other species showed that *CsVg* contains a conserved DUF1943 and VWD domains (Figure 7A). However, the typical lipoprotein N-terminal domain of known lipid transport proteins was not found in the amino acid sequence of *CsVg*. Finally, the phylogenetic tree obtained by NJ method revealed that the *CsVg* from bivalves was clustered in a separate clade from the *CsVg* from vertebrates and invertebrates (Figure 7B). Evolutionarily, the protein sequence of CsVg is more similar to that of the Pacific abalone *Haliotis discus hannai*.

3.7 Tissue distribution and temporal expression profiles during gonadal development of *CsVg*

Tissue distribution analysis demonstrated that *CsVg* was expressed in various tissues of female *C. sinensis* (Figure 7C).

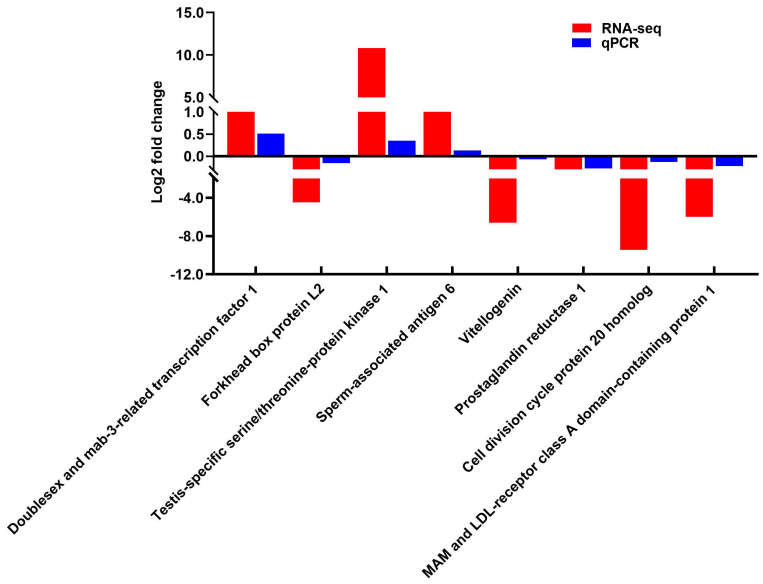

FIGURE 6
Expression levels of eight selected DEGs normalized to β-actin of *C. sinensis* was determined by qPCR.

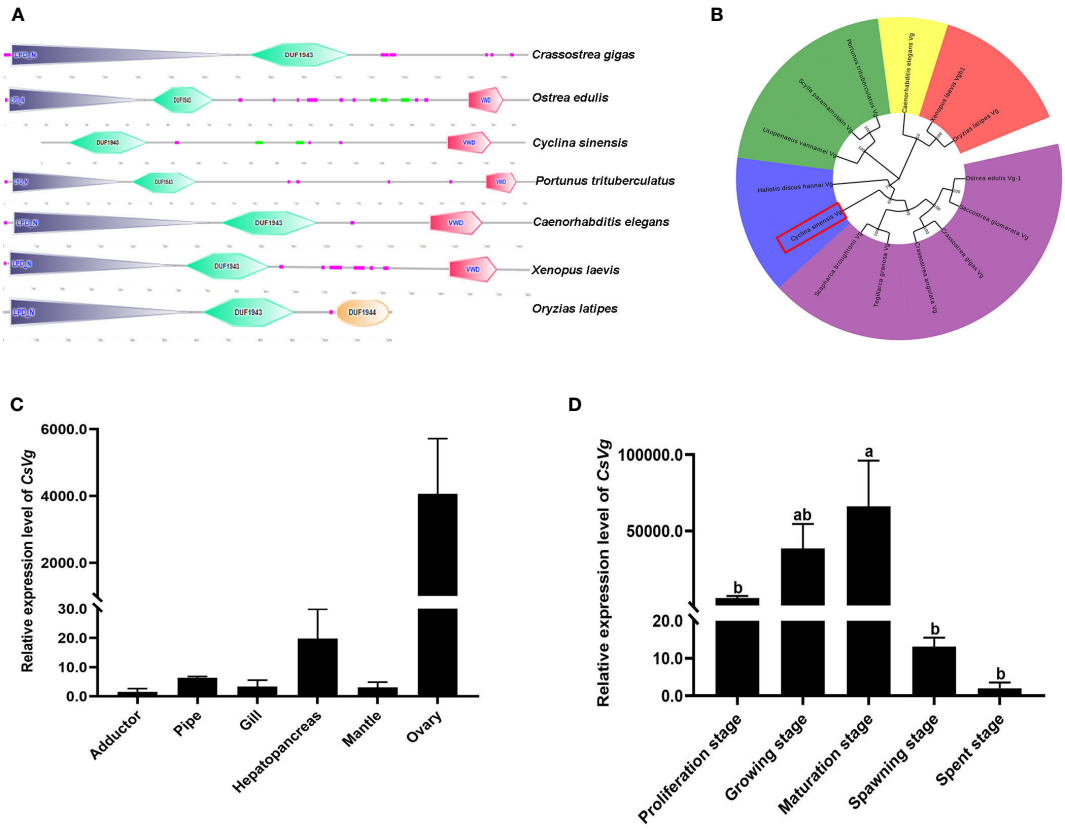

FIGURE 7
Sequence analysis of *CsVg* and its expression profile in tissues of *C sinensis*. **(A)** Domain structures of *CsVg* and other selected species. **(B)** Phylogenetic tree based on amino acid sequences of *Vg* gene **(C)** Relative expression of *CsVg* in different tissues **(D)** Relative expression of *CsVg* in different ovarian development stages. The columns with different letter indicate significant difference ($P < 0.05$).

Remarkably, *CsVg* had significantly high expression level in the ovary and hepatopancreas. To test the correlation of *CsVg* expression level with the gonadal development stages, the relative abundance of *CsVg* transcripts was detected in different stages of ovarian development by qPCR. As shown in Figure 7D, the expression level of *CsVg* in the ovary increased continuously from proliferation stage to maturation stage of *C. sinensis*, and it reached the peak level at maturation stage. However, the expression level of *CsVg* in the ovary decreased from spawning stage to spent stage.

3.8 *In vivo* effect of estradiol on *CsVg* expression

The expression level of *CsVg* in the ovary of *C. sinensis* exposure with estradiol is shown in Figure 8A. Compared with the control treatment, the expression level of *CsVg* in the ovary increased in a dose-dependent manner by estradiol treatments. Moreover, the expression levels of *CsVg* in the ovary of *C. sinensis* significantly increased in the 50μg/L estradiol treatment. In the hepatopancreas, estradiol treatments (5μg/L, 50μg/L) also significantly up-regulated the expression levels of *CsVg* compared with the control (Figure 8B).

4 Discussion

The reproduction of marine invertebrates demonstrates a wide range of sexual reproduction traits, which often manifests through free spawning (Ostrovsky, 2021; Picard et al., 2021). As a typical buried shellfish, the research on the molecular mechanism of *C. sinensis* reproduction is a key basis work for its genetic selection. Therefore, the present study firstly sequenced *C. sinensis* gonad transcriptomes, screened out several candidate genes involved in the process of sexual determination/differentiation and gonadal development, and then analyzed the responses of several genes to estradiol. The results of this study will help us understand the general underlying molecular mechanisms of bivalve reproduction and provide a scientific basis for the sexual control and breeding of shellfish.

In this study, serveral DEGs were mapped to several pathways related with to reproduction, including progesterone-mediated oocyte maturation, cell cycle, cAMP signaling pathway, oocyte meiosis and estrogen signaling pathway, which suggests the significance of signal transduction systems and endocrine regulation in gonadal development of *C. sinensis*. Importantly, twenty-three potential sexual determination/differentiation genes were identified by analysis of the female and male gonad transcriptomes of *C. sinensis*, these genes included *Dmrt1*, *Sox9*, *Wnt-4a*, *Foxl2*, *GATA-type zinc finger protein 1-like*, *Elongation factor 1 alpha* (*EF-1-alpha*), *Transformer-2 protein homolog alpha isoform X5*, *Follistatin* and *Fem-1*. The discovery of these reported genes suggests that, similar to other bivalves and mammalian, these genes also play an important role in sexual determination/differentiation of *C. sinensis* (Li et al., 2016a; Yang et al., 2016; Yao et al., 2021). Robinson et al. (2022) reported that *Dmrt* are key genes for male and female development of mollusk by the analysis of RNAseq data from eight phylogenetically diverse bivalve species. Adzigbli et al. (2019) reported that *Sox9* and *Gata-type zinc finger protein 1* are involved in genetic sex determination of pearl oysters. The signalling molecule Wnt-4 is not only crucial for female sexual development, but its signalling is also well implicated in mammalian testis development (Vainio et al., 1999; Naillat et al., 2015). Foxl2 plays a major role in initiating ovarian differentiation in fish and bivalves (Jin et al., 2022; Sun et al., 2022). Follistatin1 not only acts as an inhibitory binding protein of activin in the regulation of oocyte maturation in adult females but also plays a potential role in the masculinization of juveniles (Jiang et al., 2012). *EF-1-alpha* has been reported to be expressed in male and female germ cells, and it may contribute to the massive protein synthesis required for egg production (Kinoshita et al., 2000; Zhou et al., 2002). Wang et al. (2021a) reported that Transformer-2 plays a potential regulatory role in embryonic sex determination and early gonadal development of Freshwater Pearl Mussel *Hyriopsis cumingii*. Differently to what reported in *H. cumingii*, the present study showed the higher expression level of *Fem-1* in the testis than in the ovary of *C. sinensis* (Wang et al., 2021b). The opposite result can potentially be explained by the different functions of various *Fem-1* isoforms in distinct species. Tan et al. (2001) reported that Fem-1 plays pivotal roles in sex determination of *Caenorhabditis elegans*, whereas Fem-2 has a role in apoptosis signaling. Therefore, further research is required in *C. sinensis* regarding what these genes target and how they function to determine sex.

Spermatogenesis is a complicated process of proliferation and division and involves numerous genes (Yu et al., 2009; Yue et al., 2018). Previous study reported that *spermatogenesis-associated*

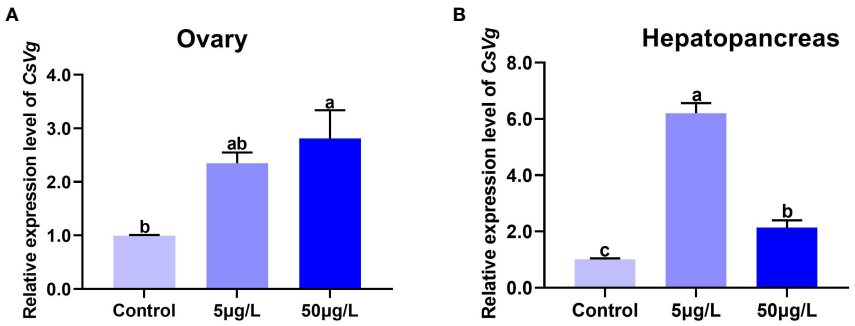

FIGURE 8
The expression level of *CsVg* in the ovary **(A)** and hepatopancreas **(B)** of *C sinensis* by different concentrations of estradiol. The columns with different letter indicate significant difference ($P < 0.05$).

protein 17 is a testis-specific apoptosis genes and plays important roles in the gonadogenesis and testis development (Nie et al., 2011). *Meiotic recombination protein REC8* is a prominent component of the meiotic prophase chromosome axis, whereas *Meiotic recombination protein SPO11* initiates meiotic recombination by generating DNA double-strand breaks (Yoon et al., 2016; Paiano et al., 2020). Ropporin is a spermatogenic cell-specific protein and may be involved in sperm maturation (Chen et al., 2009). In this study, the *spermatogenesis-associated protein 17-like isoform X1*, *meiotic recombination protein SPO11-like isoform X1*, *meiotic recombination protein REC8 homolog isoform X2* and *Ropporin-1-like protein* were also identified in the testis, where all of them had higher transcript levels in the testis, demonstrating that the *spermatogenesis-associated protein 17-like isoform X1*, *meiotic recombination protein SPO11-like isoform X1 meiotic recombination protein REC8 homolog isoform X2* and *Ropporin-1-like protein* are involved in the spermatogenesis of *C. sinensis*. Notably, members of testis-specific serine/threonine kinases (Tssk) family are required for male fertility in mammals, and targeted deletion of *Tssk1* and *Tssk2* results in dysregulation of spermiogenesis (Shang et al., 2013; Wang et al., 2022). Several studies reported that *Tssk1/2*, *Tssk3*, *Tssk4* and *Tssk5* play a functional role during spermatogenesis of several mollusks, including the pen shell *Atrina pectinate*, abalone *Haliotis discus hannai* and Bay Scallop *Argopecten irradians* (Li et al., 2016b; Kim et al., 2019; Xue et al., 2021). The present study showed the higher expression level of *Tssk1* and *Tssk3* in the testis of *C. sinensis*, indicating that Tssk family may have a role in sperm differentiation in the testis and/or fertilization. Moreover, Murray and Hobbs (2022) reported that *Kelch-like protein homolog 10* and *Armadillo repeat-containing protein 4 isoform X2* are involved in spermatogenesis and spermatid development/maturation of male blue mussel *Mytilus edulis*, respectively. Similarly, the *Kelch-like protein homolog 10* and *Armadillo repeat-containing protein 4 isoform X2* have previously been identified in serveral bivalve species including *Mytilus galloprovincialis*, *Nodipecten subnodosus*, *Pinctada margaritifera* and *C. gigas* (Craft et al., 2010; Llera-Herrera et al., 2013; Teaniniuraitemoana et al., 2014; Gallardi et al., 2021). In agreement with previous results, the higher expression level of *Kelch-like protein 10* and *Armadillo repeat-containing protein 4-like isoform X1* was found in the testis, illustrating that these genes play a key role in the sperm development of *C. sinensis*. Sperm-associated antigen 6 (SPAG6) is an important flagellar protein required for normal flagellar and cilia motility (Jarrell et al., 2020). De Sousa et al. (2014) reported that the mRNA levels of SPAG6 showed a significant correlation with the gonad area of European Clam *Ruditapes decussatus*. The present study revealed the higher transcript levels of *SPAG6* in the testis, suggesting that *SPAG6* is essential for the spermatogenesis of *C. sinensis*.

Ovary are the primary reproductive organs, and their normal development is crucial for bivalve reproduction (Yang et al., 2016; Zhao et al., 2022). Notably, vitellogenesis is involved in the accumulation of the major yolk protein vitellin (Vn), which is important in the development and maturation of oocytes (Saavedra et al., 2012; Kang et al., 2014). As a synthetic precursor of Vn, vitellogenin (Vg) is considered a biological marker of ovarian development in vertebrates and invertebrates (Marin and Matozzo, 2004; Porte et al., 2006). In this study, sequence analysis results showed that *CsVg* has no the typical lipoprotein N-terminal domain region compared with other known species, which may be attributed to the involvement of different mechanisms of Vg receptor binding during endocytosis (Xie et al., 2009). Previous studies showed that the lipoprotein N-terminal domain is responsible for lipid binding (Morandin et al., 2014). Tissue distribution results showed that *CsVg* was expressed in various tissues of female *C. sinensis*, which is consistent with the results on Fujian oyster *Crassostrea angulate* and *C. gigas* (Matsumoto et al., 2003; Ni et al., 2014). Remarkably, qPCR data showed that *CsVg* was abundantly expressed in the ovary, indicating that *CsVg* plays crucial roles in the ovarian development of *C. sinensis*. To search for more clues regarding the interaction between *CsVg* and ovarian development, the temporal expression patterns of *CsVg* in the ovary was analyzed during the ovarian development of *C. sinensis*. A relatively abundant expression of *CsVg* in proliferation stage to maturation stage and a significantly low expression in spent stage further demonstrated that *CsVg* is involved in the ovarian development of *C. sinensis*. These results coincide with those of previous studies on bivalve species (Ni et al., 2014; Yang et al., 2016). Vitellogenesis in bivalves is under the control of sex steroid hormone as well as other oviparous animals, and the estradiol levels of bivalve exhibit a seasonal change associated with the reproductive cycle (Osada et al., 2003; Wang and Croll, 2003; Osada et al., 2004). Therefore, to obtain further gain insights into the endocrine regulatory mechanism of *C. sinensis* reproduction, the regulation of *CsVg* mRNA expression by estradiol were analyzed in the ovary and hepatopancreas. The present results showed that estradiol treatments significantly upregulated the mRNA expression of *CsVg* in the ovary, suggesting that estradiol is a primary promoter of *Vg* mRNA transcription in *C. sinensis*. Similar estradiol inducibility of *Vg* was demonstrated in other bivalve species (Osada et al., 2003; Andrew et al., 2010; Qin et al., 2012; Ni et al., 2014). Moreover, the Cs*Vg* mRNA transcription in the hepatopancreas was induced by estradiol, which implies that hepatopancreas may also be involved in the vitellogenesis of *C. sinensis*. Hepatopancreas is another important site of vitellogenesis in crustaceans (Feng et al., 2022). Nonetheless, the regulation mechanism of estradiol in the vitellogenesis of bivalve is largely unknown. In vertebrate, it is well known that estrogen regulates *Vg* gene transcription mainly through binding to estrogen receptors (ER) on the target organ (Nelson and Habibi, 2013). In this study, the *Estrogen receptor gamma-like isoform X1* (*ERγ*) and *Estrogen-related receptor* (*ERR*) were identified in the ovary, indicating that the estradiol-*ERγ*/*ERR*-*Vg* signalling pathway may play an important role the regulation mechanism of estradiol on the vitellogenesis in bivalve. The above hypothesis was also proposed for scallop, mussels and oyster (Wang and Croll, 2003; Ciocan et al., 2010; Ni et al., 2014).

Except for *Vg*, the present study also discovered other genes associated with ovarian development and steroid biosynthesis/metabolism in the transcriptome data. Specifically, the higher expression levels of *MAM and LDL-receptor class A domain-containing protein 1*, *Melatonin receptor type 1B-B-like*, *Cell division cycle protein 20 homolog*, *Prostaglandin reductase 1* and *Transcription factor GATA-4 isoform X1* were detected in the ovary, indicating that

those genes participate in the ovarian development, steroidogenesis, folliculogenesis and oocyte maturation of *C. sinensis*. A previous study showed that *MAM and LDL-receptor class A domain-containing protein 1* may serve as oogonia or oocyte membrane protein mediating diverse signal transduction to regulate oocyte development (Yue et al., 2018). Takahashi and Ogiwara (2021) reported that melatonin can directly regulate ovarian physiology, including steroidogenesis, folliculogenesis, oocyte maturation and ovulation, by binding to melatonin receptors. *Cell division cycle protein 20* is required for spindle assembly and chromosomal segregation during oocyte maturation (Yang et al., 2014). *Prostaglandin reductase 1* plays a negative physiological role in the development of oocytes and ovaries (Prasertlux et al., 2011). *Transcription factor GATA-4* can be a downstream effector of cAMP/PKA pathway in the regulation of *CYP19* gene during folliculogenesis and luteinization (Monga et al., 2012). In addition, five genes related to steroid biosynthesis/metabolism were identified in the transcriptome data. *CYP17A*has been viewed as a critical enzyme for the biosynthesis of sexual steroid, and it performs the 17-alpha-hydroxylation of progesterone and pregnenolone to 17-hydroxyprogesterone (17OHP) and 17-hydroxypreg nenolone, respectively (Athanasoulia et al., 2013). *17 beta-Hydroxysteroid dehydrogenases* (*17 beta-HSDs*) plays a key role in estrogen and androgen steroid metabolism by catalyzing the final steps of steroid biosynthesis (Marchais-Oberwinkler et al., 2011). The present study showed that the *CYP17A* and three genes related to beta hydroxysteroid dehydrogenase enzymes (17-beta-hydroxysteroid dehydrogenase 14-like, Estradiol 17-beta-dehydrogenase 2-like, Hydroxysteroid dehydrogenase-like protein 2) were identified in the gonad, suggesting that these genes are involved in the biosynthesis of sexual steroids in the *C. sinensis*. Moreover, the *Estrogen sulfotransferase-like isoform X2* was also found in the gonad, which indicates the presence ofa balance system of steroid hormone synthesis in clam gonads. A previous study reported that Estrogen sulfotransferase is a cytosolic enzyme that sulphatesestrogens to inactivate them and regulate their homeostasis (Yi et al., 2021).

5 Conclusion

In this study, transcriptome sequencing was used to explore the expression level of genes associated with sexual determination/differentiation and gonadal development of *C. sinensis*. The present study identified 23 genes (*Dmrt1*, *Sox2/4/9*, *Foxl2*, *β-catenin* and *GATA-type zinc finger protein 1-like*) involved in sexual determination/differentiation, 20 genes (*Spermatogenesis-associated protein 17-like isoform X1, Meiotic recombination protein SPO11-like isoform X1, Meiotic recombination protein REC8 homolog isoform X2, Testis-specific serine/threonine-protein kinase 1, Testis-specific serine/threonine-protein kinase 3-like, Sperm-associated antigen 6* and *Kelch-like protein 10*) related to spermatogenesis, 15 genes (*Vitellogenin, MAM and LDL-receptor class A domain-containing protein 1* and *Cell division cycle protein 20 homolog*) associated with the ovarian development and 5 genes involved in steroid biosynthesis/metabolism, respectively. Theresults will provide new insights into the mechanisms of sexual determination/differentiation and gonadal development in marine bivalves. In the future, the roles of these genes need to be elucidated to provide a scientific basis for the sexual control and breeding of shellfish.

Data availability statement

The datasets presented in this study can be found in online repositories. The names of the repository/repositories and accession number(s) can be found below: NCBI - PRJNA906186.

Author contributions

ML: Experimental design, Writing - Original Draft, Data Curation. HN: Formal analysis, Data Curation. ZR: Data Curation, Validation. ZW: Formal analysis, Visualization. SY: Data Curation, Visualization. XL: Experimental design, Formal analysis. ZD: Writing-Editing, Funding acquisition. All authors contributed to the article and approved the submitted version.

Funding

This study was funded by the projects (No.42106088) from the Natural Science Foundation of China, the projects (CARS-49) from Modern Agro-industry Technology Research System; the projects (JBGS [2021]034) from the 'JBGS' Project of Seed Industry Revitalization in Jiangsu Province; an Open-end Funds (SH20201205) of Jiangsu Key Laboratory of Marine Bioresources and Environment, two practice innovation training program projects (No. 202111641127Y and No. SY202257X) for the Jiangsu College students. Infrastructure costs were partially supported by the Project of Jiangsu Fisheries Science and Technology (SZ-LYG202029).

Conflict of interest

The authors declare that the research was conducted in the absence of any commercial or financial relationships that could be construed as a potential conflict of interest.

Publisher's note

References

Adzigbli, L., Wang, Z., Lai, Z., Li, J., and Deng, Y. (2019). Sex determination in pearl oyster: A mini review. *Aquacult. Rep.* 15, 100214. doi: 10.1016/j.aqrep.2019.100214

Andrew, M., O'Connor, W., Dunstan, R., and Macfarlane, G. (2010). Exposure to 17α-ethynylestradiol causes dose and temporally dependent changes in intersex, females and vitellogenin production in the Sydney rock oyster. *Ecotoxicology* 19 (8), 1440–1451. doi: 10.1007/s10646-010-0529-5

Athanasoulia, A., Auer, M., Riepe, F., and Stalla, G. (2013). Rare missense P450c17 (CYP17A1) mutation in exon 1 as a cause of 46, XY disorder of sexual development: Implications of breast tissue 'Unresponsiveness' despite adequate estradiol substitution. *Sex Dev.* 7 (4), 212–215. doi: 10.1159/000348301

Barrionuevo, F., Georg, I., Scherthan, H., Lecureuil, C., Guillou, F., Wegner, M., et al. (2009). Testis cord differentiation after the sex determination stage is independent of Sox9 but fails in the combined absence of Sox9 and Sox8. *Dev. Biol.* 327 (2), 301–312. doi: 10.1016/j.ydbio.2008.12.011

Bertho, S., Pasquier, J., Pan, Q., Le Trionnaire, G., Bobe, J., Postlethwait, J., et al. (2016). Foxl2 and its relatives are evolutionary conserved players in gonadal sex differentiation. *Sex Dev.* 10 (3), 111–129. doi: 10.1159/000447611

Broquard, C., Saowaros, S., Lepoittevin, M., Degremont, L., Lamy, J., Morga, B., et al. (2021). Gonadal transcriptomes associated with sex phenotypes provide potential Male and female candidate genes of sex determination or early differentiation in *Crassostrea gigas*, a sequential hermaphrodite mollusc. *BMC Genomics* 22 (1), 609. doi: 10.1186/s12864-021-07838-1

Capel, B. (2006). R-spondin1 tips the balance in sex determination. *Nat. Genet.* 38 (11), 1233–1234. doi: 10.1038/ng1106-1233

Chaboissier, M., Kobayashi, A., Vidal, V., Lutzkendorf, S., Van de Kant, H., Wegner, M., et al. (2004). Functional analysis of Sox8 and Sox9 during sex determination in the mouse. *Development* 131 (9), 1891–1901. doi: 10.1242/dev.01087

Chen, J., Cai, Z., and Gui, Y. (2009). Advances in the researches of spermatogenic protein, ropporin. *Natl. J. Androl.* 15 (9), 833–835.

Chen, H. P., Xiao, G., Chai, X., Lin, X., Fang, J., and Teng, S. (2017). Transcriptome analysis of sex-related genes in the blood clam *Tegillarca granosa*. *PloS One* 12 (9), e0184584. doi: 10.1371/journal.pone.0184584

Chen, S., Zhou, Y., Chen, Y., and Gu, J. (2018). Fastp: an ultra-fast all-in-one FASTQ preprocessor. *Bioinformatics* 34 (17), 884–890. doi: 10.1093/bioinformatics/bty560

Ciocan, C., Cubero-Leon, E., Puinean, A., Hill, E., Minier, C., Osada, M., et al. (2010). Effects of estrogen exposure in mussels, *Mytilus edulis*, at different stages of gametogenesis. *Environ. pollut.* 158 (9), 2977–2984. doi: 10.1016/j.envpol.2010.05.025

Craft, J., Gilbert, J., Temperton, B., Dempsey, K., Ashelford, K., Tiwari, B., et al. (2010). Pyrosequencing of *Mytilus galloprovincialis* cDNAs: Tissue-specific expression patterns. *PloS One* 5 (1), e8875. doi: 10.1371/journal.pone.0008875

De Sousa, J., Milan, M., Bargelloni, L., Pauletto, M., Matias, D., Joaquim, S., et al. (2014). A microarray-based analysis of gametogenesis in two Portuguese populations of the European clam *Ruditapes decussatus*. *PloS One* 9 (3), e92202. doi: 10.1371/journal.pone.0092202

Devlin, R., and Nagahama, Y. (2002). Sex determination and sex differentiation in fish: an overview of genetic, physiological, and environmental influences. *Aquaculture* 208 (3-4), 191–364. doi: 10.1016/S0044-8486(02)00057-1

Dong, Z., Duan, H., Zheng, H., Ge, H., Wei, M., Liu, M., et al. (2021). Research progress in genetic resources assessment, culture technique and exploration utilization of *Cyclina sinensis*. *J. Fish. China* 45 (12), 2083–2098. doi: 10.11964/jfc.20201212545

Estermann, M., Major, A., and Smith, C. (2020). Gonadal sex differentiation: Supporting versus steroidogenic cell lineage specification in mammals and birds. *Front. Cell Dev. Biol.* 8, 616387. doi: 10.3389/fcell.2020.616387

Farhadi, A., Fang, S., Zhang, Y., Cui, W., Fang, H., Ikhwanuddin, M., et al. (2021). The significant sex-biased expression pattern of sp-Wnt4 provides novel insights into the ovarian development of mud crab (*Scylla paramamosain*). *Int. J. Biol. Macromol.* 183, 490–501. doi: 10.1016/j.ijbiomac.2021.04.186

Feng, Q., Liu, M., Cheng, Y., and Wu, X. (2022). Comparative transcriptome analysis reveals the process of ovarian development and nutrition metabolism in Chinese mitten crab. *Eriocheir Sinensis. Front. Genet.* 13, 910682. doi: 10.3389/fgene.2022.910682

Fu, L., Niu, B., Zhu, Z., Wu, S., and Li, W. (2012). CD-HIT: accelerated for clustering the next-generation sequencing data. *Bioinformatics* 28 (23), 3150–3152. doi: 10.1093/bioinformatics/bts565

Gallardi, D., Xue, X., Mercier, E., Mills, T., Lefebvre, F., Rise, M., et al. (2021). RNA-Seq analysis of the mantle transcriptome from *Mytilus edulis* during a seasonal spawning event in deep and shallow water culture sites on the northeast coast of Newfoundland, Canada. *Mar. Genomics* 60, 100865. doi: 10.1016/j.margen.2021.100865

Ge, H., Liang, X., Liu, J., Cui, Z., Guo, L., Li, L., et al. (2021). Effects of acute ammonia exposure on antioxidant and detoxification metabolism in clam *Cyclina sinensis. Ecotox. Environ. Safe.* 211, 111895. doi: 10.1016/j.ecoenv.2021.111895

Grabherr, M., Haas, B., Yassour, M., Levin, J., Thompson, D., Amit, I., et al. (2011). Full-length transcriptome assembly from RNA-seq data without a reference genome. *Nat. Biotechnol.* 29 (7), 644–U130. doi: 10.1038/nbt.1883

Jarrell, Z., Ahammad, M., Sweeney, K., Wilson, J., and Benson, A. (2020). Characterization of sperm-associated antigen 6 expression in the reproductive tract of the domestic rooster (*Gallus domesticus*) and its impact on sperm mobility. *Poultry Sci.* 99 (11), 6188–6195. doi: 10.1016/j.psj.2020.08.009

Jiang, N., Jin, X., He, J., and Yin, Z. (2012). The roles of follistatin 1 in regulation of zebrafish fecundity and sexual differentiation. *Biol. Reprod.* 87 (3), 099689. doi: 10.1095/biolreprod.112.099689

Jin, L., Sun, W., Bao, H., Liang, X., Li, P., Shi, S., et al. (2022). The forkhead factor Foxl2 participates in the ovarian differentiation of Chinese soft-shelled turtle *Pelodiscus sinensis*. *Dev. Biol.* 492, 101–110. doi: 10.1016/j.ydbio.2022.10.001

Kang, B., Okutsu, T., Tsutsui, N., Shinji, J., Bae, S., and Wilder, M. (2014). Dynamics of vitellogenin and vitellogenesis-inhibiting hormone levels in adult and subadult whiteleg shrimp, *Litopenaeus vannamei*: Relation to molting and eyestalk ablation. *Biol. Reprod.* 90 (1), 112243. doi: 10.1095/biolreprod.113.112243

Kim, E., Kim, S., Park, C., and Nam, Y. (2019). Characterization of testis-specific serine/threonine kinase 1-like (TSSK1-like) gene and expression patterns in diploid and triploid pacific abalone (*Haliotis discus hannai*; gastropoda; Mollusca) males. *PloS One* 14 (12), 0226022. doi: 10.1371/journal.pone.0226022

Kinoshita, M., Kani, S., Ozato, K., and Wakamatsu, Y. (2000). Activity of the medaka translation elongation factor 1 alpha-a promoter examined using the GFP gene as a reporter. *Dev. Growth Differ.* 42 (5), 469–478. doi: 10.1046/j.1440-169x.2000.00530.x

Liao, X., Sun, Z., Cui, Z., Yan, S., Fan, S., Xia, Q., et al. (2022). Effects of different sources of diet on the growth, survival, biochemical somposition and physiological metabolism of clam (*Cyclina sinensis*). *Aquac. Res.* 53 (10), 3797–3806. doi: 10.1111/are.15886

Li, H., Kong, L., Yu, R., and Li, Q. (2016b). Characterization, expression, and functional analysis of testis-specific serine/threonine kinase 1 (Tssk1) in the pen shell *Atrina pectinata*. *Invertebr. Reprod. Dev.* 60 (2), 118–125. doi: 10.1080/07924259.2016.1161667

Liu, X., Li, Y., Liu, J., Cui, L., and Zhang, Z. (2016). Gonadogenesis in scallop *Chlamys farreri* and cf-foxl2 expression pattern during gonadal sex differentiation. *Aquac. Res.* 47 (5), 1605–1611. doi: 10.1111/are.12621

Livak, K., and Schmittgen, T. (2001). Analysis of relative gene expression data using real-time quantitative PCR and the 2(T)(-delta delta c) method. *Methods* 25 (4), 402–408. doi: 10.1006/meth.2001.1262

Li, R., Zhang, L., Li, W., Zhang, Y., Li, Y., Zhang, M., et al. (2018). FOXL2 and DMRT1L are yin and yang genes for determining timing of sex differentiation in the bivalve mollusk *Patinopecten yessoensis*. *Front. Physiol.* 9, 01166. doi: 10.3389/fphys.2018.01166

Li, Y., Zhang, L., Sun, Y., Ma, X., Wang, J., Li, R., et al. (2016a). Transcriptome sequencing and comparative analysis of ovary and testis identifies potential key sex-related genes and pathways in scallop *Patinopecten yessoensis*. *Mar. Biotechnol.* 18 (4), 453–465. doi: 10.1007/s10126-016-9706-8

Llera-Herrera, R., Garcia-Gasca, A., Abreu-Goodger, C., Huvet, A., and Ibarra, A. (2013). Identification of Male gametogenesis expressed genes from the scallop *Nodipecten subnodosus* by suppressive subtraction hybridization and pyrosequencing. *PloS One* 8 (9), 0073176. doi: 10.1371/journal.pone.0073176

Major, A., Ayers, K., Chue, J., Roeszler, K., and Smith, C. (2019). FOXL2 antagonises the Male developmental pathway in embryonic chicken gonads. *J. Endocrinol.* 243 (3), 211–228. doi: 10.1530/JOE-19-0277

Manni, M., Berkeley, M., Seppey, M., Simao, F., and Zdobnov, E. (2021). BUSCO update: Novel and streamlined workflows along with broader and deeper phylogenetic coverage for scoring of eukaryotic, prokaryotic, and viral genomes. *Mol. Biol. Evol.* 38 (10), 4647–4654. doi: 10.1093/molbev/msab199

Marchais-Oberwinkler, S., Henn, C., Moeller, G., Klein, T., Negri, M., Oster, A., et al. (2011). 17 beta-hydroxysteroid dehydrogenases (17 beta-HSDs) as therapeutic targets: Protein structures, functions, and recent progress in inhibitor development. *J. Steroid Biochem. Mol. Biol.* 125 (1-2), 66–82. doi: 10.1016/j.jsbmb.2010.12.013

Marin, M., and Matozzo, V. (2004). Vitellogenin induction as a biomarker of exposure to estrogenic compounds in aquatic environments. *Mar. pollut. Bull.* 48 (9-10), 835–839. doi: 10.1016/j.marpolbul.2004.02.037

Matsumoto, T., Nakamura, A., Mori, K., and Kayano, T. (2003). Molecular characterization of a cDNA encoding putative vitellogenin from the pacific oyster *Crassostrea gigas*. *Zool. Sci.* 20 (1), 37–42. doi: 10.2108/zsj.20.37

Monga, R., Ghai, S., Datta, T., and Singh, D. (2012). Involvement of transcription factor GATA-4 in regulation of CYP19 gene during folliculogenesis and luteinization in buffalo ovary. *J. Steroid Biochem. Mol. Biol.* 130 (1-2), 45–56. doi: 10.1016/j.jsbmb.2011.12.010

Morandin, C., Havukainen, H., Kulmuni, J., Dhaygude, K., Trontti, K., and Helantera, H. (2014). Not only for egg yolk-functional and evolutionary insights from expression, selection, and structural analyses of Formica ant vitellogenins. *Mol. Biol. Evol.* 31 (8), 2181–2193. doi: 10.1093/molbev/msu171

Murray, H., and Hobbs, K. (2022). Spatial expression patterning of kelch-like protein homolog 10 (KLHL10), armadillo repeat-containing protein 4 isoform x2 (ARMC4), and a gamete-specific mitochondrial cytochrome c oxidase (MT-CO1) during Spermatogenesis/Spermiogenesis in the mantle of Male blue mussel (*Mytilus edulis*). *J. Shellfish Res.* 41 (1), 109–117. doi: 10.2983/035.041.0108

Nagaraju, G. (2011). Reproductive regulators in decapod crustaceans: An overview. *J. Exp. Biol.* 214 (1), 3–16. doi: 10.1242/jeb.047183

Naillat, F., Yan, W., Karjalainen, R., Liakhovitskaia, A., Samoylenko, A., Xu, Q., et al. (2015). Identification of the genes regulated by wnt-4, a critical sSignal for commitment of the ovary. *Exp. Cell Res.* 332 (2), 163–178. doi: 10.1016/j.yexcr.2015.01.010

Nelson, E., and Habibi, H. (2013). Estrogen receptor function and regulation in fish and other vertebrates. *Gen. Comp. Endocr.* 192, 15–24. doi: 10.1016/j.ygcen.2013.03.032

Nie, D., Liu, Y., and Xiang, Y. (2011). Overexpression a novel zebra fish spermatogenesis-associated gene 17 (SPATA17) induces apoptosis in GC-1 cells. *Mol. Biol. Rep.* 38 (6), 3945–3952. doi: 10.1007/s11033-010-0511-6

Ning, J., Cao, W., Lu, X., Chen, M., Liu, B., and Wang, C. (2021). Identification and functional analysis of a sex-biased transcriptional factor Foxl2 in the bay scallop *Argopecten irradians* irradians. *Comp. Biochem. Phys. B* 256, 110638. doi: 10.1016/j.cbpb.2021.110638

Ni, J., Zeng, Z., Kong, D., Hou, L., Huang, H., and Ke, C. (2014). Vitellogenin of fujian oyster, *Crassostrea angulata*: Synthesized in the ovary and controlled by estradiol-17 beta. *Gen. Comp. Endocr.* 202, 35–43. doi: 10.1016/j.ygcen.2014.03.034

Osada, M., Harata, M., Kishida, M., and Kijima, A. (2004). Molecular cloning and expression analysis of vitellogenin in scallop, *Patinopecten yessoensis* (Bivalvia, Mollusca). *Mol. Reprod. Dev.* 67 (3), 273–281. doi: 10.1002/mrd.20020

Osada, M., Takamura, T., Sato, H., and Mori, K. (2003). Vitellogenin synthesis in the ovary of scallop, *Patinopecten yessoensis*: Control by estradiol-17 beta and the central nervous system. *J. Exp. Zool. A Comp. Exp. Biol.* 299 (2), 172–179. doi: 10.1002/jez.a.10276

Ostrovsky, A. (2021). Reproductive strategies and patterns in marine invertebrates: Diversity and evolution. *Paleontological J.* 55 (7), 803–810. doi: 10.1134/S003103012107008X

Paiano, J., Wu, W., Yamada, S., Sciascia, N., Callen, E., Cotrim, A., et al. (2020). ATM And PRDM9 regulate SPO11-bound recombination intermediates during meiosis. *Nat. Commun.* 11 (1), 857. doi: 10.1038/s41467-020-14654-w

Picard, M., Vicoso, B., Bertrand, S., and Escriva, H. (2021). Diversity of modes of reproduction and sex determination systems in invertebrates, and the putative contribution of genetic conflict. *Genes* 12 (8), 1136. doi: 10.3390/genes12081136

Porte, C., Janer, G., Lorusso, L., Ortiz-Zarragoitia, M., Cajaraville, M., Fossi, M., et al. (2006). Endocrine disruptors in marine organisms: Approaches and perspectives. *Comp. Biochem. Phys. C.* 143 (3), 303–315. doi: 10.1016/j.cbpc.2006.03.004

Prasertlux, S., Sittikankaew, K., Chumtong, P., Khamnamtong, B., and Klinbunga, S. (2011). Molecular characterization and expression of the prostaglandin reductase 1 gene and protein during ovarian development of the giant tiger shrimp *Penaeus monodon*. *Aquaculture* 322, 134–141. doi: 10.1016/j.aquaculture.2011.09.037

Qian, X., Ba, Y., Zhuang, Q., and Zhong, G. (2014). RNA-Seq technology and its application in fish transcriptomics. *Omics* 18 (2), 98–110. doi: 10.1089/omi.2013.0110

Qin, Z., Li, Y., Sun, D., Shao, M., and Zhang, Z. (2012). Cloning and expression analysis of the vitellogenin gene in the scallop *Chlamys farreri* and the effects of estradiol-17 beta on its synthesis. *Invertebr. Biol.* 131 (4), 312–321. doi: 10.1111/ivb.12006

Robinson, W., Robinson, W., Krick, K., Murray, H., and Poynton, H. (2022). Comparative phylotranscriptomics reveals putative sex differentiating genes across eight diverse bivalve species. *Comp* 41, 100952.

Saavedra, L., Leonardi, M., Morin, V., and Quinones, R. (2012). Induction of vitellogenin-like lipoproteins in the mussel *Aulacomya ater* under exposure to 17 beta-estradiol. *Rev. Biol. Mar. Oceanog.* 47 (3), 429–438. doi: 10.4067/S0718-19572012000300006

Sandra, G., and Norma, M. (2010). Sexual determination and differentiation in teleost fish. *Rev. Fish Biol. Fisher.* 20 (1), 101–121. doi: 10.1007/s11160-009-9123-4

Santerre, C., Sourdaine, P., Adeline, B., and Martinez, A. (2014). Cg-SoxE and cg-beta-catenin, two new potential actors of the sex-determining pathway in a hermaphrodite lophotrochozoan, the pacific oyster *Crassostrea gigas*. *Comp. Biochem. Physiol. A.* 167, 68–76. doi: 10.1016/j.cbpa.2013.09.018

Senthilkumaran, B. , and Kar, S. (2021). Advances in reproductive endocrinology and neuroendocrine research using catfish models. *Cells* 10 (11) 2807. doi: 10.3390/cells10112807

Shangguan, X., Mao, Y., Wang, X., Liu, M., Wang, Y., Wang, G., et al. (2022). Cyp17a effected by endocrine disruptors and its function in gonadal development of *Hyriopsis cumingii*. *Gen. Comp. Endocr.* 323, 114028. doi: 10.1016/j.ygcen.2022.114028

Shang, P., Hoogerbrugge, J., Baarends, W., and Grootegoed, J. (2013). Evolution of testis-specific kinases TSSK1B and TSSK2 in primates. *Andrology* 1 (1), 160–168. doi: 10.1111/j.2047-2927.2012.00021.x

Smith-Unna, R., Boursnell, C., Patro, R., Hibberd, J., and Kelly, S. (2016). TransRate: reference-free quality assessment of *De novo* transcriptome assemblies. *Genome Res.* 26 (8), 1134–1144. doi: 10.1101/gr.196469.115

Sun, D., Yu, H., and Li, Q. (2022). Examination of the roles of Foxl2 and Dmrt1 in sex differentiation and gonadal development of oysters by using RNA interference. *Aquaculture* 548 (2), 737732. doi: 10.1016/j.aquaculture.2021.737732

Takahashi, T., and Ogiwara, K. (2021). Roles of melatonin in the teleost ovary: A review of the current status. *Comp. Biochem. Physiol. A.* 254, 110907. doi: 10.1016/j.cbpa.2021.110907

Tan, K., Chan, S., Tan, K., and Yu, V. (2001). The *Caenorhabditis elegans* sex-determining protein FEM-2 and its human homologue, hFEM-2, are Ca (2+)/calmodulin-dependent protein kinase phosphatases that promote apoptosis. *J. Biol. Chem.* 276 (47), 44193–44202. doi: 10.1074/jbc.M105880200

Teaniniuraitemoana, V., Huvet, A., Levy, P., Klopp, C., Lhuillier, E., Gaertner-Mazouni, N., et al. (2014). Gonad transcriptome analysis of pearl oyster *Pinctada margaritifera*: Identification of potential sex differentiation and sex determining genes. *BMC Genomics* 15, 491. doi: 10.1186/1471-2164-15-491

Tong, Y., Zhang, Y., Huang, J., Xiao, S., Zhang, Y., Li, J., et al. (2015). Transcriptomics analysis of *Crassostrea hongkongensis* for the discovery of reproduction-related genes. *PloS One* 10 (8), e0134280. doi: 10.1371/journal.pone.0134280

Trapnell, C., Williams, B., Pertea, G., Mortazavi, A., Kwan, G., van Baren, M., et al. (2010). Transcript assembly and quantification by RNA-seq reveals unannotated transcripts and isoform switching during cell differentiation. *Nat. Biotechnol.* 28 (5), 511–U174. doi: 10.1038/nbt.1621

Vainio, S., Heikkila, M., Kispert, A., Chin, N., and McMahon, A. (1999). Female development in mammals is regulated by wnt-4 signalling. *Nature* 397 (6718), 405–409. doi: 10.1051/medsci/2002182149

Vidal, V., Chaboissier, M., and Schedl, A. (2002). Sox9 gene induces testis development XX transgenic mice. *M S-Med. Sci.* 18 (2), 49–151.

Wang, C., and Croll, R. (2003). Effects of sex steroids on in vitro gamete release in the Sea scallop, *Placopecten magellanicus*. *Invertebr. Reprod. Dev.* 44 (2-3), 89–100. doi: 10.1080/07924259.2003.9652559

Wang, G., Dong, S., Guo, P., Cui, X., Duan, S., and Li, J. (2020). Identification of Foxl2 in freshwater mussel *Hyriopsis cumingii* and its involvement in sex differentiation. *Gene* 754, 144853. doi: 10.1016/j.gene.2020.144853

Wang, Y., Duan, S., Dong, S., Cui, X., Wang, G., and Li, J. (2021b). Comparative proteomic study on fem-1b in female and Male gonads in *Hyriopsis cumingii*. *Aquacult. Int.* 29 (1), 1–18. doi: 10.1007/s10499-020-00605-1

Wang, X., Pei, J., Xiong, L., Guo, S., Cao, M. , Kang, Y., et al. (2022). Identification of the TSSK4 alternative spliceosomes and analysis of the function of the TSSK4 protein in yak (*Bos grunniens*). *Animals* 12 (11) 1380. doi: 10.3390/ani12111380

Wang, Y., Wang, X., Ge, J., Wang, G., and Li, J. (2021a). Identification and functional analysis of the sex-determiner transformer-2 homologue in the freshwater pearl mussel, *Hyriopsis cumingii*. *Front. Physiol.* 12, 704548. doi: 10.3389/fphys.2021.704548

Wei, M., Ge, H., Shao, C., Yan, X., Nie, H., Duan, H., et al. (2020). Chromosome-level clam genome helps elucidate the molecular basis of adaptation to a buried lifestyle. *Iscience* 23 (6), 101148. doi: 10.1016/j.isci.2020.101148

Wu, Q., Tan, Y., Wang, J., Xie, Q., Huo, Z., Fang, L., et al. (2019). Effect of estradiol stimulation on dmrt gene expression in Manila clam ruditapes philippinarum. *J. Dalian Ocean Univ.* 34 (3), 362–369. doi: 10.16535/j.cnki.dlhyxb.2019.03.009

Xie, C., Mao, X., Huang, J., Ding, Y., Wu, J., Dong, S., et al. (2011). KOBAS 2.0: A web server for annotation and identification of enriched pathways and diseases. *Nucleic Acids Res.* 39, W316–W322. doi: 10.1093/nar/gkr483

Xie, S., Sun, L., Liu, F., and Dong, B. (2009). Molecular characterization and mRNA transcript profile of vitellogenin in Chinese shrimp, *Fenneropenaeus chinensis*. *Mol. Biol. Rep.* 36 (2), 389–397. doi: 10.1007/s11033-007-9192-1

Xue, X., Zhang, L., Li, Y., Wei, H., Wu, S., Liu, T., et al. (2021). Expression of the testis-specific Serine/Threonine kinases suggests their role in spermiogenesis of bay scallop *Argopecten irradians*. *Front. Physiol.* 12, 657559. doi: 10.3389/fphys.2021.657559

Yan, H. (2009). *Studies on reproductive physiology of sinonovacula constricta and cyclina sinensis. master thesis* (Ocean University of China). doi: 10.7666/d.y1502788

Yang, W., Li, J., An, P., and Lei, A. (2014). CDC20 downregulation impairs spindle morphology and causes reduced first polar body emission during bovine oocyte maturation. *Theriogenology* 81 (4), 535–544. doi: 10.1016/j.theriogenology.2013.11.005

Yang, D., Yin, C., Chang, Y., Dou, Y., Hao, Z., and Ding, J. (2016). Transcriptome analysis of Male and female mature gonads of Japanese scallop *Patinopecten yessonsis*. *Genes Genom.* 38 (11), 1041–1052. doi: 10.1007/s13258-016-0449-8

Yao, H., Lin, Z., Dong, Y., Kong, X., He, L., and Xue, L. (2021). Gonad transcriptome analysis of the razor clam (*Sinonovacula constricta*) revealed potential sex-related genes. *Front. Mar. Sci.* 8, 725430. doi: 10.3389/fmars.2021.725430

Yi, M., Negishi, M., and Lee, S. C. (2021). Estrogen sulfotransferase (SULT1E1): Its molecular regulation, polymorphisms, and clinical perspectives. *J. Pers. Med.* 11 (3), 194. doi: 10.3390/jpm11030194

Yoon, S., Lee, M., Xaver, M., Zhang, L., Hong, S., Kong, Y., et al. (2016). Meiotic prophase roles of Rec8 in crossover recombination and chromosome structure. *Nucleic Acids Res.* 44 (19), 9296–9314. doi: 10.1093/nar/gkw682

Yue, C., Li, Q., and Yu, H. (2018). Gonad transcriptome analysis of the pacific oyster *Crassostrea gigas* identifies potential genes regulating the sex determination and differentiation process. *Mar. Biotechnol.* 20 (2), 206–219. doi: 10.1007/s10126-018-9798-4

Yu, K., Hou, L., Zhu, J., Ying, X., and Yang, W. (2009). KIFC1 participates in acrosomal biogenesis, with discussion of its importance for the perforatorium in the Chinese mitten crab *Eriocheir sinensis*. *Cell Tissue Res.* 337 (1), 113–123. doi: 10.1007/s00441-009-0800-3

Zeng, Q., Hu, B., Blanco, A., Zhang, W., Zhao, D., Martinez, P., et al. (2022). Full-length transcriptome sequences provide insight into hermaphroditism of freshwater pearl mussel *Hyriopsis schlegelii*. *Front. Genet.* 13, 868742. doi: 10.3389/fgene.2022.868742

Zhang, N., Xu, F., and Guo, X. (2014). Genomic analysis of the pacific oyster (*Crassostrea gigas*) reveals possible conservation of vertebrate sex determination in a mollusc. *G3-Genes Genom. Genet.* 4 (11), 2207–2217. doi: 10.1534/g3.114.013904

Zhao, W., Li, Y., Wang, Y., Luo, X., Wu, Q., Huo, Z., et al. (2022). Gonadal development and the reproductive cycle of the geoduck clam (*Panopea japonica*) in the Sea of Japan. *Aquaculture* 548, 737606. doi: 10.1016/j.aquaculture.2021.737606

Zhou, S., Zhang, J., Fam, M., Wyatt, G., and Walker, V. (2002). Sequences of elongation factors-1 alpha and -1 gamma and stimulation by juvenile hormone in *Locusta migratoria*. *Insect Biochem. Mol. Biol.* 32 (11), 1567–1576. doi: 10.1016/S0965-1748(02)00077-2

frontiers | Frontiers in Marine Science

TYPE Original Research
PUBLISHED 17 January 2023
DOI 10.3389/fmars.2023.1105065

OPEN ACCESS

EDITED BY
Menghong Hu,
Shanghai Ocean University, China

REVIEWED BY
Yan Fang,
Ludong University, China
Qichen Jiang,
Freshwater Fisheries Research Institute of Jiangsu Province, China

*CORRESPONDENCE
Zhiguo Dong
dzg7712@163.com

†These authors have contributed equally to this work

SPECIALTY SECTION
This article was submitted to Marine Biology, a section of the journal Frontiers in Marine Science

RECEIVED 22 November 2022
ACCEPTED 02 January 2023
PUBLISHED 17 January 2023

CITATION
Wang S, Ren G, Li D, Fan S, Yan S, Shi J, Liu M and Dong Z (2023) Transcriptome reveals the immune and antioxidant effects of residual chlorine stress on *Cyclina sinensis*. *Front. Mar. Sci.* 10:1105065. doi: 10.3389/fmars.2023.1105065

Transcriptome reveals the immune and antioxidant effects of residual chlorine stress on *Cyclina sinensis*

Siting Wang[1,2†], Guoliang Ren[1,3†], Desheng Li[1,2], Sishao Fan[1,2], Susu Yan[1,2], Junjie Shi[1,2], Meimei Liu[1,2] and Zhiguo Dong[1,2*]

[1]Jiangsu Key Laboratory of Marine Bioresources and Environment, Jiangsu Ocean University, Lianyungang, China, [2]Co-Innovation Center of Jiangsu Marine Bio-industry Technology, Jiangsu Institute of Marine Resources Development, Jiangsu Ocean University, Lianyungang, China, [3]Affair Center of Animal Husbandry and Aquaculture, XiangXi Autonomous Prefecture, Jishou, China

Residual chlorine is a common by-product of warm drainage in coastal nuclear power plants. when accumulating to some limit, it may threaten marine ecosystem especially for benthic clam. However, there are few studies on the molecular mechanisms related to immunity and antioxidant of residual chlorine stress on clams. In this study, the clam (*Cyclina sinensis*) was exposed for 96 h at different concentrations (0, 50, 100, 150, 200, 250, 300, 350, 400, 450 and 500 mg/L) of residual chlorine to observe its mortality, measure the activity of antioxidant and immune-related enzymes, and analyses the gene expression level in the hepatopancreas by using the transcriptome sequencing. The results showed that the mortality rate increased with the increase of stress time and concentration, and the mortality rate in the 400, 450 and 500 mg/L groups reached 100% at 96 h. The tolerance to residual chlorine of *C. sinensis* decreased with the increase of chlorine dioxide concentration, and the LC_{50} of 96 h was 217.6 mg/L by linear regression method. After residual chlorine stress, the activity of antioxidant-related enzymes (T-AOC and SOD) in the hepatopancreas showed a trend of first increase and then decrease with the extension of stress time. The immune-related enzyme activities of AKP and LZM showed a downward trend between 0 and 96 h, while the ACP enzyme activity showed a trend of first rising and then decreasing. Transcriptome analysis showed that residual chlorine stress significantly changed the expression levels of immune-related molecules associated with signal transduction, prophenoloxidase cascade, cell apoptosis and pattern recognition protein/receptor. Moreover, glutathione S-transferase (*GST*), heat shock protein (*HSP*) and other antioxidant-related genes were significantly affected under residual chlorine stress. This study provided valuable information for understanding the effects of residual chlorine stress on survival, physiological metabolism and molecular mechanisms of immune and antioxidant functions of *C. sinensis*.

KEYWORDS

Cyclina sinensis, residual chlorine, immunity, antioxidants, transcriptome

1 Introduction

Chlorine residual is a common by-product of the warm water discharge from coastal nuclear power stations. In order to prevent seawater organisms from damaging the cooling system, seawater needs to be electrolysed so that the cooling water contains a certain concentration of chlorine, thereby killing all kinds of organisms in the seawater. The seawater enters the cooling system and carries away the waste heat from the nuclear reaction to become warm water, but the residual chlorine in the water also enters the ocean with the warm water. Chlorination of seawater is the main cause of killing organisms in cooling water, while the thermal shock from waste heat in nuclear power plants has less impact (Zeng, 2008). At the same time, in shellfish seedling production, the washing and scrubbing of ponds after transfer, the disinfection of bait cultivation and the daily cleaning of equipment and tools such as nets and bags often involve the use of disinfectants such as bleach. Although the whole process requires strict control, omissions and misuse are inevitable, allowing residual chlorine to flow into the seedling pond to varying degrees, with unpredictable effects on the production of *Cyclina sinensis* seedling (Xu et al., 2007; Wu et al., 2018).

In response to environmental changes, organisms need to use their own antioxidant and immune systems to counteract external stimuli (Eppley et al., 1976; Dempsey, 1986; Pan et al., 2006; Alexandre et al., 2022). The antioxidant response of aquatic organisms to acute or chronic stimuli has been studied mostly in fish and shrimps (Hegazi et al., 2010; Liang et al., 2016; Liu C et al., 2022). In the available studies, fish death under residual chlorine stress is mainly caused by asphyxiation (Jiang et al., 2009), which is also consistent with the mechanism of toxicity of chlorine damage to the respiratory systems of humans and animals. Residual chlorine causes lesions in the gill tissue of aquatic organisms, such as hyperplasia, hypertrophy and accumulation of mucus (Li et al., 2017; Nikolaivits et al., 2020). Swelling of the gill filaments separates the gill filaments from the capillaries and prevents oxygen from entering the capillaries properly in gill tissue, which causes reduced oxygen supply and lower blood oxygen levels in the organism. This phenomenon increases the respiratory rate in order to provide the oxygen levels required for activity. The free chlorine in residual chlorine has strong oxidizing property and can enter the bloodstream through the gills, where it can undergo redox reactions with haemoglobin in the blood. Thereby it disrupts the oxygen transport role of haemoglobin and reduces the oxygen content in the fish blood, inhibits the ability of the fish blood to transport oxygen (Zeitoun, 1977). The immune and antioxidant enzyme activities of bivalves are important physiological parameters of shellfish. Hepatopancreas are important detoxigenic organs and the first barrier against the interference of the whole organism (Pawert et al., 1996; Opstvedt et al., 2000; Zhao L et al., 2016). However, only a few studies have combined molecular and biochemical procedures to describe the relationship between the transcription of specific immune and antioxidant genes and their activity (Qiu et al., 2018; Chen et al., 2021; Qiao et al., 2022), and the response mechanism of shellfish to residual chlorine stress is also rarely studied.

Cyclina sinensis is a common buried shellfish, also known as the venus clam and black clam, and is one of the main cultured shellfish in China's aquaculture industry (Dong et al., 2021). The clam is very widely distributed in the coastal areas, from Korea to the north and south coasts of China, mainly in coastal mudflat areas, with river inlets and is a common shellfish species in China's coastal areas (Dong et al., 2021). Due to the advantages of strong resistance to adversity, tasty meat and high culture yield, the clam has become an ideal cultured shellfish with huge production and sales in China (Zhang, 2014; Shi et al., 2019). As a typical burial-type economic shellfish, *C. sinensis*, is good bioindicator for coastal pollution investigations and has been widely cultivated and proliferated in China (Wei et al., 2020; Ge et al., 2021; Liao et al., 2022). Therefore, *C. sinensis* could be used as a model species to understand the potential toxicity effects of marine bivalves exposed to residual chlorine.

In the present study, we observed the mortality of *C. sinensis* under residual chlorine stress, determined the antioxidant and immune-related enzymes and analysed transcriptome. This study will provide insight into the mechanism of residual chlorine toxicity in *C. sinensis* and provide some theoretical references for the understanding of the toxic effects of residual chlorine on bivalves.

2 Materials and methods

2.1 Animals

Juvenile clam (shell length: 1.20 ± 0.10 cm, weight: 0.70 g ± 0.2 g) was collected from a reproduction farm along coastal of Lianyungang China. Juvenile clam was acclimated for one week in an indoor circulating water system. One week before the experiment, we selected the healthy clams, cleaned their surface stains and disinfected, and then temporarily reared them in natural seawater (salinity: 22 ppt, DO: 8.00-9.00 mg/L, pH: 7.40-7.75) and kept aerating and no bait during the temporary rearing period to enable the clam to expel internal dirt. Meanwhile, we removed the deformed and diseased individuals during the temporary rearing period. All clams were treated in strict accordance with the guidelines for the care and use of experimental animals established by the Administration of Affairs Concerning Experimental Animals of the State Council of the People's Republic of China and approved by the Committee on Experimental Animal Management of the Jiangsu Ocean University.

2.2 Chlorine dioxide concentration challenge

The *C. sinensis* were randomly divided into ten groups (10 individuals in each group) and were subjected to different chlorine dioxide (chlorine dioxide effervescent tablets, South Ranch) concentration levels of 0 mg/L (C_0), 50 mg/L (C_1), 100 mg/L (C_2), 150 mg/L (C_3), 200 mg/L (C_4), 250 mg/L (C_5), 300 mg/L (C_6), 350 mg/L (C_7), 400 mg/L (C_8), 450 mg/L (C_9) and 500 mg/L (C_{10}) with C_0 set as control. Three parallel experiments were conducted for each chlorine dioxide concentration level, and used a residual chlorine meter (Pocket Colorimeter II, DR 800, HATCH) to measure the residual chlorine concentration in each group. The treatment continued for 96 h.

2.3 Mortality and median lethal concentration (LC_{50}) analysis and tissue sampling

The mortality of *C. sinensis* was measured after 24, 48, 72, and 96 h of treatment. The death of individuals in each group was recorded. The mortality rate was calculated as $D_f \times O_i^{-1} \times 100\%$, where D_f is the number of the clams killed at the end of each stress in each group and O_i is the total number of the clams in each group at the start of the stress. The LC_{50} of chlorine dioxide for *C. sinensis* at 96 h were analyzed by linear regression analysis on the basis of mortality data. The calculation formula and method were referred from Li et al. (2012). The safe concentration (*SC*) was calculated as following: SC = 0.1 × 96 h LC_{50}.

Choosing 10%, 25% and 50% of the LC_{50} of chlorine dioxide at 96 h for *C. sinensis* obtained from above, i.e., 21.76 mg/L, 54.4 mg/L and 108.8 mg/L as stress concentrations, while as the concentrations could not be set precisely due to the large size of the culture water. So we set three stress concentrations of 20 mg/L (a), 50 mg/L (b) and 100 mg/L (c), and three replicates in each group (10 individuals in each group) in this experiment. The hepatopancreas samples from each individual in groups a, b and c were collected at 0, 3, 6, 12, 24, 48, 72, and 96 h of treatment for enzyme activity determination and only hepatopancreas at 96 h were collected for transcriptomic analysis, with three biological replicates for each experiment.

2.4 Determination of antioxidant and immunity enzymes activity

During sampling, 5 clams from each replicate were pooled together to eliminate any effect of tank, and each clam was collected hepatopancreas at each point of sampling time, immediately frozen in liquid nitrogen and stored at -80°C. The frozen samples were ground in liquid nitrogen, diluted with physiological saline and stored in a refrigerator at 4°C before the assay for subsequent biochemical determination. The activities of enzymes including Lysozyme (LZM), Alkaline phosphatase (AKP), Acid phosphatase (ACP), Superoxide dismutase (SOD) and Total antioxidant capacity (T-AOC) were determined through biochemical analysis kits (Nanjing Jiancheng Bioengineering Institute, China) according to the manufacturer's instructions.

2.5 RNA extraction and transcriptomic sequencing

Selecting the hepatopancreas of *C. sinensis* treated with different concentrations (a, b, c) for 96 h in Section **2.3** described as samples, marked as H-96a, H-96b and H-96c, respectively, and the 0 h stress group was used as the control, marked as H-0. Total RNA was extracted from the hepatopancreas using Trizol method, and genomic DNA was removed with DNase I (Takara). Subsequently, the integrity and purity were estimated by a NanoDrop 2000 (Thermo Fisher Scientific Inc., USA), respectively. Only high-quality RNA samples (OD260/OD280 ranged 1.8-2.2, RIN ≥8.0) were used to construct the sequencing library. Then, these libraries were sequenced on the Illumina sequencing platform (HiSeqTM 2500 or Illumina HiSeq X Ten), and 125 bp/150 bp paired-end reads were generated. After removing adaptor and low-quality sequences, the clean reads were assembled into expressed sequence tag clusters (contigs) and *de novo* assembled into transcripts by using Trinity with the paired-end method (Grabherr et al., 2011). The longest transcript was chosen as an unigene based on the similarity and length of a sequence for subsequent analysis.

The function of assembled unigenes was annotated by alignment of the unigenes with the NCBI nonredundant (NR), SwissProt, and Clusters of Orthologous Groups for Eukaryotic Complete Genomes (KOG) databases using Blastx with a threshold E-value of 10^{-5}. GO and Pfam annotations were performed by Blast2GO and HMMER software, respectively. Database annotation was performed with KEGG. The gene expression level was calculated by using the FPKM (fragments per kb per million reads) method. To identify differentially expressed genes (DEGs) across samples, $|\log2(\text{fold change})| > 1$ and P-value < 0.05 were set to be the thresholds for significantly different expression levels. The gene expression profiles were compared among the four groups, control (H-0, 0 mg/L), a (H-96a, 20mg/L), b, (H-96b, 50 mg/L) and c, (H-96c, 100 mg/L) treatments, and then all DEGs in each comparison were submitted to GO functional and KEGG pathway enrichment analysis using the GO database and KEGG database, respectively.

2.6 qPCR verification

According to the transcriptome sequencing results, 10 immune and antioxidant related genes were randomly selected to detect Illumina by qRT - PCR. The reliability of sequencing was verified. All the 10 target gene primers were designed using Primer 5.0 and were synthesized by Shanghai Sangon Biological Company. Each pair of primers was validated by gel electrophoresis prior to qPCR. Primers used in the experiment are shown in Table 1.

The cDNA of hepatopancreas of *C. sinensis* treated with different residual chlorine concentrations for 96 h was used as the template for qPCR. TransGen Biotech's PerfectStart® Green qPCR SuperMix kit was used for quantitative analysis of gene expression levels. The qRT-PCR assays were performed with three replicates, and the β-actin gene was used as an internal control to normalize the expression level of the target genes The reaction system with a volume of 10 μL was as follows: 2×PerfectStart® Green qPCR SuperMix (5.0μL), Passive Reference Dye (50×) (0.2μL), primer F (0.2μL), primer R (0.2μL), cDNA template (1μL) and Nuclease-free Water (3.4 μL). The qPCR analyses were performed in triplicate on a StepOnePlus Real-Time PCR (Applied Biosystems, USA) as follows: was used, and the reaction procedure was: predenatured at 94 °C for 30 s; followed by 40 cycles of 94 °C for 5 s and 60 °C for 30 s. Using the $2^{-\Delta\Delta Ct}$ method to calculate relative quantification of qRT-PCR data.

2.7 Statistical analysis

SPSS 26.0 software was used for data analysis in this study. Use One-way ANOVA and Duncan's analysis to compare the difference of the data. Differences were considered significant at $P < 0.05$.

10.3389/fmars.2023.1105065

TABLE 1 Primer sequence for qRT-PCR verification.

Gene	Primer sequence (5′ - 3′)	Primer length (bp)	Tm (°C)
β-actin	CCTGGTATTGCCGACCGTAT	20	59.9
	TTGGAAGGTGGACAGTGAAGC	21	59.9
CLE	GAAGTCAAACTGCGACCTCA	20	55.8
	CAATCTTTACCCCACTCCATA	20	54.6
CYP450	ATGGCAAATGCGACAGAGAA	20	58.9
	AAGTGGTGGAACCCAAGGAC	20	58.5
CTL6	ACACAGGACAGCGTGGTTCT	20	57.5
	TTCATTCTCTCTGCTACTGGTAAG	24	55.8
Itgbl1	AAGTTTGATGTTTCCCCCAG	20	56.5
	AGTTTATTTCGTAGCCGTGC	20	55.2
TIRB	CCAGCACCAAGCAGTTTATT	20	55.6
	TTTCAAGCTCATCTCGACCA	20	56.4
Bcl - 2	TTACGGGATAGAATACACGACC	22	60.7
	CGCACAAACACCAAGCACAG	20	58.4
T151B	CAGGAATAAACGGCAGGACT	20	57.0
	CTTGAAAGTAAAGCCAGACCA	21	55.1
LPR4	GAACTGGTATTCTGCCTAACG	21	55.6
	CCCATCTATTCTCACCTCTCG	20	56.4
samA	TGCTGAACAACACAGACAAGA	21	54.5
	GTAGATACCAAACGACGACACA	22	55.4
RDE2	GACATACAGAACACCCCGCT	20	57.2
	CCATTTTGCCTCCCAAGATT	20	59.1

3 Results

3.1 Effect of chlorine dioxide stress on the mortality of *C. sinensis*

The mortality rate of *C. sinensis* after chlorine dioxide treatment and residual chlorine concentration for different chlorine dioxide concentrations are shown in Table 2. As can be seen, the mortality rate in the control group (C_0) remained zero during the whole experiment period, indicating the clam individuals used were all in good health.

At the same time, there was a concentration-time effect on the resistance of *C. sinensis* to residual chlorine. The results showed that the mortality increased with time, and as the concentration of chlorine dioxide increased, the tolerance of *C. sinensis* to residual chlorine decreased. Among the different concentration groups, only the groups of C_8, C_9 and C_{10} showed mortality at 24 h. At 48 h, no death occurred in the C_0 group and C_1 group, but all the other groups occurred dead individuals, but the mortality was less than 50%. At 72 h the mortality rates of the C_8, C_9 and C_{10} groups exceeded 50%, with the mortality rate in the C_{10} group reached 83.33%, and the mortality rate in the C_8, C_9 and C_{10} groups reached 100% at 96 h.

As can be seen from the concentration-mortality curve of chlorine dioxide on clams (Figure 1), using the linear regression method, the 96 h LC_{50} was 217.6 mg/L, corresponding to a residual chlorine concentration of 0.22 mg/L. The safe concentration (*SC*) was 21.76 mg/L, corresponding to a residual chlorine concentration of 0.01 mg/L.

3.2 Antioxidant and immune enzymes activity in hepatopancreas of *C. sinensis* under different concentration of residual chlorine

The activities of T-AOC and SOD in hepatopancreas of clams subjected to residual chlorine stress showed a wavy trend from 0 to 96 h (Figure 2). The maximum value of T-AOC in 20 mg/L stress group at 72 h was significantly different from that at 0 h ($P < 0.05$), the enzyme activity at 96 h was the lowest, and lower than that at 0 h, but the difference was not significant ($P > 0.05$). The T-AOC activity in 50 mg/L stress group also reached the maximum value at 72 h, and the difference was significant compared with 0 h ($P < 0.05$), the activity at the 6 h was the lowest, and there was no significant difference from the initial value ($P > 0.05$). The T-AOC in the 100 mg/L group

TABLE 2 Experimental results of acute lethal effect of chlorine dioxide on *C. sinensis*.

Treatment	Chlorine dioxide concentration (mg/L)	Corresponding residual chlorine concentration (mg/L)	Mean mortality at different times of stress (%)			
			24 h	48 h	72 h	96 h
C_0	**0**	0	0.00	0.00	0.00	0.00
C_1	**50**	0.03 ± 0.06	0.00	0.00	0.00	10.00
C_2	**100**	0.08 ± 0.16	0.00	3.33	0.00	16.67
C_3	**150**	0.13 ± 0.22	0.00	3.33	6.67	26.67
C_4	**200**	0.20 ± 0.81	0.00	6.67	3.33	33.33
C_5	**250**	0.71 ± 0.43	0.00	10.00	10.00	56.67
C_6	**300**	1.52 ± 0.35	0.00	10.00	16.67	66.67
C_7	**350**	2.33 ± 0.19	0.00	13.33	36.67	73.33
C_8	**400**	2.94 ± 0.31	3.33	26.67	63.33	100
C_9	**450**	3.57 ± 0.21	6.67	33.33	76.67	100
C_{10}	**500**	6.81 ± 0.37	6.67	23.33	83.33	100

reached its maximum value at 48 h and was significantly different from that at 0 h ($P < 0.05$), while it was lowest at 6 h and 96 h with no significant difference from the initial value ($P > 0.05$). Compared with the other two groups, the maximum T-AOC took a shorter time in the 100 mg/L group than that in the other two groups.

The SOD enzyme activity of all three concentration groups showed an increasing trend from 0 to 12 h, after which the SOD enzyme activity started to decrease. The SOD enzyme activity of the 20 mg/L group showed an overall increasing trend, and started to decrease at 24 h, and the enzyme activity was still higher than the initial value, but was not significantly different from the initial value ($P > 0.05$), and started to increase again at 48 h. At 96 h, the SOD enzyme activity decreased significantly ($P < 0.05$) and reached the lowest value. The SOD enzyme activity in the 50 mg/L group reached its maximum value at 12 h and was significantly different from the initial value ($P < 0.05$), then the enzyme activity decreased slightly, but was still higher than the initial value and significantly different from the initial value ($P < 0.05$) and the lowest value was reached at 6 h, which was not significantly different from the initial value ($P > 0.05$).

The effect of residual chlorine stress on ACP activity in the hepatopancreas of *C. sinensis* showed a general trend of increasing and then decreasing, as seen in Figure 3A. In the 20 mg/L group, the ACP activity showed fluctuating changes, reaching two peaks at 6 h and 48 h respectively, with a maximum value at 48 h, which was significantly different from the initial value ($P < 0.05$), and the lowest ACP activity at 96 h, which was lower than the initial value, but not significantly different from the initial value ($P > 0.05$). The ACP activity in the 50 mg/L group showed a trend of increasing and then decreasing, and reached a maximum value at 48 h, which was significantly different from the initial value ($P < 0.05$), and a minimum value at 96 h, which was lower than the initial value, but not significantly different from the initial value ($P > 0.05$). The ACP activity in the 100 mg/L group showed a tendency to increase and then decrease, and reached a maximum value at 6 h, which was significantly different from the initial value ($P < 0.05$), and a minimum value at 72 h, which was lower than the initial value but not significantly different from the initial value ($P > 0.05$).

As seen in Figure 3B, the effect of residual chlorine stress on AKP activity in the hepatopancreas of *C. sinensis* showed fluctuating changes. The AKP activity in the 20 mg/L group reached its maximum value at 12 h and was significantly different from the initial value ($P < 0.05$), and reached its lowest value at 48 h and was lower than the initial value and the difference was significant compared with the initial value ($P < 0.05$). The AKP enzyme activity in the 100 mg/L group also showed fluctuating changes, but the enzyme activity was lower than that of the control group in all period of time and was significantly different from that of the control group ($P < 0.05$). The lowest value was found at 72 h.

The effect of residual chlorine stress on LZM enzyme activity in the hepatopancreas of *C. sinensis* showed fluctuating changes as can be seen in Figure 3C. The LZM activity in the 20 mg/L group showed fluctuating changes, reaching a maximum value at 12 h with no significant difference from the initial value ($P > 0.05$) and a minimum value at 48 h with significant difference ($P < 0.05$). The LZM activity in the 100 mg/L group was lower than the initial value after 0 h and was significantly different from the initial value ($P < 0.05$), with the lowest value occurring at 72 h.

3.3 Assembly, function enrichment analysis and identification of differentially expressed genes

In this study, the H-0 group was used as the control, and the number of differential genes in H-96a, H-96b and H-96c groups were counted (Figures 4, 5). The ILLUMINA data were submitted to the National Center for Biotechnology Information (NCBI, PRJNA904083). The results showed that compared with the control group, 13, 17 and 16 unigenes were up-regulated and 23, 34 and 13 unigenes were down-regulated in group H-96a, H-96b and H-96c, respectively. Compared with group H-96a at 96 h of residual chlorine stress, 19 and 23 unigenes were up-regulated and 17 and 16 unigenes were down-regulated in group H-96b and group H-96c, respectively. Finally, 23 and 27 unigenes were up-regulated and down-regulated in

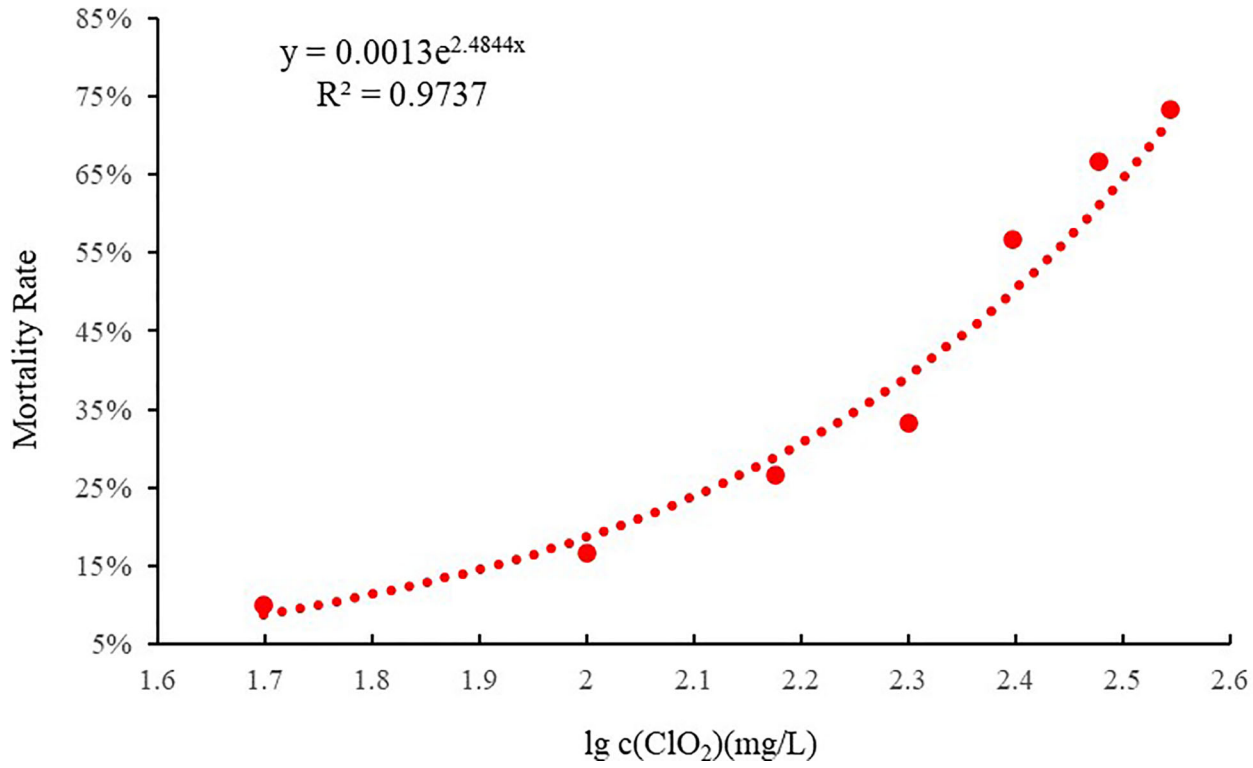

FIGURE 1
The Concentration - Mortality curve of chlorine dioxide to *C. sinensis* at 96 h (R^2 = 0.9737).

group H-96c, respectively, compared with group H-96b at 96 h. Most of the genes in groups H-96a, H-96b, and H-96c were down-regulated compared with the control group, and most of the genes in groups H-96a, H-96b, and H-96c were up-regulated compared with each other.

To analyse the functions of these DGEs, GO assignments were made. These DGEs were assigned to major GO categories (level 3), i.e., biological process, cellular component, and molecular function (Figure 6). KO annotation of transcriptome results classified differentially expressed genes (referred to as differential genes) into 5 categories based on metabolic pathways categories, which belong to Metabolism, Organismal systems, Cellular Processes, Genetic information processing, and Environmental information processing. The annotation of the number of differential genes is shown in Figure 7: In KEGG annotation, the most single gene pathways among groups were: cofactors in metabolic pathways and signal transduction in vitamin metabolism and environmental information processing; Transport and catabolism in cellular processes and Signal transduction in environmental information processing.

3.4 Key genes involved in immunity and antioxidation response to residual chlorine stress in *C. sinensis*

In the present study, DEGs associated with immune defence were divided into 5 groups (Table 3). There were 31 genes associated with signal transduction, the most of the 5 groups, followed by other immune molecules (10), pattern recognition proteins/receptors (8), apoptosis (8), antimicrobial peptides (8) and genes associated with the pre-phenol oxidase cascade (3).

Compared with the control group H-0, the expression levels of genes in H-96a related to signal transduction, such as caspase 9 (*CASP9*), HRAS-like suppressor 3, Thrombospondin-4, Dual oxidase 2-like isoform X2, C-terminal-binding protein-like isoform X1 were significantly up-regulated, while the expression levels of phospholipid phosphatase 3-like, pantetheinase-like, Follistatin, ADP-ribosylation factor-like and other genes were significantly down-regulated. In addition, residual chlorine at group H-96a down-regulated the expression levels of genes in the C-Type Lectin family of pattern recognition proteins/receptors, such as C-type lectin domain family member isoform crab 3, C-type lectin domain family 6 member A, and genes in the prophenoloxidase cascade system, such as serine protease, Kazal-type serine protease genes. The expression levels of Baculoviral IAP repeat-containing protein 7-B were significantly upregulated in genes related to apoptosis, while the expression levels of cathepsin L, inhibitor of apoptosis protein-like were significantly downregulated. In addition, the expression levels of pantetheinase-like, deleted in malignant brain tumors 1 protein-like, gelsolin-like protein 2 and legumain-like were also altered in the concentration treatment group compared to the control group.

Compared to the control group, the expression levels of genes related to signal transduction such as guanylate cyclase soluble subunit beta-2-like, MMP-19 and mitogen-activated protein kinase/p38 were significantly up-regulated in the H-96b group, while the expression levels of phospholipid phosphatase 3-like, ADP-ribosylation factor-like, Protocadherin Fat 4, and fatty acid synthase were significantly down-regulated. At the same time, the expression

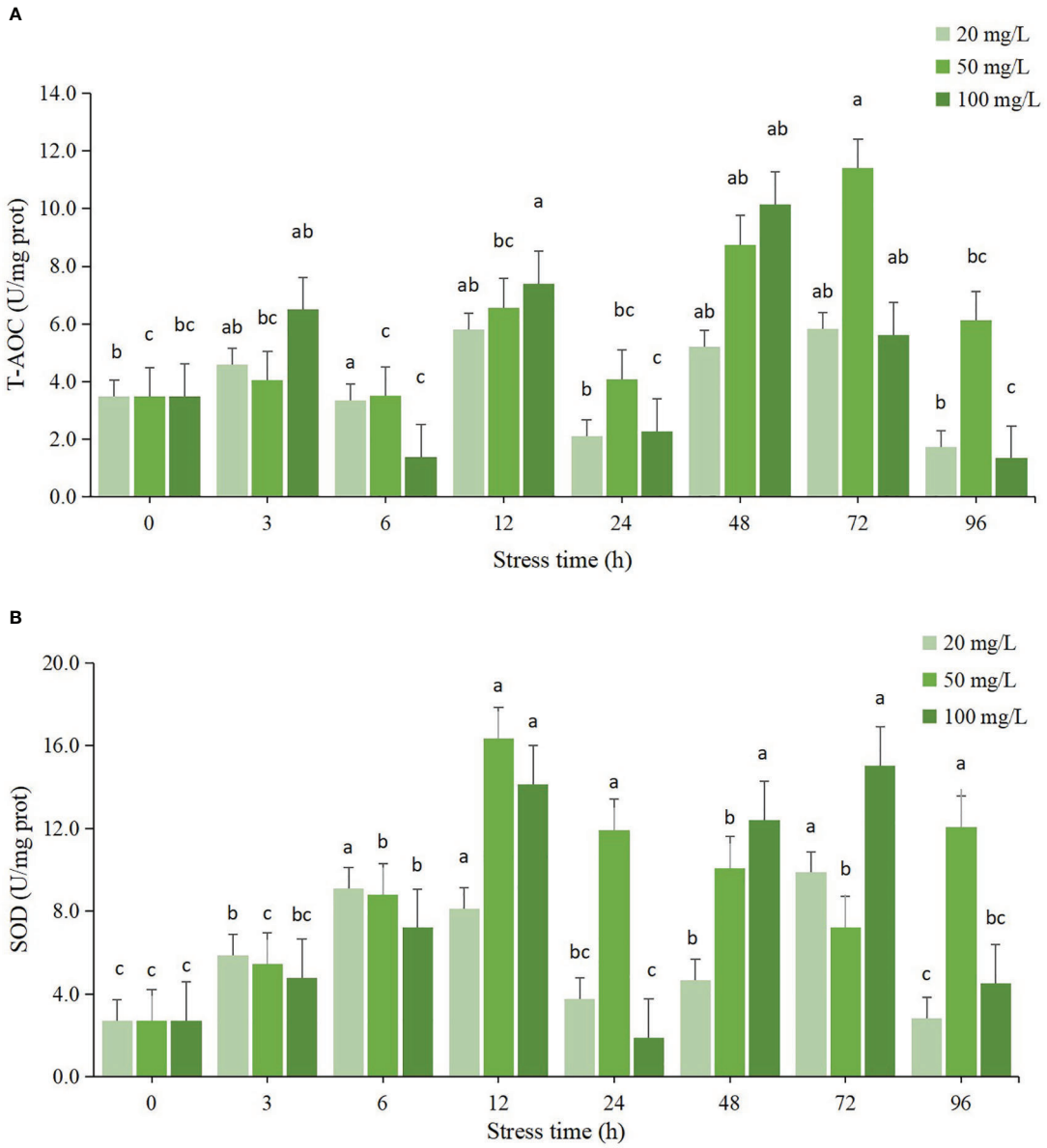

FIGURE 2
Changes of antioxidant enzyme activities in hepatopancreas of *C sinensis* at different time points after different residual chlorine stress. **(A)** T-AOC activitiy, **(B)** SOD activitiy. Different letters indicate statistically significant differences between different time points for the same treatment using one-way ANOVA and Tukey's comparison of the means test ($P < 0.05$).

levels of leptin precursor 4, C-type lectin domain family 6 member A and C-type lectin were significantly down-regulated in genes related to pattern recognition proteins/receptors (*PRPs*), while the expression levels of mitogen-activated protein kinase/p38 were significantly up-regulated. The expression levels of mitogen-activated protein kinase/p38 were significantly up-regulated. The expression of cathepsin L, Bcl-2 like 2 protein and baculoviral IAP repeat-containing protein 5-like, which are genes related to apoptosis, were all down-regulated. In addition, the expression levels of genes such as guanylate cyclase soluble subunit beta-2-like and Full=G2/mitotic-specific cyclin-B were also altered in the b concentration treatment group.

The expression levels of signal transduction-related protein crumbs homolog 1-like and MASP-related molecule Type 1 genes were significantly down-regulated in group H-96c compared to the H-0, while in the phenol oxidase progenitor system, the expression levels of serine/threonine-protein kinase TBK1 like isoform X1 were significantly up-regulated. Meanwhile, the expression levels of inhibitor of apoptosis 1, a gene related to apoptosis, were significantly up-regulated, while the expression levels of C-type lectin, electin precursor 4 and toll-like receptor 13, a gene related to pattern recognition protein/receptor, were significantly down-regulated. In addition, the c-treatment group also caused deleted in malignant brain tumors 1 protein-like, proteasome activator complex subunit 3-like, Full=G2/mitotic-specific cyclin-B and NRAMP gene expression levels were altered.

Meanwhile, several DEGs are involved in various processes of animal antioxidant mechanisms in the hepatopancreas (Table 4). Compared with the H-0 treated group, the expression levels of omega

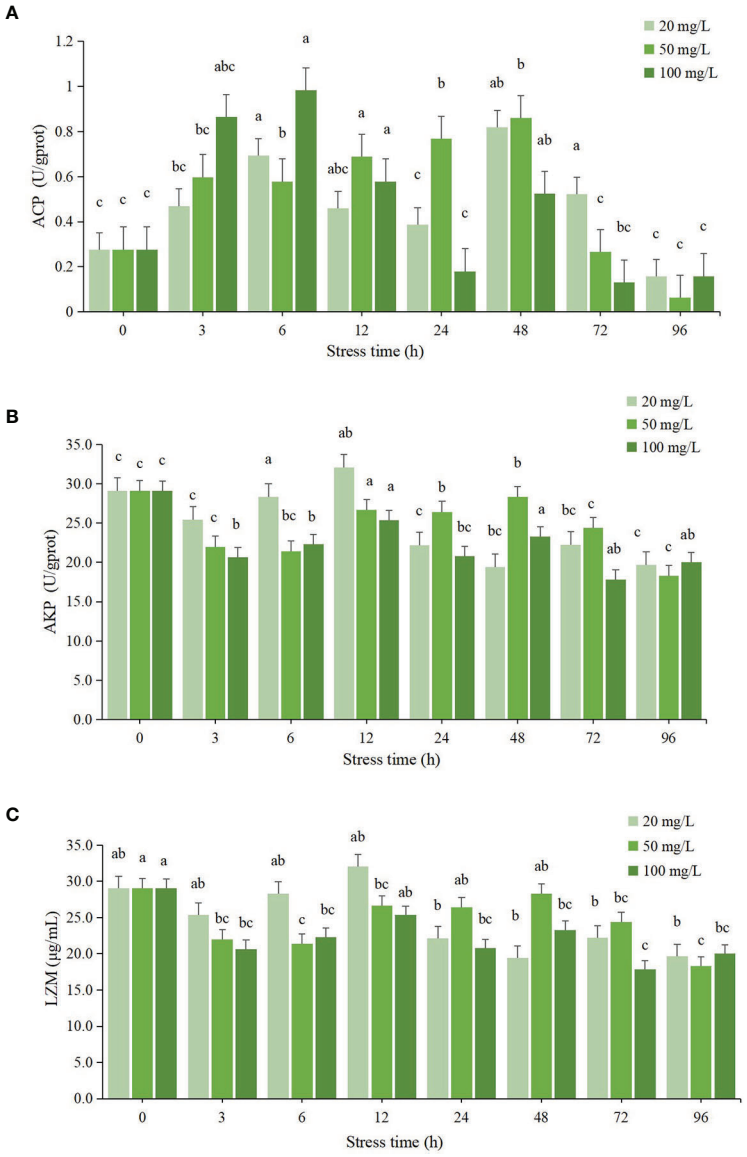

FIGURE 3
Changes of immune enzyme activities in hepatopancreas of *C sinensis* at different time points after different residual chlorine stress. **(A)** ACP activitiy, **(B)** AKP activitiy and **(C)** LZM activitiy. Different letters indicate statistically significant differences between different time points for the same treatment using one-way ANOVA and Tukey's comparison of the means test ($P < 0.05$).

glutathione S-transferase, glutathione S-transferase and mu class glutathione S-transferase genes associated with antioxidant were significantly up-regulated in the H-96a group, while the expression levels of Thioredoxin-like fold genes were significantly down-regulated in the H-96a group. The expression levels of alanine—glyoxylate aminotransferase 2, pi-class glutathione S-transferase, and thioredoxin genes were significantly up-regulated in the H-96b group, while the expression levels of genes such as ribosyldihydronicotinamide dehydrogenase, thioredoxin-like fold, and asparagine synthetase were significantly downregulated. The expression levels of omega glutathione S-transferase, pi-class glutathione S-transferase, and pi-class glutathione S-transferase were significantly up-regulated in the H-96c group, while the expression levels of Thioredoxin-like fold and peroxiredoxin V genes were significantly down-regulated. As a response to environmental stress, chaperone genes in the organism showed significant variation at the transcriptional or translational level. In the present study, the expression levels of heat shock protein were significantly up-regulated in group H-96a compared to the H-0; in group H-96c, the expression levels of heat shock protein 70 and heat shock protein were significantly up-regulated, while the expression levels of heat shock protein 60 gene were significantly down-regulated. In addition, residual chlorine stress also altered the expression levels of metal-binding proteins, including heavy metal-binding protein HIP-like, metallothionein and ferritin subunit.

3.5 Validation of gene expression by qPCR

The transcriptome results were verified by qPCR (Figure 8), and selected 10 immune and antioxidant related genes (5 up-regulated and 5 down-regulated) randomly. The verification results were

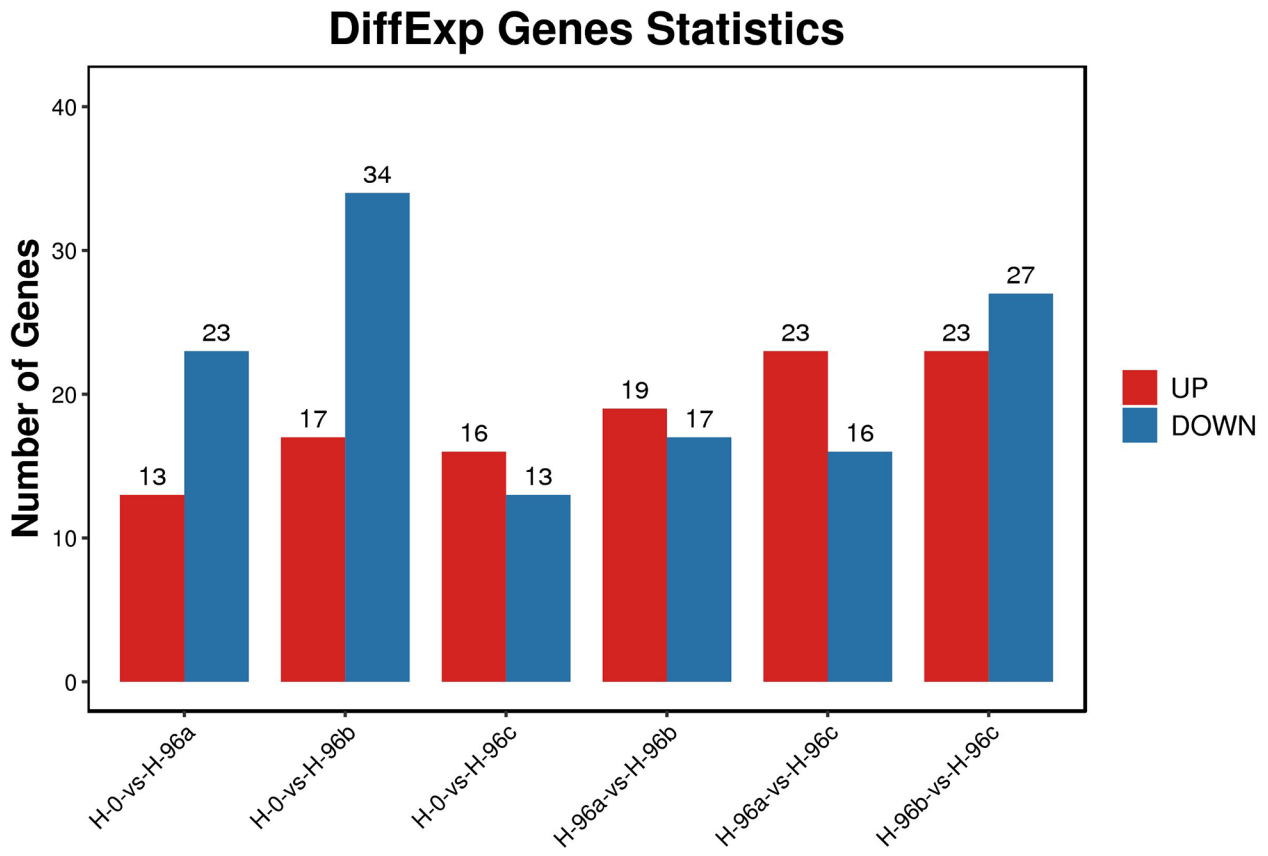

FIGURE 4
Statistical chart of DEGs. H-0: Control group; H-96a: concentration of 20 mg/L group; H-96b: concentration of 50 mg/L group; H-96c: concentration of 100 mg/L group. Up- and down-regulated genes are shown in red and blue, respectively.

consistent with the sequencing results, indicating that the transcriptome sequencing results were authentic and reliable.

4 Discussion

4.1 Effects of acute residual chlorine on the mortality of *C. sinensis*

The mortality of aquatic organisms can be affected by changes in the water environment and chemical stimuli, such as temperature (Casas et al., 2020; Syafaat et al., 2021), salinity (Nie et al., 2018; Zhang Y et al., 2020), pH (Swezey et al., 2020; Liew et al., 2022), and feed (Willer and Aldridge, 2019; Mohan et al., 2019). Chlorine and compounds in water can undergo complex chemical reactions to synthesise a range of compounds under different conditions, such as the chloramine family of compounds. Electrolytic chlorine for the disinfection of cooling water in nuclear power plants is usually free chlorine, which is unstable in its state and very easily dissipated in seawater (Venkatnarayanan et al., 2021). The main sources of chlorine for production activities are several common disinfectants such as bleach, chlorine dioxide and trichloroisocyanuric acid. Also, during the shellfish culture and nursery phase, the cleaning and disinfection of various types of equipment and ponds inevitably involves the use of disinfectants such as bleach and chlorine dioxide, in which residual chlorine is inevitably produced.

The LC_{50} is an important index to measure the toxin tolerance of an organism. This study calculated the 96-h LC_{50} of juvenile *C. sinensis* to chlorine dioxide exposure, based on linear regression method ($y = 0.0013e^{2.4844x}$, $R^2 = 0.9737$, where y = % mortality and x = lg c (ClO_2)) was 217.6 mg/L. The results of the present studies were similar to those reported in other aquatic organisms. The LC_{50} of residual chlorine (Cl^-) in STEL water for brood-stock and 2-mo-old shrimp were 2.3 and 3.2 ppm, respectively (Park et al., 2004). The Manila clam *Ruditapes philippinarum* exhibited strong tolerance to hypoxia as the 20-day LC_{50} for dissolved oxygen (DO) was estimated to be 0.57 mg L^{-1} (Li et al., 2019). The 96-h LC_{50} at 22 and 26°C values was 28.591 and 11.761 mg/L, respectively, for $NiCl_2$ exposure in the abalone (Min et al., 2015).

Studies on the effects of residual chlorine on mussels showed that the time of death of mussels at the same concentration depended on the size of the mussel, with smaller mussels taking less time to reach 100% mortality than larger mussels. In addition, the death time of mussels with the same size depends on the residual chlorine concentration, with higher concentrations of residual chlorine taking less time to reach 100% mortality than lower concentrations (Zhang et al., 2000; Masilamoni et al., 2002). In the present study, the mortality of bay scallop (*Argopectens irradias*) parents (Chen, 2009) and yellow clam (*Corbicula fluminea*) (Zou and Cheng, 2003) showed a gradual increase in mortality with increasing chlorine dioxide concentration in the water column and the extension of soaking time. In this study, chlorine dioxide concentration and duration of stress directly affected the survival and growth of first instar clams,

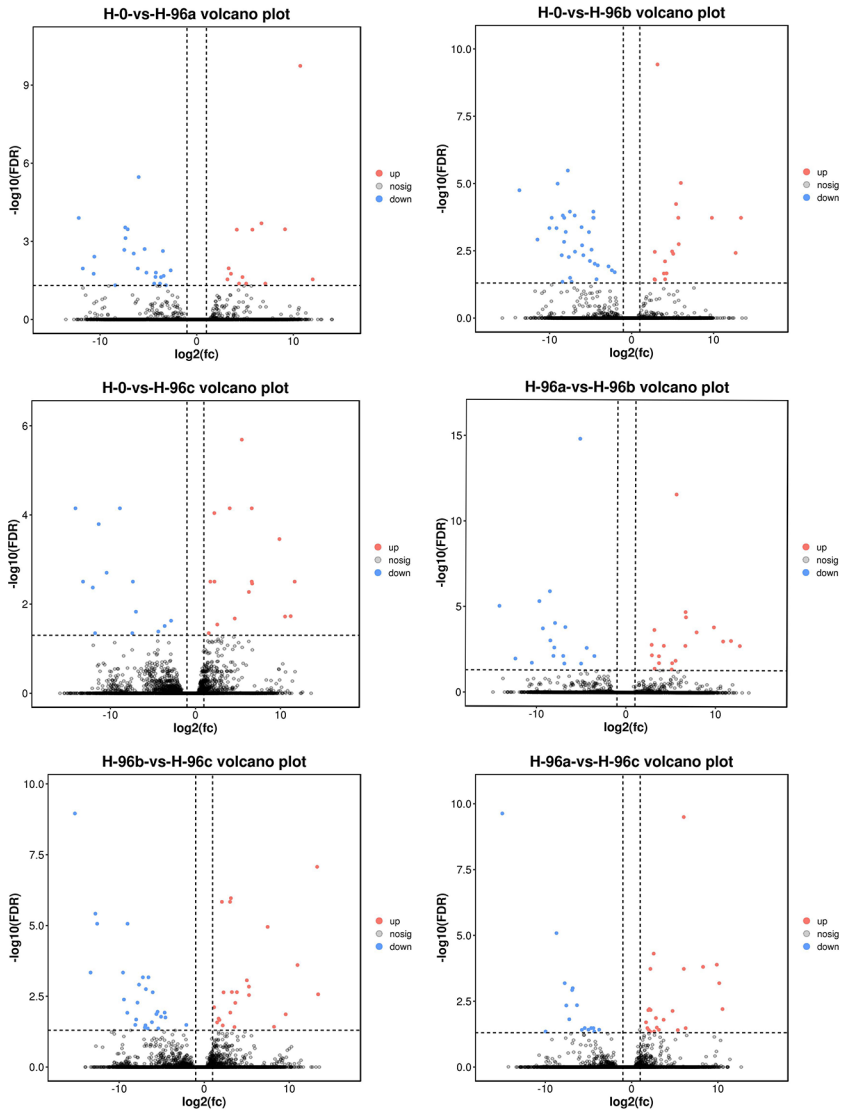

FIGURE 5
Difference comparison volcano map. H-0: Control group; H-96a: concentration of 20 mg/L group; H-96b: concentration of 50 mg/L group; H-96c: concentration of 100 mg/L group. Up- and down-regulated genes are shown in red and blue, respectively.

and the mortality rate of clams increased with increasing chlorine dioxide concentration and duration of stress.

4.2 Effects of residual chlorine on physiological metabolism of *C. sinensis*

The living environment of the *C. sinensis* is near the estuary of the freshwater river, and the outlet of the warm water drainage of the coastal nuclear power plant is one of the main habitats of *C. sinensis*. When faced with changes in the external environment, the immune system of the clam undergoes stress behaviour, resulting in the production of large amounts of reactive oxygen species (ROS), and the sharp increase in ROS places a great burden on the organism, generating oxidative stress and causing a decrease in immune function (Liang et al., 2016). The antioxidant system consists of antioxidant enzymes (Lian et al., 2019; Dong et al., 2022; Holen et al., 2022) (e.g., SOD, CAT, T-AOC), which have a strong detoxifying effect on ROS. The activity of antioxidant enzymes also reflects the physiological state of aquatic organisms in response to environmental changes to a certain extent. The immune system of shellfish consists of immune-related enzymes (e.g., ACP, AKP, LZM) and changes in the activity of immune-related enzymes also show changes in immune function.

T-AOC reflects the total antioxidant capacity of organisms. In this study, it can be seen that the T-AOC in the three concentration groups tended to increase significantly at the beginning of the experiment, with the 20 mg/L and 50 mg/L groups reaching their maximum values at 72 h and the 100 mg/L group reaching its maximum value at 48 h. The T-AOC activity of the three concentration groups remained at a higher level at 96 h and was significantly different compared to the initial value ($P < 0.05$). It is speculated that high concentration of chlorine stimulates the stress response of *C. sinensis* to produce a large number of ROS. In order to prevent its own damage, the body improves the enzymatic reaction, secretes a large amount of SOD and antioxidant-related enzymes, and improves the total antioxidant capacity. The changes in SOD enzyme

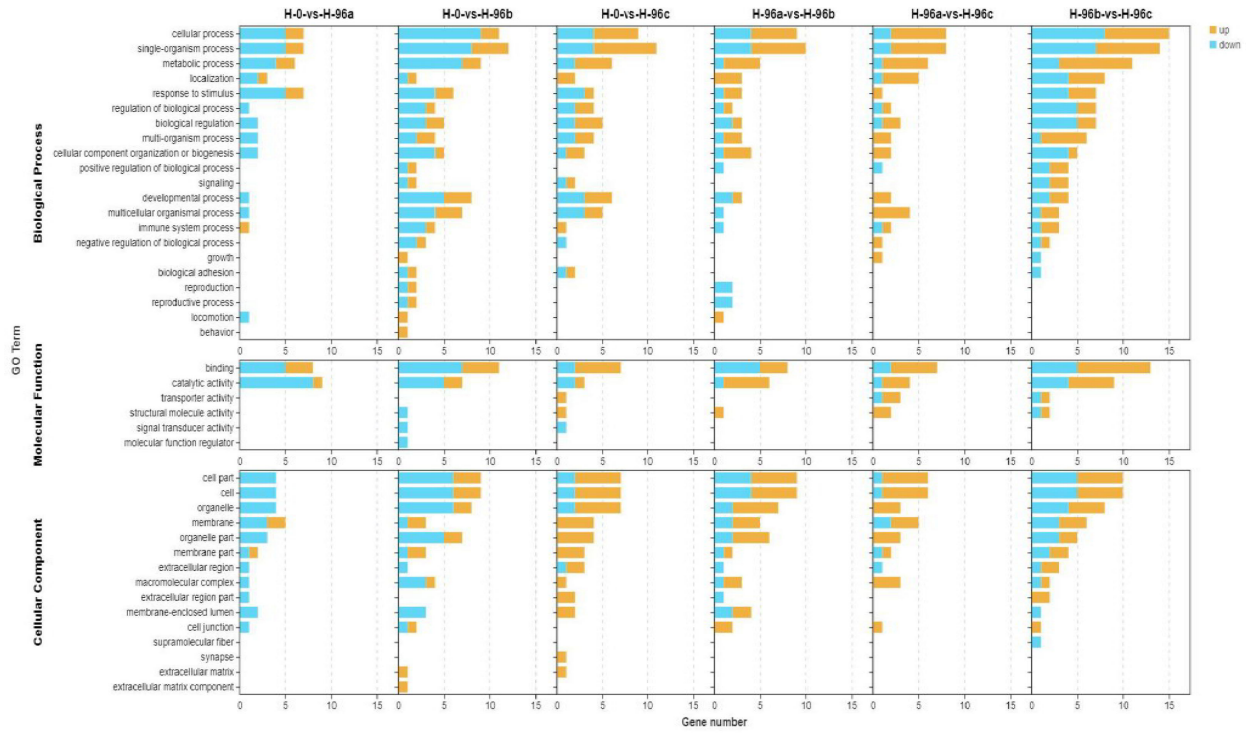

FIGURE 6
GO enrichment analyses of differentially expressed genes (DEGs) in hemolymph transcriptome. H-0: Control group; H-96a: concentration of 20 mg/L group; H-96b: concentration of 50 mg/L group; H-96c: concentration of 100 mg/L group.

activity were the same as those in *T*-AOC, showing a trend of increasing, then decreasing and then increasing. The SOD activity of all three concentration groups reached its maximum at 12 h, and the activity remained at a high level afterwards, which was significantly different from that of the control group ($P < 0.05$). This result was also consistent with the results of T-AOC.

ACP and AKP are two common immune-related enzymes, both of which are involved in the detoxification process of the organism

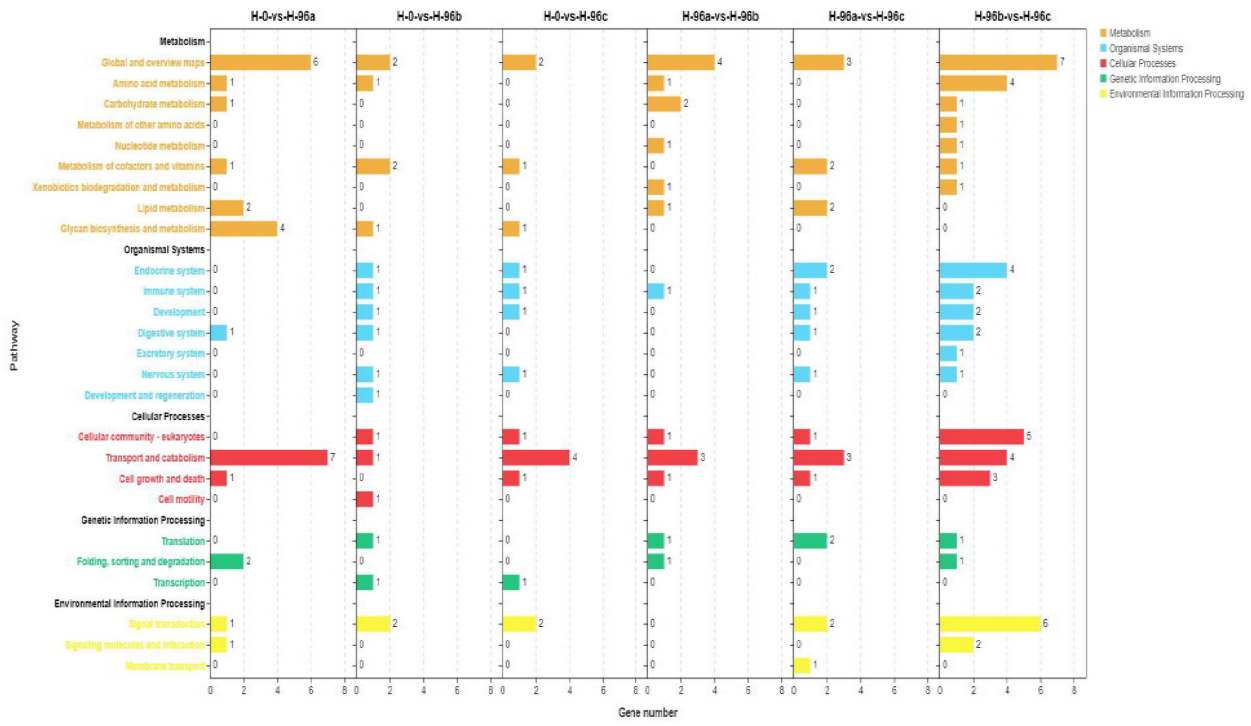

FIGURE 7
KEGG enrichment analyses of differentially expressed genes (DEGs) in hemolymph transcriptome. H-0: Control group; H-96a: concentration of 20 mg/L group; H-96b: concentration of 50 mg/L group; H-96c: concentration of 100 mg/L group.

10.3389/fmars.2023.1105065

TABLE 3 Summary of differential expressed genes related to immune in transcriptome of *C. sinensis*.

Functional category	ID	Treatment	Fullname	log2(fc)	PValue
Prophenoloxidase cascade					
	evm.TU.Hic_asm_14.1340	H-0 vs H-96a	serine protease	-11.499	2.35E-04
	evm.TU.Hic_asm_14.1339	H-0 vs H-96a	Kazal-type serine protease	-2.517	2.48E-04
	evm.TU.Hic_asm_12.1545	H-0 vs H-96c	serine/threonine-protein kinase TBK1-like isoform X1	1.351	3.67E-02
Pattern recognition proteins/receptors					
	MSTRG.3775	H-0 vs H-96a	C-type lectin domain family member isoform crab 3	-1.133	2.66E-02
	MSTRG.16577	H-0 vs H-96a	C-type lectin 5	-1.935	6.99E-03
	MSTRG.14827	H-0 vs H-96c	C-type lectin	-5.457	4.45E-02
	evm.TU.Hic_asm_5.816	H-0 vs H-96a	lectin precursor 4	-5.535	1.30E-02
	evm.TU.Hic_asm_5.430	H-0 vs H-96a	C-type lectin	-7.141	1.02E-07
	evm.TU.Hic_asm_5.382	H-0 vs H-96b	lectin precursor 4	-6.244	5.81E-04
	evm.TU.Hic_asm_5.382	H-0 vs H-96c	lectin precursor 4	-5.115	4.31E-03
	evm.TU.Hic_asm_3.81	H-0 vs H-96a	C-type lectin domain family 6 member A	-1.665	4.55E-02
	evm.TU.Hic_asm_3.302	H-0 vs H-96b	C-type lectin domain family 6 member A	-3.322	2.56E-02
	evm.TU.Hic_asm_15.1667	H-0 vs H-96a	perlucin-like protein isoform X2	-3.786	3.78E-02
	evm.TU.Hic_asm_13.1924	H-0 vs H-96b	C-type lectin	-2.797	7.25E-03
	evm.TU.Hic_asm_12.301	H-0 vs H-96b	mitogen-activated protein kinase/p38	1.101	5.26E-02
	evm.TU.Hic_asm_11.26	H-0 vs H-96c	toll-like receptor 13	-7.409	2.07E-02
Signal transduction					
	MSTRG.7549	H-0 vs H-96a	phospholipid phosphatase 3-like	-2.040	7.06E-03
	MSTRG.7549	H-0 vs H-96b	phospholipid phosphatase 3-like	-2.598	9.09E-04
	MSTRG.7457	H-0 vs H-96c	protein crumbs homolog 1-like	-2.045	4.65E-02
	MSTRG.25534	H-0 vs H-96a	tumor necrosis factor ligand superfamily member 6-like	-2.037	3.45E-02
	MSTRG.19434	H-0 vs H-96a	pantetheinase-like	-2.024	1.34E-02
	MSTRG.1925	H-0 vs H-96a	caspase 9, partial	1.632	3.55E-02
	evm.TU.Hic_asm_8.972	H-0 vs H-96b	low-density lipoprotein receptor-related protein 1-like, partial	1.444	4.88E-02
	evm.TU.Hic_asm_7.39	H-0 vs H-96a	HRAS-like suppressor 3	3.107	8.80E-03
	evm.TU.Hic_asm_6.906	H-0 vs H-96b	guanylate cyclase soluble subunit beta-2-like	1.464	1.06E-02
	evm.TU.Hic_asm_3.1133	H-0 vs H-96b	MMP-19	1.587	2.75E-02
	evm.TU.Hic_asm_2.761	H-0 vs H-96a	Thrombospondin-4	1.643	1.75E-02
	evm.TU.Hic_asm_17.1590	H-0 vs H-96b	solute carrier family 2 facilitated glucose transporter member 1 protein	-1.298	4.04E-02
	evm.TU.Hic_asm_16.997	H-0 vs H-96a	Follistatin	-3.195	6.00E-03
	evm.TU.Hic_asm_16.161	H-0 vs H-96a	dual oxidase 2-like isoform X2	1.163	3.23E-02
	evm.TU.Hic_asm_15.13	H-0 vs H-96a	C-terminal-binding protein-like isoform X1	1.174	4.53E-02
	evm.TU.Hic_asm_12.301	H-0 vs H-96b	mitogen-activated protein kinase/p38	1.101	5.26E-02
	evm.TU.Hic_asm_12.1630	H-0 vs H-96c	MASP-related molecule Type 1	-3.027	7.05E-03
	evm.TU.Hic_asm_12.1627	H-0 vs H-96a	chymotrypsin-like protease	2.105	3.06E-02
	evm.TU.Hic_asm_12.127	H-0 vs H-96a	gelsolin-like protein 2	1.164	2.93E-02
	evm.TU.Hic_asm_11.1497	H-0 vs H-96a	serine palmitoyltransferase 1-like	1.463	1.84E-02
	evm.TU.Hic_asm_10.963	H-0 vs H-96a	probable 4-coumarate–CoA ligase 5	2.128	3.41E-02

(Continued)

TABLE 3 Continued

Functional category	ID	Treatment	Fullname	log2(fc)	PValue
	evm.TU.Hic_asm_10.2188	H-0 vs H-96a	ADP-ribosylation factor-like	-3.022	1.01E-03
	evm.TU.Hic_asm_10.2172	H-0 vs H-96a	ADP-ribosylation factor-like	-3.060	6.31E-04
	evm.TU.Hic_asm_10.2172	H-0 vs H-96b	ADP-ribosylation factor-like	-3.367	2.21E-03
	evm.TU.Hic_asm_10.1800	H-0 vs H-96a	Collagen alpha-4(VI) chain	1.723	1.74E-03
	evm.TU.Hic_asm_10.1800	H-0 vs H-96b	Collagen alpha-4(VI) chain	1.202	2.55E-03
	evm.TU.Hic_asm_10.1718	H-0 vs H-96a	legumain-like	-1.174	3.66E-02
	evm.TU.Hic_asm_1.865	H-0 vs H-96b	angiotensin-converting enzyme-like isoform X4	-2.578	1.28E-02
	evm.TU.Hic_asm_0.82	H-0 vs H-96b	Protocadherin Fat 4	-3.026	1.19E-02
	evm.TU.Hic_asm_0.599	H-0 vs H-96b	acyl-CoA desaturase isoform X2	-1.919	4.28E-03
	evm.TU.Hic_asm_0.560	H-0 vs H-96b	fatty acid synthase	-3.889	2.62E-03
	evm.TU.Hic_asm_0.1830	H-0 vs H-96b	protocadherin-like wing polarity protein stan	-6.038	2.17E-06
	evm.TU.Hic_asm_0.1428	H-0 vs H-96a	lethal(2) giant larvae protein homolog 1-like	1.407	3.61E-02
	evm.TU.Hic_asm_0.1423	H-0 vs H-96a	peptidyl prolyl cis-trans isomerase A (II)	-3.253	2.00E-02
	evm.TU.Hic_asm_0.1347	H-0 vs H-96a	calcium-activated potassium channel slowpoke-like isoform X6	4.051	1.60E-03
Apoptosis					
	MSTRG.6005	H-0 vs H-96c	inhibitor of apoptosis 1	2.463	1.33E-03
	MSTRG.29423	H-0 vs H-96a	cathepsin L	-2.101	3.18E-02
	MSTRG.29423	H-0 vs H-96b	cathepsin L	-2.396	1.01E-02
	MSTRG.1925	H-0 vs H-96a	caspase 9, partial	1.632	3.55E-02
	MSTRG.1925	H-0 vs H-96b	caspase 9, partial	1.620	5.04E-03
	MSTRG.13361	H-0 vs H-96a	inhibitor of apoptosis 2, partial	-1.881	2.32E-02
	evm.TU.Hic_asm_9.458	H-0 vs H-96a	cathepsin L	-1.550	4.39E-03
	evm.TU.Hic_asm_9.458	H-0 vs H-96b	cathepsin L	-1.698	1.75E-02
	evm.TU.Hic_asm_6.810	H-0 vs H-96a	Baculoviral IAP repeat-containing protein 7-B	10.728	7.75E-15
	evm.TU.Hic_asm_16.1565	H-0 vs H-96b	Bcl-2 like 2 protein	-1.251	2.23E-02
	evm.TU.Hic_asm_11.2315	H-0 vs H-96a	inhibitor of apoptosis protein-like	-11.978	3.72E-02
	evm.TU.Hic_asm_0.1758	H-0 vs H-96b	baculoviral IAP repeat-containing protein 5-like	-1.954	3.86E-02
Other immune molecules					
	MSTRG.19434	H-0 vs H-96a	pantetheinase-like	-2.024	1.34E-02
	evm.TU.Hic_asm_6.906	H-0 vs H-96b	guanylate cyclase soluble subunit beta-2-like	1.464	1.06E-02
	evm.TU.Hic_asm_5.1466	H-0 vs H-96a	deleted in malignant brain tumors 1 protein-like	1.390	4.98E-02
	evm.TU.Hic_asm_5.1466	H-0 vs H-96c	deleted in malignant brain tumors 1 protein-like	1.568	5.55E-05
	evm.TU.Hic_asm_3.513	H-0 vs H-96c	proteasome activator complex subunit 3-like	-2.384	1.68E-02
	evm.TU.Hic_asm_17.964	H-0 vs H-96b	b(0,+)-type amino acid transporter 1-like isoform X3	-1.587	2.04E-02
	evm.TU.Hic_asm_16.193	H-0 vs H-96b	Full=G2/mitotic-specific cyclin-B	-1.844	3.02E-02
	evm.TU.Hic_asm_16.193	H-0 vs H-96c	Full=G2/mitotic-specific cyclin-B	-3.579	6.28E-04
	evm.TU.Hic_asm_15.1378	H-0 vs H-96b	uracil-DNA glycosylase-like	-2.100	2.23E-02
	evm.TU.Hic_asm_12.127	H-0 vs H-96a	gelsolin-like protein 2	1.164	2.93E-02
	evm.TU.Hic_asm_10.1718	H-0 vs H-96a	legumain-like	-1.174	3.66E-02
	evm.TU.Hic_asm_1.1054	H-0 vs H-96c	NRAMP	1.415	7.18E-04

10.3389/fmars.2023.1105065

TABLE 4 Summary of differential and non-differentially expressed genes related to antioxidative capability in transcriptome of *C. sinensis*.

Functional category	ID	Treatment	Fullname	log2(fc)	PValue
Nrf2 signalling pathway					
	evm.TU.Hic_asm_14.463	H-0 vs H-96a	mitogen-activated protein kinase kinase kinase 7-like isoform X2	1.1162	6.65E-02
	evm.TU.Hic_asm_12.301	H-0 vs H-96a	mitogen-activated protein kinase/p38	1.1641	8.56E-02
	evm.TU.Hic_asm_11.1866	H-0 vs H-96b	kelch-like protein 30	4.1859	2.79E-02
Antioxidant					
	MSTRG.11302	H-0 vs H-96b	ribosyldihydronicotinamide dehydrogenase	-1.6087	4.83E-02
	evm.TU.Hic_asm_18.94	H-0 vs H-96a	Thioredoxin-like fold	-1.7154	1.90E-03
	evm.TU.Hic_asm_18.94	H-0 vs H-96b	Thioredoxin-like fold	-2.0399	1.80E-02
	evm.TU.Hic_asm_18.94	H-0 vs H-96c	Thioredoxin-like fold	-1.5592	4.66E-02
	evm.TU.Hic_asm_18.402	H-0 vs H-96c	glutathione S-transferase theta-1-like	0.9051	1.55E-02
	evm.TU.Hic_asm_18.377	H-0 vs H-96b	asparagine synthetase	-1.2806	4.34E-02
	evm.TU.Hic_asm_17.1421	H-0 vs H-96a	omega glutathione S-transferase	0.9259	6.86E-02
	evm.TU.Hic_asm_17.1421	H-0 vs H-96c	omega glutathione S-transferase	0.5777	4.31E-02
	evm.TU.Hic_asm_17.122_	H-0 vs H-96b	alanine–glyoxylate aminotransferase 2	1.3636	1.09E-02
	evm.TU.Hic_asm_17.1077	H-0 vs H-96a	omega glutathione S-transferase	1.9723	6.10E-02
	evm.TU.Hic_asm_14.810	H-0 vs H-96b	pi-class glutathione S-transferase	-1.3021	2.20E-02
	evm.TU.Hic_asm_14.808	H-0 vs H-96b	pi-class glutathione S-transferase	1.5357	3.00E-02
	evm.TU.Hic_asm_14.808	H-0 vs H-96c	pi-class glutathione S-transferase	1.5711	1.30E-03
	evm.TU.Hic_asm_12.1240	H-0 vs H-96a	glutathione S-transferase	2.5167	7.41E-03
	evm.TU.Hic_asm_12.1240	H-0 vs H-96c	glutathione S-transferase	2.1996	1.16E-03
	evm.TU.Hic_asm_12.1238	H-0 vs H-96a	mu class glutathione S-transferase	2.3959	2.43E-02
	evm.TU.Hic_asm_12.1235	H-0 vs H-96c	glutathione S-transferase	1.5995	1.65E-03
	evm.TU.Hic_asm_11.1942	H-0 vs H-96b	thioredoxin	3.5194	2.48E-02
	evm.TU.Hic_asm_10.1023	H-0 vs H-96c	peroxiredoxin V	-1.9552	1.14E-02
	evm.TU.Hic_asm_0.2822	H-0 vs H-96b	glutamate dehydrogenase	-1.8303	1.84E-02
Chaperones					
	evm.TU.Hic_asm_13.1719	H-0 vs H-96a	heat shock protein	1.0017	5.14E-02
	evm.TU.Hic_asm_4.634	H-0 vs H-96c	heat shock protein 70	1.8990	3.67E-03
	evm.TU.Hic_asm_16.191	H-0 vs H-96c	heat shock protein 70	3.7798	1.69E-04
	evm.TU.Hic_asm_13.392	H-0 vs H-96c	heat shock protein 70	2.4537	8.60E-03
	evm.TU.Hic_asm_13.1719	H-0 vs H-96c	heat shock protein	0.7215	1.07E-02
	evm.TU.Hic_asm_10.736	H-0 vs H-96c	heat shock protein 70	2.2761	5.50E-03
	evm.TU.Hic_asm_7.742	H-0 vs H-96c	heat shock protein 60	-1.7482	2.89E-02
Metal-binding protein					
	evm.TU.Hic_asm_5.725	H-0 vs H-96a	heavy metal-binding protein HIP-like	-4.2672	2.45E-05
	evm.TU.Hic_asm_5.725	H-0 vs H-96b	heavy metal-binding protein HIP-like	-1.8680	1.89E-01
	evm.TU.Hic_asm_5.725	H-0 vs H-96c	heavy metal-binding protein HIP-like	-2.8378	3.87E-02
	evm.TU.Hic_asm_4.572	H-0 vs H-96c	heavy metal-binding protein HIP-like	1.8727	2.87E-03
	evm.TU.Hic_asm_3.88	H-0 vs H-96a	heavy metal-binding protein HIP-like	-0.9580	2.50E-02
	evm.TU.Hic_asm_16.1511	H-0 vs H-96a	metallothionein	-2.2738	5.84E-02

(Continued)

TABLE 4 Continued

Functional category	ID	Treatment	Fullname	log2(fc)	PValue
	evm.TU.Hic_asm_16.1511	H-0 vs H-96c	metallothionein	-3.4181	7.44E-03
	evm.TU.Hic_asm_12.1610	H-0 vs H-96a	ferritin subunit	-0.9914	7.17E-02

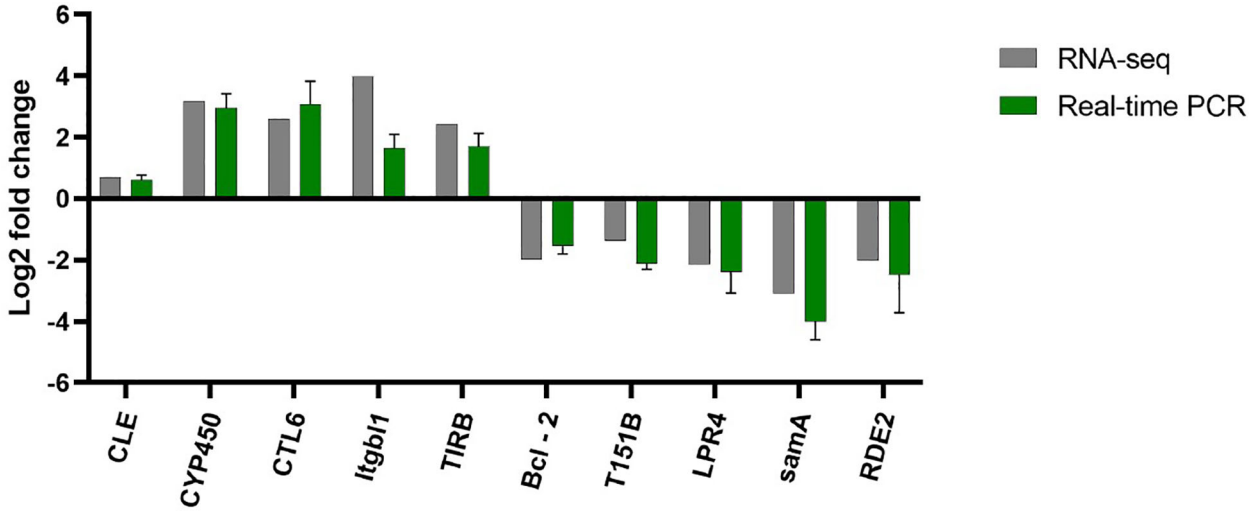

FIGURE 8
Transcriptome result validation. RNA seq and Real-time PCR are shown in grey and green, respectively.

when aquatic organisms are affected by external environmental factors (Chi et al., 2019). The study about the ACP and AKP activities in deltamethrin stressed *Macrobrachium rosenbergii* found that the ACP activity showed a wavy change and the AKP activity showed a trend of increasing and then decreasing after acute stress (Guo et al., 2021; Jiang et al., 2021). A similar conclusion was reached by Peng., in his study on the acute toxicity of the proposed cave green crab (*Cyprinus carpio*) (Peng et al., 2018). In this study, the ACP activity in the 20 mg/L group showed fluctuating changes, while the ACP *a*ctivity in the 50 mg/L and 100 mg/L groups both showed an increase followed by a decrease. There was no significant difference between the initial values. It is assumed that the prolonged survival in a high chlorine environment affected the expression of enzyme activity. The AKP activity in this study showed an overall decreasing trend, with all three concentration groups having lower AKP activity than the initial value after 96 h but no significant difference, suggesting that the AKP activity of the *C. sinensis* organism is inhibited in a high chlorine environment.

LZM protects the organism from foreign bacteria by hydrolyzing the mucopolysaccharides in bacteria (Yin et al., 2022). In a study by Zhou Y., it was found that LZM activity increased during stress after starvation stress in *Oratosquilla oratoria* and began to decrease beyond a certain range (Zhou, 2014). In the present study, the LZM activity of *C. sinensis* showed a decrease, then an increase and then a decrease after chlorine stimulation, and all three concentration groups showed this wavelike change. At 96 h, the LZM activities of all three concentration groups were significantly lower than the initial values ($P < 0.05$). It is hypothesized that the immune function of the *C. sinensis* was reduced after high chloride stress and the LZM activity was inhibited.

4.3 Transcriptome analysis of the effects of residual chlorine stress on hepatopancreas of *C. sinensis*

Studies have shown that residual chlorine stress affects the growth and survival of organisms and their physiological changes, but the molecular mechanisms involved are not well understood. In this study, the transcriptome of the hepatopancreas of *C. sinensis* stressed with residual chlorine for 96 hours was sequenced using RNA-seq technology. These transcriptional data provide a resource for further studies on the molecular mechanisms by which residual chlorine affects immune responses in molluscs. The data from this study indicate that residual chlorine stress has an effect on both the immune and antioxidant systems of the clam.

Serine proteases (*SP*) are a group of widely distributed protein hydrolases that perform a range of important physiological functions, including participation in digestion, blood coagulation, embryonic development and immune response processes (Yin S et al., 2022; Liu H et al., 2022), and play an important role in the innate immune defence of invertebrates (Hu et al., 2018; Xu et al., 2018). When invertebrates are stimulated or infected by microorganisms (Faisal et al., 1998; Xue et al., 2006), *SP* in their bodies can rapidly activate the body's immune system to produce the corresponding immune effects and kill the invading pathogens. However, the benzoquinone and ROS produced during the reaction can cause cellular damage, and serine protease inhibitors (*SPI*) can precisely regulate this process to avoid serious damage to the body (Ding et al., 2011; Chen et al., 2020). In this study, *SP* expression level was down-regulated at safe concentrations compared to the control group, while the expression

levels of *SP* in the high residual chlorine stress group were not significantly different from the control group, which is consistent with previous findings (Zhang et al., 2016; Mao et al., 2018), indicating that that residual chlorine stress induces *SP* in the clam to protect the organism by activating cascade processes and phenol oxidase pathways.

The C-type lectin family is an important class of pattern recognition receptors that trigger processes such as agglutination of microorganisms, induction of phagocytosis and activation of complement by recognizing glycan structures on the surface of microorganisms (Vasta et al., 2004; Osorio and Sousa, 2011) and participate in the regulation of specific immunity with the emergence of specific immunity (van Vliet et al., 2008), playing an important role in shellfish innate immunity (Wang et al., 2007; Zhu et al., 2008; Hu et al., 2011), but has rarely been studied in *C. sinensis*. The results of the present study showed that the expression levels of C-type lectins were significantly down-regulated in both groups a and b after 96 h of residual chlorine stress compared to the control group, with no significant difference in expression levels in group c. This is consistent with the previous findings that the expression of the C-type lectin gene tends to decrease when the stimulation time exceeds 72 hours (Shen et al., 2018), indicating that the clam is affected by residual chlorine and adapts to the environment by regulating the secretion of C-type lectin in the body to protect itself from the stimulus. The regulatory mechanism of the body becomes slower when the stimulation time is too long, and the higher the concentration of residual chlorine, the higher the level of gene expression.

Cathepsin L (*Cts L*) is a major member of the papain C1 family of cysteine proteases. Studies have shown that *Cts L* is involved in a variety of physiological and pathological processes in the organism, such as antigen presentation, hormone protein maturation and processing, tumour invasion and metastasis, apoptosis, bone resorption, individual development and tissue differentiation. In addition, *Cts L* may also mediate the immune defence of the organism (Ma et al., 2010; Peng et al., 2012). Consistent with previous studies (Wang et al., 2013; Liu S et al., 2014) in the present study, *Cts L* expression was significantly down-regulated in both groups a and b after 96 h of residual chlorine stimulation compared to the control group, while no significant difference was observed in group c. This may imply that residual chlorine stress induced an inflammatory response in the organism, which was in a post-infection recovery period after 96 h.

It has been shown that apoptosis is a highly regulated programmed cell death and that the Caspase family plays a pivotal role in apoptosis, with Caspase 9 (*CASP9*) being the initiator of apoptosis (Yu, 2017; Lu et al., 2021; Zhu et al., 2022). In the present study, *CASP9* expression was up-regulated at a and b stress concentrations compared to the control, while no significant difference was observed in group c. This suggests that residual chlorine stress initiated an apoptotic response, but the initiation of the response became slower with increasing residual chlorine concentrations after 96 hours of stress. Previous studies on stress in aquatic animals such as carp (*Ctenopharyngodon idella*) (Luan et al., 2022), yellow catfish (*Pelteobagrus fulvidraco*) (Li et al., 2020) and grouper bream (*Megalobrama amblycephala*) (Zhang, 2015) are consistent with the results of this experiment, suggesting that *CASP9* is associated with apoptosis induced by stress.

The effects of Glutathione S-transferase (*GST*) molecule are both antidotal and antioxidant. When shellfish are stimulated by environmental pollutants, the *GST* activity in their organism is significantly increased (Sandamalika et al., 2019) and protects cells from external stressful environmental damage by catalyzing the redox reaction of hydrogen peroxide and scavenging oxygen radicals and peroxides generated by metabolic reactions in the body (Samaraweera et al., 2019). pi type is a typical representative of many *GST* isoforms and is widely involved in the metabolism of toxins in immune cells and the production of lipophilic compounds and their derivatives (Liu et al., 2020). The *GST* in marine shellfish is basically of the pi type (Liu H et al., 2014). Under the stimulation of pathogenic bacteria, the respiratory burst of cells increases significantly and induces the production of large amounts of ROS. ROS protect the organism from oxidative damage by killing bacteria (Zhang et al., 2017). The antibacterial process of ROS refers to that overly high concentration of ROS breaks the antioxidant defense mechanism in cells and reacts with genetic materials, enzymes, proteins and other substances in bacteria to cause oxidative damage, or reacts with structural components of cell membrane (wall) to cause lipid peroxidation in cells, causing damage and death of bacteria (Zhou et al., 2021). However, excess ROS can cause damage to host cell structure and function, oxidizing cell membrane phospholipids and leading to alterations in cell membrane fluidity and permeability. *GST*s, as an important antioxidant enzyme, play an important role in detoxification of exogenous organisms and protection of cells from excess effects, and ROS regulate cell function by affecting the end products formed from macromolecules damaged by oxidative stress. Therefore, the antioxidant function of *GST*s is essential for the survival of molluscs, as these enzymes (Hu et al., 2012) can rapidly scavenge excess ROS. In the present study, the expression of *GST* was significantly higher in the H-96a, H-96b and H-96c treated groups than in the control group, which is consistent with previous findings (Zheng et al., 2019; Zhang H et al., 2020). This suggests that *C. sinensis* are sensitive to residual chlorine stress and that *GST* are involved in the detoxification process of residual chlorine, thus maintaining the stability of the organism.

Heat shock proteins (*Hsp*), also known as stress proteins, are a group of highly structurally conserved peptide protein family molecules that perform important physiological functions under both normal and stressful conditions. *Hsp70*s are members of a family of 70 kDa heat shock proteins that are widely present in prokaryotic and eukaryotic cells (Gong et al., 2020). *Hsp70* is an inducibly expressed protein that is one of the first protective molecules to appear in response to cellular injury, which helps denatured proteins to recuperate and clear permanently denatured proteins, and its expression increases significantly in response to stimulation by contaminants (Guo et al., 2020; Wang et al., 2020; Cui et al., 2022; Roh and Kim, 2022). In this study, the expression level of *Hsp70* gene was significantly increased in the H-96c group compared to the control group, while there was no significant change in the other two groups, which is consistent with the results of previous studies (Shao and Zhang, 2015; Zhao H et al., 2016; Jing et al., 2019), indicating that the stress response of hepatopancreatic cells increased

with the increase of residual chlorine concentration and the expression level of *Hsp70* gradually increased.

This study showed that residual chlorine stress significantly altered the expression of antioxidant and immune-related genes in the hepatopancreas of *C. sinensis*, providing evidence at the gene transcriptional level for a potential mechanism by which excessive residual chlorine residues in the culture environment affect basal immunity in molluscs. Among the DEGs between the control and three different residual chlorine concentration treatment groups, 68 DEGs were associated with immune responses and 29 DEGs were involved in antioxidant mechanisms. Specifically, genes associated with the proPO cascade system, *PRRs* and signal transduction play an important role in residual chloride-stimulated immune defence to maintain the normal physiological state of the green clam. In addition, molecules associated with the *GST*-dependent antioxidant system are highly involved in antioxidant defence against residual chlorine stress. Thus, these results not only provide some evidence that residual chlorine affects immune homeostasis in aquatic animals, but also contribute to further understanding of the molecular mechanisms and potential pathways of immune function and antioxidant capacity in larval *C. sinensis* under residual chlorine stress.

5 Conclusion

The study showed that the mortality rate of the *C. sinensis* increased with the increase of stress time and concentration. The antioxidant-related T-AOC and SOD activities and immune-related ACP, AKP and LZM enzyme activities of hepatopancreas of *C. sinensis* after residual chlorine stress were significantly changed between 0 and 96 h ($P < 0.05$). Meanwhile, transcriptome analysis showed that residual chlorine stress significantly altered the expression levels of immune and antioxidant related genes. Thus, this study provided valuable information for understanding the effects of residual chlorine stress on survival, physiological metabolism and molecular mechanisms of immune and antioxidant functions of the *C. sinensis* and provided some theoretical references for the understanding of the toxic effects of residual chlorine on bivalves.

Data availability statement

The datasets presented in this study can be found in online repositories. The names of the repository/repositories and accession number(s) can be found in the article/supplementary material.

Ethics statement

All clams were treated in strict accordance with the guidelines for the care and use of experimental animals established by the Administration of Affairs Concerning Experimental Animals of the State Council of the People's Republic of China and approved by the Committee on Experimental Animal Management of the Jiangsu Ocean University.

Author contributions

SW: validation, writing - original draft, visualization, data curation. GR: formal analysis, data curation. DL: data curation, writing - review and editing. SF: data curation, writing - review and editing. SY: data curation, writing - review and editing. JS: data curation, writing - review and editing. ML: supervision, project administration. ZD: data curation, writing - review and editing, funding acquisition, project administration, conceptualization. All authors contributed to the article and approved the submitted version.

Funding

This work was supported by Jiangsu Natural Resources Development Special-Marine Science and Technology Innovation Project (JSZRHYKJ202008); Jiangsu Modern Agriculture Independent Innovation Project (CX (20) 3150); The "JBGS" Project of Seed Industry Revitalization in Jiangsu Province (JBGS〔2021〕034); Modern Agro-industry Technology Research System (CARS-49) and Jiangsu Graduate Research and Practice Innovation Program (KYCX2021-035, KYCX22_3388).

Conflict of interest

The authors declare that the research was conducted in the absence of any commercial or financial relationships that could be construed as a potential conflict of interest.

Publisher's note

All claims expressed in this article are solely those of the authors and do not necessarily represent those of their affiliated organizations, or those of the publisher, the editors and the reviewers. Any product that may be evaluated in this article, or claim that may be made by its manufacturer, is not guaranteed or endorsed by the publisher.

References

Alexandre, L., Christelle, C., Olivier, B., Jean-Marc, L., Antoine, L., Katherine, C., et al. (2022). Effects of chronic exposure of metals released from the dissolution of an aluminium galvanic anode on the pacific oyster *Crassostrea gigas*. *Aquat. Toxicol.* 249, 106223. doi: 10.1016/j.aquatox.2022.106223

Casas, S., La,, and Peyre, J. (2020). Heat shock protein 70 levels and post-harvest survival of eastern oysters following sublethal heat shock in the laboratory or conditioning in the field. *Cell Stre. Chaper* 25 (2), 369–378. doi: 10.1007/s12192-019-01056-1

Chen, J. (2009). Tolerance of chlorine dioxide in parent, larvae and juvenile scallops of the bay scallop (*Scallopus* spp.). *Chin. Agron. Bull.* 07), 279–283.

Chen, D., Guo, L., Yi, C., Wang, S., Ru, Y., and Wang, H. (2021). Hepatopancreatic transcriptome analysis and humoral immune factor assays in red claw crayfish (*Cherax quadricarinatus*) provide insight into innate immunomodulation under vibrio parahaemolyticus infection. *Ecotoxicol. Environ. Saf.* 217, 112266. doi: 10.1016/j.ecoenv.2021.112266

Chen, S., Liang, J., and Zhang, R. (2020). Cloning and expression of the serine protease inhibitor gene pfser1 from the hepu mother-of-pearl shell. *J. GD. Ocean Univer.* 40 (01), 1–7.

Chi, C., Yun, S., Giri, S., Kim, H., Kim, S., Kang, J., et al. (2019). Effect of the algicide thiazolidinedione 49 on immune responses of bay scallop argopecten irradians. *Molecules* 24 (19), 3579. doi: 10.3390/molecules24193579

Cui, Y., Zhao, N., Wang, C., Long, J., Chen, Y., Deng, Z., et al. (2022). Acute ammonia stress-induced oxidative and heat shock responses modulated by transcription factors in *Litopenaeus vannamei*. *Fish Shellfish Immunol.* 128, 181–187. doi: 10.1016/j.fsi.2022.07.060

Dempsey, C. (1986). The exposure of herring postlarvae to chlorine in coastal power stations. *Mari. Environ. Res.* 20 (4), 279–290. doi: 10.1016/0141-1136(86)90053-X

Ding, J., Zhang, G., and Li, L. (2011). Cloning and expression analysis of a serine protease inhibitory factor from abalone cuniculus. *Aquatic. Sci.* 30 (12), 731–738. doi: 10.16378/j.cnki.1003-1111.2011.12.001

Dong, Z., Duan, H., Zheng, H., Ge, H., Wei, M., Liu, M., et al. (2021). Research progress on germplasm, culture and exploitation of *Cyclina sinensis*. *J. Aquac.* 12), 2083–2098.

Dong, X., Yang, Z., Liu, Z., Wang, X., Yu, H., Peng, C., et al. (2022). Metabonomic analysis provides new insights into the response of zhikong scallop (*Chlamys farreri*) to heat stress by improving energy metabolism and antioxidant capacity. *Antioxidants (Basel)* 11 (6), 1084. doi: 10.3390/antiox11061084

Eppley, R., Renger, E., and Williams, P. (1976). Chlorine reactions with seawater constituents and the inhibition of photosynthesis of natural marine phytoplankton. *Estua. Coast. Mar. Sci.* 4 (2), 147–161. doi: 10.1016/0302-3524(76)90039-6

Faisal, M., MacIntyre, E., Adham, K., Tall, B., Kothary, M., La,, et al. (1998). Evidence for the presence of protease inhibitors in eastern (*Crassostrea virginica*) and pacific (*Crassostrea gigas*) oysters. *Comp. Biochem. Physiol. B Biochem. Mol. Biol.* 121 (2), 161–168. doi: 10.1016/S0305-0491(98)10084-6

Ge, H., Liang, X., Liu, J., Cui, Z., Guo, L., Sun, Y., et al. (2021). Effects of acute ammonia exposure on antioxidant and detoxification metabolism in clam *Cyclina sinensis*. *Ecotoxicol. Environ. Saf.* 211, 111895. doi: 10.1016/j.ecoenv.2021.111895

Gong, Y., Kong, T., Ren, X., Chen, J., Lin, S., Zhang, Y., et al. (2020). Exosome-mediated apoptosis pathway during WSSV infection in crustacean mud crab. *PloS. Pathog.* 16 (5), e1008366. doi: 10.1371/journal.ppat.1008366

Grabherr, M., Haas, B., Yassour, M., Levin, J., Thompson, D., Amit, I., et al. (2011). Full-length transcriptome assembly from RNA-seq data without a reference genome. *Nat. Biotechnol.* 29 (7), 644–652. doi: 10.1038/nbt.1883

Guo, J., Pu, Y., Zhong, L., Wang, K., Duan, X., and Chen, D. (2021). Lead impaired immune function and tissue integrity in yellow catfish (*Peltobargus fulvidraco*) by mediating oxidative stress, inflammatory response and apoptosis. *Ecotoxicol. Environ. Saf.* 226, 112857. doi: 10.1016/j.ecoenv.2021.112857

Guo, K., Ruan, G., Fan, W., Wang, Q., Fang, L., Luo, J., et al. (2020). Immune response to acute heat stress in the intestine of the red swamp crayfish, *Procambarus clarkii*. *Fish Shellfish Immunol.* 100, 146–151. doi: 10.1016/j.fsi.2020.03.017

Hegazi, M., Attia, Z., and Ashour, O. (2010). Oxidative stress and antioxidant enzymes in liver and white muscle of Nile tilapia juveniles in chronic ammonia exposure. *Aquat. Toxicol.* 99 (2), 118–125. doi: 10.1016/j.aquatox.2010.04.007

Holen, E., Espe, M., Larsen, A., and Olsvik, P. (2022). Dietary chlorpyrifos-methyl exposure impair transcription of immune, detoxification and redox signaling genes in leukocytes isolated from cod (*Gadus morhua*). *Fish Shellfish Immunol.* 127, 549–560. doi: 10.1016/j.fsi.2022.06.060

Hu, J., Chen, Y., Duan, X., Jin, T., Li, Y., Zhang, L., et al. (2018). Involvement of clip-domain serine protease in the anti-vibrio immune response of abalone (*Haliotis discus hannai*)-molecular cloning, characterization and functional analysis. *Fish Shellfish Immunol.* 72, 210–219. doi: 10.1016/j.fsi.2017.10.062

Hu, B., Deng, L., Wen, C., Yang, X., Pei, P., Xie, Y., et al. (2012). Cloning, identification and functional characterization of a pi-class glutathione-s-transferase from the freshwater mussel *Cristaria plicata*. *Fish Shellfish Immunol.* 32 (1), 51–60. doi: 10.1016/j.fsi.2011.10.018

Hu, Y., Zhang, D., Cui, S., Guo, H., Chen, M., Jiang, S., et al. (2011). Sequence features and functional analysis of the c-type lectin gene(PoLEC1)from pearl oyster *Pinctada fucata*. *J. Fish. China* 35 (9), 1327–1336.

Jiang, Q., Jiang, Z., Ao, S., Gao, X., Zhu, X., Zhang, Z., et al. (2021). Multi-biomarker assessment in the giant freshwater prawn *Macrobrachium rosenbergii* after deltamethrin exposure. *Ecotoxicol. Environ. Saf.* 214, 112067. doi: 10.1016/j.ecoenv.2021.112067

Jiang, Z., Liao, Y., Gao, A., Chen, Q., and Zeng, J. (2009). Progress in the study of residual chlorine effects on fish toxicity. *Oceano. Res.* 27 (04), 86–94.

Jing, Y., Zhang, T., Liu, E., Chen, Q., Sun, M., Guo, W., et al. (2019). Effect of cadmium on the expression of heat shock protein 70 gene in different tissues of pacific oysters at different salinities. *J. GX Acad. Sci.* 35 (04), 332–336. doi: 10.13657/j.cnki.gxkxyxb.20191129.002

Liang, Z., Liu, R., Zhao, D., Wang, L., Sun, M., Wang, M., et al. (2016). Ammonia exposure induces oxidative stress, endoplasmic reticulum stress and apoptosis in hepatopancreas of pacific white shrimp (*Litopenaeus vannamei*). *Fish Shellfish Immunol.* 54, 523–528. doi: 10.1016/j.fsi.2016.05.009

Lian, S., Zhao, L., Xun, X., Lou, J., Li, M., Li, X., et al. (2019). Genome-wide identification and characterization of sods in zhikong scallop reveals gene expansion and regulation divergence after toxic dinoflagellate exposure. *Mar. Drugs* 17 (12), 700. doi: 10.3390/md17120700

Liao, X., Sun, Z., Cui, Z., Yan, S., Fan, S., Xia, Q., et al. (2022). Effects of different sources of diet on the growth, survival, biochemical composition and physiological metabolism of clam (*Cyclina sinensis*). *Aquac. Res.* 00, 1–10. doi: 10.1111/are.15886

Liew, H., Rahmah, S., Tang, P., Waiho, K., Fazhan, H., Rasdi, N., et al. (2022). Low water pH depressed growth and early development of giant freshwater prawn *Macrobrachium rosenbergii* larvae. *Heliyon* 8 (7), e09989. doi: 10.1016/j.heliyon.2022.e09989

Li, Q., Sun, S., Zhang, F., Wang, M., and Li, M. (2019). Effects of hypoxia on survival, behavior, metabolism and cellular damage of Manila clam (*Ruditapes philippinarum*). *PloS. One* 14 (4), e0215158. doi: 10.1371/journal.pone.0215158

Liu, H., He, J., Zhao, R., and Xue, C. (2014). Analysis of glutathione s-transferase gene expression in the thick-shelled mussel *Mytilus edulis* under heavy metal stress. *Ocean Lake Marsh* 45 (02), 274–280.

Liu, H., Yang, R., Chen, Y., Zhang, L., Sun, L., Liu, G., et al. (2022). Cloning, expression and properties of myogenic fibril-binding serine protease from rhubarb fish. *J. Aquac.* 46 (07), 1154–1166.

Liu, H., Zhang, H., Cheng, D., Tan, K., Ye, T., Ma, H., et al. (2020). Differential responses of a pi-class glutathione s-transferase (CnGSTp) expression and antioxidant status between golden and brown noble scallops under pathogenic stress. *Fish Shellfish Immunol.* 105, 144–151. doi: 10.1016/j.fsi.2020.07.004

Liu, C., Zhang, W., Jiang, P., Lin, Y., and Lu, W. (2022). The anti-stress effect of taurine in fish: Assessments based on repeat acute stress and animal individuality. *Aquaculture* 561, 738685. doi: 10.1016/j.aquaculture.2022.738685

Liu, S., Zhao, T., Zhang, H., and Pan, B. (2014). Expression and recombinant protein activity analysis of the histone l gene of the clam (*Cyclina sinensis*). *Mar. Lake. Marsh.* 01), 134–140.

Li, C., Wu, M., and Wang, H. (2012). LC_{50} caculated by kochi, probit analysis and linear regression methods. *Prog. Veteri. Medi.* 33 (09), 89–92. doi: 10.16437/j.cnki.1007-5038.2012.09.012

Li, M., Zhang, M., Qian, Y., Shi, G., and Wang, R. (2020). Ammonia toxicity in the yellow catfish (*Pelteobagrus fulvidraco*): The mechanistic insight from physiological detoxification to poisoning. *Fish Shellfish Immunol.* 02, 195–202. doi: 10.1016/j.fsi.2020.04.042

Li, Y., Zhang, X., Yang, M., Liu, J., Li, W., Graham, N., et al. (2017). Three-step effluent chlorination increases disinfection efficiency and reduces DBP formation and toxicity. *Chemosphere* 168, 1302–1308. doi: 10.1016/j.chemosphere.2016.11.137

Luan, P., Zhang, H., Zhang, X., Hu, G., and Zhang, Z. (2022). Cadmium regulates FKBP5 through miR-9-5p and induces carp lymphocyte apoptosis. *Fish Shellfish Immunol.* 120, 353–359. doi: 10.1016/j.fsi.2021.12.006

Lu, J., Zhang, J., Zhou, G., Wang, P., and Qing, H. (2021). Effects of acute high temperature stress on liver apoptosis-related enzyme activity and gene expression in largemouth bass (*Percus macrocephalus*). *Freshw. Fisher* 02), 81–86. doi: 10.13721/j.cnki.dsyy.2021.02.010

Mao, Z., Lin, Q., Wang, B., Zhang, C., Chen, C., Jian, S., et al. (2018). Effects of Cu~(2+) stress on toxic effects and immune-related gene expression in the Chinese mitten crab *Eriocheir sinensis*. *J. JX Agricul. Univer.* 40 (02), 358–364. doi: 10.13836/j.jjau.2018047

Masilamoni, G., Jesudoss, K., Nandakumar, K., Satapathy, K., Azariah, J., and Nair, K. (2002). Lethal and sub-lethal effects of chlorination on green mussel *Perna viridis* in the context of biofouling control in a power plant cooling water system. *Mar. Environ. Res.* 53 (1), 65–76. doi: 10.1016/s0141-1136(01)00110-6

Ma, J., Zhang, D., Jiang, J., Cui, S., Pu, H., and Jiang, S. (2010). Molecular characterization and expression analysis of cathepsin L1 cysteine protease from pearl oyster *Pinctada fucata*. *Fish Shellfish Immunol.* 29 (3), 501–507. doi: 10.1016/j.fsi.2010.05.006

Min, E., Cha, Y., and Kang, J. (2015). Effects of waterborne nickel on the physiological and immunological parameters of the pacific abalone haliotis *discus hannai* during thermal stress. *Environ. Sci. pollut. Res. Int.* 22 (17), 13546–13555. doi: 10.1007/s11356-015-4597-1

Mohan, K., Ravichandran, S., Muralisankar, T., Uthayakumar, V., Chandirasekar, R., Seedevi, P., et al. (2019). Application of marine-derived polysaccharides as immunostimulants in aquaculture: A review of current knowledge and further perspectives. *Fish Shellfish Immunol.* 86, 1177–1193. doi: 10.1016/j.fsi.2018.12.072

Nie, H., Zuo, S., Li, L., Tian, C., Cao, C., and Yan, X. (2018). Physiological and biochemical responses of *Dosinia corrugata* to different thermal and salinity stressors. *J. Exp. Zool A Ecol. Integr. Physiol.* 329 (1), 15–22. doi: 10.1002/jez.2152

Nikolaivits, E., Agrafiotis, A., Baira, E., Le Goff, G., Tsafantakis, N., Chavanich, S., et al. (2020). Degradation mechanism of 2,4-dichlorophenol by fungi isolated from marine invertebrates. *Int. J. Mol. Sci.* 21 (9), 3317. doi: 10.3390/ijms21093317

Opstvedt, J., Mundheim, H., Nygrd, E., Aase, H., and Pike, I. (2000). Reduced growth and feed consumption of Atlantic salmon (*Salmo salar l.*) fed fish meal made from stale fish is not due to increased content of biogenic amines. *Aquaculture* 188 (3-4), 323–337. doi: 10.1016/S0044-8486(00)00343-4

Osorio, F., and Sousa, C. (2011). Myeloid c-type lectin receptors in pathogen recognition and host defense. *Immunol.* 34 (5), 651–664. doi: 10.1016/j.immuni.2011.05.001

Pan, L., Ren, J., and Liu, J. (2006). Responses of antioxidant systems and LPO level to benzo (a) pyrene and benzo (k) fluoranthene in the haemolymph of the scallop *Chlamys ferrari*. *Environ. pollut.* 141 (3), 443–451. doi: 10.1016/j.envpol.2005.08.069

Park, J., Seok, S., Cho, S., Baek, M., Lee, H., Kim, D., et al. (2004). Safety and protective effect of a disinfectant (STEL water) for white spot syndrome viral infection in shrimp. *Dis. Aquat Organ.* 60 (3), 253–257. doi: 10.3354/dao060253

Pawert, M., Triebskorn, R., Gräff, S., Berkus, M., Schulz, J., and Köhler, H. (1996). Cellular alterationsin collembolan midgut cellsasa marker of heavy metal exposure: ultrastructure and intracellular metal distribution. *Sci. Total Environ.* 181 (3), 187–200. doi: 10.1016/0048-9697(95)05009-4

Peng, J., Chen, L., Cheng, C., Feng, J., Ma, H., and Guo, Z. (2018). Acute toxicity of ammonia nitrogen to the caveman green crab (*Cyprinus carpio*) and effects on its serum immune-related enzyme activity. *Adv. Fish. Sci.* 05), 114–121. doi: 10.19663/j.issn2095-9869.20170907001

Peng, K., Wang, J., Liu, T., Sheng, J., Shi, J., Shao, P., et al. (2012). Tissue expression and immune stress analysis of the histone l gene in the pond mussel, *Phyllostomus pelagicus*. *J. Aquatic. Bio.* 36 (06), 128–1134.

Qiao, Y., Zhou, L., Qu, Y., Lu, K., Han, F., and Li, E. (2022). Effects of different dietary β-glucan levels on antioxidant capacity and immunity, gut microbiota and transcriptome responses of white shrimp (*litopenaeus vannamei*) under low salinity. *Antioxidants (Basel)* 11 (11), 2282. doi: 10.3390/antiox11112282

Qiu, L., Shi, X., Yu, S., Han, Q., Diao, X., and Zhou, H. (2018). Changes of ammonia-metabolizing enzyme activity and gene expression of two strains in shrimp *Litopenaeus vannamei* under ammonia stress. *Front. Physiol.* 9. doi: 10.3389/FPHYS.2018.00211

Roh, H., and Kim, D. (2022). Identification, classification and functional characterization of HSP70s in rainbow trout (*Oncorhynchus mykiss*) through multi-omics approaches. *Fish Shellfish Immunol.* 121, 205–214. doi: 10.1016/j.fsi.2021.12.059

Samaraweera, A., Sandamalika, W., Liyanage, D., Lee, S., Priyathilaka, T., and Lee, J. (2019). Molecular characterization and functional analysis of glutathione s-transferase kappa 1 (GSTκ1) from the big belly seahorse (*Hippocampus abdominalis*): Elucidation of its involvement in innate immune responses. *Fish Shellfish Immunol.* 92, 356–366. doi: 10.1016/j.fsi.2019.06.010

Sandamalika, W., Priyathilaka, T., Lee, S., Yang, H., and Lee, J. (2019). Immune and xenobiotic responses of glutathione s-transferase theta (GST-θ) from marine invertebrate disk abalone (*Haliotis discus discus*): With molecular characterization and functional analysis. *Fish Shellfish Immunol.* 91, 159–171. doi: 10.1016/j.fsi.2019.04.004

Shao, C., and Zhang, Z. (2015). Response of the heat shock protein 70 gene to tributyltin in the near-river oyster (*Oyster sinensis*). *Environ. Sci. Res.* 28 (05), 745–751. doi: 10.13198/j.issn.1001-6929.2015.05.11

Shen, S., Zhu, L., Li, J., Xue, S., Li, Y., Chen, Q., et al. (2018). Cloning and expression analysis of the cDNA of c-type lectin gene in the ark clam (*Arca inflata*). *Adv. Fish Sci.* 39 (01), 128–136.

Shi, P., Bi, X., Dong, S., Song, L., Dai, W., and Zhang, S. (2019). Preparation of baited microalgae slow release cake and its preliminary application in *Cyclina sinensis* pond culture. *J. Dalian Ocean Uni.* 03), 310–315. doi: 10.16535/j.cnki.dlhyxb.2019.03.002

Swezey, D., Boles, S., Aquilino, K., Stott, H., Bush, D., Whitehead, A., et al. (2020). Evolved differences in energy metabolism and growth dictate the impacts of ocean acidification on abalone aquaculture. *Proc. Natl. Acad. Sci. U S A.* 117 (42), 26513–26519. doi: 10.1073/pnas.2006910117

Syafaat, M., Azra, M., Mohamad, F., Che-Ismail, C., Amin-Safwan, A., Asmat-Ullah, M., et al. (2021). Thermal tolerance and physiological changes in mud crab, *Scylla paramamosain crablet* at different water temperatures. *Ani. (Basel)* 11 (4), 1146. doi: 10.3390/ani11041146

van Vliet, S., Garcíavallejo, J., and Van, K. (2008). Dendritic cells and c-type lectin receptors: coupling innate to adaptive immune responses. *Immun. Cell Bio.* 86 (7), 580–587. doi: 10.1038/icb.2008.55

Vasta, G., Ahmed, H., and Odom, E. (2004). Structural and functional diversity of lectin repertoires in invertebrates, protochordates and ectothermic vertebrates. *Curr. Opin. Struc. Bio.* 14 (5), 617–630. doi: 10.1016/j.sbi.2004.09.008

Venkatnarayanan, S., Murthy, P., Kirubagaran, R., Veeramani, P., and Venugopalan, V. (2021). Response of green mussels (*Perna viridis*) subjected to chlorination: investigations by valve movement monitoring. *Environ. Monit. Assess.* 193 (4), 202. doi: 10.1007/s10661-021-09008-y

Wang, Z., Jian, J., Lu, Y., Ding, Y., Wang, B., Chen, G., et al. (2013). Cloning and expression analysis of the histone l gene from the mother-of-pearl mussel (*Pinctada fucata*). *Mar. Lake* 06), 1604–1611.

Wang, H., Song, L., Li, C., Zhao, J., Zhang, H., Ni, D., et al. (2007). Cloning and characterization of a novel c-type lectin from *Chlamys farreri*. *Mole Immun.* 44 (5), 722–731. doi: 10.1016/j.molimm.2006.04.015

Wang, Z., Zhou, J., Li, J., Zou, J., and Fan, L. (2020). The immune defense response of pacific white shrimp (*Litopenaeus vannamei*) to temperature fluctuation. *Fish Shellfish Immunol.* 103, 103–110. doi: 10.1016/j.fsi.2020.04.053

Wei, M., Ge, H., Shao, C., Yan, X., Nie, H., Duan, H., et al. (2020). Chromosome-level genome assembly of the Venus clam, *Cyclina sinensis*, helps to elucidate the molecular basis of the adaptation of buried life. *iScience* 23 (6), 101148. doi: 10.1016/j.isci.2020.101148

Willer, D., and Aldridge, D. (2019). Microencapsulated diets to improve growth and survivorship in juvenile European flat oysters (*Ostrea edulis*). *Aquaculture* 505, 256–262. doi: 10.1016/j.aquaculture.2019.02.072

Wu, Y., Chen, A., Zhang, Y., Cao, Y., Chen, S., and Zhang, Z. (2018). Study on the toxicity and median lethal concentration of residual chlorine on larval razor clams. *Aquat. Sci. Techno. Inform* 03), 158–161. doi: 10.16446/j.cnki.1001-1994.2018.03.009

Xue, Q., Waldrop, G., Schey, K., Itoh, N., Ogawa, M., Cooper, R., et al. (2006). A novel slow-tight binding serine protease inhibitor from eastern oyster (*Crassostrea virginica*) plasma inhibits perkinsin, the major extracellular protease of the oyster protozoan parasite perkinsus marinus. *Comp. Biochem. Physiol. B Biochem. Mol. Biol.* 145 (1), 16–26. doi: 10.1016/j.cbpb.2006.05.010

Xu, Y., Liao, D., Zhang, C., and Qin, S. (2007). Research on clam purification technology in the *Philippines*. *Fish. Modern* 04), 9–12.

Xu, X., Liu, J., Wang, Y., Si, Y., Wang, X., Wang, Z., et al. (2018). Kunitz-type serine protease inhibitor is a novel participator in anti-bacterial and anti-inflammatory responses in Japanese flounder (*Paralichthys olivaceus*). *Fish Shellfish Immunol.* 80, 22–30. doi: 10.1016/j.fsi.2018.05.058

Yin, S., He, Y., Yu, J., Zhang, Y., Liu, Y., Geng, X., et al. (2022). Cloning and immune response characteristics of the serine protease homologue gene (Lv-SPH) in *Penaeus vannamei*. *J. Aquac.* 46 (05), 815–824.

Yin, Z., Nie, H., Jiang, K., and Yan, X. (2022). Molecular mechanisms underlying vibrio tolerance in *ruditapes philippinarum* revealed by comparative transcriptome profiling. *Front. Immunol.* 13. doi: 10.3389/fimmu.2022.879337

Yu, Q. (2017). Effects of copper, cadmium and their combined exposure on oxidative stress and apoptosis in rare minnow (Xianyang: MAster's thesis, Northwest Agriculture and Forestry University).

Zeitoun, I. (1977). The effect of chlorine toxicity on certain blood parameters of adult rainbow trout (*Salmo gairdneri*). *Environ. Bio. Fish.* 1 (2), 189–195. doi: 10.1007/BF00000410

Zeng, J. (2008). *Study on the ecological impact of coastal power plant warm water drainage on subtropical seas* (Hangzhou: Doctoral dissertation, Zhejiang University).

Zhang, X. (2014). *Cyclina sinensis* and shrimp pond mixed culture technology. *Hebei Fishery* 09), 31–32.

Zhang, Q. (2015). Full-length cDNA cloning and expression analysis of g-type lysozyme and caspase family genes in g. regia under ammonia nitrogen stress (Master's thesis (Nanjing: Nanjing Agricultural Universit).

Zhang, H., Dong, Y., Yao, H., Yu, K., Hu, Y., and Lin, Z. (2020). Cloning of GST and HSP90 genes in razor clams (*Sinonovacula constricta*) and characterization of their expression under ammonia nitrogen stress. *J. Oceano.* 04), 66–78.

Zhang, S., Huang, H., Chen, H., Peng, Y., Wang, Z., Fang, Z., et al. (2000). Impact of residual chlorine discharge from daya bay nuclear power station on the environment of adjacent sea areas. *Mar. Environ. Sci.* 19 (2), 14–18.

Zhang, Z., Lv, Z., Shao, Y., Qiu, Q., Zhang, W., Duan, X., et al. (2017). Microsomal glutathione transferase 1 attenuated ROS-induced lipid peroxidation in *Apostichopus japonicus*. *Dev. Comp. Immunol.* 73, 79–87. doi: 10.1016/j.dci.2017.03.011

Zhang, J., Wei, K., and Zhao, T. (2016). Effect of Cu~(2+) stress on the activity of phenol oxidase pro-activation system in crayfish (*Procambarus clarkii*). *J. Agricul. Environ. Sci.* 35 (05), 865–870.

Zhang, Y., Wu, Q., Fang, S., Li, S., Zheng, H., Zhang, Y., et al. (2020). mRNA profile provides novel insights into stress adaptation in mud crab megalopa, *Scylla paramamosain* after salinity stress. *BMC Genomics* 21 (1), 559. doi: 10.1186/s12864-020-06965-5

Zhao, H., Li, W., Wan, L., Yang, D., and Monday, B. (2016). Effect of cd (II) and Cu (II) stress on heat shock protein 70 (HSP70) gene expression in the double-toothed fence silkworm, silkworm (*Serratia marcescens*). *J. DL Ocean Univer.* 31 (02), 156–161. doi: 10.16535/j.cnki.dlhyxb.2016.02.007

Zhao, L., Yang, X., Cheng, Y., and Yang, S. (2016). Effect of dietary histamine supplementation on growth, digestive enzyme activities and morphology of intestine and hepatopancreas in the Chinese mitten crab *Eriocheir sinensis*. *Springerplus.* 5, 552. doi: 10.1186/s40064-016-2105-9

Zheng, S., Liu, Q., Zhang, X., and Xie, Y. (2019). Analysis of GST mRNA expression and enzyme activity in the viscera of river clams under heavy metal stress. *J. Eco. Environ.* 02), 369–375. doi: 10.16258/j.cnki.1674-5906.2019.02.019

Zhou, Y. (2014). Preliminary study on the characteristics of digestive enzymes and immune factors in the mouth shrimp, phyllostomus spp. (Dalian: Master's thesis, Dalian Ocean University).

Zhou, Z., Li, B., Liu, X., Li, Z., Zhu, S., Liang, Y., et al. (2021). Recent progress in photocatalytic antibacterial. *ACS Appl. Bio Mater.* 4 (5), 3909–3936. doi: 10.1021/acsabm.0c01335

Zhu, L., Song, L., Xu, W., and Qian, P. (2008). Molecular cloning and immune responsive expression of a novel c-type lectin gene from bay scallop *Argopecten irradians*. *Fish Shellfish Immunol.* 25 (3), 231–238. doi: 10.1016/j.fsi.2008.05.004

Zhu, P., Sun, Y., Wang, H., Ji, X., and Zeng, Y. (2022). Molecular insight into the hepatopancreas of oriental river prawn (*Macrobrachium nipponense*) in response to residual chlorine stimulus. *Aquat. Toxicol.* 243, 106052. doi: 10.1016/j.aquatox.2021.106052

Zou, L., and Cheng, X. (2003). Study on the tolerance of chlorine dioxide in *Corbicula fluminea*. *Freshw. Fisheries* 02), 8–10.

frontiers | Frontiers in Marine Science

TYPE Original Research
PUBLISHED 27 January 2023
DOI 10.3389/fmars.2023.1076870

OPEN ACCESS

EDITED BY
Thanos Dailianis,
Hellenic Centre for Marine Research, Greece

REVIEWED BY
Yao Zheng,
Freshwater Fisheries Research Center, Chinese Academy of Fishery Sciences, China
Chuangye Yang,
Guangdong Ocean University, China
Youji Wang,
Shanghai Ocean University, China

*CORRESPONDENCE
Zhiguo Dong
dzg7712@163.com

†These authors have contributed equally to this work

SPECIALTY SECTION
This article was submitted to Marine Biology, a section of the journal Frontiers in Marine Science

RECEIVED 22 October 2022
ACCEPTED 16 January 2023
PUBLISHED 27 January 2023

CITATION
Liu M, Fan S, Rong Z, Qiu H, Yan S, Ni H and Dong Z (2023) Exposure to polychlorinated biphenyls (PCBs) affects the histology and antioxidant capability of the clam *Cyclina sinensis*. *Front. Mar. Sci.* 10:1076870. doi: 10.3389/fmars.2023.1076870

Exposure to polychlorinated biphenyls (PCBs) affects the histology and antioxidant capability of the clam *Cyclina sinensis*

Meimei Liu[1,2†], Sishao Fan[1,2†], Zhichao Rong[1,2], Hao Qiu[1,2], Susu Yan[1,2], Hongwei Ni[1,2] and Zhiguo Dong[1,2,3*]

[1]Jiangsu Key Laboratory of Marine Bioresources and Environment, Jiangsu Ocean University, Lianyungang, China, [2]Co-Innovation Center of Jiangsu Marine Bio-industry Technology, Jiangsu Institute of Marine Resources Development, Lianyungang, China, [3]Jiangsu Institute of Marine Resources Development, Jiangsu Ocean University, Lianyungang, China

Polychlorinated biphenyls (PCBs) are environmentally persistent and highly toxic organochlorine compounds that may cause toxic effects on aquatic animals. In this study we assess the toxic effect of PCBs on a bivalve used in aquaculture, the clam *Cyclina sinensis*. To this end, individuals of *C. sinensis* were exposed for 72 h at two PCB concentrations (1 ng/L and 10 ng/L) and control (absence of PCBs). At the end of the exposure, the hemolymph, hepatopancreas, and gills samples of *C. sinensis* were harvested for analysis of the enzyme activity and histology. The results showed that acute PCBs exposure decreased the survival rate of *C. sinensis* compared to the control. Acute PCBs exposure up-regulated the enzymatic activity of superoxide dismutase (SOD), catalase (CAT) and glutathione peroxidase (GSH-Px) and the content of malondialdehyde (MDA) in the hemolymph of *C. sinensis*, while down-regulated the non-specific enzymatic activity of alkaline phosphatase (AKP). For the hepatopancreas, 1 ng/L PCBs exposure up-regulated the enzymatic activity of SOD while down-regulated the enzymatic activity of CAT of *C. sinensis*. In the gill, the enzymatic activity of CAT decreased significantly and the MDA content increased of *C. sinensis* after 10 ng/L PCBs exposure. Moreover, histological observations showed that acute exposure to PCBs caused loss of gill filaments and lateral cilia and shortening of their length, in the studied organism. The present study will provide valuable reference data for marine shellfish aquaculture and toxicology research.

KEYWORDS

bivalve, ecotoxicology, aquaculture, non-specific immunity, chemical stress

1 Introduction

Polychlorinated biphenyls (PCBs) are synthetic organochlorine compounds consisting of 209 congeners that have been used in hundreds of industrial and commercial applications due to their non-flammability, chemical stability, high boiling point and electrical insulation properties in the early years (Rudel et al., 2008; Weis et al., 2011). However, research showed that PCBs are environmentally persistent, highly toxic and bioaccumulate (EUA, 2000; Cao et al., 2008). Thus, concerns over the toxicity and persistence of PCBs in the environment led to the usage of PCBs was banned in the 1970s (Dodoo et al., 2013). Nevertheless, PCBs continue to enter nearby waterways in most developing countries through the uncontrolled spillage, stream transport, surface runoff and atmospheric deposition and that accumulated through the food pyramid (Beate and Ralf, 2004; Lin et al., 2020; Xiao et al., 2021). Recent surveys have found that the concentration of PCBs ranges from 15.1 to 57.9 ng/g (mean: 34.5 ng/g) in the sediment of the Minjiang River in southern China (Zhang et al., 2003).

The most obvious signs of environmental harm caused by PCBs are in the aquatic ecosystems (Environment Canada, 2008). Once PCBs are released into the aquatic environment, they can be bioaccumulate along the food chain and pose potential hazards to other organisms and human consumers (Ashley et al., 2000; Fontenot et al., 2000; Pruell et al., 2000; Dodoo et al., 2013). As the second largest phylum of invertebrates, molluscs are major aquaculture species worldwide and its aquaculture accounts for approximately 27% of the total world aquaculture production (Guo, 2009). With the improvement of people's understanding of the safety of aquatic products, more and more research focus on the detection of the accumulation level of PCBs in wild and farmed mollusk (Madureira et al., 2014; Sun et al., 2015; Zaynab et al., 2021). Take the oysters *Crassostrea tulipa* as an example, the content of PCBs in oysters ranged from 2.95-11.41 mg/kg wet weight (Dodoo et al., 2013). Similarly, Milun et al. (2016) reported that the concentrations of PCBs ranged from 1.53 to 21.1(ng g^{-1} dry weight) in the soft tissue of bivalves. However, the studies regarding the toxic effects of PCB in bivalves is poorly understood.

The clam *Cyclina sinensis* are widely distributed in the coastal beaches and estuaries of China, Japan and North Korea, and have been widely cultivated and proliferated in China (Ge et al., 2021; Dong et al., 2021; Ge et al., 2022). In recent years, extensive *C. sinensis* culture have been carried out in coastal areas, but diseases are frequent, including germplasm decline, environmental pollution and pathogenic stimulation have resulted in high mortality in this species and resulted in huge economic losses (Liang et al., 2000; Ni et al., 2021). As a shellfish with typical filter-feeding behavior, PCBs may accumulate in the gills and digestive glands of *C. sinensis* through their presence in the aquatic environment and in food. Studies have shown that when the concentration of organic contaminants in the environment is above the toxic tolerance limit, it will have serious negative effects on farm animals (Xiao et al., 2021). Several studies have reported that the bivalves in this type of environment suffer from increased mortality, elevated oxidative stress, immune dysfunction, and disturbed energy metabolism (Stewart et al., 2020; Klimova et al., 2021; Balbi et al., 2021).

Antioxidants related to glutathione (GSH) metabolism, and antioxidant enzymes such as superoxide dismutase (SOD) and catalase (CAT), are current topics in biomarker in bivalves during environmental pollutants or factors stress (Liu and Wang, 2016; Danielli et al., 2017; Liang et al., 2022). Some hydrolytic enzymes like alkaline phosphatase (AKP) and ACP (acid phosphatase) also play a role in bivalve non-specific immunity because they may accelerate phagocytosis by modifying pathogen surface molecule (Cheng, 1978; Tang et al., 2010; Adzigbli et al., 2020; Sun et al., 2022). It has been reported that the bivalve gill is the tissue that first comes into contact with foreign particles, which is highly susceptible to damage from environmental pollutants (Cui et al., 2019; Teng et al., 2021; De Campos et al., 2021). The hemolymph and Hepatopancreas also played key role in innate immunity or detoxification for bivalve (Kasturi et al., 2006; Bouallegui, 2019; Zhang et al., 2019). Therefore, the gill, hemolymph and hepatopancreas of mollusks are three target organs that are very valuable to study in acute stress experiments.

To study the toxic effects of PCBs on the bivalves, the clams (*Cyclina sinensis*) were exposed at three different concentrations of PCBs (control, 1 ng/LPCB, 10 ng/L PCBs) for 72 h in this study. At the end of the exposure, the hemolymph, hepatopancreas, and gills samples of *C. sinensis* were harvested for analysis of the enzyme activity and histology. These results will explore the PCBs toxicity to *C. sinensis*, and this study may provide valuable reference data for marine shellfish aquaculture and toxicology research.

2 Materials and methods

2.1 Animal and culture conditions

The *C. sinensis* (shell lengths: 3.5-4.1 cm; body weight: 17.5-18.7 g) were obtained from seaside aquaculture base of Jiangsu Ocean University, Ganyu District, Lianyungang City, Jiangsu Province, China. The *C. sinensis* were transported alive to Shellfish Laboratory of Jiangsu Ocean University, Lianyungang, China, and maintained in cement tanks (length × width × depth=100 cm × 100 cm × 80 cm) filled with natural seawater (salinity 25 ± 1 ppt). During acclimatization, the clams were fed with microalgae *Chaeroeeros moelleri* twice in the 8:30am and 18:00pm. The microalgae *Chaeroeeros moelleri* was purchased from Wudi Zaocheng Biotechnology company (Shandong, China). The water quality was maintained at: ammonia-N<0.5 mg L^{-1}; nitrite<0.10 mg L^{-1}; DO>5 mg L^{-1} and pH 7.0–9.0. After acclimated for seven days, the individual *C. sinensis* of similar size (body weight: 18 ± 0.2g) were selected for the following acute PCBs exposure experiments.

2.2 PCBs exposure and sampling

Polychlorinated biphenyls (P115160, 100μg/mL) were purchased from Bilan Marine Bio-Technology company (Jiangsu, China). Prior to the experiment, the PCBs solution was diluted using the ethanol, the solvent control with 0.001% ethanol was used as the negative control. The exposure experiment is divided into three groups (control, 1 ng/L PCBs treatment and 10 ng/L PCBs treatment)

based on a review of the literature (Dong et al., 2017; Zha et al., 2019a; Zha et al., 2019b; Xiao et al., 2021). 63 clams were used in this experiment and each group had three replicates. Throughout the experiment, the seawater with PCBs was changed every 24 h to ensure that the concentration of PCBs in each group remained invariable during the experiment. Moreover, the number of deaths of clams was recorded for subsequent calculation of the survival rate. The survival rate was calculated using the following formulas:

$$Survival\ \ rate = \frac{X_0 - X}{X_0} \times 100\,\%$$

Where X is the number of final clams, X_0 is the number of initial clams.

In order to study the effect of acute PCB stress on *C. sinensis*, we chose the time point of 72 h exposure as the duration of the stress experiment based on previous studies in zebrafish (Licata et al., 2019a; Licata et al., 2019b). After PCBs exposure for 72 h, fifteen clams were sampled randomly from each group. Approximately 500 μL hemolymph was collected from the adductor muscle of each clams using a sterilized syringe and placed in a 1.5 mL centrifuge tube for the measurement of enzyme activities. The hepatopancreas and gills from each sampled clam were divided into two sub-samples: one was fixed in 4% Paraformaldehyde for histological sectioning, and the remaining tissue was frozen in liquid nitrogen and stored at -40°C for following biochemical analysis.

2.3 Determination of biochemical parameters after acute PCBs exposure

Hemolymph samples were firstly thawed and homogenized using an IKA homogenizer (T10B, IKA Co., Germany). The resultant homogenates were then centrifuged at 12000 rpm for 10 min at 4° C, and the supernatant were placed in sterile centrifuge tubes and stored in 4°C refrigerator for subsequent measurement. Around 0.1 g of hepatopancreas and gills was weighted and added to ice-cold physiological saline solution in a proportion of 1:9 (w/v), and then were homogenized using an IKA homogenizer in a 2 mL centrifuge tube. The homogenate was then centrifuged at 10,000 rpm for 10 min at 4°C, and the supernatant phase was taken and stored at 4°C for later analysis. The same volume of supernatant phase from each sample at the same replicate tank were pooled and mixed prior to later analysis. Thus, three pooled samples for each treatment were detected in this study.

The activities of superoxide dismutase (SOD, A001-3), catalase (CAT, A007-1), glutathione peroxidase (GSH-Px, A005-1), acid phosphatase (ACP, A060-2), alkaline phosphatase (AKP, A059-2) and malondialdehyde (MDA, A003-1) content in the gill, hemolymph and hepatopancreas were analyzed with a spectrophotometer and corresponding detection kits (Nanjing Jiancheng Biological Product, China) according to the manufacturer's guidelines. The total protein contents of the tissue samples were determined using a Coomassie Brilliant Blue Total Protein Assay Kit (Nanjing Jiancheng Bioengineering Research Institute, Nanjing, China). The enzyme activities in the gill and hepatopancreas were expressed as enzyme unit perprotein (U/mg), while the enzyme activities in the hemolymph were expressed as enzyme unit permilliliter (U/mL).

2.4 Histologic observation of gills and hepatopancreas after acute PCBs exposure

The gills and hepatopancreas were fixed in 4% Paraformaldehyde for 24 h and then dehydrated in ascending concentrations of ethanol solutions, cleared in xylene and embedded in paraffin wax. Embedded tissues were cut into 6-μm-thick sections using a rotary microtome (Leica RM2125RTS, Leica Microsystems, Bannockburn, IL, U.S.A.). Sections of gills and hepatopancreas were stained with hematoxylin-eosin for observation under a light microscope (Nikon, Japan) equipped with an automated Leica digital camera system (Nikon, Japan and image manager software (Nikon, Japan). The gill filament and lateral cilia length of *C. sinensis* were measured with Image J 1.8.0 software. 5 individuals and 15 sections in each group were randomly selected for histological observation. The histological structure of the gills and hepatopancreas of *C. sinensis* according to the previous study (Cui et al., 2005; Teng et al., 2021; Liang, 2022). Specifically, the gill filaments are arranged parallel, wider on the outside, thinner on the center and inside, and the outer 1/3 to 1/2 of the gill filaments are covered with a single layer of columnar epithelium, and the lateral cilia are longer. Interfilament connections are covered with cuboidal or flattened epithelium, with abundant connective tissue under the epithelium. The hepatopancreas of clam is composed of multiple blind-end tubules with walls consisting of four kinds of cells: the embryonic cell (E cell), blister-like cell (B cell), resorptive cell (R cell) and fibrillar cell (F cell).

2.5 Data analysis

Data were presented as the mean ± standard error (SE). Homogeneity of the variance of relevant data was tested with Levene's test. When necessary, an arcsine-square root or logarithmic transformation was performed prior to analysis. One-way ANOVA and Duncan's multiple range determine significant differences between groups. All statistical analysis was performed using SPSS 19.0 statistical software (IBM, USA). The level of significance was set to $P< 0.05$. The graphs are drawn by software Graphpad Prism 9 (Graphpad Software Inc., USA).

3 Results

3.1 Impacts of acute PCBs exposure on *C. sinensis* survival rate

As shown in Figure 1, the survival rate of *C. sinensis* after acute PCBs exposure was decreased. The results showed that the lowest survival rate of 81% for the 10 ng/L PCBs group and the highest survival rate of 95% for the control group. There was no significant difference in the survival rate of *C. sinensis* among the three treatment groups.

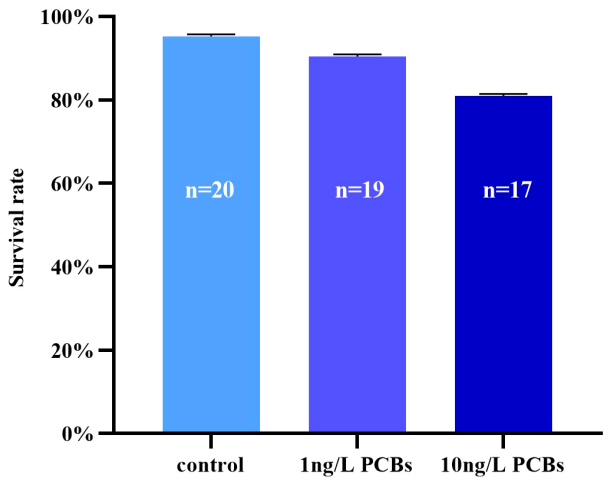

FIGURE 1
Survival rate of *C. sinensis* under different concentrations of PCBs exposure for 72h.

3.2 Impacts of acute PCBs exposure on the non-specific immunity and antioxidant capability

To investigate the effects of acute PCBs exposure on antioxidant capability and non-specific immunity of *C. sinensis*, the activities of SOD, CAT, GSH-Px and MDA content in hemolymph, hepatopancreas and gills were detected. The results further showed that the SOD activity in the hemolymph of *C. sinensis* increased gradually with the increasing of PCBs concentration (Figure 2A). Compared to the control group, the CAT, MDA, GSH-Px in the hemolymph increased significantly in 1 ng/L PCBs group (Figures 2B–D). As shown in Figure 3, the hepatopancreatic SOD activity of *C. sinensis* showed a trend of first increasing and then decreasing after acute PCBs exposure. Compared to the control group, the hepatopancreatic CAT, MDA and GSH-Px decreased in a dose-dependent manner by PCBs groups (Figures 3B–D). In the gills, the SOD, MDA and GSH-Px a trend of first decreasing and then increasing followed by an increase with PCBs concentration, while there was no significant difference among the three groups (Figures 4A, C, D). However, the CAT activity in the gills decreased significantly with the ascending of PCBs concentration (Figure 4B, $P<0.05$).

The enzyme activities of ACP and AKP in hemolymph and hepatopancreas after acute PCBs exposure have also been examined. In the hemolymph, no observable changes were evident in the ACP activity among the three groups (Figure 5A). However, the enzyme activity of AKP in the PCBs treatments significantly lower than that of the control group (Figure 5B). As shown in Figures 5C, D, after 72 h PCBs exposure, the activities of ACP and AKP in the hepatopancreas decreased gradually in comparison to the control, while there was no significant difference among the different groups.

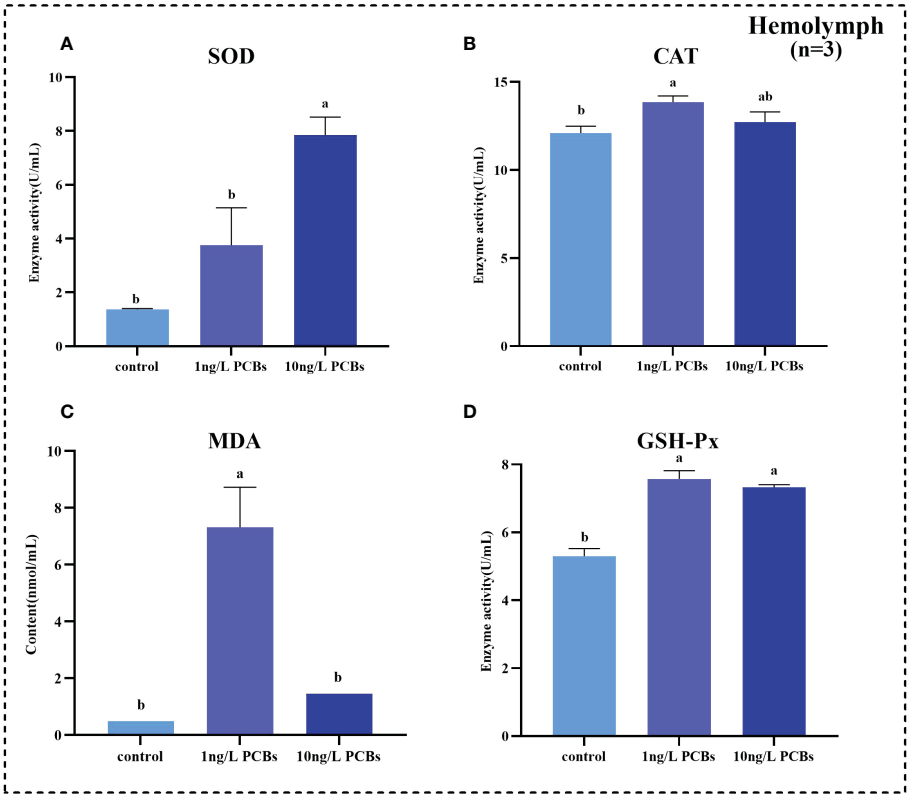

FIGURE 2
Effect of PCBs on the antioxidant capacity in the hemolymph of *C. sinensis*. The columns with different letter indicate significant difference ($P< 0.05$). SOD: superoxide dismutase; CAT: catalase; MDA: malonaldehyde; GSH-Px: glutathione peroxidase.

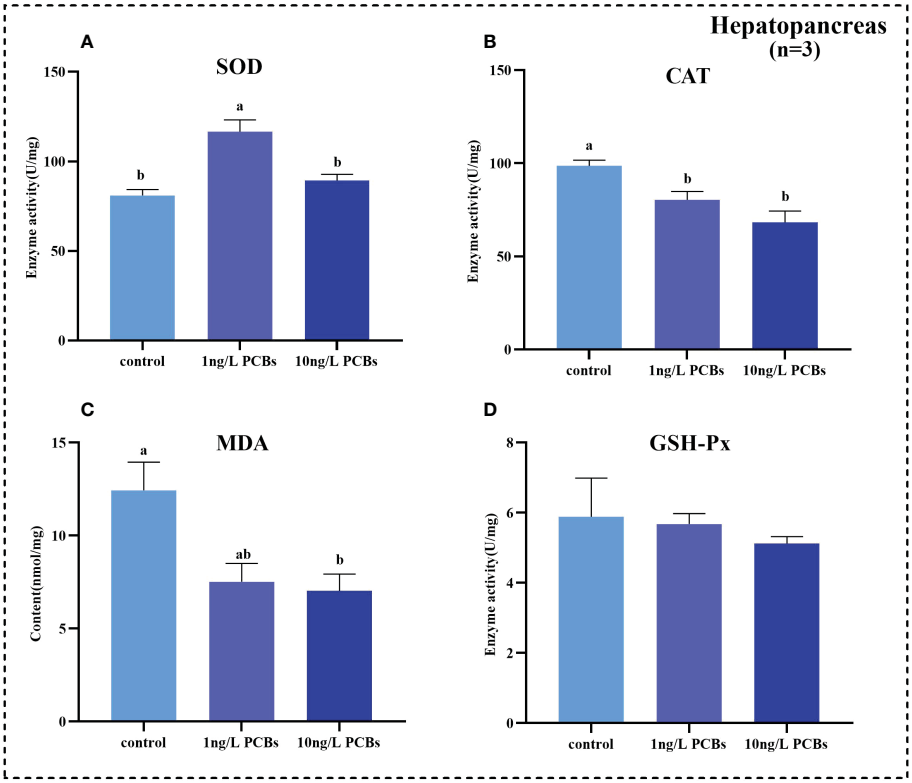

FIGURE 3
Effect of PCBs on the antioxidant capacity in the hepatopancreas of *C. sinensis*. The columns with different letter indicate significant difference ($P< 0.05$). SOD: superoxide dismutase; CAT: catalase; MDA: malonaldehyde; GSH-Px: glutathione peroxidase.

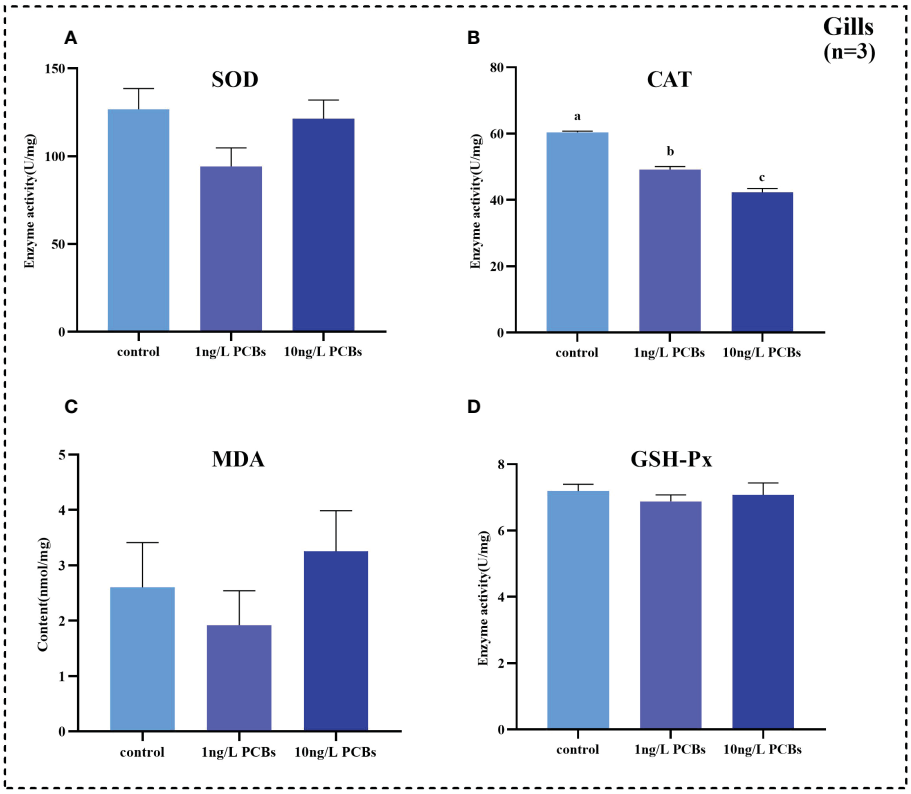

FIGURE 4
Effect of PCBs on the antioxidant capacity in the gills of *C. sinensis*. The columns with different letter indicate significant difference ($P< 0.05$). SOD: superoxide dismutase; CAT: catalase; MDA: malonaldehyde; GSH-Px: glutathione peroxidase.

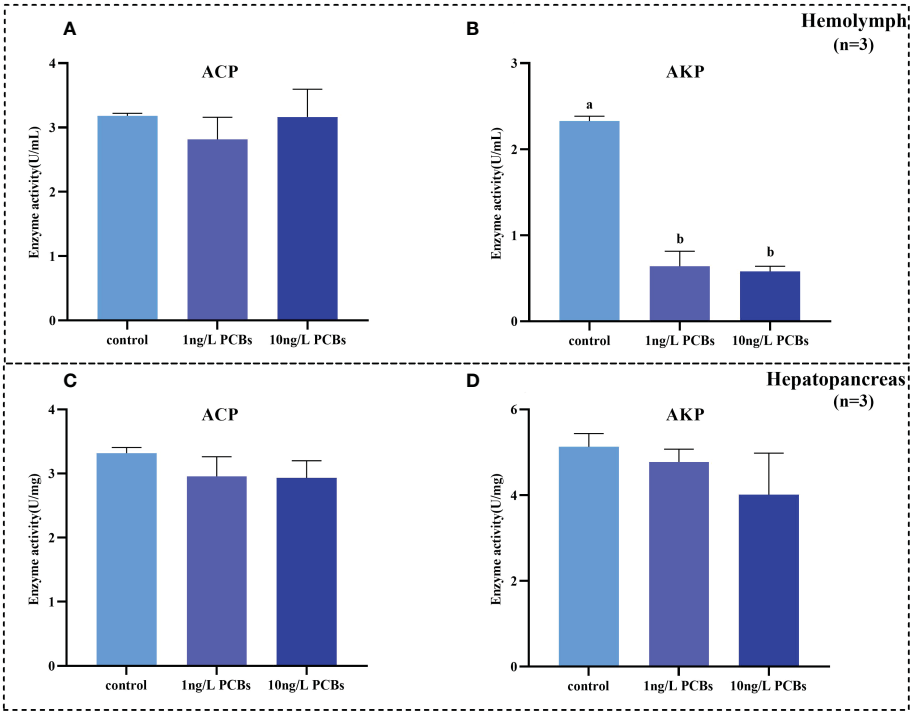

FIGURE 5
Effect of PCBs on the non-specific immunity indices in the hemolymph and hepatopancreas of *C. sinensis*. The columns with different letter indicate significant difference ($P< 0.05$). AKP: alkaline phosphatase; ACP: acid phosphatase.

3.3 Histological effect of acute PCBs exposure on gills and hepatopancreas

Compared with the control group, with the increase of PCBs concentration, the gill plate gap gradually widened and the tissue structure was incomplete and appeared to be detached and defective of *C. sinensis* (Figure 6). After 72 h PCBs exposure, most of the gill filaments and lateral cilia in the clam gills in the 10 ng/L PCBs group were shed, and the connective tissue inside the columnar cells on the gills basically disappeared (Figure 6C). Meanwhile, the length of gill filament and lateral cilia of *C. sinensis* in the 10 ng/L PCBs group were significantly shorter than those in the control group (Table 1).

The histological results showed that the number of blister-like cells in the hepatopancreatic ducts tended to increase with increasing PCB concentration, but there was no significant difference between the groups (Figure 7). Furthermore, the hepatopancreatic tubular lumen of *C. sinensis* gradually shrinks with the increase of PCBs concentration (Figure 7).

4 Discussion

In this study, the relationship among the survival rate, non-specific immunity antioxidant capability, histology and concentrations of PCBs were investigated using clams, *Cyclina sinensis*, as the experimental animal. The results are envisaged to be important towards increasing knowledge of physiological response in the *C. sinensis*, and also shading some lights on the possible ecotoxicological effects of PCBs contamination in effluent seawaters. PCBs are frequently detected in aquatic environments, which particularly toxic to fishes and invertebrates and are fatal to these animals in even small concentrations (McGraw-Hill, 1987; Encyclopedia, 2003). Previous studies showed that the toxicity of

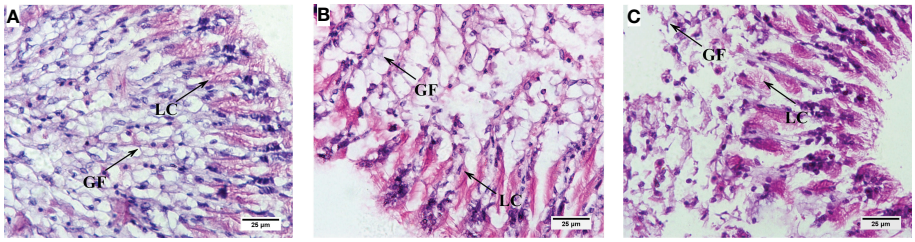

FIGURE 6
Histological changes in the gills of (*C*) *sinensis* under different concentrations of PCBs. Notes: **(A)** control; **(B)** 1ng/L PCBs group; **(C)** 10 ng/L PCBs group; GF: gill filament; LC: lateral cilia.

TABLE 1 The Gill filament and Lateral cilia length of *C. sinensis* after exposure to different concentration of PCBs for 72 h. (N=5).

Groups	Gill filament length(μm)	Lateral cilia length(μm)
Control	124.4 ± 5.4[a]	10.8 ± 1.3[a]
1ng/L PCBs	86.3 ± 3.7[b]	7.2 ± 1.5[b]
10ng/L PCBs	53.2 ± 4.1[c]	5.8 ± 1.2[c]

Values are presented as mean ± SE. Different superscript letters within a same column indicate significantly different (P< 0.05).

PCBs is thought to be solely mediated through binding to aryl hydrocarbon receptor, AhR (Safe et al., 1985; Yuan et al., 2014). Thus, the adverse effects of PCBs in mammal were reported such as hepatotoxicity, endocrine effects, immunotoxicity, body weight loss, teratogenicity and carcinogenicity (Yuan et al., 2014). Recently, several studies reported that PCBs treatment significantly decreased the survival rate of aquatic animals (He et al., 2010; Adams et al., 2016; Xiao et al., 2021). In present study, the survival rate of *C. sinensis* also decreased after exposure to PCBs for 72 h, further indicating that PCBs have toxic effects on aquatic organisms even in the low concentration (Berg et al., 2011; Gard et al., 2021).

Identifying how environmental pollutants reduce the antioxidant capacity and innate immunity of farmed animals has become an important topic in the aquaculture research (Xiao et al., 2021). Several studies have reported that the bivalves in organic pollutants of environment suffer from elevated oxidative stress, immune dysfunction, and disturbed energy metabolism (Stewart et al., 2020; Klimova et al., 2021; Balbi et al., 2021). Therefore, in order to protect themselves, the activities of enzymes related to the antioxidant system in the organism are altered in response to oxidative stress (Karakoc et al., 1997). As the important intracellular primary antioxidant enzymes, SOD neutralizes O_2^- and converts it into the less reactive H_2O_2, while CAT catalyses the conversion of H_2O_2 to water and molecular oxygen during the process of ROS elimination (Valko et al., 2006; Newsholme et al., 2016). GSH-Px catalyse the removal of hydroperoxides using the tripeptide glutathione as reducing substrate (Duan et al., 2015). MDA is formed as a byproduct caused by oxidative stress, which is generally used as a biomarker for oxidative damage (Lopes et al., 2001; Aldini et al., 2010). In this study, PCBs exposure up-regulated the enzymatic activities of SOD, CAT and GSH-Px and the content of MDA in the hemolymph of *C. sinensis*, indicating that hemolymph is very sensitive to PCBs exposure and that it mobilizes a variety of antioxidant enzymes to cope with the oxidative damage caused by PCB to maintain biological homeostasis. Similarly, He and Chen (2010) reported that PCBs treatment significantly increased the enzymatic activities of SOD, CAT and GSH-Px and the content of MDA in the mudskipper *Boleophthalmus pectinirostris* compared to the control group. Feng et al. (2019) reported that the PCBs treatment significantly increased the enzymatic activities of SOD, CAT and the content of MDA in the hemolymph of Chinese mitten crab *Eriocheir sinensis*. Moreover, the enzymatic activity of CAT decreased significantly and the MDA content increased in the gills of *C. sinensis* after 10 ng/L PCBs exposure, indicating that PCBs treatment caused the body to produce excess ROS, which in turn damaged the gills and reduced enzyme activity (Cheng et al., 2020; Cheng et al., 2021). For the hepatopancreas, 1 ng/L PCBs exposure up-regulated the enzymatic activity of SOD while down-regulated the enzymatic activity of CAT of *C. sinensis*. It was speculated that the hepatopancreas is under low oxidative stress and it can eliminate damage caused by PCBs by regulating the balance of the oxidative system in the hepatopancreas (Vieira et al., 2012; Zheng et al., 2016). The low content of MDA in the hepatopancreas also further indicated that the antioxidant enzymes alleviate oxidative stress, and thereby were likely to have limited the accumulation of MDA (Han et al., 2014).

The innate immune response of marine bivalve molluscs is the main immune system against the stressful conditions (Pourmozaffar et al., 2019). In this study, non-specific immune-related enzymes ACP and AKP were studied to assessment the non-specific immune response to PCBs stress of *C. sinensis*. ACP and AKP, important lysosomal marker enzymes, played an important role in non-specific immune responses and were often used as indicators to evaluate the immune status of organisms (Rahman and Siddiqui, 2004; Ma et al., 2013; Liang et al., 2014). In bivalve's species, the activities of ACP and AKP is often measured to evaluate their immune response to adverse environmental and biological factors, such as heat, pH, temperature, heavy metals and virus, etc (Tang et al., 2010; Hu et al., 2015; Yang et al., 2019; Adzigbli et al., 2020; Xu et al., 2021; Yang et al., 2021). Moreover, a previous study in crustacean have shown that the enzyme activities of ACP were decreased in the hemolymph after PCBs treatment (Feng et al., 2019). In agreement with previous results,

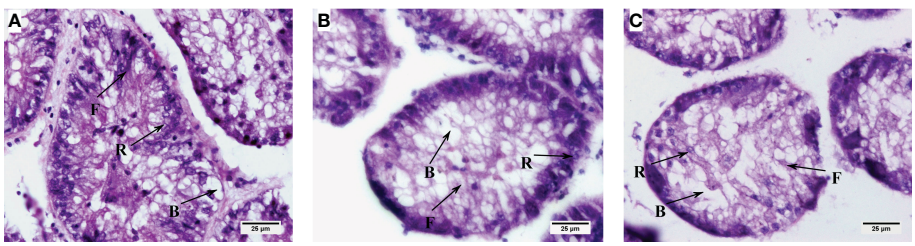

FIGURE 7
Histological changes in the hepatopancreas of (*C*) *sinensis* under different concentrations of PCBs. Notes: **(A)** control; **(B)** 1ng/L PCBs group; **(C)** 10 ng/L PCBs group. B: blister-like cell; F: fibrillar cell; R: resorptive cell.

this study also found that the enzymatic activities of AKP and ACP in the hemolymph and hepatopancreas decline after acute PCBs exposure, indicating that PCB damages the non-specific immune system of *C. sinensis* through inhibited the enzymatic activities of AKP and ACP.

Gill is the respiratory organ as well as the feeding organ of shellfish. Shellfish can filter food, transport food particles, conduct gas, ion exchange and other activities through gill structures, such as cilia (Li, 2008; De Campos et al., 2021). Biotransformation of organic xenobiotics, excretion of harmful trace metals and food digestion and storage are the main hepatopancreas functions (Hinton et al., 2001; Zhang et al., 2019). Besides the measurement/evaluation of chemical and physical parameters, evidence arising from histo-cytopathological examinations has been increasingly recognised as valuable tool to evaluate the impact of pollutants on aquatic animals (Au, 2004; Carballeira et al., 2011; Sikdokur et al., 2020). Thus, PCBs exposure caused histological changes in the gills and hepatopancreas of clams was also investigated in this study. Based on the histological analysis generated in this study, it was shown that PCBs expose caused the gill plate gap widened and tissue structure appeared to be detached and defective of *C. sinensis*. These results indicate that PCBs impacts physiological metabolism also by causing damage to structure of gills. Differently to what reported in crustaceans, the present study showed that histological structure of the hepatopancreas in the PCBs treatments of *C. sinensis* did not show significant changes compared to the control group. The possible reasons for the contradictory results on the PCBs may related to the period of exposure experiment (Feng et al., 2019; Xiao et al., 2021).

5 Conclusion

This study investigated the effect of acute PCBs exposure on the survival, non-specific immunity, antioxidant capability and histology of the *C. sinensis*. The results showed that acute PCBs exposure down-regulated the survival rate, the CAT activity and MDA content in the hepatopancreas, while up-regulated the CAT, SOD, GSH-Px activities and MDA content in the hemolymph of *C. sinensis*. Moreover, PCBs exposure caused the gill plate gap widened and tissue structure appeared to be detached and defective of *C. sinensis*, and down-regulated the CAT activity in the gills (Figure 8). These data will provide valuable reference data for further understanding the effects of PCBs on marine shellfish toxicology. In the future, tailored studies on the toxicological mechanisms of PCBs regulating the physiological metabolism of shellfish are therefore warranted.

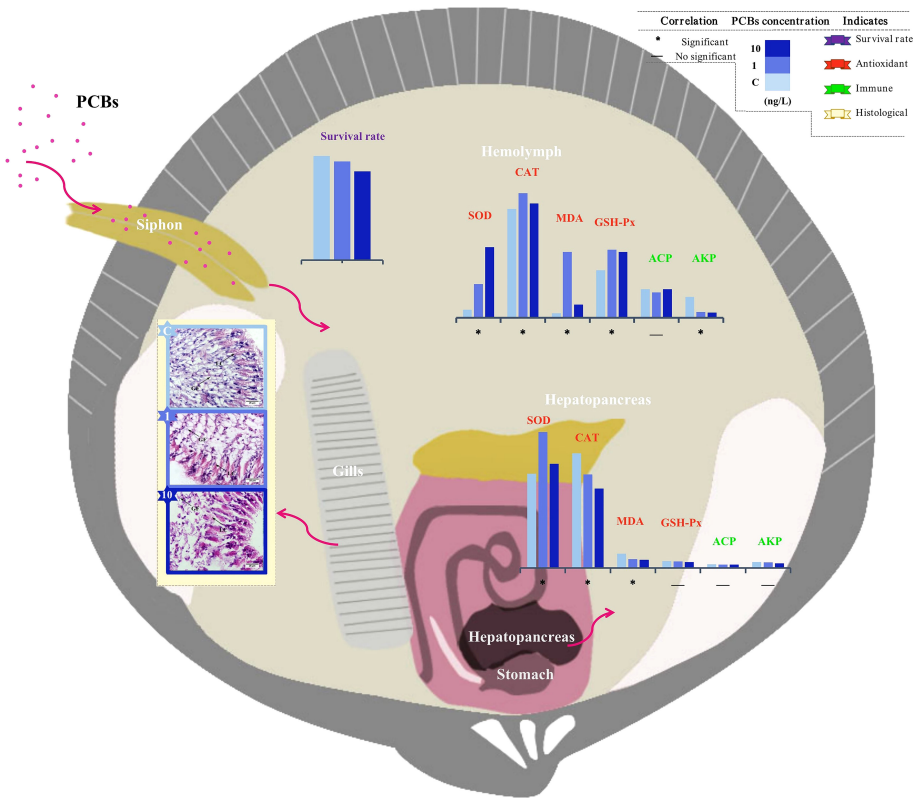

FIGURE 8
Schematic of the effects of acute PCBs exposure on the histological changes of the gills, and antioxidant capacity and non-specific immunity response of hemolymph as well as hepatopancreas of *C. sinensis*. SOD: superoxide dismutase; CAT: catalase; MDA: malonaldehyde; GSH-Px: glutathione peroxidase. AKP: alkaline phosphatase; ACP: acid phosphatase.

Data availability statement

The original contributions presented in the study are included in the article/supplementary material. Further inquiries can be directed to the corresponding author.

Author contributions

ML: Experimental design, writing - original draft, data curation. SF: Formal analysis, data curation. ZR: Data curation, validation. HQ: Data curation, visualization. SY: Experimental design, formal analysis. ZD: Writing-editing, funding acquisition. All authors contributed to the article and approved the submitted version.

Funding

This study was funded by the"JBGS"Project of Seed Industry Revitalization in Jiangsu Province(JBGS[2021]034), an Open-end Funds (SH20201205) of Jiangsu Key Laboratory of Marine Bioresources and Environment, two practice innovation training program projects (No. 202111641127Y and No. SY202257X) for the Jiangsu College students. Infrastructure costs were partially supported by the Project of Jiangsu Fisheries Science and Technology (SZ-LYG202029) and Modern Agro-industry Technology Research System (CARS-49).

Conflict of interest

The authors declare that the research was conducted in the absence of any commercial or financial relationships that could be construed as a potential conflict of interest.

Publisher's note

All claims expressed in this article are solely those of the authors and do not necessarily represent those of their affiliated organizations, or those of the publisher, the editors and the reviewers. Any product that may be evaluated in this article, or claim that may be made by its manufacturer, is not guaranteed or endorsed by the publisher.

Supplementary material

The Supplementary Material for this article can be found online at: https://www.frontiersin.org/articles/10.3389/fmars.2023.1076870/full#supplementary-material

References

Adams, M., Baker, J., and Kjellerup, B. (2016). Toxicological effects of polychlorinated biphenyls (PCBs) on freshwater turtles in the united states. *Chemosphere.* 154, 148–154. doi: 10.1016/j.chemosphere.2016.03.102

Adzigbli, L., Wang, Z., Li, J., and Deng, Y. (2020). Survival, retention rate and immunity of the black shell colored stocks of pearl oyster *Pinctada fucata martensii* after grafting operation. *Fish. Shellfish Immun.* 98, 691–698. doi: 10.1016/j.fsi.2019.11.003

Aldini, G., Dalle-Donne, I., Facino, R., Milzani, A., and Carini, M. (2010). Intervention strategies to inhibit protein carbonylation by lipoxidation-derived reactive carbonyls. *Med. Res. Rev.* 27 (6), 817–868. doi: 10.1002/med.20073

Ashley, J., Secor, D., and Slokovitz, E. (2000). Linking habitat use of Hudson river striped bass to the accumulation of polychlorinated biphenyls. *Environ. Sci. Technol.* 34, 1023–1029. doi: 10.1021/es990833t

Au, D. (2004). The application of histo-cytopathological biomarkers in marine pollution monitoring: a review. *Mar. pollut. Bull.* 48, 817–834. doi: 10.1016/j.marpolbul.2004.02.032

Balbi, T., Auguste, M., Ciacci, C., and Canesi, L. (2021). Immunological responses of marine bivalves to contaminant exposure: contribution of the omics approach. *Front. Immun.* 12. doi: 10.3389/FIMMU.2021.618726

Beate, U., and Ralf, S. (2004). Developmental toxicity of polychlorinated biphenyls (PCBs): a systematic review of experimental data. *Arch. Toxicol.* 78, 483–487. doi: 10.1007/s00204-004-0583-y

Berg, K., Puntervolland, P., Klungsøyr, J., and Goksøyr, A. (2011). Brain proteome alterations of atlantic cod (*Gadus morhua*) exposed to PCB 153. *Aquat. Toxicol.* 105 (3-4), 206–217. doi: 10.1016/j.aquatox.2011.06.010

Bouallegui, Y. (2019). Immunity in mussels: An overview of molecular components and mechanisms with a focus on the functional defenses. *Fish Shellfish Immun.* 89, 158–169. doi: 10.1016/j.fsi.2019.03.057

Cao, X., Chen, H., Shen, S., Song, Y., and Lian, X. (2008). The nature and environmental impact of PCBs. *Sciencepa. On.* 5), 375–381.

Carballeira, C., Espinosa, J., and Carballeira, A. (2011). Linking δ15n and histopathological effects in molluscs exposed *in situ* to effluents from land-based marine fish farms. *Mar. pollut. Bull.* 62 (12), 2633–2641. doi: 10.1016/j.marpolbul.2011.09.034

Cheng, T. (1978). *The role of lysosmal hydrolases in moluscan cellular response to immunologic challenge* (US: Springer). doi: 10.1007/978-1-4757-1278-0_4

Cheng, C., Ma, H., Deng, Y., Feng, J., Jie, Y., and Guo, Z. (2021). Oxidative stress, cell cycle arrest, DNA damage and apoptosis in the mud crab (*Scylla paramamosain*) induced by cadmium exposure. *Chemosphere.* 263, 128277. doi: 10.1016/j.chemosphere.2020.128277

Cheng, C., Su, Y., Ma, H., Deng, Y., Feng, J., Chen, X., et al. (2020). Effect of nitrite exposure on oxidative stress, DNA damage and apoptosis in mud crab (*Scylla paramamosain*). *Chemosphere.* 239, 124668. doi: 10.1016/j.chemosphere.2019.124668

Cui, L., Kong, J., and Zhou, X. (2005). Observation on the gill of *Mactra chinensis* with optical and scanning electron microscopes. *Prog. Fish. Sci.* 4), 60–63. doi: 10.3969/j.issn.1000-7075.2005.04.010

Cui, Q., Qiu, L., and Yang, X. (2019). Transcriptome profiling of the low-salinity stress responses in the gills of the juvenile *Pseudopleuronectes yokohamae*. *Comp. Biochem. Phys. D.* 32, 100612. doi: 10.1016/j.cbd.2019.100612

Danielli, N., Trevisan, R., Mello, D., Fischer, K., Deconto, V., Acosta, D., et al. (2017). Upregulating Nrf2-dependent antioxidant defenses in pacific oysters *Crassostrea gigas*: Investigating the Nrf2/Keap1 pathway in bivalves. *Comp. Biochem. Physiol. C.* 195, 16–26. doi: 10.1016/j.cbpc.2017.02.004

De Campos, B. G., Fontes, M. K., Gusso-Chioueri, P. K., Marinsek, G. P., Nobre, C. R., Moreno, B. B., et al. (2021). A preliminary study on multi-level biomarkers response of the tropical oyster *Crassostrea brasiliana* to exposure to the antifouling biocide DCOIT. *Mar. pollut. Bull.* 174, 113241. doi: 10.1016/j.marpolbul.2021.113241

Dodoo, D., Essumang, D., and Jonathan, J. (2013). Accumulation profile and seasonal variations of polychlorinated biphenyls (PCBs) in bivalves *Crassostrea tulipa* (oysters) and *Anadara senilis* (mussels) at three different aquatic habitats in two seasons in Ghana. *Ecotoxicol. Environ. Saf.* 88, 26–34. doi: 10.1016/j.ecoenv.2012.10.013

Dong, Z., Duan, H., Zheng, H., Ge, H., Wei, M., Liu, M., et al. (2021). Research progress in genentic resources assessment, culture technique and exploration utilization of *Cyclina sinensis*. *J. Fish. China.* 45 (12), 2083–2098. doi: 10.11964/jfc.20201212545

Dong, Y., Zhang, X., Tian, H., Li, X., Wang, W., and Ru, S. (2017). Effects of polychlorinated biphenyls on metamorphosis of a marine fish Japanese flounder (*Paralichthys olivaceus*) in relation to thyroid disruption. *Mar. pollut. Bull.* 119, 325–331. doi: 10.1016/j.marpolbul.2017.04.033

Duan, Y., Zhang, J., Dong, H., Wang, Y., Liu, Q., and Li, H. (2015). Oxidative stress response of the black tiger shrimp *Penaeus monodon* to *Vibrio parahaemolyticus* challenge. *Fish. Shellfish Immun.* 46 (2), 354–365. doi: 10.1016/j.fsi.2015.06.032

Environment Canada (2008). Pollution and wastes-polychlorinated biphenyls (PCBs).

EUA (2000). Department of health and human services. agency for toxic substances and disease registry. toxicological profile for polychlorinated biphenyls (Update). *ATSDR toxicological profile.*

Encyclopedia, B (2003). *The New Encyclopedia Britannica* (Chicago: Encyclopedia Britannica Inc) 9, 577.

Feng, D., Wang, X., Li, E., Bu, X., Qiao, F., Qin, J., et al. (2019). Dietary aroclor 1254-induced toxicity on antioxidant capacity, immunity and energy metabolism in Chinese

mitten crab *Eriocheir sinensis*: Amelioration by vitamin a. *Front. Physiol.* 10. doi: 10.3389/fphys.2019.00722

Fontenot, L., Noblet, G., and Atkins, J. (2000). Bioaccumulation of polychlorinated biphenyls in ranid frogs and northern water snakes from a hazardous waste site and a contaminated watershed. *Chemosphere.* 40, 803–809. doi: 10.1016/S0045-6535(99)00329-X

Gard, N., Edwards, M., Kulacki, K., and Ginn, T. (2021). Limitations on development of polychlorinated biphenyl tissue concentration thresholds for survival, growth, and reproduction in fish. *Environ. Toxicol. Chem.* 40 (8), 2085–2097. doi: 10.1002/ETC.5071

Ge, H., Liu, J., Ni, Q., Wang, F., and Dong, Z. (2022). Effects of acute ammonia exposure and post-exposure recovery on nonspecific immunity in clam cyclina sinensis. *Isr. J. Aquacult-Bamid.* 74, 1–10. doi: 10.46989/001c.32647

Ge, H., Shi, J., Liu, J., Liang, X., and Dong, Z. (2021). Combined analysis of mRNA-miRNA reveals the regulatory roles of miRNAs in the metabolism of clam *Cyclina sinensis* hepatopancreas during acute ammonia nitrogen stress. *Aquacult. Res.* 53 (4), 1492–1506. doi: 10.1111/ARE.15683

Guo, X. (2009). Use and exchange of genetic resources in molluscan aquaculture: Genetic resources in molluscan aquaculture. *Rev. Aquacult.* 1 (3-4), 251–259. doi: 10.1111/j.1753-5131.2009.01014.x

Han, X., Gao, B., Wang, H., Liu, P., Chen, P., and Li, H. (2014). Effects of low salinity stress on microstructure of gill and hepatopancreas and family survival rate of *Portunus trituberculatus*. *Pro. Fish. Sci.* 35 (1), 104–110. doi: 10.3969/j.issn.1000-7075.2014.01.015

He, S., and Chen, B. (2010). Effects of aroclor 1248 on oxidative stress and toxicity in *Boleophthalmus pectinirostris*. *Acta Hydrobio. Sini.* 34 (2), 442–447. doi: 10.3724/SP.J.1035.2010.00442

Hinton, D., Segner, H., and Braunbeck, T. (2001). "Toxic responses of the liver," in *Toxicity in marine and freshwater teleosts*, vol. 1 . Eds. D. Schlenk and W. H. Bensen (London: Taylor & Francis), 224–268.

Hu, M., Li, L., Sui, Y., Li, L., Wang, Y., Lu, W., et al. (2015). Effect of pH and temperature on antioxidant responses of the thick shell mussel *Mytilus coruscus*. *Fish. Shellfish Immun.* 46 (2), 573–583. doi: 10.1016/j.fsi.2015.07.025

Karakoc, F., Hewer, A., Philips, D., Gaines, A., and Yuregir, G. (1997). Biomarkers of marine pollution observed in species of mullet living in two eastern Mediterranean harbours. *Biomarkers* 2 (5), 303–309. doi: 10.1080/135475097231535

Kasturi, R., Lutz, A., and Peter, C. (2006). Ammonia toxicity and its effect on the growth of the south African abalone *Haliotis midae* Linnaeus. *Aquaculture.* 261 (2), 678–687. doi: 10.1016/j.aquaculture.2006.06.020

Klimova, Y., Chuiko, G., Pesnya, D., and Ivanova, E. (2021). Biomarkers of oxidative stress in freshwater bivalve mollusks (Review). *Inland Water Biol.* 13 (4), 674–683. doi: 10.1134/S1995082920060073

Li, J. (2008). *Studies on the shell characters, feeding, and digestive systems and nuclear DNA of saxidomus purpuratus (Sowerby)* (Shaodong Qingdao: Ocean University of China). Master Thesis.

Liang, X. (2022). *Effects of ammonia nitrogen stress on detoxification metabolism and functional verification of related genes in cyclina sinensis* (Jiangsu Liangyungang: Jiangsu Ocean University). Master Thesis. doi: 10.44354/d.cnki.gjsuy.2022.000260

Liang, J., Liu, Y., Zhu, F., Li, Y., Liang, S., and Guo, Y. (2022). Impact of ocean acidification on the physiology of digestive gland of razor clams *Sinonovacula constricta*. *Front. Mar. Sci.* 9. doi: 10.3389/FMARS.2022.1010350

Liang, S., Luo, X., You, W., Luo, L., and Ke, C. (2014). The role of hybridization in improving the immune response and thermal tolerance of abalone. *Fish. Shellfish Immun.* 39 (1), 69–77. doi: 10.1016/j.fsi.2014.04.014

Liang, Y., Yang, B., Wang, L., Zhang, X., Wu, Z., Jiang, Y., et al. (2000). Disease triggering mechanism and protecting policy of the mariculture shellfish in coast of yellow sea. *Mar. Environ. Res.* 1), 5–10. doi: 10.3969/j.issn.1007-6336.2000.01.002

Licata, P., Piccione, G., Fazio, F., Lauriano, E., and Calò, M. (2019a). Protective effects of genistein on cytochrome p-450 and vitellogenin expression in liver of zebrafish after PCB-126 exposure. *Sci. Total Environ.* 674, 71–76. doi: 10.1016/j.scitotenv.2019.03.467

Licata, P., Tardugno, R., Pergolizzi, S., Capillo, G., Aragona, M., Colombo, A., et al. (2019b). *In vivo* effects of PCB-126 and genistein on vitellogenin expression in zebrafish. *Nat. Prod. Res.* 33 (17), 2507–2514. doi: 10.1080/14786419.2018.1455048

Lin, S., Zhao, B., Ying, Z., Fan, S., Hu, Z., Xue, F., et al. (2020). Residual characteristics and potential health risk assessment of polychlorinated biphenyls (PCBs) in seafood and surface sediments from xiangshan bay, China, (2011-2016). *Food Chem.* 327, 126994. doi: 10.1016/j.foodchem.2020.126994

Liu, X., and Wang, W. (2016). Antioxidant and detoxification responses of oysters *Crassostrea hongkongensis* in a multimetal-contaminated estuary. *Environ. Toxicol. Chem.* 35 (11), 2798–2805. doi: 10.1002/etc.3455

Lopes, P., Pinheiro, T., Santos, M., Da, L., Collares-Pereira, M., and Viegas-Crespo, A. (2001). Response of antioxidant enzymes in freshwater fish populations (*Leuciscus alburnoides* complex) to inorganic pollutants exposure. *Sci. Total Environ.* 280, 153–163. doi: 10.1016/S0048-9697(01)00822-1

Madureira, T., Santos, C., Velhote, S., Cruzeiro, C., Rocha, E., and Rocha, M. (2014). Contamination levels of polychlorinated biphenyls in wild versus cultivated samples of female and male mussels (*Mytilus* sp.) from the Northwest coast of Iberian peninsula-new application for QuEChERS (Quick, easy, cheap, effective, rugged, and safe) methodology. *Environ. Sci. pollut. Res. Int.* 21 (2), 1528–1540. doi: 10.1007/s11356-013-2017-y

Ma, Y., Liu, Z., Yang, Z., Li, M., Liu, J., and Song, J. (2013). Effects of dietary live yeast *Hanseniaspora opuntiae* C21 on the immune and disease resistance against *Vibrio splendidus* infection in juvenile sea cucumber *Apostichopus japonicus*. *Fish. Shellfish Immun.* 34 (1), 66–73. doi: 10.1016/j.fsi.2012.10.005

McGraw-Hill (1987). *Encyclopedia of science and technology* Vol. 14 (McGraw-Hill), 127–128.

Milun, V., Lušić, J., and Despalatović, M. (2016). Polychlorinated biphenyls, organochlorine pesticides and trace metals in cultured and harvested bivalves from the eastern Adriatic coast (Croatia). *Chemosphere.* 153, 18–27. doi: 10.1016/j.chemosphere.2016.03.039

Newsholme, P., Cruzat, V., Keane, K., Carlessi, R., and Bittencourt, P. (2016). Molecular mechanisms of ROS production and oxidative stress in diabetes. *Biochem. J.* 473 (24), 4527–4550. doi: 10.1042/BCJ20160503C

Ni, Q., Li, W., Liang, X., Liu, J., Ge, H., and Dong, Z. (2021). Gill transcriptome analysis reveals the molecular response to the acute low-salinity stress in *Cyclina sinensis*. *Aquacult. Rep.* 19, 100564. doi: 10.1016/J.AQREP.2020.100564

Pourmozaffar, S., Tamadoni, J., Rameshi, H., Sadeghi, A., Bagheri, T., Behzadi, S., et al. (2019). The role of salinity in physiological responses of bivalves. *Rev. Aquacult.* 12, 1548–1566. doi: 10.1111/raq.12397

Pruell, J., Taplin, B., and Mcgovern, D. (2000). Organic contaminant distributions in sediments, polychaetes (*Nereis virens*) and American lobster (*Homarus americanus*) from a laboratory food chain experiment. *Mar. Environ. Res.* 49, 19–36. doi: 10.1016/S0141-1136(99)00046-X

Rahman, M., and Siddiqui, M. (2004). Biochemical effects of vepacide (from azadirachta indica) on wistar rats during subchronic exposure. *Ecotoxicol. Environ. Saf.* 59 (3), 332–339. doi: 10.1016/j.ecoenv.2003.07.013

Rudel, R., Seryak, L., and Brody, J. (2008). PCB-Containing wood floor finish is a likely source of elevated PCBs in resident's blood, household air and dust: a case study of exposure. *Environ. Health* 7, 2. doi: 10.1186/1476-069x-7-2

Safe, S., Bandiera, S., Sawyer, T., Robertson, L., Safe, L., Parkinson, A., et al. (1985). PCBs: structure-function relationships and mechanism of action. *Environ. Health Perspect.* 60, 47–56. doi: 10.2307/3429944

Sikdokur, E., Belivermis, M., Sezer, N., Pekmez, M., Bulan, O., and Kilic, O. (2020). Effects of microplastics and mercury on manila clam *Ruditapes philippinarum*: feeding rate, immunomodulation, histopathology and oxidative stress. *Environ. pollut.* 7), 262. doi: 10.1016/j.envpol.2020.114247

Stewart, B., Jenkins, S., Boig, C., Sinfield, C., Kennington, K., and Brand, A. (2020). Metal pollution as a potential threat to shell strength and survival in marine bivalves. *Sci. Total Environ.* 755 (1), 143019. doi: 10.1016/j.scitotenv.2020.143019

Sun, Y., Guo, K., Yu, X., Li, Y., Yao, W., and Wu, Z. (2022). Molecular and biochemical effects on metabolism and immunity of *Hyriopsis cumingii* fed with four different microalgae. *Front. Mar. Sci.* 9. doi: 10.3389/FMARS.2022.970781

Sun, X., Hu, H., Zhong, Z., Jin, Y., Zhang, X., and Guo, Y. (2015). Ultrasound-assisted extraction and solid-phase extraction as a cleanup procedure for organochlorinated pesticides and polychlorinated biphenyls determination in aquatic samples by gas chromatography with electron capture detection. *J. Sep. Sci.* 38 (4), 626–633. doi: 10.1002/jssc.201400880

Tang, B., Liu, B., Wang, X., Yue, X., and Xiang, J. (2010). Physiological and immune responses of zhikong scallop *Chlamys farreri* to the acute viral necrobiotic virus infection. *Fish. Shellfish Immun.* 29 (1), 42–48. doi: 10.1016/j.fsi.2010.02.019

Teng, J., Zhao, J., Zhu, X., Shan, E., Zhang, C., Zhang, W., et al. (2021). Toxic effects of exposure to microplastics with environmentally relevant shapes and concentrations: Accumulation, energy metabolism and tissue damage in oyster crassostrea gigas. *Environ. pollut.* 269, 116169. doi: 10.1016/j.envpol.2020.116169

Valko, M., Rhodes, C., Moncol, J., Izakovic, M., and Mazur, M. (2006). Free radicals, metals and antioxidants in oxidative stress-induced cancer. *Chem.-Biol. Interact.* 160 (1), 1–40. doi: 10.1016/j.cbi.2005.12.009

Vieira, M., Torronteras, R., Córdoba, F., and Canalejo, A. (2012). Acute toxicity of manganese in goldfish *Carassius auratus* is associated with oxidative stress and organ specific antioxidant responses. *Ecotoxicol. Environ. Saf.* 78, 212–217. doi: 10.1016/j.ecoenv.2011.11.015

Weis, J., and Monosson, E. (2011). PCBs. *Encyclopedia of earth*, Ed. C. J. Cleveland, 23.

Xiao, C., Zhang, Y., and Zhu, F. (2021). Immunotoxicity of polychlorinated biphenyls (PCBs) to the marine crustacean species, *Scylla paramamosain*. *Environ. pollut.* 291, 118229. doi: 10.1016/j.envpol.2021.118229

Xu, Y., Zhang, Y. H., Liang, J., He, G. X., Liu, X. L., Zheng, Z., et al. (2021). Impacts of marine heatwaves on pearl oysters are alleviated following repeated exposure. *Mar. pollut. Bull.* 173, 112932. doi: 10.1016/j.marpolbul.2021.112932

Yang, C., Du, X., Hao, R., Wang, Q., Deng, Y., and Sun, R. (2019). Effect of vitamin D3 on immunity and antioxidant capacity of pearl oyster *Pinctada fucata martensii* after transplantation: Insights from LC-MS-based metabolomics analysis. *Fish. Shellfish Immun.* 94, 271–279. doi: 10.1016/j.fsi.2019.09.017

Yang, X., Zhang, Y., Liang, J., He, G., Liu, X., and Zheng, Z. (2021). Impacts of marine heatwaves on pearl oysters are alleviated following repeated exposure. *Mar. pollut. Bull.* 173, 112932. doi: 10.1016/J.MARPOLBUL.2021.112932

Yuan, J., Pu, Y., and Yin, L. (2014). Prediction of binding affinities of PCDDs, PCDFs and PCBs using docking-based comparative molecular similarity indices analysis. *Environ. Toxicol. Pharmacol.* 38 (1), 1–7. doi: 10.1016/j.etap.2014.04.019

Zaynab, M., Fatima, M., Sharif, Y., Sughra, K., Sajid, M., and Khan, K. (2021). Health and environmental effects of silent killers organochlorine pesticides and polychlorinated bipheny. *J. King Saud Univ. Sci.* 33 (6), 101511. doi: 10.1016/J.JKSUS.2021.101511

Zhang, Z., Hong, H., Zhou, J., Huang, J., and Yu, G. (2003). Fate and assessment of persistent organic pollutants in water and sediment from minjiang river estuary, southeast China. *Chemosphere.* 52 (9), 1423–1430. doi: 10.1016/S0045-6535(03)00478-8

Zhang, T., Yan, Z., Zheng, X., Fan, J., Wang, S., Wei, Y., et al. (2019). Transcriptome analysis of response mechanism to ammonia stress in Asian clam (*Corbicula fluminea*). *Aquat. Toxicol.* 214, 105235. doi: 10.1016/j.aquatox.2019.105235

Zha, S., Rong, J., Guan, X., Tang, Y., Han, Y., and Liu, G. (2019a). Immunotoxicity of four nanoparticles to a marine bivalve species, *Tegillarca granosa*. *J. Hazard Mater.* 377, 237–248. doi: 10.1016/j.jhazmat.2019.05.071

Zha, S., Shi, W., Su, W., Guan, X., and Liu, G. (2019b). Exposure to 2,3,7,8-tetrachlorodibenzo-paradioxin (TCDD) hampers the host defense capability of a bivalve species, *Tegillarca granosa*. *Fish Shellfish Immun.* 86, 368–373. doi: 10.1016/j.fsi.2018.11.058

Zheng, Y., Qiu, L., Meng, S., Fan, L., Song, C., Li, D., et al. (2016). Effect of polychlorinated biphenyls on oxidation stress in the liver of juvenile GIFT, *Oreochromis niloticus*. *Genet. Mol. Res.* 15 (3), 15038613. doi: 10.4238/gmr.15038613

frontiers | Frontiers in Marine Science

TYPE Original Research
PUBLISHED 13 February 2023
DOI 10.3389/fmars.2023.1122668

OPEN ACCESS

EDITED BY
Pedro Morais,
Florida International University,
United States

REVIEWED BY
Verginica Schröder,
Ovidius University, Romania
Qi Li,
Ocean University of China, China

*CORRESPONDENCE
Tao Zhang
zhangtaocas@126.com
Hao Song
haosong@qdio.ac.cn

SPECIALTY SECTION
This article was submitted to Marine Biology, a section of the journal Frontiers in Marine Science

RECEIVED 13 December 2022
ACCEPTED 27 January 2023
PUBLISHED 13 February 2023

CITATION
Yang M-J, Shi Y, Lin Z-S, Shi P, Hu Z, Zhou C, Hu P-P, Yu Z-L, Zhang T and Song H (2023) RNA-seq analysis reveals the effect of the metamorphic cue (juvenile oysters) on the *Rapana venosa* larvae. *Front. Mar. Sci.* 10:1122668. doi: 10.3389/fmars.2023.1122668

RNA-seq analysis reveals the effect of the metamorphic cue (juvenile oysters) on the *Rapana venosa* larvae

Mei-Jie Yang[1,2,3,4,5], Ying Shi[6], Zhi-Shu Lin[6], Pu Shi[1,2,3,4,5,7], Zhi Hu[1,2,3,4,5,7], Cong Zhou[1,2,3,4,5,7], Peng-Peng Hu[1,2,3,4,5,7], Zheng-Lin Yu[3,8], Tao Zhang[1,2,3,4,5]* and Hao Song[1,2,3,4,5]*

[1]CAS Key Laboratory of Marine Ecology and Environmental Sciences, Institute of Oceanology, Chinese Academy of Sciences, Qingdao, China, [2]Laboratory for Marine Science and Technology, Qingdao National Laboratory for Marine Science and Technology, Qingdao, China, [3]Center for Ocean Mega-Science, Chinese Academy of Sciences, Qingdao, China, [4]CAS Engineering Laboratory for Marine Ranching, Institute of Oceanology, Chinese Academy of Sciences, Qingdao, China, [5]Shandong Province Key Laboratory of Experimental Marine Biology, Qingdao, China, [6]Qingdao Marine Management Support Center, Qingdao, China, [7]University of Chinese Academy of Sciences, Beijing, China, [8]Research and Development Center for Efficient Utilization of Coastal Bioresources, Yantai Institute of Coastal Zone Research, Chinese Academy of Sciences, Yantai, China

As a vital developmental event, metamorphosis controls the population dynamics of most marine invertebrates and affects the breeding of economic shellfish. *Rapana venosa* is an economically important species in China, but artificial aquaculture has hampered its metamorphosis process. Previous studies have found that juvenile oysters can effectively induce the metamorphosis of *R. venosa*, but the specific induction mechanism is not clear. Here, we investigated the mechanism underlying the response of *R. venosa* to juvenile oysters through the RNA-seq analysis. In this study, the gene set responses to metamorphosis cues (juvenile oysters) in *R. venosa* were identified, and GO and KEGG enrichment analyses were further performed on these gene sets. The results showed that the expression of the prototype of the class of immediate early genes, the transcription factor AP-1, was rapidly and significantly increased, and the molecular chaperone of NOS, HSP90, exhibited lower expression in the M12 group than in the control group. In contrast, the expression of inhibitors of apoptosis (IAPs) was significantly increased upon exposure to juvenile oysters. Additionally, the Wnt signaling pathway and MAPK signaling pathway were enriched in the trend analysis. These pathways may also play critical regulatory roles in the response to juvenile oysters. Taken together, the results show that competent larvae rapidly respond to the inducing effects of oysters *via* some immediate early genes, such as the transcription factor AP-1, which may further regulate downstream pathways such as the MAPK signaling pathway to cause subsequent changes, including a decrease in HSP90 and an increase in IAPs. These changes together may regulate the metamorphosis of *R. venosa*. This study provides further evidence that juvenile oysters are the metamorphosis cues of *R. venosa*, which may enhance our understanding of the metamorphosis mechanism in this marine invertebrate.

KEYWORDS

rapana venosa, metamorphic cue, RNA-Seq, juvenile oyster, trend analysis

1 Introduction

Rapana venosa is an economically important gastropod in China. Recently, with the increasing market demand, fishing of *R. venosa* has intensified, which has severely damaged wild resources. These situations have attracted widespread attention from domestic researchers, and the artificial culture industry of *R. venosa* will continue to develop in the future (Yu et al., 2020). However, *R. venosa* is a successful worldwide invader, including in the Black Sea, the Mediterranean Sea, the Adriatic and Aegean seas, the coasts of France and the Netherlands, the Chesapeake Bay on the Atlantic coast of the United States, and the Río de la Plata between Uruguay and Argentina, and it causes great damage to the wild resources of oysters and other bivalves in the above areas (Xue et al., 2018). This problem has also attracted widespread concern. Therefore, the invasion mechanism urgently needs to be elucidated.

Given the special ecological status of this species, in recent years, there have been a number of studies on the behavior, reproduction and development, environmental suitability, ecological effects, and technology of artificial breeding and culturing of *R. venosa* (Song et al., 2016a; Song et al., 2016b; Song et al., 2016c; Zhang et al., 2017; Xu et al., 2019; Yu, 2019; Yang et al., 2020a; Yang et al., 2020b; Zhang et al., 2020; He et al., 2021; Shi et al., 2022; Yang et al., 2022). However, we have found that the metamorphosis rate of *R. venosa* has become extremely low in its early development stage with the development of the artificial breeding and culturing industry, resulting in a low breeding survival rate (Yu et al., 2020). This low survival rate severely restricts the development of this industry.

Metamorphosis is critical for most marine invertebrates due to the sensitivity and vulnerability of organisms during this time, which affect the population dynamics and resource recruitment of marine invertebrates (Song et al., 2021). Therefore, it is very important to reveal the regulatory mechanisms of metamorphosis for the development of the artificial culture industry and the illumination of the invasion mechanism. In previous studies, we have found that the metamorphosis rate of *R. venosa* increases by more than 60% when juvenile oysters (*Crassostrea gigas*, with a shell length less than 3 cm) are present, although the metamorphosis process cannot be completed spontaneously (Cavalcanti et al., 2020). Meanwhile, Xu et al. (2019) indicated that oyster reefs can significantly promote the recovery of *R. venosa* resources. This may partly explain why these mollusks are destroying oyster resources. However, the specific mechanism by which oysters induce metamorphosis of *R. venosa* larvae is not clear.

Considering the importance of metamorphosis, its regulatory mechanism has been widely researched in species including sponges, tubeworm, coral and mollusks, especially in bivalves and herbivorous gastropods (Cavalcanti et al., 2020). Most of these species use cues from bacteria. For example, Song et al. (2021) showed that in the marine sponge *Amphimedon queenslandica*, bacterial symbionts can play a critical role in animal development by providing their host with the arginine needed for larval settlement and metamorphosis. Shikuma et al., (2016) found that larvae of the tubeworm *Hydroides elegans* metamorphose in response to surface-bound *Pseudoalteromonas luteoviolacea* bacteria, further inducing the regulation of mitogen-activated protein kinase (MAPK) signaling. Conspecific adults and food are also important cues of metamorphosis in some species. The metamorphosis of *Mytilopsis sallei* and *Balanus amphitrite* is stimulated by conspecific adults (Matsumura et al., 1998; He et al., 2021). Metamorphosis is usually food-stimulated in some gastropods, including the herbivorous gastropods *Haliotis rufescens* and *Crepidula fornicata* (Morse et al., 1979; Taris et al., 2010) and the carnivorous gastropod *Onchidoris bilamellata*, whose metamorphosis cues are juvenile barnacles (Rodriguez et al., 1993).

As *R. venosa* is a typical carnivorous gastropod, its metamorphosis cue is also its food, juvenile oysters (Yu et al., 2020), consistent with that in *O. bilamellata*. We have also performed many studies on the metamorphosis of *R. venosa*, including studies on its morphology, behavior, enzyme kinetics, symbiotic microbiota, metabolome, proteome, transcriptome and critical genes (Song et al., 2016a; Song et al., 2016b; Song et al., 2016c; Zhang et al., 2017; Yu et al., 2020; Yang et al., 2020a; Yang et al., 2020b; Shi et al., 2022; Yang et al., 2022). However, a comprehensive analysis of the metamorphosis regulation mechanism in *R. venosa* has not been conducted.

Transcriptomics has been widely applied to investigate the mechanisms underlying metamorphosis in invertebrates, revealing the critical pathways and genes that regulate metamorphosis and providing novel insights (Shikuma et al., 2016; He et al., 2021). Herein, to further investigate the mechanism by which juvenile oysters induce the metamorphosis of *R. venosa* larvae, we obtained the mRNA expression profiles of competent larvae exposed to juvenile oysters for 2 hours (M2) and 12 hours (M12) and before exposure to juvenile oysters (control, Con) *via* sequencing on an Illumina NovaSeq 6000 platform. Furthermore, we identified the differentially expressed mRNAs (differentially expressed genes, DEGs) and performed trend analysis of gene expression based on their transcripts per million (TPM) values to further screen out the genes that were consistently regulated during exposure to juvenile oysters. Then, these genes were subjected to Gene Ontology (GO) and Kyoto Encyclopedia of Genes and Genomes (KEGG) enrichment analyses. The findings of this study will enhance understanding of the metamorphosis mechanism of *R. venosa*, which may not only aid in the development of artificial breeding and culturing but also reveal the invasion mechanism and support the protection of wild populations of oysters and other bivalves.

2 Materials and methods

2.1 Larval culture and sample collection

Culturing of *R. venosa* larvae and sample collection were performed according to Yang et al. (2022), and the competent larvae (shell height > 1,200 μm) were used to conduct the assay. Three cement pools (3.5 × 5.2 × 1.5 m) were used to culture these larvae, and the assay was performed with a larval density of 0.1 ind/mL. First, we randomly collected 100 larvae from each pool as the Con group. Then, the juvenile oysters (*Crassostrea gigas*) were placed evenly in pools (50 oysters on each scallop, added about 25000 scallop shells to each pool), and 100 larvae were collected at 2 and 12 hours

thereafter from each pool as the oyster-exposed groups (M2 and M12, respectively). During the whole process of experiment and sampling, the three pools were closed with no water in or out, and maintain a stable experimental conditions (23 ± 1°C, 30‰ salinity, 7mg/L dissolved oxygen). A total of nine samples were obtained from the Con, M2 and M12 groups, which were washed with PBS and stored at -80°C for RNA extraction.

2.2 RNA extraction, library preparation and sequencing

Total RNA was extracted from the larval samples using TRIzol® Reagent (Invitrogen, USA) according the manufacturer's recommendations, and 1% agarose gels were used to monitor the degradation and contamination of RNA. The integrity and quantification of RNA samples were evaluated using a 2100 Bioanalyzer (Agilent Technologies, USA), and RNA samples with integrity numbers (RINs) > 8.0 were used for construction of an mRNA library. The library was prepared using a TruSeq™ RNA Sample Preparation Kit (Illumina, USA) and sequenced on an Illumina NovaSeq 6000 platform (*Majorbio*. Shanghai, China), and 125-bp paired-end reads were generated and deposited in the Sequence Read Archive (ncbi.nlm.nih.gov/sra) under BioProject PRJNA855327.

2.3 Read mapping and quantification of gene expression levels

The raw reads were trimmed and quality-controlled *via* SeqPrep and Sickle with default parameters, and the clean reads were separately aligned to the reference genome of *R. venosa* (unpublished data) with orientation mode using HISAT2 software (Kim et al., 2015). The mapped reads of each sample were assembled by StringTie *via* a reference-based approach (Pertea et al., 2015), and then the paired-end clean reads were aligned to the reference genome of R. venosa (unpublished data) using TopHat v2.0.12. HTSeq v0.6.1 was used to count the reads mapped to each gene. Known genes and novel transcripts were identified by Reference Annotation Based Transcript (RABT) assembly method, the Cufflinks v2.1.1. Subsequently, the TPM of each gene was calculated based on the length of the gene and the number of reads mapped to the gene.

2.4 Differential expression analysis and trend analysis of genes

DEG analysis was conducted among the three groups, and the TPM algorithm was used to normalize the expression level of each transcript. RSEM was used to quantify gene abundances. Briefly, DEG analysis was performed using the DESeq2 R package with the significance thresholds set to a P-adjusted value < 0.05 and a $|\log_2 FC| \geq 1$. Additionally, after filtering out the genes with TPM = 0 and normalizing the TPM by log2 transformation, the trend analysis of *R. venosa* transcriptome data was performed on the Majorbio Cloud Platform by Short Time-series Expression Miner (STEM) software.

2.5 Functional enrichment analysis

To further explore the biological functions of the DEGs and these genes with significant trends, GO and KEGG enrichment analyses were performed. GO enrichment analysis was implemented using the GOseq package in R, and KOBAS was used to analyze the statistical enrichment of genes in KEGG pathways. GO terms and KEGG pathways with the significance enrichment threshold set to a P-adjusted value < 0.05 corrected by the Bonferroni method.

2.6 Verification by quantitative real-time PCR (qRT–PCR)

To validate the accuracy of the RNA-Seq profiling results, critical genes were selected for qRT–PCR analysis. The cDNA for qRT–PCR was synthesized using the Prime Script™ RT Reagent Kit with gDNA Eraser (TaKaRa, Japan). The primers used in the mRNA qRT–PCR assay were designed using Primer 5, and 60S ribosomal protein L28 (RL28) was selected as a housekeeping gene to normalize the data (Song et al., 2017). A SYBR PrimeScript RT–PCR Kit II (TaKaRa, Japan) was used to quantify the expression levels. The relative expression levels of genes were estimated by the $2^{-\Delta\Delta CT}$ method. All data are presented as the means ± SEs (N = 3). Statistical significance was analyzed using SPSS v.19, with a P value < 0.05 considered to indicate significance.

3 Results

3.1 Overview of RNA-seq and quantitative RT-PCR validation

Nine libraries of *R. venosa* larvae were constructed from the Con group and oyster-exposed groups (M2 and M12), from which 63.84 Gb of clean reads were generated. Each cDNA library was greater than 6.09 Gb in size (Q30 > 93.36%), and the rate of successful mapping to the reference genome ranged from 75.32 to 76.71% (Table 1). A total of 37,493 genes were obtained, including 24,662 known genes and 12,831 novel genes. Gene function annotations showed that 19,629 genes (79.59% of known genes) had significant matches in the COG, GO, KEGG, KOG, Pfam, SwissProt, eggNOG, or NR databases (Table 2). Nine random genes were then chosen to verify the accuracy of the transcriptome sequence data by qRT-PCR. The results were shown in Figure 1. Altogether, the transcriptome data were consistent with the qRT-PCR results, which further reinforced our findings.

3.2 Sample clustering and heatmap analysis

Hierarchical clustering analysis (HCA) showed that the groups exposed to oysters for 12 hours (M12) were clustered as one branch,

TABLE 1 Statistics of RNA-sequencing.

Sample	Total reads	Total mapped	Multiple mapped	Uniquely mapped
Con_1	50320292	38417313 (76.35%)	1496708 (2.97%)	36920605 (73.37%)
Con_2	40928390	31300196 (76.48%)	1188816 (2.9%)	30111380 (73.57%)
Con_3	47522032	36256374 (76.29%)	1371018 (2.89%)	34885356 (73.41%)
M12_1	46871404	35711880 (76.19%)	1336336 (2.85%)	34375544 (73.34%)
M12_2	48148090	36898017 (76.63%)	1369664 (2.84%)	35528353 (73.79%)
M12_3	48464624	37176764 (76.71%)	1417883 (2.93%)	35758881 (73.78%)
M2_1	48812826	36767047 (75.32%)	1394099 (2.86%)	35372948 (72.47%)
M2_2	50221540	38236981 (76.14%)	1541732 (3.07%)	36695249 (73.07%)
M2_3	49247810	37291896 (75.72%)	1536689 (3.12%)	35755207 (72.6%)

TABLE 2 Statistics of gene annotation.

	Expre_Gene number (percent)	Expre_Transcript number (percent)	All_Gene number (percent)	All_Transcript number (percent)
GO	14733 (0.5974)	12972 (0.5836)	15783 (0.5323)	15783 (0.5323)
KEGG	12180 (0.4939)	10649 (0.4791)	13111 (0.4422)	13111 (0.4422)
COG	14773 (0.599)	12864 (0.5787)	15527 (0.5236)	15527 (0.5236)
NR	19007 (0.7707)	16817 (0.7565)	20483 (0.6908)	20483 (0.6908)
Swiss-Prot	14209 (0.5761)	12353 (0.5557)	14866 (0.5013)	14866 (0.5013)
Pfam	16111 (0.6533)	14134 (0.6358)	17310 (0.5838)	17310 (0.5838)
Total_anno	19629 (0.7959)	17416 (0.7835)	21341 (0.7197)	21341 (0.7197)
Total	24662 (1.0)	22229 (1.0)	29652 (1)	29652 (1)

while the group exposed to oysters for 2 hours (M2) was clustered with the Con group (Figure 2A). Additionally, principal component analysis (PCA) showed that all three groups were significantly separated from each other (Figure 2B). These results may mean that exposure to oysters has a significant effect on the mRNA profile of *R. venosa* larvae and that the effect increases with time.

3.3 Differential expression analysis and functional enrichment analysis

Differential expression analysis of genes among the three groups was also performed based on the TPM value. The DEGs in the Con vs. M2, Con vs. M12 and M2 vs. M12 comparisons were regarded as those induced by juvenile oysters but participating in different time periods of the induced-regulation process. In total, there were 189 DEGs in Con vs. M2, 597 DEGs in Con vs. M12 and 744 DEGs in M2 vs. M12 (Figure 3A). Additionally, a Venn diagram showed that 42 DEGs were shared between the Con vs. M2 and Con vs. M12 comparisons, 55 DEGs were shared between the Con vs. M2 and M2 vs. M12 comparisons, and 292 DEGs were shared between the Con vs. M12 and M2 vs. M12 comparisons (Figure 3B). In contrast, 92 DEGs were unique to Con vs. M2 comparisons, 263 DEGs were unique to Con vs. M12 comparisons, and 397 DEGs were unique to M2 vs. M12 comparisons.

The 189 DEGs in the Con vs. M2 comparison were regarded as the initial-response genes (I-DEGs) to oyster presence, which were significantly enriched with 2 GO terms: DNA-binding transcription factor activity and transcription regular activity (Figure 4A). There were no significantly enriched pathways (P adjust < 0.05). We further analyzed the expression of these genes enriched with the 2 GO terms. As shown in Figure 4B, 12 genes were upregulated in the M2 group compared with the Con group, including some nuclear receptor genes (nuclear receptor subfamily 1 and nuclear hormone receptor E75), CREBRF, the transcription factor Maf/MafK/AP-1, dendritic arbor reduction protein 1, cAMP-responsive element-binding protein, CCAAT/enhancer-binding protein beta and transforming protein v-Fos/v-Fox. Five other genes were downregulated in the M2 group, including the transcription factor MafAa, forkhead box protein B1, vitamin D3 receptor, deformed epidermal autoregulatory factor 1 and nuclear factor interleukin-3-regulated protein.

The 597 DEGs in Con vs. M12 were regarded as the final-response genes (F-DEGs) to oyster presence, which were significantly enriched in 3 pathways, including ribosome biogenesis in eukaryotes, antigen processing and presentation, and RNA transport (P adjusted < 0.05) (Figure 5A). There were 36 DEGs in the 3 pathways, and all of them were downregulated in the M12 group compared with the Con group, which suggested that these 3 pathways were suppressed in the presence of oysters or were inhibited by oyster exposure. There were 36 DEGs in the 3 pathways, including many heat shock

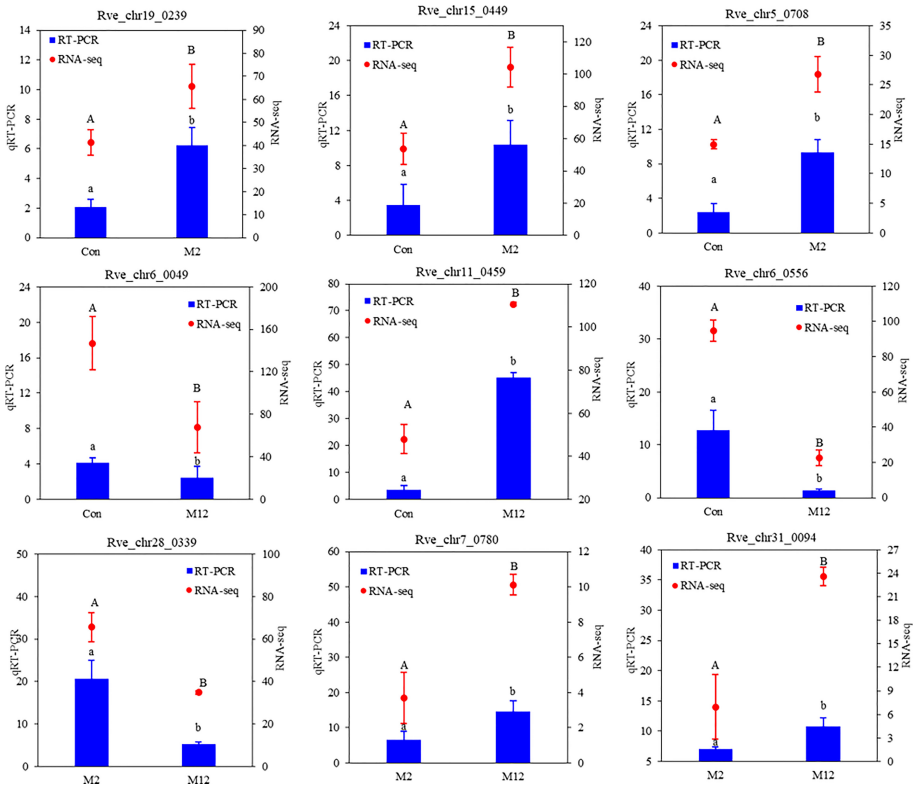

FIGURE 1
Validation of the 9 random DEGs involved in different pairwise comparisons by qRT-PCR. RL28 was selected to normalize the gene expression levels. The data are shown as means (± SE) of three replicates. Different superscripted letters indicate significant differences (P < 0.05).

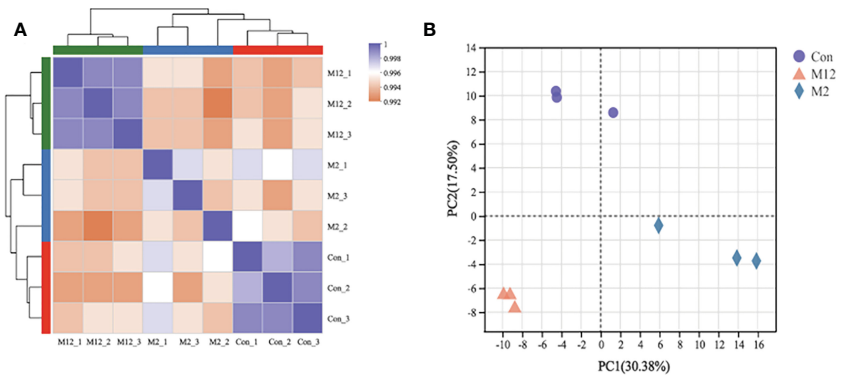

FIGURE 2
Relationships analysis between samples: Hierarchical clustering analysis **(A)** and principal component analysis **(B)**.

proteins (HSPs), such as HSP70 proteins (heat shock protein 68, heat shock 70 kDa protein A1, heat shock cognate 71 kDa protein and so on) and HSP90 proteins (97 kDa heat shock protein and heat shock protein HSP 90-beta) (Figure 5C). These DEGs were significantly enriched with 52 GO terms (top 20 were shown), and the small-subunit processome term was the most enriched (Figure 5B).

In addition to the initial-response and final-response genes that were altered in response to oysters, 397 DEGs existed only in the M2 vs. M12 comparison. These genes may respond to oyster presence slowly and ultimately not significantly change but still have an important regulatory effect; therefore, they should not be ignored. We regarded them as late-response genes (L-DEGs) to oyster exposure. The 397 DEGs were significantly enriched with 3 GO terms, including rRNA metabolic process, ncRNA metabolic process and rRNA processing. Furthermore, we analyzed the expression of 14 genes enriched with 3 GO terms (Figure 6A). All 14 genes were downregulated in the M12 group compared with the M2 group, which may mean that the metabolic processes related to rRNA and ncRNA were slowed down in the later stage in the presence of oysters (Figure 6B).

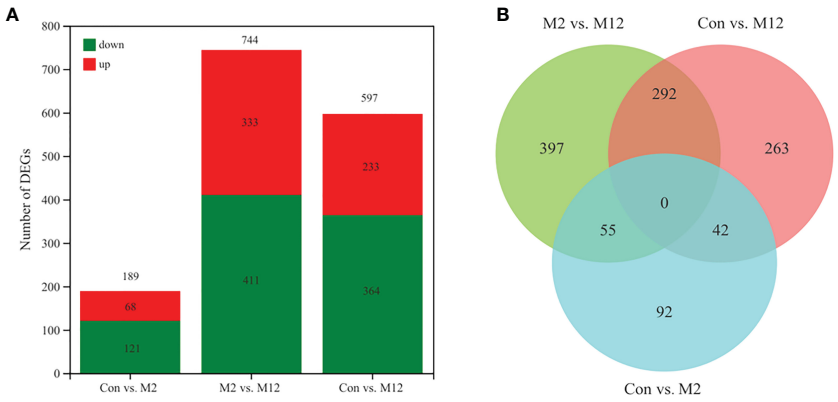

FIGURE 3
Statistics of differentially expressed genes **(A)** and Venn diagram of differentially expressed genes **(B)**.

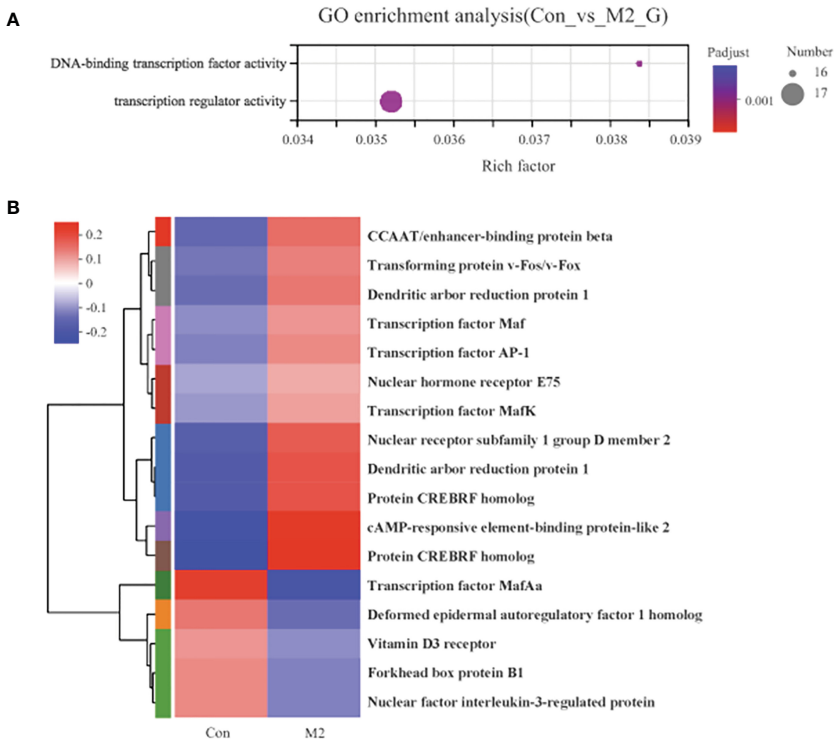

FIGURE 4
The functional enrichment and expression analysis of initial-response genes to oyster induction. **(A)** GO enrichment results of 92 DEGs in Con vs. M2 comparison. (P adjust < 0.05). **(B)** Heat map of the expression analysis of 17 DEGs in GO:0003700 (DNA-binding transcription factor activity) and GO:0140110 (transcription regulator activity).

3.4 Analysis of gene expression trends and functional enrichment analysis

A total of 22,662 genes were used to perform trend analysis, and 8 model profiles were used to summarize the expression patterns. The genes in the same profile presented similar expression patterns. As shown in Figure 7A, 3 profiles labeled with different colors were statistically significant, including profile 2 (3563 genes), profile 4 (1308 genes), and profile 1 (751 genes). These genes with different expression trends may have different functions in the metamorphosis induced by oysters. To further understand the functions of these genes in the 3 profiles, GO and KEGG enrichment analyses were performed. The top 20 significantly enriched GO terms and pathways are illustrated. For the genes in profile 2, 10 of the significantly enriched pathways were in the "human disease" category, 5 were in the "organismal systems" category, and only one was in the "cellular process" category. Four were in the "Environmental Information Processing" category, including the Ras signaling pathway (62 genes with adjusted $P < 0.05$), the Wnt signaling pathway (46 genes with adjusted $P < 0.05$), the MAPK signaling pathway (62 genes with

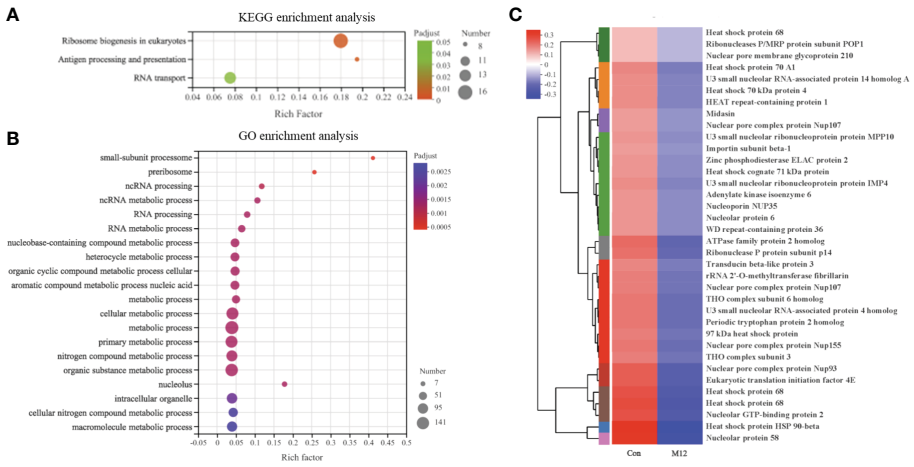

FIGURE 5
The functional enrichment and expression analysis of final-response genes to oyster induction. **(A)** KEGG enrichment results of 597 DEGs in Con vs. M12 comparison. (P adjust < 0.05). **(B)** GO enrichment results of 597 DEGs in Con vs. M12 comparison. (P adjust < 0.05). **(C)** Heat map of the expression analysis of 36 DEGs in the enriched pathways: "Ribosome biogenesis in eukaryotes", "Antigen processing and presentation" and "RNA transport".

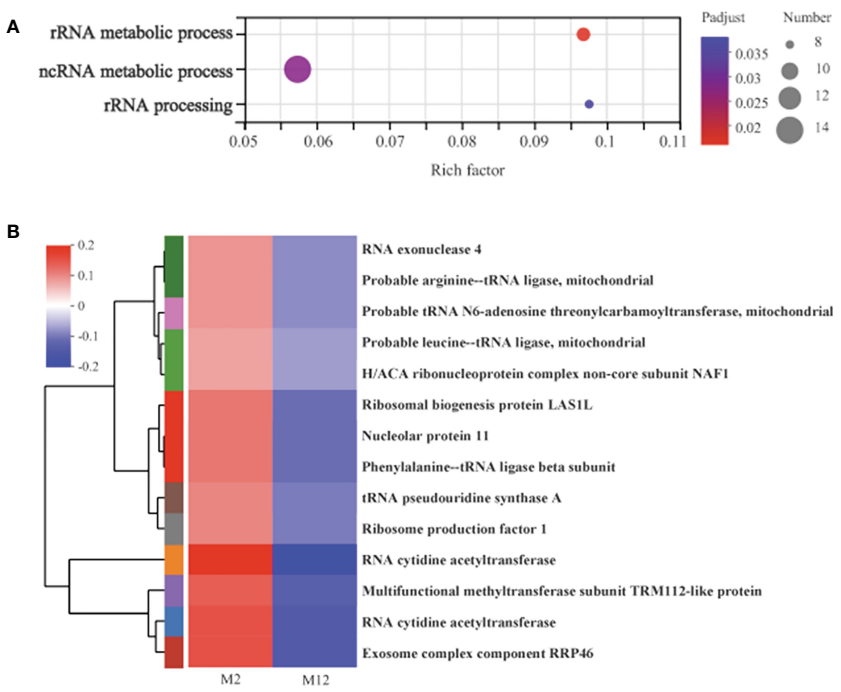

FIGURE 6
The functional enrichment and expression analysis of late-response genes to oyster induction. **(A)** GO enrichment results of 397 DEGs in M2 vs. M12 comparison. (P adjust < 0.05). **(B)** Heat map of the expression analysis of 14 DEGs in GO:0016072 (rRNA metabolic process) and GO:0034660 (ncRNA metabolic process), GO:0006364 (rRNA processing).

adjusted P < 0.05), and the Rap1 signaling pathway (64 genes with adjusted P < 0.05) (Figure 7B). In addition, the genes in profile 2 were significantly enriched in 10 GO terms belonging to the "biological process" category, 1 belonging to the "cellular component" category, and 9 belonging to the "molecular function" category, which also contained the Wnt signaling pathway (22 genes with adjusted P < 0.05) (Figure 7C). For the genes in profile 4, only one pathway, autophagy - animal (18 genes with adjusted P < 0.05), was significantly enriched, and no significantly enriched GO term was identified. For the genes in profile 1, there were also no significantly enriched GO terms or pathways. Furthermore, we analyzed the expression of the genes in the Wnt signaling pathway and animal autophagy.

4 Discussion

The food or prey of some animals not only provides them with the necessary nutrients for growth and development but also plays an important role in their development at a critical time. One of the most

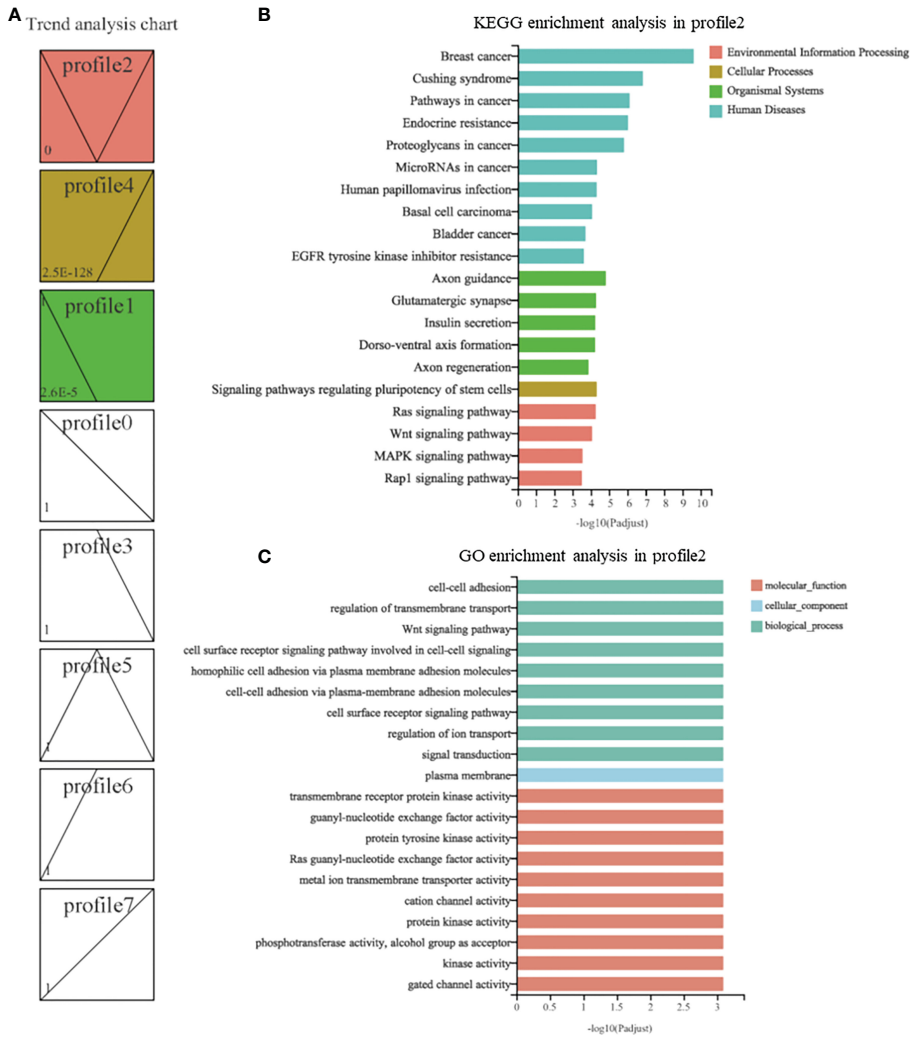

FIGURE 7
Trend analysis of genes in *R. venosa* transcriptome. **(A)** Different expression patterns of all genes. Each box represents a model profile. The upper number in the box represents the serial number of profiles and the lower one is the P value. Boxes with P values <0.05 are colored. GO **(B)** and KEGG **(C)** enrichment analysis of genes in profile 2.

dramatic examples is when the food or prey induces animal metamorphosis (Morse et al., 1979; Rodriguez et al., 1993; Taris et al., 2010). Although representative species from diverse taxa undergo food-induced metamorphosis, little is known about the processes that occur within the animals as they detect the cues produced by their food. To further understand the mechanism by which juvenile oysters induce the metamorphosis of *R. venosa* larvae, we performed RNA-seq and analyzed changes in gene expression at different time points upon exposure to metamorphosis cues, the juvenile oysters. Then, we conducted functional enrichment for these genes and identified the critical signaling pathways in the process. The present results may provide new insights into the regulatory mechanisms of metamorphosis in marine invertebrates.

In the present study, GO enrichment analysis revealed that 189 DEGs that responded early to the presence of juvenile oysters were significantly enriched with two GO terms: DNA-binding transcription factor activity and transcription regulator. These genes included some critical transcription factor genes, such as Maf, AP-1, MafK, MafAa, and transforming protein v-Fos/v-Fox, and most of the genes were upregulated. A previous study has also indicated that these genes are Jun or Fos genes (transcription factor AP-1 gene family), which are prototypical immediate early genes. Immediate early genes are characterized by a rapid and transient activation of transcription in response to changes of environmental conditions, such as growth factors, cytokines, tumor promoters, carcinogens, and expression of certain oncogenes (Angel and Hess, 2010). The transcription factor AP-1 gene family participates in many pathways, such as the MAPK signaling pathway, Wnt signaling pathway and apoptosis, which have been proven to be important in the metamorphoses of marine invertebrate animals (Angel and Hess, 2010). Therefore, we speculate that the transcription factor AP-1 may be a critical initiator in competent larvae of *R. venosa* in response to the metamorphosis cues of juvenile oysters that regulates other subsequent processes.

A previous study has indicated that the most critical members of the class of protein kinases regulating the activity of AP-1 in response to extracellular stimuli are MAPKs (Angel and Hess, 2010). In addition, researchers have shown that the MAPK signaling pathway

is induced by the metamorphosis cue in tubeworm *Hydroides elegans* and regulates the downstream process of metamorphosis (Shikuma et al., 2016; Wang and Qian, 2010), which also occurs in other marine invertebrate animals, such as corals, ascidians and barnacles (Chambon et al., 2007; He et al., 2012; Siboni et al., 2014). Interestingly, we also found that the MAPK signaling pathway was significantly enriched in the gene set of profile 2 in the trend analysis, which may mean that in competent larvae of *R. venosa*, MAPK signaling participates in the response to metamorphosis cues.

Chambon et al. (2007) found that the MAPK signaling pathway regulates gene networks that stimulate metamorphosis and apoptosis in tail tissues of ascidian tadpoles, and apoptosis occurs during metamorphosis in almost all invertebrates, including *R. venosa* (Song et al., 2016a). In the present study, we found that the expression of IAPs was significantly increased upon exposure to juvenile oysters. IAP expression is also upregulated after metamorphosis in juveniles of *R. venosa* (Shi, 2022). IAPs are important regulators that participate in the sophisticated molecular machineries in cells that guard against inappropriate or premature apoptosis to counter various stimuli capable of triggering death (Song et al., 2021). IAPs are also highly upregulated in response to various environmental stresses, including heat, air exposure, and low-salinity stress, in some marine invertebrate animals (Hu et al., 2022). The presence of oysters can also be considered an environmental factor for competent *R. venosa* larvae, and the upregulation of IAPs in the present results indicates that apoptosis is tightly regulated during the metamorphosis of *R. venosa*. The observed upregulation also suggests that apoptosis is induced by the presence of oysters during the metamorphosis of *R. venosa*. Furthermore, we found that the transcription factor AP-1 affected the expression of some proapoptotic genes, including p53, Fas, Fas-L, Bim and HRK, which supports the findings of a previous study showing that AP-1 target genes are involved in the regulation of apoptosis (Angel and Hess, 2010).

Past studies have revealed that, as a molecular chaperone of nitric oxide synthase (NOS), HSP90 is also a negative regulator (repressor) of metamorphosis in a diverse range of marine invertebrates (Bishop and Brandhorst, 2001; Bishop et al., 2001; Hens et al., 2006; Taris et al., 2009). However, Ueda and Degnan (2014) had a different discovery: that inhibition of NOS reduces rates of metamorphosis, which means that NO facilitates, rather than represses, induction of metamorphosis in *Haliotis asinina*. Additionally, Ueda and Degnan (2014) tested the hypothesis of NOS-HSP90 interaction at the initiation of settlement and metamorphosis because they found that the spatial and temporal expression trends of NOS and HSP90 were not consistent. In the present study, we found that HSP90 genes were significantly downregulated after exposure to oysters for 12 hours (Figure 4C), which might be considered to be a signal of metamorphosis induced by the oysters, but the specific function of HSP90 needs further investigation.

In addition to HSP90 genes, several HSP70 genes were also significantly downregulated in oysters (Figure 4C). Similar trends of downregulation were observed in a study on gene expression during the metamorphosis of *R. venosa* (Shi et al., 2022). HSP70 first received attention for its role in the response to heat shock (Welch, 1993) and has also been found to be critical for the folding and assembly of other cellular proteins (Ritossa, 1962). HSP70 genes also participate in the regulation of the MAPK signaling pathway (Patel, 2009), which has been widely reported to participate in the regulation of metamorphosis in several marine invertebrate animals mentioned above. Porto et al. (2018) reported that HSP70 can act as a signaling molecule, modulating MAPK downstream signaling during memory consolidation in the hippocampus. Patel (2009) also indicated that HSP70 plays a role in the induction of p38MAPK in animals to respond differently to high osmotic stress. Therefore, we speculate that HSP70 may also participate in the MAPK signaling pathway and be related to the metamorphosis of *R. venosa*; however, the specific effect of HSP70 on metamorphosis needs further investigation, especially since no previous studies have reported the relationship between HSP70 and metamorphosis in marine invertebrates.

The Wnt signaling pathway, which has been widely studied, regulates cell proliferation, migration, differentiation and survival during animal development as well as the maintenance of homeostasis and regeneration (Liu et al., 2008; De Robertis, 2010; Clevers and Nusse, 2012). In the trend analysis, we found that the Wnt signaling pathway was significantly enriched in profile 2, a gene set that was decreased at the early stage during exposure to juvenile oysters. This finding may suggest that the Wnt signaling pathway participates in the metamorphosis of *R. venosa*. Chandramouli et al. (2013) also found Wnt signaling pathway enrichment during the larval metamorphosis of the polychaete worm *Pseudopolydora vexillosa* in transcriptome studies. Furthermore, Yue et al. (2012) have reported that Wnt signaling pathways may be involved in the metamorphosis of the bryozoan *Bugula neritina*. However, the specific function of the Wnt signaling pathway in the metamorphosis of marine invertebrates needs further investigation.

5 Conclusion

In this study, the gene set responses to metamorphosis cues (juvenile oysters) in *R. venosa* (I-DEGs and F-DEGs) were identified, and GO and KEGG enrichment analyses were further performed on these gene sets. We found that DNA-binding transcription factor activity and transcription regulator activity were enriched for the I-DEGs, such as the transcription factor AP-1, which is a prototypical immediate early gene that rapidly and transiently activates transcription in response to changes in environmental conditions. The molecular chaperone of NOS, HSP90, exhibited lower expression in the M12 group than in the Con group, while the expression of IAPs was significantly increased upon exposure to juvenile oysters. Additionally, the Wnt signaling pathway and MAPK signaling pathway were enriched in the trend analysis. These pathways may also play critical regulatory roles in the response to juvenile oysters. Taken together, the results show that competent larvae rapidly respond to the presence of oysters by expressing some immediate early genes, such as the transcription factor AP-1. These genes may further regulate downstream pathways such as the MAPK signaling pathway and result in subsequent changes, including a decrease in HSP90 and an increase in IAPs. These changes together may regulate the metamorphosis of the larvae.

Data availability statement

The datasets presented in this study can be found in online repositories. The names of the repository/repositories and accession number(s) can be found in the article/Supplementary Material.

Ethics statement

The studies involving animals were reviewed and approved by the Animal Welfare Committee of the Institute of Oceanology, Chinese Academy of Sciences.

Author contributions

TZ and HS conceived and designed the experiments. M-JY and HS conducted the experiments. M-JY analyzed the data. YS, Z-SL, PS, ZH, CZ, P-PH and Z-LY contributed reagents, materials, and analytical tools. M-JY wrote the manuscript. All authors contributed to the article and approved the submitted version.

Funding

This research was supported by the National Natural Science Foundation of China (Grant No. 42206086 & 31972814 & 32002409 & 32002374), the China Postdoctoral Science Foundation (Grant No. 2021M703248), the China Agriculture Research System of MOF and MARA, the Young Elite Scientists Sponsorship Program by CAST (Grant No. 2021QNRC001), the 'Double Hundred' Blue Industry Leader Team of Yantai (Recipient: Tao Zhang), and the Creative Team Project of the Laboratory for Marine Ecology and Environmental Science, Qingdao National for Marine Science and Technology (no. LMEESCTSP-2018). The funders had no role in the study design, data collection and analysis, decision to publish or preparation of the manuscript.

Conflict of interest

The authors declare that the research was conducted in the absence of any commercial or financial relationships that could be construed as a potential conflict of interest.

Publisher's note

Supplementary material

The Supplementary Material for this article can be found online at: https://www.frontiersin.org/articles/10.3389/fmars.2023.1122668/full#supplementary-material

References

Angel, P., and Hess, J. (2010). The multi-gene family of transcription factor AP-1. *Handb. Cell Signaling (Second Edition)* 152 (1), 2059–2068. doi: 10.1016/B978-0-12-374145-5.00251-5

Bishop, C. D., Bates, W. R., and Brandhorst, B. P. (2001). A. regulation of metamorphosis in ascidians involves NO/cGMP signaling and HSP90. *J. Exp. Zool.* 289 (6), 374–384. doi: 10.1002/jez.1019

Bishop, C. D., and Brandhorst, B. P. (2001b). NO/cGMP signaling and HSP90 activity represses metamorphosis in the sea urchin lytechinus pictus. *Biol. Bull.* 201 (3), 394–404. doi: 10.2307/1543617

Cavalcanti, G. S., Alker, A. T., Delherbe, N., Malter, K. E., and Shikuma, N. J. (2020). The influence of bacteria on animal metamorphosis. *Annu. Rev. Microbiol.* 74, 137–158. doi: 10.1146/annurev-micro-011320-012753

Chambon, J. P., Nakayama, A., Takamura, K., McDougall, A., and Satoh, N. (2007). ERK- and JNK signalling regulate gene networks that stimulate metamorphosis and apoptosis in tail tissues of ascidian tadpoles. *Development* 134 (6), 1203–1219. doi: 10.1242/dev.002220

Chandramouli, K. H., Sun, J., Mok., F. S. Y., Liu, L. L., Qiu, J. W., Ravasi, T., et al. (2013). Transcriptome and quantitative proteome analysis reveals molecular processes associated with larval metamorphosis in the polychaete pseudopolydora vexillosa. *J. Proteome Res.* 12 (3), 1344–1358. doi: 10.1021/pr3010088

Clevers, H., and Nusse, R. (2012). Wnt/β-catenin signaling and disease. *Cell* 149, 1192–1205. doi: 10.1016/j.cell.2012.05.012

De Robertis, E. M. (2010). Wnt signaling in axial patterning and regeneration: lessons from planaria. *Sci. Signal.* 3 (127), pe21. doi: 10.1126/scisignal.3127pe21

He, L. S., Xu, Y., Matsumura, K., Zhang, Y., Zhang, G., Qi, S. H., et al. (2012). Evidence for the involvement of p38 MAPK activation in barnacle larval settlement. *PloS One* 7 (10), e47195. doi: 10.1371/journal.pone.0047195

He, J., Wu, Z. W., Chen, L. Y., Dai, Q., Hao, H. H., Su, P., et al. (2021). Adenosine triggers larval settlement and metamorphosis in the mussel *Mytilopsis sallei* through the ADK-AMPK-FoxO pathway. *ACS Chem. Biol.* 16 (8), 1390–1400. doi: 10.1021/acschembio.1c00175

Hens, M. D., Fowler, K. A., and Leise, E. M. (2006). Induction of metamorphosis decreases nitric oxide synthase gene expression in larvae of the marine mollusc *Ilyanassa obsoleta* (Say). *Biol. Bull.* 211, 208–211. doi: 10.2307/4134543

Hu, Z., Feng, J., Song, H., Zhou, C., Yu, Z. L., Yang, M. J., et al (2022). Mechanisms of heat and hypoxia defense in hard clam: Insights from transcriptome analysis. *Aquaculture* 549, 737792.

Kim, D., Langmead, B., and Salzberg, S. L. (2015). HISAT: a fast spliced aligner with low memory requirements. *Nat. Meth.* 12, 357–360. doi: 10.1038/nmeth.3317

Liu, Y., Wang, X., Lu, C. C., Kerman, R., Steward, O., Xu, X. M., et al. (2008). Repulsive wnt signaling inhibits axon regeneration after CNS injury. *J. Neurosci.* 28 (33), 8376–8382. doi: 10.1523/JNEUROSCI.1939-08.2008

Matsumura, K., Nagano, M., and Fusetani, N. (1998). Purification of a larval settlement-inducing protein complex (SIPC) of the barnacle, *Balanus amphitrite*. *J. Exp. Zool.* 281, 12–20. doi: 10.1002/(SICI)1097-010X(19980501)281:1<12::AID-JEZ3>3.0.CO;2-F

Morse, D. E., Hooker, N., Duncan, H., and Jensen, J. (1979). γ-aminobutyric acid, a neurotransmitter, induces planktonic abalone larvae to settle and begin metamorphosis. *Science* 204, 407–410. doi: 10.1126/science.204.4391.407

Patel, P. L. (2009). *Role of p38MAPK, heat shock proteins, HSP27 and HSP70 in osmotic stress in renal vs. blood cells: A comparative study* (University of the Sciences in Philadelphia).

Pertea, M., Pertea, G. M., Antonescu, C. M., Chang, T. C., Mendell, J. T., Salzberg, S. L., et al. (2015). StringTie enables improved reconstruction of a transcriptome from RNA-seq reads. *Nat. Biotechnol.* 33, 290–295. doi: 10.1038/nbt.3122

Porto, R. R., Dutra, F. D., Crestani, A. P., Holsinger, R. M. D., Quillfeldt, J. A., Bittencourt, P. D., et al. (2018). HSP70 facilitates memory consolidation of fear conditioning through mapk pathway in the hippocampus. *Neuroscience* 375, 108–118. doi: 10.1016/j.neuroscience.2018.01.028

Ritossa, F. (1962). A new puffing pattern induced by temperature shock and DNP in drosophila. *Experientia* 18 (12), 571–573. doi: 10.1007/BF02172188

Rodriguez, S. R., Ojeda, F. P., and Inestrosa, N. C. (1993). Settlement of benthic marine invertebrates. *Mar. Ecol. Prog. Ser.* 97, 193–207. doi: 10.3354/meps097193

Shi, P. (2022). Effects of autophagy and apoptosis on the regulation of metamorphosis and seedling of *Rapana venosa*. *Institute Oceanol. Chin. Acad. Sci*. doi: 10.1111/1749-4877.12675

Shi, P., Song, H., Jie, F., Yang, M. J., Yu, Z. L., Hu, Z., et al. (2022). Molecular response and developmental speculations in metamorphosis of the veined rapa whelk, *Rapana venosa* (Valenciennes 1846). *Integr. Zool.* doi: 10.1111/1749-4877.12675

Shikuma, N. J., Antoshechkin, I., Medeiros, J. M., Pilhofer, M., and Newman, D. K. (2016). Stepwise metamorphosis of the tubeworm hydroides elegans is mediated by a bacterial inducer and MAPK signaling. *PNAS* 113 (36), 10097–10102. doi: 10.1073/pnas.1603142113

Siboni, N., Abrego, D., Motti, C. A., Tebben, J., and Harder, T. (2014). Gene expression patterns during the early stages of chemically induced larval metamorphosis and settlement of the coral *Acropora millepora*. *PloS One* 9 (3), e91082. doi: 10.1371/journal.pone.0091082

Song, H., Dang, X., He, Y. Q., Zhang, T., and Wang, H. Y. (2017). Selection of housekeeping genes as internal controls for quantitative rt-pcr analysis of the veined rapa whelk (*rapana venosa*). *PeerJ* 5 (7), e3398. doi: 10.7717/peerj.3398

Song, H., Hewitt, O. H., and Degnan, S. M. (2021). Arginine biosynthesis by a bacterial symbiont enables nitric oxide production and facilitates larval settlement in the marine-sponge host. *Curr. Biol.* 31, 1–5. doi: 10.1016/j.cub.2020.10.051

Song, H., Wang, H. Y., and Zhang, T. (2016b). Comprehensive and quantitative proteomic analysis of metamorphosis-related proteins in the veined rapa whelk, *rapana venosa*. *Int. J. Mol. Sci.* 17, 924. doi: 10.3390/ijms17060924

Song, H., Yu, Z. L., Sun, L. N., Xue, D. X., Zhang, T., Wang, H. Y., et al. (2016c). Transcriptomic analysis of differentially expressed genes during larval development of *rapana venosa* by digital gene expression profiling. *G3-Gene. Genom. Genet.* 6, 2181–2193. doi: 10.1534/g3.116.029314

Song, H., Zhang, T., and Hadfield, M. G. (2021). Metamorphosis in warming oceans: a microbe-larva perspective. *Trends Ecol. Evol.* 36, 976–977. doi: 10.1016/j.tree.2021.07.010

Song, H., Zhang, T., Yu, Z. L., Sun, L. N., Xue, D. X., Zhang, T., et al. (2016a). Metabolomic analysis of competent larvae and juvenile veined rapa whelks (*rapana venosa*). *Mar. Biol.* 163, 145. doi: 10.1007/s00227-016-2919-6

Taris, N., Comtet, T., Stolba, R., Lasbleiz, R., Pechenik, J. A., Viard, F., et al. (2010). Experimental induction of larval metamorphosis by a naturally-produced halogenated compound (dibromomethane) in the invasive mollusc *Crepidula fornicata* (L.). *J. Exp. Mar. Biol. Ecol.* 393, 71–77. doi: 10.1016/j.jembe.2010.07.001

Taris, N., Comtet, T., and Viard, F. (2009). Inhibitory function of nitric oxide on the onset of metamorphosis in competent larvae of *Crepidula fornicata*: a transcriptional perspective. *Mar. Genom.* 2, 161–167. doi: 10.1016/j.margen.2009.08.002

Ueda, N., and Degnan, S. M. (2014). Nitric oxide is not a negative regulator of metamorphic induction in the abalone haliotis asinine. *Front. Mar. Sci.* 1, 21. doi: 10.3389/fmars.2014.00021

Wang, H., and Qian, P. Y. (2010). Involvement of a novel p38 mitogen-activated protein kinase in larval metamorphosis of the polychaete *Hydroides elegans* (Haswell). *J. Exp. Zool. Part B.* 314 (5), 390–402. doi: 10.1002/jez.b.21344

Welch, W. J. (1993). How cells respond to stress. *Sci. Am.* 268 (5), 56–56. doi: 10.1038/scientificamerican0593-56

Xu, M., Qi, L., Zhang, L. B., Zhang, T, Yang, H. S., and Zhang, Y. L. (2019). Ecosystem attributes of trophic models before and after construction of artificial oyster reefs using ecopath. *Aquacult. Env. Interac.* 11, 111–127. doi: 10.3354/aei00284

Xue, D. X., Graves, J., Carranza, A., Sylantyev, S., Snigirov, S., Zhang, T., et al. (2018). Successful worldwide invasion of the veined rapa whelk, *Rapana venosa*, despite a dramatic genetic bottleneck. *Biol. Invasions* 20, 3297–3314. doi: 10.1007/s10530-018-1774-4

Yang, M. J., Song, H., Feng, J., Yu, Z. L., Shi, P., Liang, J., et al. (2022). Symbiotic microbiome and metabolism profiles reveal the effects of induction by oysters on the metamorphosis of the carnivorous gastropod *Rapana venosa*. *Comput. Struct. Biotec.* 20, 1–14. doi: 10.1016/j.csbj.2021.11.041

Yang, M. J., Song, H., Yu, Z. L., Bai, Y. C., Hu, Z., Hu, N., et al. (2020a). Expression and activity of critical digestive enzymes during early larval development of the veined rapa whelk, *Rapana venosa* (Valenciennes 1846). *Aquaculture* 519, 734722. doi: 10.1016/j.aquaculture.2019.734722

Yang, M. J., Song, H., Yu, Z. L., Hu, Z., Zhou, C., Wang, X. L., et al. (2020b). Changes in symbiotic microbiota and immune responses in early development stages of *Rapana venosa* (Valenciennes 1846) provide insights into immune system development in gastropods. *Front. Microbiol.* 11, 1265. doi: 10.3389/fmicb.2020.01265

Yu, Z. L. (2019). A study on the behavior of the early developmental stage of Rapana venosa. *Doctoral dissertation* Institute of Oceanology, Chinese Academy of Science.

Yu, Z. L., Yang, M. J., Song, H., Hu, Z., Zhou, C., Wang, X. L., et al. (2020). Settlement and metamorphosis of *Rapana venosa* (Gastropoda: Muricidae) with implications for artificial culture. *J. Oceanol. Limnol.* 38, 249–259. doi: 10.1007/s00343-019-9107-8

Yue, H. W., Wang, H., Ravasi, T., and Qian, P. Y. (2012). Involvement of wnt signaling pathways in the metamorphosis of the bryozoan *Bugula neritina*. *PLoS One* 7 (3), e33323. doi: 10.1371/journal.pone.0033323

Zhang, T., Song, H., Bai, Y. C., Sun, J. C., Zhang, X. F., Ban, S. J., et al. (2017). Effects of temperature, salinity, diet and stocking density on development of the veined rapa whelk, *Rapana venosa* (Valenciennes 1846) larvae. *Aquacult. Int.* 25, 1577–1590. doi: 10.1007/s10499-017-0140-3

Zhang, Z., Zhang, H., Yu, D., Song, J., and Wang, M. (2020).). influence of spatial heterogeneity of artificial reefs on food sources and trophic levels of marine animals based on stable isotope ratios. *Ecol. Indic.* 118, 106779. doi: 10.1016/j.ecolind.2020.106779

frontiers | Frontiers in Marine Science

TYPE Original Research
PUBLISHED 17 February 2023
DOI 10.3389/fmars.2023.1120015

OPEN ACCESS

EDITED BY
Yafei Duan,
South China Sea Fisheries Research Institute, China

REVIEWED BY
Yongbo Bao,
Zhejiang Wanli University, China
Yuehuan Zhang,
South China Sea Institute of Oceanology (CAS), China
Zhiyi Bai,
Shanghai Ocean University, China

*CORRESPONDENCE
Zhiguo Dong
dzg7712@163.com

SPECIALTY SECTION
This article was submitted to Marine Biology, a section of the journal Frontiers in Marine Science

RECEIVED 09 December 2022
ACCEPTED 06 February 2023
PUBLISHED 17 February 2023

CITATION
Yan S, Xu M, Xie J, Liao X, Liu M, Wang S, Fan S and Dong Z (2023) Characterization, expression profiling, and estradiol response analysis of *DMRT3* and *FOXL2* in clam *Cyclina sinensis*.
Front. Mar. Sci. 10:1120015.
doi: 10.3389/fmars.2023.1120015

Characterization, expression profiling, and estradiol response analysis of *DMRT3* and *FOXL2* in clam *Cyclina sinensis*

Susu Yan[1,2], Mengge Xu[1,2], Jing Xie[1,2], Xiaoting Liao[1,2], Meimei Liu[1,2], Siting Wang[1,2], Sishao Fan[1,2] and Zhiguo Dong[1,2,3]*

[1]Jiangsu Key Laboratory of Marine Bioresources and Environment, Jiangsu Ocean University, Lianyungang, China, [2]Co-Innovation Center of Jiangsu Marine Bio-industry Technology, Jiangsu Institute of Marine Resources Development, Lianyungang, China, [3]Jiangsu Institute of Marine Resources Development, Lianyungang, China

The clam *Cyclina sinensis* is one of the important economical aquaculture shellfish in China. However, the mechanisms of sex determination and differentiation in *C. sinensis* have not been fully studied. In this study, full-length cDNAs of *DMRT3* and *FOXL2* were cloned and functionally characterized. The ORF region of *CsDMRT3* consists of 1137 nucleotides, which encode 378 amino acids contains a conserved DM domain of *DMRT* family. The ORF region of *CsFOXL2* is 1245 bp, encodes 414 amino acids, and contains a conserved FH domain. Tissue-specific expression results showed that the higher expression level of *CsDMRT3* and *CsFOXL2* was found in the ovary and testis of *C. sinensis*. The expression levels of *CsDMRT3* and *CsFOXL2* also peaked at the maturation stage of male and female gonadal development, respectively. Moreover, the expression levels of *CsDMRT3* and *CsFOXL2* were significantly higher in the trochophore and D-larval stages than in other stages. The transcript levels of *CsDMRT3* reached the highest level at 11 months of age, while the *CsFOXL2* reached the highest level at 7 months of age. In estradiol-treated experiments, the expression levels of *CsDMRT3* and *CsFOXL2* in the gonads were highest at 5 μg/L estradiol treatment, and histologically, it was observed that the oocytes diameters became larger with increasing estradiol concentration. These results suggest that *CsDMRT3* and *CsFOXL2* play an important role in gonadal development and sex differentiation of *C. sinensis*.

KEYWORDS

***Cyclina sinensis*, *DMRT3*, *FOXL2*, expression analysis, estradiol response**

1 Introduction

Sex differences are essential characteristics of sexually reproducing organisms. In aquatic animals, species of both sexes grow at different rates (Liao, 2022). Therefore, understanding the sex development of aquatic animals is important. Key sex-related genes have been identified in bivalves, including *FOXL2*, *DMRT* family, *WNT4*, *FST*, *β-CATENIN*, and *SOXE*, which are involved in the development, gonad maintenance and germ cell formation of individual organisms (Christelle et al., 2014; Shi et al., 2014; Tong et al., 2015).

The *DMRT* (double-sex and mab-3-related transcription factor) gene family was first detected from fruit fly *Drosophila melanogaster*, where all genes in the family are transcription factors. The *DMRT* family is involved in the sex determination and differentiation of organisms, as well as in embryonic development and organ formation (Hildreth, 1965). Shinseog et al. (2003) found that *DMRT3*, *DMRT5*, and *DMRT7* exhibit sex specificity, suggesting their involvement in the gonadal development of mouse *Mus culus*. *DMRT3* transcripts in Japanese pufferfish *Takifugu rubripes* begin to express at the larval stage and are highly expressed in adult testes (Akihiko et al., 2006). Similar results were found in experiments with Atlantic cod (Hanne and Øivind, 2012).

FOXL2, forkhead transcription factor gene 2, is a member of the forkhead (FOX) family. The *FOXL2* coding region is highly conserved in *Homo*, *Capra hircus*, and *M. culus*. (Cocquet et al., 2002). *FOXL2* represses the male gene pathway during female gonadal differentiation and regulates and maintains ovarian development in mice (Loffler et al., 2003; Chris et al., 2005). Previous experiments have shown that *FOXL2* is expressed very differently in the testis and ovary of chicken *Gallus gallus domesticus*, and its testis expression is much lower than the ovary expression (Govoroun et al., 2004). Similar results were found during gonadal differentiation in frog *Rana rugosa* (Yuki et al., 2008). In invertebrates, *FOXL2* is involved in regulating embryonic development in sea urchin *Strongylocentrotus purpuratus* (Tu et al., 2006). Liu et al. (2013) found that *FOXL2* was expressed at a higher level in the D-larval stage of Zhikong scallop *Chlamys farreri*. The expression level of *FOXL2* in the freshwater mussel *Hyriopsis cumingii* gonad gradually decreases with age (Wang et al., 2020).

Estradiol (E2) is a sex steroid hormone produced by cholesterol metabolism and plays an important role in gonadal development and sex differentiation in animals. Specifically, Ni et al. (2012) found that the injection of estradiol into oysters induces sex reversal from male to female. Yan et al. (2011) treated razor clam *Sinonovacula constricta* with estradiol, causing an increase in oocyte diameter, suggesting that estradiol plays an endogenous regulatory role in the gonadal development of razor clam. Estradiol affects on the expression levels of sex-related genes. Estradiol exposure decreases the expression levels of *DMRT1* and *SOX9*, which are male key factors in *Pelodiscus sinensis* (Wang et al., 2014). The expression level of *FOXL2* was elevated in the ovaries of sea urchins *Mseocentrotus nudus* after estradiol exposure (Hu et al., 2021). The same result was also found in blue tilapia *Oreochromis aureus* (Cao et al., 2010).

To date, studies on genes related to sexual differentiation and the mechanisms of sexual differentiation among mollusks have mainly focused on oyster *C. gigas*, scallop *C. farreri*, and freshwater mussel *H. cumingii* (Liu, 2012; Tian et al., 2012; Christelle et al., 2014). However, detailed findings on the sex determination and differentiation of *C. sinensis* have not been reported. Understanding the sex determination and differentiation of *C. sinensis* is important for the reproduction and breeding of clams (Wei et al., 2020; Dong et al., 2021; Liao et al., 2022). In the present study, the full-length cDNAs of *DMRT3* and *FOXL2* were cloned first. The changes in the expression patterns of *DMRT3* and *FOXL2* were analyzed in different tissues, gonadal development stages, larval developmental stages, and different month-old clams. Finally, the expression levels of *DMRT3* and *FOXL2* of *C. sinensis* in response to estradiol exposure were investigated. This study will provide a reference for subsequent studies on gonad development and sex differentiation of *C. sinensis*.

2 Materials and methods

2.1 Ethics statement

All animal experiments were conducted in accordance with the guidelines and approval of the Animal Experiment Ethics Committee at Jiangsu Ocean University.

2.2 Animals and sampling

All clams of this study were obtained from Lianyungang Comprehensive Experimental Station, the national shellfish industry system of China. The clams were acclimated in a seawater tank (salinity: 25‰) for a week before experimental processing. During the acclimatization, the clams were fed with microalgae *Chaeroeeros moelleri* twice in the 8:30am and 18:00pm. The microalgae *Chaeroeeros moelleri* was purchased from Wudi Zaocheng Biotechnology company (Shandong, China).

Past studies have shown that the gonadal development of *C. sinensis* can be divided into five stages: proliferation stage, growing stage, maturation stage, spawning stage, and spent stage (Racotta et al., 2003; Liao, 2022). Based on above gonadal staging system, eight male and eight female clams in the growing stage were selected and adductor, mantle, pipe, gill, foot, hepatopancreas and gonad were collected. Ovarian and testis samples were also collected from *C. sinensis* with different gonadal development stages, respectively. During the larval development of *C. sinensis*, the fertilized egg, trochophore, D-larvae, and umbo larvae were sampled in a 1.5 mL DNase/RNase-free centrifuge tube. In addition, the gonads of juvenile clams aged 3–12 months were also collected every month from October 2020 to September 2021. All tissues were immediately frozen in liquid nitrogen and stored at −80°C for RNA extraction.

2.3 RNA isolation, cDNA synthesis, and RACE PCR

Total RNA from the clam tissues was isolated using TRIzol reagent (TaKaRa, Japan), following the manufacturer's instruction, and then stored at −80°C. PrimeScript RT reagent kit with gDNA Eraser (TaKaRa, Tokyo, Japan) was used for first-strand cDNA synthesis. Ready-cDNA, which was used as the template for RACE PCR, was synthesized using the SMART™ RACE cDNA Amplification Kit (Clontech, USA) in accordance with the manufacturer's instructions.

The program of touchdown PCR was conducted in the 5′- and 3′-RACE PCR amplification as follows: 5 cycles of 95°C for 30 s, 72°C for 30 s, 72°C for 2 min; 5 cycles of 95°C for 30 s, 70°C for 30 s, 72°C for 2 min; 5 cycles of 95°C for 30 s, 68°C for 30 s, 72°C for 2 min; and 20 cycles of 95°C for 30 s, 66°C for 30 s, 72°C for 2 min, and then 72°C for 7 min for elongation. The PCR products were purified using a DNA Purification Kit (CWBiotech, Beijing, China), and the purified products were subcloned into a pEASY-T1 vector (Transgen, China) and sequenced by Ruibiotech Company (Beijing, China). The sequences of all the primers used are displayed in Table 1.

2.4 Sequence and phylogenetic analysis

All the sequence data were analyzed using DNAStar 11.1. The open reading frame (ORF) of genes was predicted by the ORF finder. The conserved domains and genomic structures were analyzed using the online software Simple Modular Architecture Research Tool (SMART) (http://smart.embl.de/) and Splign (https://www.ncbi.nlm.nih.gov/sutils/splign/splign.cgi), respectively. Phylogenetic trees were constructed using MEGA 5.0 with the Neighbor-joining (NJ) method. Amino acid sequences from other species were downloaded from the GenBank database.

2.5 Quantitative real-time PCR

Primer Premier 5.0 was used to design specific primers for qPCR (Table 1). The qPCR was then conducted using the SYBR Premix Ex Taq™ kit (Takara, Japan) on a StepOnePlus Real-Time PCR system (Applied Biosystems) according to the instructions. *β-actin* was selected as the reference gene in the qPCR reaction system. The $2^{-\Delta\Delta CT}$ method was used for the analysis of the relative gene expression.

2.6 Estradiol exposure

Estradiol regent was obtained from Sigma (St. Louis, MO, USA). The stock solution (4 mg/mL) of estradiol was prepared in ethanol. Two-year-old *C. sinensis* samples in the growing stage were selected for the experiment. The average length and body weight of the clams were in the range of 3.2–3.4 cm and 13–15 g, respectively. First, 180 healthy clams were randomly divided into three groups of 60 with three duplicates in each group. Clams were exposed to estradiol (E2: control group, 5 μg/L, and 50 μg/L; Wu, 2019). The same feeding regime was kept during the exposure. Uneaten food and feces were removed before water renewal. The water was changed daily, and fresh hormones were

TABLE 1 Primers used in this study.

Primer	Sequence (5′–3′)	Purpose
DMRT3-5GSP	GCGTCGGAATACGTCTGTGTCCATCT	RACE
DMRT3-5NGSP	TTCTGTCGCCTGCTGTCTTTTC	RACE
DMRT3-3GSP	AATCGGCGTTCAAGCCATTACCAA	RACE
DMRT3-3NGSP	CAATCTTGGACTTCCGTTTCCGCAT	RACE
FOXL2-5GSP	TTTCCTTGTCGGCAACAGAGCG	RACE
FOXL2-NGSP	ACGGTGACAGGATTGGATTTAGG	RACE
Upm-long	CTAATACGACTCACTATAGGGCAAGCAGTGGTATCAACGCAGAGT	RACE
Upm-short	CTAATACGACTCACTATAGGGC	RACE
NUP	AAGCAGTGGT AACAACGCAGAGT	RACE
DMRT3-F	CTGAAAAGACAGCAGGCGACA	qPCR
DMRT3-R	GCTTGACTTGCGGGTATCGA	qPCR
FOXL2- F	ACTTGCTTCCTGTGGATACGG	qPCR
FOXL2- R	TAAATGGCTCGCTCTGTTGC	qPCR
β-actin-F	CCTGGTATTGCCGACCGTAT	qPCR
β-actin-R	TTGGAAGGTGGACAGTGAAGC	qPCR

10.3389/fmars.2023.1120015

added. After 21 days of exposure, the gonad tissues of the clam were frozen in liquid nitrogen and stored at −80°C for RNA extraction. The remaining ovaries were fixed in 4% paraformaldehyde (PFA) overnight. Then, paraffin-embedded ovary samples were sliced on a microtome, and hematoxylin-eosin staining was carried out. Finally, ovary sections of 12 clams were observed under a Nikon 90i microscope, and the oocyte diameter was recorded.

2.7 Statistical analyses

All experimental data are expressed as mean ± SD and were analyzed using SPASS 23.0. The homogeneity of variance for all data was tested using Levene's method. When the homogeneity variance was unsatisfactory, the percentage data were processed by taking the arcsine or square root. Statistical analysis was conducted using one-way analysis of variance (ANOVA) with Duncan's test on the gene expression levels, and statistical significance was defined at P value <0.05.

3 Results

3.1 Sequence analysis of *DMRT3* and *FOXL2* in *C. sinensis*

In the study, the cDNA sequences of *CsDMRT3* (GenBank accession No: OP970557) and *CsFOXL2* (GenBank accession No: OP970558) were obtained by partial cDNA cloning and RACE technique. The ORF region of *CsDMRT3* was 1137 bp, which encoded 378 amino acids containing the DM domain (16–69 aa) and DMA domain (189–228 aa; Figure 1A). The ORF sequence of *CsFOXL2* was 1245 bp. The deduced amino acid sequence was 414 aa and contains the FH domain (177–267 aa; Figure 1B).

The predicted molecular weight of the *CsDMRT3*-encoded protein was 41.38 kDa, whereas the theoretical isoelectric point was 8.05. The α helix of the CsDMRT3 protein was 25.93%, the extended strand was 2.65%, the β strand was 3.17%, and the disordered was 68.25% (Figures 2A, C). Among the protein encoded by *CsFOXL2*, the proportions of α-helix, extended chain, β-turn, and irregular coiling were 27.54%, 8.94%, 5.80%, and

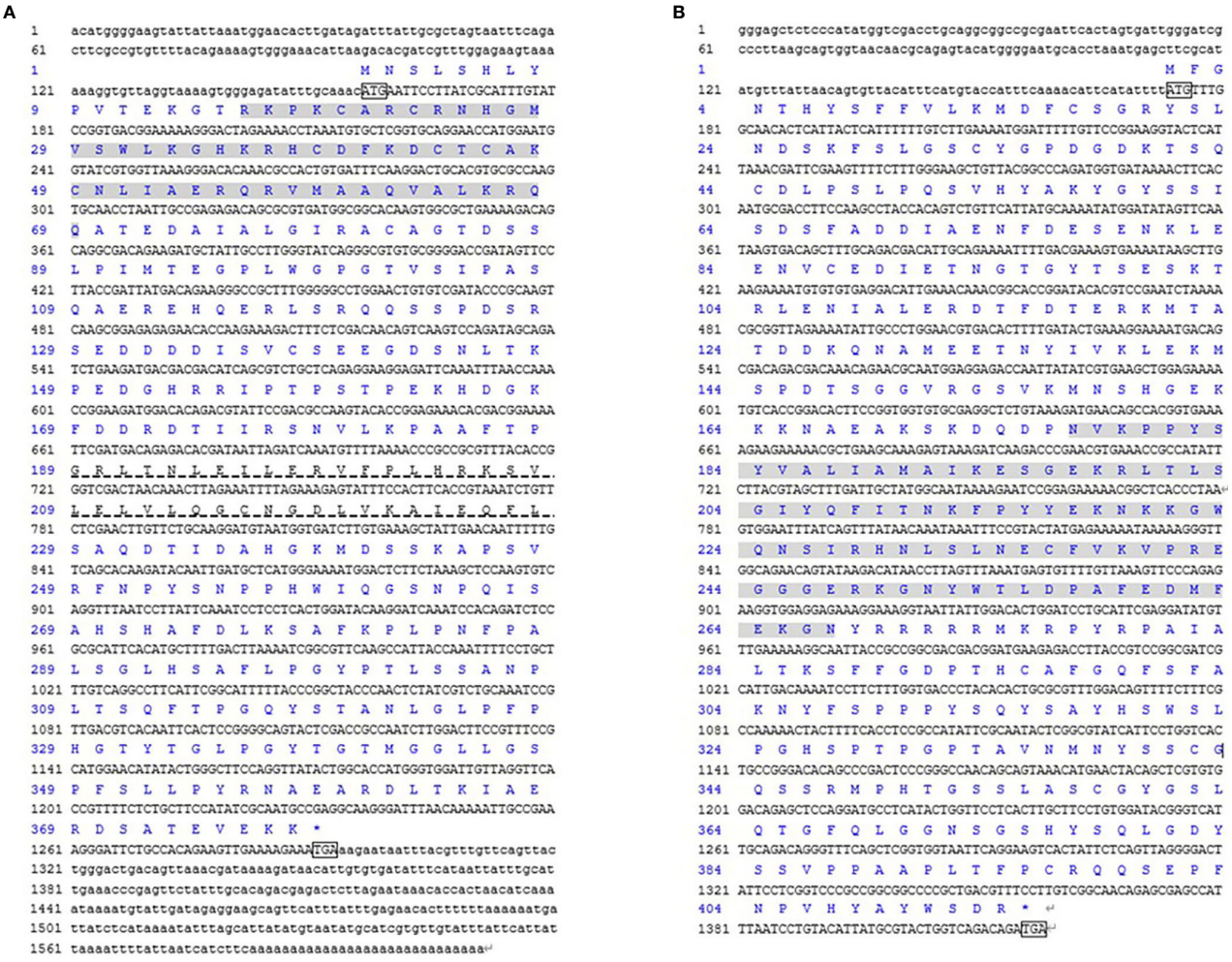

FIGURE 1
The *DMRT3* **(A)** and *FOXL2* **(B)** cDNA and deduced amino acid sequence of *C. sinensis*. The ATG/TGA indicated by the box starts codon/stop codon; shaded regions represent the DM domain and the FH domain, respectively. The DMA domain was indicated by virtual underline.

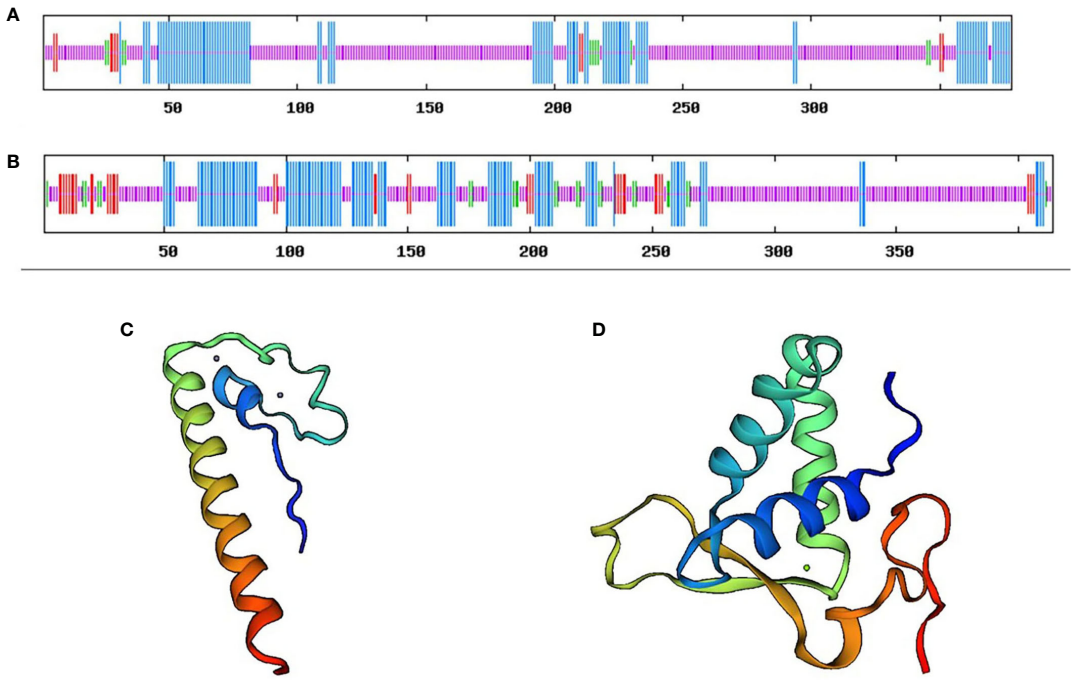

FIGURE 2
The secondary structure and tertiary structure prediction of *DMRT3* **(A)** and *FOXL2* **(B)** in *C. sinensis*. Blue represents the alpha helix, red represents the extended strand, green represents the beta-turn, and orange represents the random coil.

57.73%, respectively (Figures 2B, D). The predicted molecular weight of the *CsFOXL2*-encoded protein was 46.55 kDa, whereas the theoretical isoelectric point was 7.55.

A comparison of the amino acid sequence encoded by the *CsDMRT3* with other species (Figure 3A) showed that *DMRT3* contains a conserved DM domain. The highest identity of *CsDMRT3* with *Mercenaria mercenaria* was 85.1%, and it shares 40.5%, 48.4%, 48.7%, 35.8%, and 36.2% identity with homologs in *Pomacea canaliculate*, *Aplysia californica*, *Crassostrea virginica*, *Acanthaster planci*, and *Limulus polyphemus*, respectively. Therefore, *DMRT3* is relatively conserved in shellfish, especially in bivalves. The comparison of the sequence of *FOXL2* (Figure 3B) showed that the FH domain is also present in other species. *CsFOXL2* shares 84.7%, 62.3%, 58.1%, 57.9%, 51.4%, and 49.0% identity with homologs in *Mercenaria mercenaria*, *Dreissena polymorpha*, *Haliotis rubra*, *Gigantopelta aegis*, *Octopus bimaculoides*, and *Owenia fusiformis*, respectively.

Phylogenetic tree was constructed based on the sequence of the *CsDMRT3* with 12 species by using the Neighbor-Joining method, and the results indicate that *CsDMRT3* cluster with the other bivalves and stay farther away from humans and mice (Figure 4A). Phylogenetic analysis showed that *CsFOXL2* formed a cluster with those of other bivalve shellfish species (Figure 4B).

3.2 Expression levels of *DMRT3* and *FOXL2* in different tissues and gonadal development stages of *C. sinensis*

Tissue-specific expression results showed that the expression level of *CsDMRT3* in the testes significantly higher than that of other tissues, including the hepatopancreas, ovary, and foot (Figure 5A). During the gonadal development of *C. sinensis*, the expression level of *CsDMRT3* in the testis increased significantly from the proliferation stage to maturation stage, and reached the peak level at the maturation stage (Figure 6A). Subsequently, the expression of *CsDMRT3* in the testis of *C. sinensis* continued to decline from spawning stage to spent stage (Figure 6A).

The present result showed that the highest expression level of *CsFOXL2* was found in the foot of *C. sinensis*. Moreover, the results showed that the levels of *CsFOXL2* in the ovaries of *C. sinensis* were higher than that in the testis (Figure 5B). Further analysis revealed that the expression level of *CsFOXL2* in the ovary increased significantly from the proliferation stage to maturation stage, and reached the peak level at the maturation stage throughout the reproductive cycle of *C. sinensis*. Then, the expression level of *CsFOXL2* in the ovary decreased significantly from spawning stage to spent stage. The lowest expression level of *CsFOXL2* was found in the spent stage (Figure 6B).

10.3389/fmars.2023.1120015

FIGURE 3
The amino acid alignment of *DMRT3* **(A)** and *FOXL2* **(B)** from *C. sinensis* and other species. Different colors represent residues sharing homology, cyan, pink and black regions indicate homology above 50%, above 75%, and equal to 100%, respectively.

3.3 Expression levels of *DMRT3* and *FOXL2* in larvae development and different months of *C. sinensis*

During the period of larval development of *C. sinensis*, *CsDMRT3* had the lower expression level in fertilized egg and umbo larval stages. However, the expression level of *CsDMRT3* in the trochophore and D-larval stages was significantly higher than that of other two stages. (Figure 7A). For the expression levels of *CsDMRT3* in *C. sinensis* at different months of age, the results showed that the transcript level of *CsDMRT3* in the gonads at different months of age showed a sharp increase from 5 months of

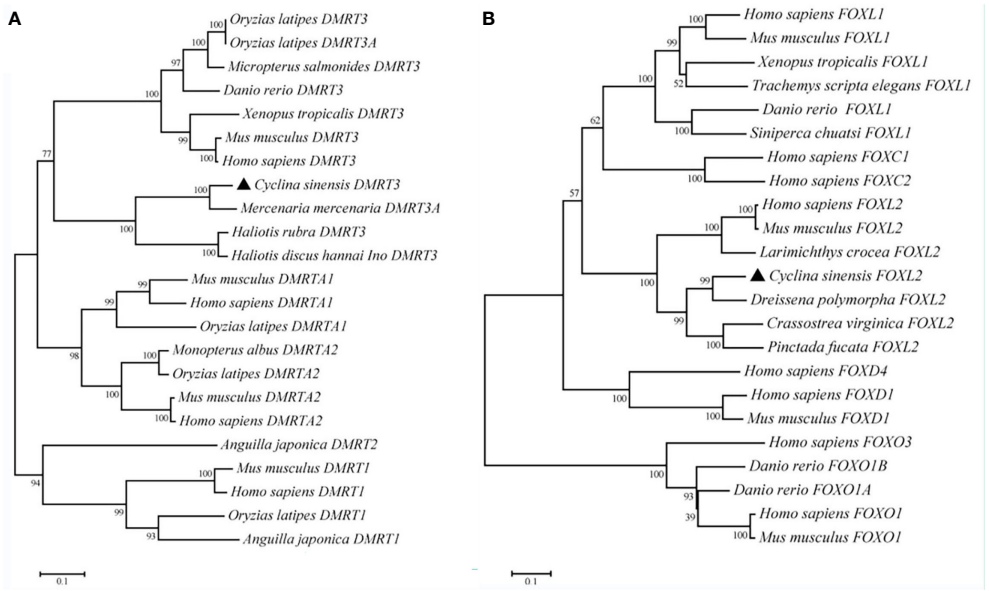

FIGURE 4
The phylogenetic tree of *DMRT3* **(A)** and *FOXL2* **(B)** from *C. sinensis* and other species. *Note: C. sinensis* were marked by a black triangle.

age to 11 months of age. Moreover, the expression level of *CsDMRT3* reached the lowest level in the gonads of 12-month-old *C. sinensis* (Figure 8A).

The expression level of *CsFOXL2* increased significantly from the fertilized egg to D-larval stage, while the expression level of *CsFOXL2* declined sharply in the umbo larval stage (Figure 7B). For the expression levels of *CsFOXL2* in *C. sinensis* at different months of age, the results showed that the low transcript levels of *CsFOXL2* were found in 3 to 5 months of age, increased at 6 months of age, and then dropped at 9 months of age (Figure 8B).

3.4 Expression levels of *CsDMRT3* and *CsFOXL2* in gonads after estradiol exposure

Results of estradiol exposure experiments showed that 5 μg/L estradiol treatment caused a significant increase in *CsDMRT3* transcript level of male gonads. However, no significant changes in *CsDMRT3* expression levels were observed at 50 μg/L estradiol treatment compared to the control group (Figure 9A). Moreover, estradiol treatment up-regulated the expression level of *CsFOXL2* in female gonads compared to the control group (Figure 9B).

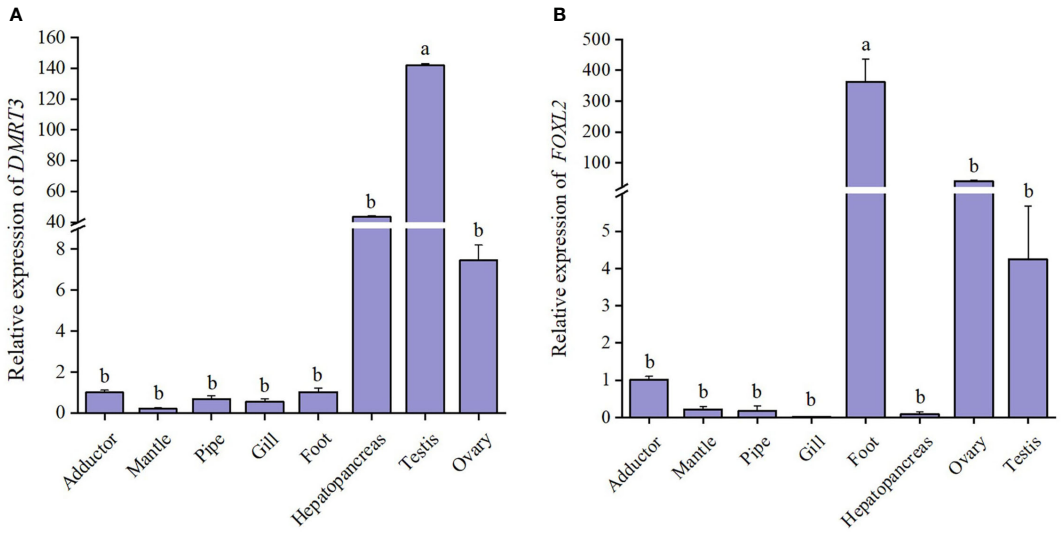

FIGURE 5
The relative expression levels of *DMRT3* **(A)** and *FOXL2* **(B)** in different tissues of *C. sinensis*. Different letters represent significant differences (*P<0.05*).

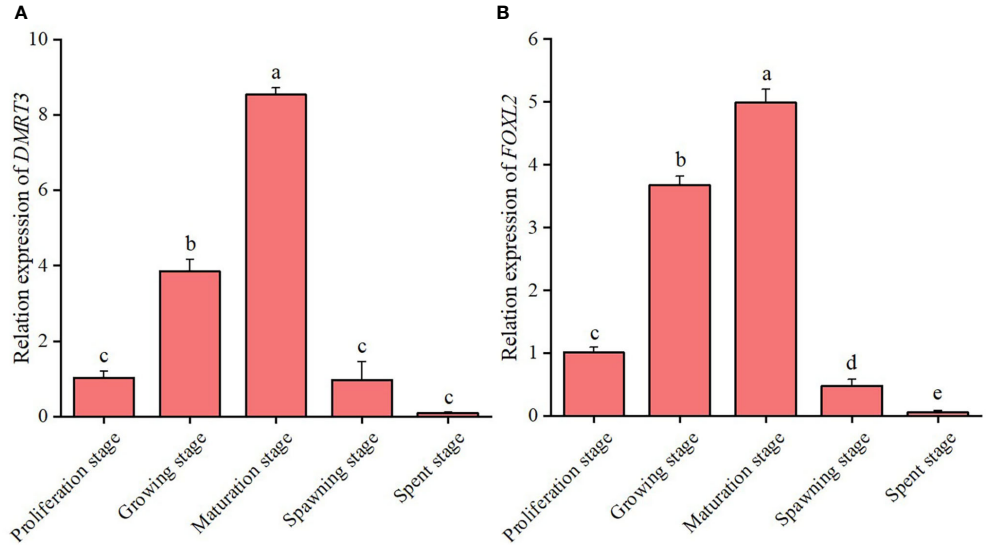

FIGURE 6
The relative expression levels of *DMRT3* **(A)** and *FOXL2* **(B)** in the different gonadal developmental stages of *C. sinensis*. The expression levels of *DMRT3* and *FOXL2* was only detected in testis and ovary, respectively. Different letters represent significant differences (*P<0.05*).

3.5 Ovaries histological analysis of estradiol exposure

Histological examination showed that estradiol exposure promoted the ovarian development of *C. sinensis* (Figure 10). Specifically, the main type of germ cells of *C. sinensis* was pre-vitellogenesis oocyte (POI) and the cytoplasm of POI was basophilic in the control group (Figure 10A). In the estradiol group (5 μg/L estradiol, 50 μg/L estradiol), the main type of germ cells of *C. sinensis* was post-vitellogenesis oocytes (POL) and the cytoplasm of POL is eosinophilic (Figures 10B, C). Further analysis revealed that the mean long diameters of the oocytes in control group, 5μg/L group and 50 μg/L group were 42.62 ± 1.50 μm, 59.56 ± 2.22 μm, and 69.05 ± 1.99 μm, respectively. The short diameters of oocytes after different estradiol treatments were 28.23 ± 1.01 μm, 38.30 ± 1.29 μm, and 46.82 ± 1.52 μm (Table 2).

4 Discussion

The *DMRT* family is a class of sex-determination and differentiation-related genes that are commonly found in organisms, and the genes in this family are highly conserved in invertebrates and vertebrates (Zhang et al., 2015; Craig et al., 2002).

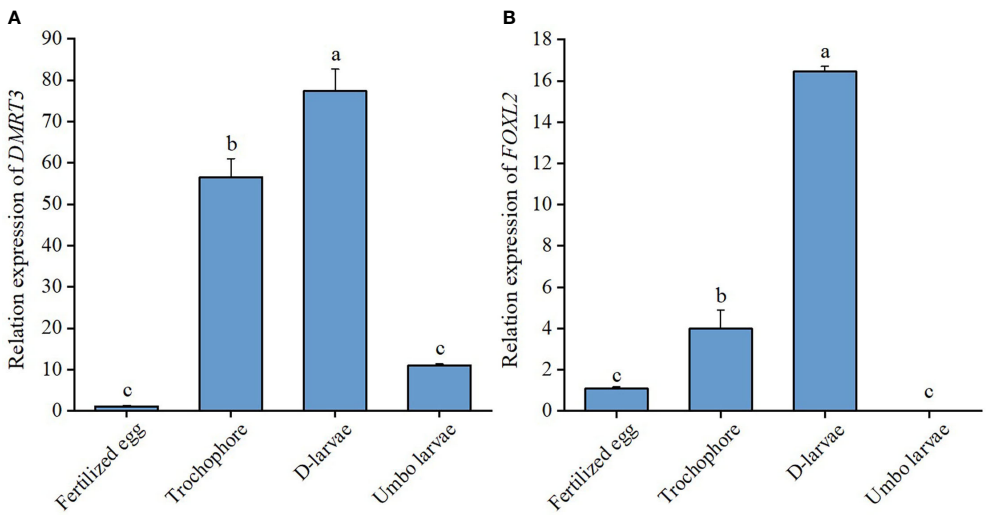

FIGURE 7
The relative expression levels of *DMRT3* **(A)** and *FOXL2* **(B)** in larval development stages of *C. sinensis*. Different letters represent significant differences (*P<0.05*).

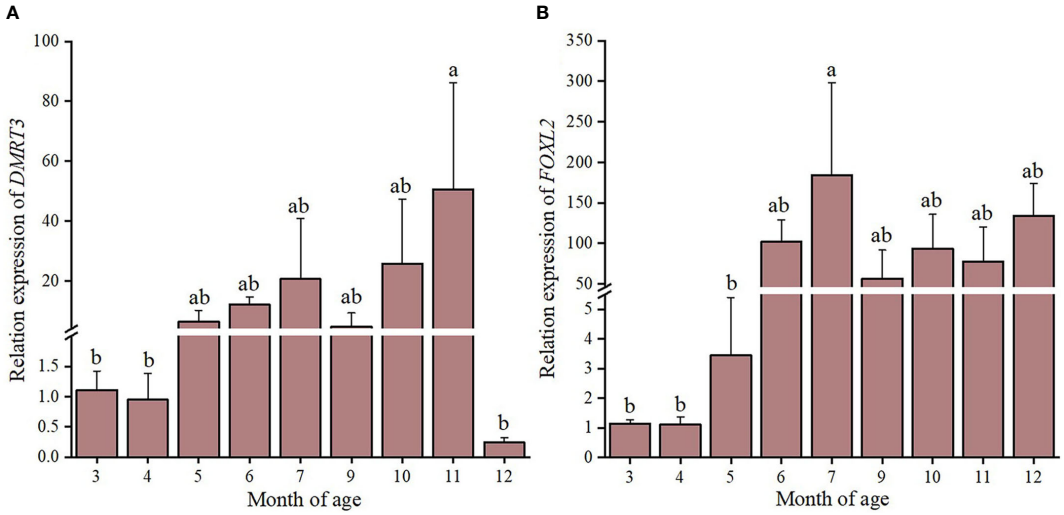

FIGURE 8
The relative expression levels of *DMRT3* **(A)** and *FOXL2* **(B)** in different months ages of *C. sinensis*. Different letters represent significant differences (*P<0.05*).

The *DMRT* family-specific DM domain, which binds specifically in a zinc finger-like manner, is the main functional domain in the gene sequence Guo et al. (2020). Sinclair et al. (1990) found that zinc finger proteins can bind to other regulated genes and then regulate downstream genes, ultimately affecting testis development. The present results showed that no transmembrane structure was detected for the CsDMRT3 protein, suggesting that the DMRT3 protein in *C. sinensis* is an intracellular protein. DMRT3 protein has also been reported in studies on largemouth bass *Micropterus salmoides*, mandarin fish *Siniperca chuatsi*, and swamp eel *Monopterus albu*. Furthermore, the DM and DMA domains were present in the protein sequence encoded by *CsDMRT3*, indicating that the structure of *DMRT3* was conserved between vertebrate and invertebrates. Yu et al. (2007) found that 68% of the amino acid sequences in DM domains of *DMRT* were identical in 16 different evolutionary positions species.

The *DMRT* family is involved in sex determination and differentiation, gonadal development, and maintenance of organ function in organisms, and plays an important role in the development of individuals (Grandi et al., 2000; Loffler et al., 2003; Li et al., 2018). Previous experiments showed that *DMRT3* was expressed only in the testes of *Carassius auratus* (Wang et al., 2014). However, *DMRT3* transcripts have been detected in both testes and ovaries of zebrafish and Mandarin fish (Li et al., 2008; Han et al., 2021). Similar results were found in scallops and ctenophores (Feng et al., 2010; Zhao, 2021). Tissue distribution

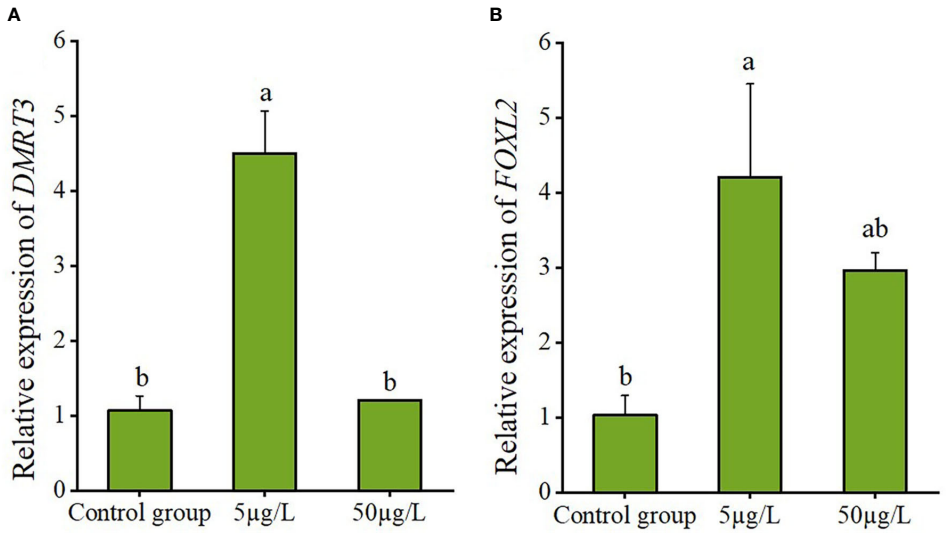

FIGURE 9
The relative expression levels of *DMRT3* in the testis **(A)** and *FOXL2* in the ovary **(B)** of *C. sinensis* under estradiol exposure treatments. Different letters represent significant differences (*P<0.05*).

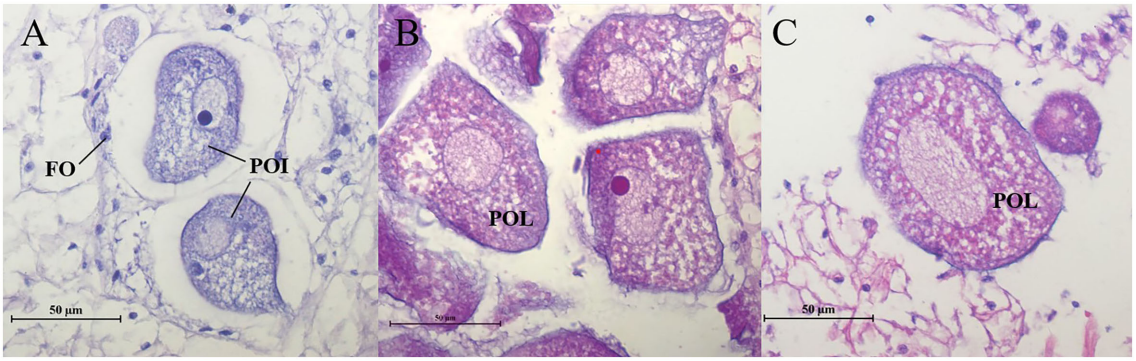

FIGURE 10
Ovaries histological characteristic of *C. sinensis* under estradiol exposure treatments. **(A)** control group, **(B)** 5 μg/L group, **(C)** 50 μg/L group. POI, pre-vitellogenesis oocyte; POL, post-vitellogenesis oocyte; FO, follicle cells.

analysis showed that the expression level of *CsDMRT3* in the testes significantly higher than in the ovary. The findings clarify that the expression level of *CsDMRT3* shows sexual dimorphism. The expression level of *CsDMRT3* in the testis reached the peak level at the maturation stage. The lowest expression level of *CsDMRT3* was found in the spent stage. Studies on the oyster *C. gigas* and scallops *Patinopecten yessoensis* yielded similar results (Amine et al., 2009; Zhao, 2021). Therefore, it is hypothesized that *DMRT3* is involved in the regulation of testis development and germ cell formation. The expression levels of *CsDMRT3* in larvae of different developmental stages were examined by qPCR. Results show that the expression level of *CsDMRT3* was the highest in the D-larval stage and low in the umbo larval stage, indicating that *CsDMRT3* was mainly synthesized in the D-larval stage. Similar features were found in the embryonic development of zebrafish and mice, and this finding is presumably related to the formation of the nervous system (Shinseog et al., 2003; Li et al., 2008; Wang and Luo, 2014). The expression level of *CsDMRT3* increased at 4 months of age and was highest at 11 months of age. Therefore, *CsDMRT3* is involved in the growth and development of the testis.

FOXL2 has an important role in sex determination and differentiation, ovarian development and maintenance, embryonic development, and immune regulation in animals (He et al., 2020; Craig et al., 2005). Sequence analysis of the *CsFOXL2* in the present study showed that *CsFOXL2* contains an FH domain. The phylogenetic tree of the *FOX* family shows that *C. gigas FOXL2* is clustered together with *FOXL2*. Therefore, *FOXL2* has a highly conserved FH domain, which is typical of the fox family (Amine et al., 2009). The expression level of *CsFOXL2* was highest in the foot. *FOXL2* was highly expressed in the foot in the study of *H. cumingii*, indicating the possible existence of a mechanism in the foot that regulates sex determination and differentiation in clams (Wang et al., 2020). The transcript levels of *CsFOXL2* were higher in the ovary than in the testis. The same result was observed in *C. gigas*, where the expression level of *CsFOXL2* does not show sexual dimorphism (Amine et al., 2009). The expression level of *CsFOXL2* during gonad development initially increased and then decreased from the proliferation stage to the spent stage. This finding is consistent with the expression characteristics of *FOXL2* during scallop gonad development (Ning et al., 2021; Zhao, 2021). The involvement of *CsFOXL2* in early ovarian development and oocyte differentiation can be hypothesized based on the trend of *CsFOXL2* expression during ovarian development. In the present study, the expression level of *CsFOXL2* during larval development was analyzed. The results showed that *CsFOXL2* was transcribed in fertilized eggs, and Liu (2012) concluded that this phenomenon occurred, because *FOXL2* was expressed maternally. *CsFOXL2* was significantly highly expressed in the D-larval stage, but barely expressed in the umbo larvae stage. Similar results were observed for *C. farreri* and the bay scallop *Argopecten irradians irradians* (Liu et al., 2013). For the result, Ning et al. (2021) suggested that primordial germ cells (PGCs) may first appear in the D-larval stage. The D-larval stage is a period of rapid construction of larvae tissue in *C. sinensis*, including the initial formation of larval shells and visceral masses. Therefore, it is hypothesized that *CsFOXL2* is involved in the formation of certain organs of the larvae. The expression level of *CsFOXL2* reached its peak at 7 months of age. Therefore, *CsFOXL2* is involved in ovarian growth and development.

Fluctuations in sex hormone levels in the organism as the sexual maturation cycle changes, suggest that sex hormones may participate in

TABLE 2 The oocytes diameters of *C. sinensis* in different estradiol treatment.

Indices	Control	5 μg/L	50 μg/L
long diameters of oocytes/μm	42.62 ± 1.50^{c}	59.56 ± 2.22^{b}	69.05 ± 1.99^{a}
short diameters of oocytes/μm	28.23 ± 1.01^{c}	38.30 ± 1.29^{b}	46.82 ± 1.52^{a}

Data are meant ± SE. Different superscript letters indicate that means are significantly different (P<0.05).

gonadal development (Reis-Henriques and Coimbra, 1990; Matsumoto et al., 1997; Shangguan et al., 2022). Estradiol injection promoted the growth of sea scallop oocytes, demonstrating that estrogen is involved in the reproductive process in invertebrates (Wang and Croll, 2004). The expression level of *CsDMRT3* was significantly higher at estradiol: 5 μg/L compared with the control group. Combined with the specific expression of *DMRT3* in the male gonads, it is hypothesized that *DMRT3* is involved in the development and the maintenance of gonadal function in *C. sinensis* (Wu et al., 2019). After estradiol treatment, the expression level of *CsFOXL2* peaked at estradiol concentration of 5 μg/L, which was significantly higher compared with the control group. The experimental results suggest that estradiol treatment induced the upregulation of *CsFOXL2*. It indicates that estradiol may play a role in ovarian development by stimulating *FOXL2* to induce estrogenic feedback mechanism (Narisato et al., 2006; Li et al., 2014; Banh Quyen et al., 2021). However, the expression level of *CsFOXL2* was decreased at estradiol concentration of 50 μg/L compared with estradiol concentration of 5 μg/L. Similar results were observed in *C. elegans*. Zhu et al. (2019) concluded that the uptake of exogenous estrogen by fry leads to high estradiol concentrations in the body, resulting in a negative feedback mechanism that inhibits the production of endogenous estrogens. In the present experiment, the diameter of oocytes in the ovaries of *C. sinensis* remarkably increased with increasing estradiol concentration. The findings of this study are consistent with the study of Wang and Croll, 2004.

The results showed that *DMRT3* and *FOXL2* were involved in the development and maintenance of gonad in different tissues and gonad stages of *C. sinensis*. *CsDMRT3* may be a candidate regulator of male development. In addition, *FOXL2* may interact with *ESR* in oyster gonads to inhibit the expression of genes related to male development (Sun et al., 2022). *CsFOXL2* was barely expressed in the umbo larvae stage, while *CsDMRT3* was expressed at different stages of larval development, suggesting that the broader function of *CsDMRT3* in early development.

5 Conclusion

The present study showed that the expression level of *DMRT3* in *C. sinensis* was sexually dimorphic, indicating that *DMRT3* is likely to be involved in male gonad development and germ cell formation. *FOXL2* is closely associated with early organogenesis and ovarian development in *C. sinensis*. In addition, estradiol exposure stimulated ovarian development and oocyte growth. The results of this study provide valuable information for the subsequent study of sex determination and gonadal development of clam *C. sinensis*.

Data availability statement

The datasets presented in this study can be found in online repositories. The the cDNA sequences of CsDMRT3 can be found at GenBank, https://www.ncbi.nlm.nih.gov/genbank/, accession No: OP970557 and the sequences of CsFOXL2 can be found at GenBank, accession No: OP970558. Further inquiries should be directed to the corresponding author

Ethics statement

The animal study was reviewed and approved by the Animal Experiment Ethics Committee at Jiangsu Ocean University.

Author contributions

SY: experimental design, formal analysis, and writing - original draft. MX: data curation, and validation. JX: data curation. XL: experimental design and data curation. ML: experimental design and formal analysis. SW: formal analysis. SF: experimental design. ZD: writing-editing and funding acquisition. All authors contributed to the article and approved the submitted version.

Funding

The work was financially supported by Jiangsu Natural Resources Development Special-Marine Science and Technology Innovation Project (JSZRHYKJ202008); Modern Agro-industry Technology Research System (CARS-49); The 'JBGS' Project of Seed Industry Revitalization in Jiangsu Province (JBGS[2021]034); Postgraduate Research & Practice Innovation Program of Jiangsu Province (SJCX201267); Jiangsu Graduate Research and Practice Innovation Program (KYCX2021-035).

Conflict of interest

The authors declare that the research was conducted in the absence of any commercial or financial relationships that could be construed as a potential conflict of interest.

Publisher's note

References

Akihiko, Y., Kyung, H. L., Hiromi, F., Kazushi, K., Susumu, Y., and Michiya, M. (2006). Expression of the DMRT gene and its roles in early gonadal development of the Japanese pufferfish *Takifugu rubripes*. *Comp. Biochem. Physiol. D.* 1 (1), 59–68. doi: 10.1016/j.cbd.2005.08.003

Amine, N., Anne-Sophie, M., Marie-Laure, S., Abdellah, M., Blandine, D., Michel, M., et al. (2009). Identification and expression of a factor of the DM family in the oyster *Crassostrea gigas*. *Comp. Biochem. Physiol. A.* 152 (2), 189–196. doi: 10.1016/j.cbpa.2008.09.019

Banh Quyen, Q. T., Guppy Jarrod, L., Domingos Jose, A., Budd Alyssa, M., Pinto Ricardo, C. C., and Marc Adrien, F. (2021). Induction of precocious females in the protandrous barramundi (*Lates calcarifer*) through implants containing 17β-estradiol-effects on gonadal morphology, gene expression and DNA methylation of key sex genes. *Aquaculture* 539 (1), 736601. doi: 10.1016/j.aquaculture.2021.736601

Cao, J. L., Chen, J. J., Wu, T. T., Gan, X., and Luo, Y. J. (2010). Molecular cloning and sexually dimorphic expression of DMRT4 gene in *Oreochromis aureus*. *Mol. Biol. Rep.* 37 (6), 2781–2788. doi: 10.1007/s11033-009-9820-z

Chris, O., Shakib, O., J Elias, G., Manuela, U., Laura, C., Antonino, F., et al. (2005). Foxl2 is required for commitment to ovary differentiation. *Hu. Mol. Genet.* 14 (14), 2053–2062. doi: 10.1093/hmg/ddi210

Christelle, S., Pascal, S., Béatrice, A., and Anne-Sophie, M. (2014). Cg-SoxE and cg-β-catenin, two new potential actors of the sex-determining pathway in a hermaphrodite lophotrochozoan, the pacific oyster *Crassostrea gigas*. *Comp. Biochem. Physiol. A.* 167, 68–76. doi: 10.1016/j.cbpa.2013.09.018

Cocquet, J., Pailhoux, E., Jaubert, F., Servel, N., Xia, X., Pannetier, M., et al. (2002). Evolution and expression of FOXL2. *J. Med. Genet.* 39 (12), 916–921. doi: 10.1136/jmg.39.12.916

Craig, R. M., Kevin, P., and Mark, Q. M. (2005). Genomic inventory and expression of sox and fox genes in the cnidarian *Nematostella vectensis*. *Dev. Genes. Evol.* 215 (12), 618–630. doi: 10.1007/s00427-005-0022-y

Craig, A. S., Tanya, M. H., Peter J, M., and Andrew H, S. (2002). Retracted: restricted expression of dmrt3 in chicken and mouse embryos. *Gene. Expr. Patterns.* 2 (1-2), 69–72. doi: 10.1016/S0925-4773(02)00360-X

Dong, Z. G., Duan, H. B., Zheng, H. F., Ge, H. X., Wei, M., Liu, M. M., et al. (2021). Research progress in genetic resources assessment, culture technique and exploration utilization of *Cyclina sinensis*. *J. Fish. China.* 45 (12), 2083–2098. doi: 10.11964/jfc.20201212545

Feng, Z. F., Shao, M. Y., Sun, D. P., and Zhang, Z. F. (2010). Cloning, characterization and expression analysis of cf-dmrt4-like gene in *Chlamys farrei*. *J. Fish. Sci. China.* 17 (05), 930–940.

Govoroun, M. S., Pannetier, M., Pailhoux, E., Cocquet, J., Brillard, J., Couty, I., et al. (2004). Isolation of chicken homolog of the FOXL2 gene and comparison of its expression patterns with those of aromatase during ovarian development. *Dev. Dynam.* 231 (4), 859–870. doi: 10.1002/dvdy.20189

Grandi, A. D., Calvari, V., Bertini, V., Bulfone, A., Peverali, G., Camerino, G., et al. (2000). The expression pattern of a mouse doublesex -related gene is consistent with a role in gonadal differentiation. *Mech. Dev.* 90 (2), 323–326. doi: 10.1016/s0925-4773(99)00282-8

Guo, P. F., Duan, S. H., Dong, S. S., Wu, C. D., and Wang, G. L. (2020). Molecular characterization and expression analysis of Dmrt1 gene in *Hyriopsis cumingii*. *GAB* 39 (5), 2033–2041. doi: 10.13417/j.gab.039.002033

Han, C., Wang, C. W., Ouyang, H. F., Zhu, Q. Y., Huang, J. J., and Han, L. Q. (2021). Characterization of dmrts and their potential role in gonadal development of mandarin fish (*Siniperca chuatsi*). *Aquacult. Rep.* 21. doi: 10.1016/j.aqrep.2021.100802

Hanne, J., and Øivind, A. (2012). Sex dimorphic expression of five dmrt genes identified in the Atlantic cod genome. the fish-specific dmrt2b diverged from dmrt2a before the fish whole-genome duplication. *Gene* 505 (2), 221–232. doi: 10.1016/j.gene.2012.06.021

He, J. Q., Zhang, H., She, Z. C., Zhen, W. Q., You, S. Y., and Wang, P. L. (2020). Cloning and expression pattern investigation of crassostrea hongkongensis Foxl2 gene. *GAB* 39 (04), 1519–1528. doi: 10.13417/j.gab.039.001519

Hildreth, P. E. (1965). Doublesex, recessive gene that transforms both males and females of *Drosophilid* into intersexes. *Genetics* 51 (4), 659–678. doi: 10.1093/genetics/51.4.659

Hu, B., Cui, Z. P., Wei, J. L., Zhang, J., Wang, Y., Zhang, W. J., et al. (2021). Effects of exogeneous hormone on expression of dmrt1, foxl2, and boule genes in gonads of Sea urchin *Mseocentrotus nudus*. *Chin. J. Fish.* 34 (04), 1–6. doi: 10.3969/j.issn.1005-3832.2021.04.001

Li, H. L., Liu, J. G., Huang, X. T., Wang, D., and Zhang, Z. F. (2014). Characterization, expression and function analysis of DAX1 gene of scallop (*Chlamys farreri* jones and preston 1904) during its gametogenesis. *J. Ocean. U. China* 13 (4), 696–704. doi: 10.1007/s11802-014-2299-9

Li, R. J., Zhang, L. L., Li, W. R., Zhang, Y., Li, Y. P., Zhang, M. W., et al. (2018). FOXL2 and DMRT1L are yin and yang genes for determining timing of sex differentiation in the bivalve mollusk *Patinopecten yessoensis*. *Front. Physiol.* 9. doi: 10.3389/fphys.2018.01166

Li, Q., Zhou, X., Guo, Y. Q., Shang, X., Chen, H., Lu, H., et al. (2008). Nuclear localization, DNA binding and restricted expression in neural and germ cells of zebrafish Dmrt3. *Biol. Cell.* 100 (8), 453–463. doi: 10.1042/bc20070114

Liao, X. T. (2022). Study on the gonadal development and expression of sex related genes Dmrt1 and Foxl2 in clam *Cyclina sinensis*. *Master's thesis of Jiangsu Ocean University*. 1, 1–63. doi: 10.44354/d.cnki.gjsuy.2022.000148

Liao, X. T., Sun, Z. P., Cui, Z. Q., Yan, S. S., Fan, S. S., Xia, Q., et al. (2022). Effects of different sources of diet on the growth, survival, biochemical composition and physiological metabolism of clam (*Cyclina sinensis*). *Aquac. Res.* 10, 53. doi: 10.1111/are.15886

Liu, X. L. (2012). Molecular cloning, expression pattern and function analysis of cf-foxl2 in the scallop *Chlamys farreri*. *Doctoral Thesis of Ocean University of China*. 1, 1–103.

Liu, X. L., Liu, J. G., Wang, D., Zhang, Z. Y., and Zhang, Z. F. (2013). Expression pattern of the foxl2 gene in the scallop *Chlamys farreri* during development. *J. Fish. Sci. China* 20 (01), 206–211. doi: 10.3724/SP.J.1118.2013.00205

Loffler, K. L., Zarkower, D., and Koopman, P. (2003). Etiology of ovarian failure in blepharophimosis ptosis epicanthus inversus syndrome: FOXL2 is a conserved, early-acting gene in vertebrate ovarian development. *Endocrinology* 144 (7), 3237–3243. doi: 10.1210/en.2002-0095

Matsumoto, T., Osada, M., Osawa, Y., and Mori, K. (1997). Gonadal estrogen profile and immunohistochemical localization of steroidogenic enzymes in the oyster and scallop during sexual maturation. *Comp. Biochem. Physiol. B.* 118 (4), 811–817. doi: 10.1016/S0305-0491(97)00233-2

Narisato, H., Ayumi, N., Masaaki, K., Takuya, K., Masatoshi, M., and Norihisa, T. (2006). Feminization of Japanese medaka (*Oryzias latipes*) exposed to 17beta-estradiol: formation of testis-ova and sex-transformation during early-ontogeny. *Aquat. Toxicol.* 77 (1), 78–86. doi: 10.1016/j.aquatox.2005.11.001

Ni, J. B., Zeng, Z., and Ke, C. H. (2012). Sex steroid levels and expression patterns of estrogen receptor gene in the oyster *Crassostrea angulata* during reproductive cycle. *Aquaculture* 376-379, 105–116. doi: 10.1016/j.aquaculture.2012.11.023

Ning, J. H., Cao, W. A., Lu, X., Chen, M., Liu, B., and Wang, C. D. (2021). Identification and functional analysis of a sex-biased transcriptional factor Foxl2 in the bay scallop *Argopecten irradians irradians*. *Comp. Biochem. Physiol. B.* 256, 11068. doi: 10.1016/j.cbpb.2021.110638

Racotta, I. S., Ramirez, J. L., Ibarra, A. M., Rodrıguez-Jaramillo, M. C., Carreño, D., and Palacios, E. (2003). Growth and gametogenesis in the lion-paw scallop *Nodipecten (Lyropecten) subnodosus*. *Aquaculture* 217 (1-4), 0–349. doi: 10.1016/s0044-8486(02)00366-6

Reis-Henriques, M. A., and Coimbra, J. (1990). Variations in the levels of progesterone in *Mytilus edulis* during the annual reproductive cycle. *Comp. Biochem. Physiol. A.* 95 (3), 343–348. doi: 10.1016/0300-9629(90)90230-P

Shangguan, X. Z., Mao, Y. R., Wang, X. Q., Liu, M. L., Wang, Y. Y., Wang, J. L., et al. (2022). Cyp17a effected by endocrine disruptors and its function in gonadal development of *Hyriopsis cumingii*. *Gen. Comp. Endocrinol.* 323-324, 114028. doi: 10.1016/j.ygcen.2022.114028

Shi, Y., Wang, Q., and He, M. X. (2014). Molecular identification of dmrt2 and dmrt5 and effect of sex steroids on their expressions in *Chlamys nobili*. *Aquaculture* 426, 21–30. doi: 10.1016/j.aquaculture.2014.01.021

Shinseog, K., Jae R, K., Robert C, A., Vivian J, B., and David, Z. (2003). Sexually dimorphic expression of multiple doublesex -related genes in the embryonic mouse gonad. *Gene. Expr. Patterns* 3 (1), 77–82. doi: 10.1016/S1567-133X(02)00071-6

Sinclair, A. H., Berta, P., Palmer, M. S., Hawkins, J. R., Griffiths, B. L., and Smith, M. J. (1990). A gene from the human sex-determining region encodes a protein with homology to a conserved DNA-binding motif. *Nature* 346 (6281), 240–244. doi: 10.1038/346240a0

Sun, D. F., Yu, H., and Li, Q. (2022). Examination of the roles of foxl2 and dmrt1 in sex differentiation and gonadal development of oysters by using RNA interference. *Aquaculture* 548, 737732. doi: 10.1016/J.AQUACULTURE.2021.737732

Tian, Y., Zhang, B. L., and Chang, Y. Q. (2012). Cloning and bioinformatics analysis of aromatization gene P450c17 in sea cucumber *Apostichopus japonicus* (Selenka). *J. Fish. Sci. China* 19 (01), 22–32. doi: 10.3724/SP.J.1118.2012.00022

Tong, Y., Zhang, Y., Huang, J. M., Xiao, S., Zhang, Y. H., Li, J., et al. (2015). Transcriptomics analysis of *Crassostrea hongkongensis* for the discovery of reproduction-related genes. *PloS. One* 10 (8), e0134280. doi: 10.1371/journal.pone.0134280

Tu, Q., Brown, C. T., Davidson, E. H., and Paola, O. (2006). Sea Urchin forkhead gene family: phylogeny and embryonic expression. *Dev. Biol.* 300 (1), 49–62. doi: 10.1016/j.ydbio.2006.09.031

Wang, C. D., and Croll, R. P. (2004). Effects of sex steroids on gonadal development and gender determination in the sea scallop, *Placopecten magellanicus*. *Aquaculture* 238 (1–4), 0–498. doi: 10.1016/j.aquaculture.2004.05.024

Wang, G. L., Dong, S. S., Guo, P. F., Cui, X. Y., Duan, S. H., and Li, J. L. (2020). Identification of Foxl2 in freshwater mussel *Hyriopsis cumingii* and its involvement in sex differentiation. *Gene* 754, 144853. doi: 10.1016/j.gene.2020.144853

Wang, L., Hu, T., Fu, M. D., Yang, K. Z., Qian, G. Y., and Ge, C. T. (2014). The effects of estrogen on gonadal differentiation and expression of dmrt1 and sox9 in *pelodiscus sinensis*. *Acta Hydrobiol. Sin.* 38 (03), 467–473. doi: 10.7541/2014.66

Wang, J., and Luo, C. (2014). Molecular cloning and expression analysis of dmrt3 in goldfish, *Carassius auratus*. *Acta Hydrobiol. Sin.* 38 (03), 548–555. doi: 10.7541/2014.77

Wei, M., Ge, H. X., Shao, C. W., Yan, X. W., Nie, H. T., Duan, H. B., et al. (2020). Chromosome-level genome assembly of the Venus clam, *Cyclina sinensis*, helps to elucidate the molecular basis of the adaptation of buried life. *iScience* 23 (6), 101148. doi: 10.1016/j.isci.2020.101148

Wu, Q. D. (2019). Molecular mechanism of sex differentiation of *Ruditapes philippinarum* under the action of estradiol. *Master's thesis of Dalian Ocean University*. 3, 1–159. doi: 10.27821/d.cnki.gdlhy.2019.000196

Wu, Q. D., Tan, Y., Wang, J. T., Xie, Q. Y., Huo, M. Z., and Fang, L. (2019). Effect of estradiol stimulation on dmrt gene expression in Manila clam *Ruditapes philippinarum*. *J. Dalian. Univ.* 34 (03), 362–369. doi: 10.16535/j.cnki.dlhyxb.2019.03.009

Yan, H. W., Li, Q., Liu, W. G., Ke, Q. Z., Yu, R. H., and Kong, L. F. (2011). Seasonal changes of oestradiol-17 and testosterone concentrations in the gonad of the razor clam *Sinonovacula constricta* (Lamarck 1818). *J. Mollus. Stud.* 77 (2), 116–122. doi: 10.1093/mollus/eyq045

Yu, F. F., Zhou, L., Wang, M. F., Yu, X. Y., and Gui, J. F. (2007). Cloning and sequence analysis of three DM domain in *Pinctada martensii*. *J. Agric. Biotechnol.* 2007 (05), 905–906. doi: 10.3969/j.issn.1674-7968.2007.05.034

Yuki, O., Yoshinobu, U., Yoichi, M., Tohru, K., and Masahisa, N. (2008). Molecular cloning and gene expression of Foxl2 in the frog *Rana rugosa*. *Gen. Comp. Endocrinol.* 159 (2-3), 170–177. doi: 10.1016/j.ygcen.2008.08.013

Zhang, N., Huang, W., Xu, F., Li, L., Zhang, G. F., and Guo, X. M. (2015). Expression of two dmrt family genes in the pacific oyster *Crassostrea gigas*. *Oceanol. Limnol. Sin.* 46 (03), 717–724. doi: 10.11693/hyhz20140900249

Zhao, D. (2021). Expression characteristics and function of genes Dmrt1 and Foxl2 in the scallop *Patinopecten yessoensis*. *Master's thesis of Shanghai Ocean University*. 1, 1–73. doi: 10.27314/d.cnki.gsscu.2021.000103

Zhu, Y. Y., Zhang, M., Ye, K., Shen, W. L., Wu, X. F., and Wang, Z. Y. (2019). Effects of 17β-estradiol on the expression of genes related to sex differentiation of the Large yellow croaker. *J. Jimei. Univ. (Natural Science)* 24 (06), 401–408. doi: 10.19715/j.jmuzr.2019.06.01

frontiers | Frontiers in Marine Science

TYPE Original Research
PUBLISHED 07 March 2023
DOI 10.3389/fmars.2023.1138074

OPEN ACCESS

EDITED BY
Ming Li,
Ningbo University, China

REVIEWED BY
Zhenlu Wang,
Guizhou University, China
Mbaye Tine,
Gaston Berger University, Senegal

*CORRESPONDENCE
Tao Zhang
tzhang@qdio.ac.cn
Hao Song
haosong@qdio.ac.cn

SPECIALTY SECTION
This article was submitted to Aquatic Physiology, a section of the journal Frontiers in Marine Science

RECEIVED 05 January 2023
ACCEPTED 22 February 2023
PUBLISHED 07 March 2023

CITATION
Zhou C, Lin Z-s, Shi Y, Feng J, Hu Z, Yang M-j, Shi P, Li Y-r, Guo Y-j, Zhang T and Song H (2023) Genome-wide identification, structural and evolutionary characteristics, and expression analysis of aquaporin gene family members in *Mercenaria mercenaria*. *Front. Mar. Sci.* 10:1138074. doi: 10.3389/fmars.2023.1138074

Genome-wide identification, structural and evolutionary characteristics, and expression analysis of aquaporin gene family members in *Mercenaria mercenaria*

Cong Zhou[1,2,3,4,5,6], Zhi-shu Lin[7], Ying Shi[7], Jie Feng[8], Zhi Hu[1,2,3,4,5,6], Mei-jie Yang[1,2,3,4,5,6], Pu Shi[1,2,3,4,5,6], Yong-ren Li[9], Yong-jun Guo[9], Tao Zhang[1,2,3,4,6]* and Hao Song[1,2,3,4,6]*

[1]CAS Key Laboratory of Marine Ecology and Environmental Sciences, Institute of Oceanology, Chinese Academy of Sciences, Qingdao, China, [2]Laboratory for Marine Ecology and Environmental Science, Qingdao National Laboratory for Marine Science and Technology, Qingdao, China, [3]Center for Ocean Mega-Science, Chinese Academy of Sciences, Qingdao, China, [4]CAS Engineering Laboratory for Marine Ranching, Institute of Oceanology, Chinese Academy of Sciences, Qingdao, China, [5]University of Chinese Academy of Sciences, Beijing, China, [6]Shandong Province Key Laboratory of Experimental Marine Biology, Qingdao, China, [7]Qingdao Marine Management Support Center, Qingdao, China, [8]North China Sea Marine Forecasting Center of State Oceanic Administration, Qingdao, China, [9]Tianjin Key Laboratory of Aqua-ecology and Aquaculture, Fisheries College, Tianjin Agricultural University, Tianjin, China

Aquaporins (AQPs) are highly-selective transmembrane water transporters that are involved in the adaptation to environmental challenges. However, the structure, function, and evolution of AQPs in bivalves remain largely unknown. In this study, AQP gene family members were identified in nine bivalve species, and their abundance rangs from 7 to 15. Nine AQPs (MmAQPs) were identified in the genome of hard clam (*Mercenaria mercenaria*), which is a euryhaline bivalve that has evolved sophisticated osmoregulatory mechanisms and salinity adaptation. Structurally, all MmAQPs contain 6 or 12 transmembrane α-helices, a major intrinsic protein (MIP) domain, and 2 asparagine-proline-alanine (NPA) motifs. MmAQPs were classified into three subfamilies based on phylogenetic analysis: AQP1-like, AQP3-like, and AQP8-like. No AQP11-like subfamily member was identified in the genome of hard clam. Tandem duplication resulted in a lineage-specific expansion in AQP8-like subfamily in hard clams. MmAQP8 genes showed different expression sensitivity to different environmental stressors. The gene expression patterns of three MmAQP8 were similar under heat, hypoxia, and air exposure stress, but differed greatly under salinity stress, indicating that tandem duplication events may accelerate the functional divergence of AQP8 genes in hard clams. AQP3-like members may have undergone gene loss during evolution, resulting in weakened glycerol and urea penetration in hard clams. Three orthologs of MmAQPs were detected in the genomes of *Cyclina sinensis* and *Archivesica marissinica* through synteny analyses. Tissue expression profiles showed that MmAQP genes were highly

expressed in the foot and hepatopancreas. Under environmental stress, the expression levels of most of the MmAQP genes changed significantly to maintain metabolic homeostasis. Several MmAQP genes were downregulated to reduce water permeability under salinity and air exposure stress. Several MmAQP genes were significantly upregulated to promote the transmembrane transport of ammonia and reactive oxygen species and activate anti-apoptotic responses to resist stress. This study provides a comprehensive understanding of the AQP gene family in hard clams, and lays a foundation for further studies to explore the functions of AQPs in bivalves.

KEYWORDS

aquaporin, evolutionary relationship, tandem duplication, environmental stress, expression pattern

1 Introduction

The water permeability of cell membranes is highly dependent on the presence of water channel proteins, also known as aquaporins (AQPs). In 1988, the first AQP was isolated from human erythrocytes and changed the concept of transmembrane water transport from involving simple diffusion across the lipid bilayer to more strictly-regulated processes (Denker et al., 1988; Preston et al., 1992). Structurally, AQPs are tetrameric membrane proteins composed of four identical 30-kDa monomers (Benga, 2012). Each monomers harbor a central water-transporting pore surrounded by six transmembrane α-helices (Gonen and Walz, 2006). The pore structure determines the substrate selectivity of AQPs and is characterised by two highly-conserved asparagine-proline-alanine (NPA) motifs (Törnroth-Horsefield et al., 2006; Ishibashi et al., 2011). The pore structure allows different small molecules, including water, glycerol, ammonia, carbon dioxide, urea, and hydrogen peroxide, to specifically penetrate the biological membranes (Krane and Goldstein, 2007; Groszmann et al., 2017). Based on the distinct sequence characteristics and substrate permeability, AQPs can be classified into four subfamilies: AQP1, AQP3, AQP8, and AQP11-like. AQP1-like subfamily consists of AQP0, 1, 2, 4, 5 and 6, which can only permeate water. AQP3-like subfamily members are AQP3, 7, 9, and 10, which can permeate glycerol, urea, and ammonia. AQP8-like subfamily member (AQP8) shows poor ability to transport water across membranes. AQP11 and 12 are the members of AQP11-like subfamily, which are also known as unorthodox AQPs and are characterized by highly-variable NPA motifs (Soto et al., 2012; FinnCerda, 2015).

AQPs are present in almost all the kingdoms of life (Heymann and Engel, 1999), among which mammalian AQPs have been the most extensively studied. To date, 13 AQPs (AQP0–AQP12) have been identified in humans (Ishibashi et al., 2009). Increasing evidence has suggested that human AQPs are involved in osmoregulation, lipid metabolism, cell adhesion and migration, and celluar stress responses (Hara-ChikumaVerkman, 2006; Maeda et al., 2008; Ishibashi et al., 2011; Tamma et al., 2018). With the increasing availability of genome and transcriptome sequencing projects, numerous homologues of human AQPs have been identified in aquatic animals (Cao and Shi, 2019). For instance, 37 AQPs have been identified in the fish *Cyprinus carpio* (Dong et al., 2016). The transcriptional regulation of AQPs has been found to be closely associated with environmental salinity changes in the crab *Portunus trituberculatus* and shrimp *Litopenaeus vannamei* (Wang et al., 2015). These studies imply that AQPs are important elements for osmoregulation and salinity adaptation in aquatic animals.

Bivalves are the second class of mollusca and one of the oldest and most evolutionarily-successful groups of invertebrates (Wang et al., 2013). Bivalves are osmoconformers whose hemolymph osmolality changes rapidly with environmental salinity fluctuations (Koprivnikar and Poulin, 2009; Sokolov and Sokolova, 2019). The osmotic gradient between hemolymph and tissues causes cellular swelling or shrinkage and disrupts normal cellular functions. Bivalves can maintain osmotic equilibrium *via* regulation of water transport and intracellular osmolytes, such as free amino acids, glycerol, and various inorganic ions (Berger and Kharazova, 1997). Hence, bivalves provide suitable models to investigate the evolutionary diversification and roles of AQPs in mollusca due to their characteristic requirement for sustained water homeostasis. To date, AQPs in mollusca have been studied mainly in gastropods. The first AQPs in gastropods was reported more than two decades later after the discovery of human AQPs (Pieńkowska et al., 2014). Genome-wide identification of AQPs and their structural and functional diversity have been reported in abalone *Haliotis discus hannai* (Jia et al., 2022). In bivalves, knowledge of AQPs remains largely limited, with only a few studies suggesting that their gene expression is related to salinity stress. For instance, a transcriptomic study reported that 7 days of hyposalinity stress induced a dwonregulation in AQP gene expression in *Crassostrea gigas* (Meng et al., 2013). Three cDNAs encoding AQPs (AQP1, AQP8, and AQP11) were cloned from *Sinonovacula constricta*, and their expression levels were significantly upregulated under salinity stress (Ruan et al., 2022). With the completion of the assembly of the reference genomes in various bivalve species, it is necessary to

study the structure, function and evolution of the AQP gene family in bivalves, especially the euryhaline species that have evolved sophisticated osmoregulatory mechanisms and salinity adaptation.

The hard clam (*Mercenaria mercenaria*) is a euryhaline bivalve species that naturally lives along the eastern coasts of the United States and Canada. Hard clams have emerged as an important pond-farmed bivalves since they have been imported into China in 1997. Salinity, temperatures and dissolved oxygen are major abiotic factors that affect the physiological status of pond-farmed hard clams. Hard clam is well-known for its "hardiness" and shows strong adaptations to salinity and other environmental stressors (Song et al., 2021). Hard clam may represent an attractive model for studying the osmoregulation and stress resistance mechanisms in bivalves. Previous studies have reported that the powerful anti-apoptotic system (Song et al., 2021), massive expansion of the heat shock protein 70 gene family (Hu et al., 2022b), and transmembrane transport of inorganic ions and free amino acids (Zhou et al., 2022) are vital stress resistance mechanisms in hard clams. However, AQP gene family and AQP-related osmoregulation and stress responses remain largely unknown in this hardy species. In this study, genome-wide identification and phylogenetic analysis of AQP gene family were performed in hard clam and eight other bivalve species. The AQPs in hard clams (MmAQPs) were selected to investigate the chromosomal locations, gene and protein structures, and evolutionary characteristics. To investigate the potential involvement of MmAQPs in stress resistance, the expression patterns of MmAQPs under salinity, air exposure, heat and hypoxia stress were examined using transcriptome data. This study provides a comprehensive understanding of AQP gene family in hard clams, and lays a foundation for further research to expolre the functions of AQPs in bivalves.

2 Materials and methods

2.1 Genome-wide identification of AQPs in various bivalve species

The whole-genome protein sequences of *M. mercenaria* were downloaded from Figshare (https://Figshare.com/s/a8378910b437fc843a46). The whole-genome protein sequences of *C. gigas*, *C. virginica*, *Pinctada fucata*, *Argopecten purpuratus*, *Chlamys farreri*, *Patinopecten yessoensis*, *Modiolus philippinarum*, and *Sinonovacula constricta* were downloaded from the MolluscDB database (http://mgbase.qnlm.ac/home). The known full-length AQPs sequences in *Homo sapiens* (13), *Danio rerio* (10), *H. discus hannai* (18), *C. gigas* (3), *C. hongkongensis* (2), *C. virginica* (1), *Ostrea edulis* (3), and *Sinonovacula constricta* (3) were downloaded from the UniProt database (https://www.uniprot.org/). These sequences were used as a query database to conduct a BLASTP search against the *M. mercenaria* genome, with a cut-off E-value of 1E-10 and identity of 30%. The hidden Markov model (HMM) profile of the conserved major intrinsic protein (MIP) domain (PF00230) was downloaded from the UniProt database. The putative *M. mercenaria* AQPs (MmAQPs) were identified using HMMER software (v3.3), with a cut-off E-value of 1E-5. The protein sequences that showed high similarities with the query sequences and conserved MIP domain were identified as candidate MmAQPs. The NCBI CD-Search tool (https://www.ncbi.nlm.nih.gov/Structure/bwrpsb/bwrpsb.cgi) was used to confirm the reliability of candidate MmAQPs (Marchler-Bauer et al., 2015). Given the molecular weights (MWs) of the water channel monomers (26–34 kDa), the MmAQPs that comprised more than 200 amino acids were selected for further analysis (Heymann and Engel, 1999). To further study the evolutionary relationship of AQPs in bivalves, AQP gene family members were also identified from the genomes of *C. gigas*, *C. virginica*, *P. fucata*, *A. purpuratus*, *C. farreri*, *P. yessoensis*, *M. philippinarum*, and *S. constricta* using the same methods described above.

2.2 Sequence alignment and phylogenetic analysis of bivalve AQPs

To classify MmAQPs, a multiple sequence alignment of the MmAQPs and other known AQPs in *H. sapiens*, *D. rerio* and *Caenorhabditis elegans* was carried out using ClustalW algorithm. An unrooted phylogenetic tree was constructed using maximum-likelihood (ML) algorithm in MEGA 11.0 software (Tamura et al., 2021). The MmAQPs were named based on the phylogenetic tree branching, BLASTP search against Swiss-Prot database, and gene positions on chromosomes. The subfamily classification and protein nomenclature of the AQPs in eight other bivalve species were performed using the same methods. A multiple sequence alignment of all bivalve AQPs was performed using ClustalW, and a phylogenetic tree was constructed using neighbor-joining (NJ) algorithm in MEGA 11.0. We further constructed an NJ tree of MmAQPs used for further analysis. To assess the reliability, the bootstrap value of each phylogenetic tree was set at 1,000 replications. The phylogenetic trees were imported into the iTOL website for embellishment (https://itol.embl.de/itol.cgi).

2.3 Physicochemical properties and subcellular localization of MmAQPs

The MWs, isoelectric points (pI), and grand averages of hydropathicity (GRAVY) of the MmAQPs were predicted using ExPASy-ProtParam tool (https://web.expasy.org/protparam/). The transmembrane structures of the MmAQPs were predicted and analyzed using DeepTMHMM software (https://dtu.biolib.com/DeepTMHMM). The subcellular localization of the MmAQPs was predicted using WoLF PSORT online software (https://wolfpsort.hgc.jp/).

2.4 Chromosomal localization, gene duplication and collinearity analysis of MmAQPs

The genome annotation file (GFF3 format) of *M. mercenaria* was downloaded from Figshare (https://Figshare.com/s/

a8378910b437fc843a46). Based on the genome annotation information, the chromosomal localization of MmAQPs was visualized using the gene location visualize from GTF/GFF tool in TBtools software (v1.1043) (Chen et al., 2020). The whole-genome protein sequences of hard clams were compared in pairs using DIAMOND software with the cut-off max-target-seqs of 5 and E-value of 1E-5 (Buchfink et al., 2015). MCScanX software was used to search for tandemly-duplicated and collinear gene pairs (Wang et al., 2012). The collinear gene pairs were visualized using the advanced circos tool in TBtools.

2.5 Gene structures and motif analysis of MmAQPs

Gene structures, including untranslated regions (UTR), coding sequences (CDS), and introns, were displayed using GSDS 2.0 (http://gsds.gao-lab.org/). To better understand the structural diversity of MmAQPs, a conserved motif analysis of MmAQPs was conducted using MEME (v5.5.0) with a maximum number of motifs of 10 (https://meme-suite.org/meme/tools/meme) (Bailey et al., 2015). The results were visualized using the simple MEME wrapper tool in TBtools.

2.6 Amino acid composition, secondary and tertiary structures of MmAQP proteins

To detect the conserved NPA motifs in MmAQPs, a multiple sequence alignment was performed using MUSCLE algorithm in MEGA 11.0. The secondary structures of MmAQPs were predicted using SOPMA web tool (https://npsa-prabi.ibcp.fr/cgi-bin/npsa_automat.pl?page=/NPSA/npsa_sopma.html) with a cut-off similarity threshold of 8. The three-dimensional (3D) tertiary structures of MmAQPs were predicted using SWISS-MODEL (https://swissmodel.expasy.org/), which is a fully-automated protein structure homology-modelling online tool (Arnold et al., 2006). The 3D structures of MmAQPs were visually edited and mapped using PyMOL molecular graphics system (v2.2.0).

2.7 Synteny analyses of AQP genes between hard clams and other bivalves

Synteny analyses were performed to detect the orthologs of MmAQPs in four chromosome-level bivalve genomes. The genome sequence and annotation file of *P. yessoensis* were downloaded from the MolluscDB database. The genome sequence and annotation file of *C. gigas* were downloaded from the NCBI genome database (https://www.ncbi.nlm.nih.gov/genome/?term=Crassostrea+gigas). The genome sequence of *Cyclina sinensis* genome was downloaded from NCBI (project PRJNA612143), and the genome annotation file was obtained from the DRYAD website (https://doi.org/10.5061/dryad.44j0zpcb5). The genome sequence and annotation file of *Archivesica marissinica* were downloaded from Figshare (https://figshare.com/articles/dataset/Host-Endosymbiont_Genome_Integration_in_a_Deep-Sea_Chemosymbiotic_Clam/12198987). Diamond software was used to perform a two-way BLASTP analysis between *M. mercenaria* and *P. yessoensis*, *M. mercenaria* and *C. gigas*, *M. mercenaria* and *C. sinensis*, and *M. mercenaria* and *A. marissinica*, with a cut-off max-target-seqs of 5 and E-value of 1E-5. Then MCScanX software was used to screened out the collinear large fragments consisting of multiple neighboring collinear gene pairs in two genomes. According to the gene ID of MmAQPs, the collinear AQP gene pairs in two genomes were identified and visualized using the systeny plot for MCScanX tool in TBtools.

2.8 Tissue expression profiles of MmAQP genes

The gills, mantles, feet, adductor muscles, hemolymph, liver, stomach, intestines, testes, and ovaries were sampled from the healthy hard clams under suitable living conditions (salinity: 30 ± 0.5 psu, temperature: 15 ± 1 °, dissolved oxygen: 8.0 ± 1.0 mg/L). The Illumina paired-end transcriptome libraries of these tissues were constructed in our previous study (Song et al., 2021). Raw data were obtained from the NCBI SRA database (accession number: PRJNA596049). The raw data were pre-processed to remove adapters, poly-N, and low-quality reads using Cutadapt (v3.3). After performing a quality control check using FastQC (v0.11.8), the high-quality reads were mapped to the *M. mercenaria* reference genome using TopHat (v2.0.12) with default parameters. HTSeq (v0.6.1) was used to count the number of reads that were mapped to each gene. FPKM value represented the gene expression levels and was calculated based on the length of the gene and its read count. The expression levels of MmAQP genes in the different tissues were standardized by Z-scores and visualized using pheatmap package in R (v4.2.2).

2.9 Environmental stress treatments and expression patterns of MmAQP genes

To clarify the role of MmAQPs in osmoregulation and stress responses, hard clams were exposed to various environmental stressors, including hyposalinity, hypersalinity, air exposure, heat, and hypoxia. Gills were selected as the target tissue because they can exchange substances with the external environment and are vital for stress resistance in bivalves (Hosoi et al., 2007). Moderate and severe hyposalinity were set at 15 practical salinity units (psu) and 5 psu, respectively. The hypersalinity was set at 40 psu (Song et al., 2021). Four groups were established in this experiment: 30 psu (control group, S30), 5 psu (S5), 15 psu (S15), and 40 psu (S40). After 10 days of salinity stress, gills were aseptically dissected from the clams and immediately stored at −80°C. To examine the effects of air exposure stress on MmAQPs, hard clams were exposed to air in a thermostatic incubator at 15°C and 50% humidity. Gills were dissected from the clams on days 0 (control group, PreAE), day 8 (PostAE8), and day 16 (PostAE16). Additional experimental details are available in Song et al. (2021). In heat and hypoxia stress experiments, the temperature was set to 35°, and the dissolved oxygen concentration was set to 0.2 mg/L (Hu et al., 2022a). Four

groups were established in this experiment: 20°, 6 mg/L (control group, C_6); 35°, 6 mg/L (heat group, H_6); 20°, 0.2 mg/L (hypoxia group, C_02); and 35°, 0.2 mg/L (combined heat and hypoxia group, H_02). After three days of stress treatments, gills were dissected from the clams and stored at −80°. Further experimental details can be found in Hu et al. (2022a). Each experimental group had three biological replicates. The frozen gill samples were used for RNA extraction and transcriptome sequencing. Raw data were obtained from the NCBI SRA database (accession number: PRJNA596049, PRJNA764366, and PRJNA764372). The quality control for the reads, genome mapping, reads counts, and gene expression level calculations were performed using the same methods described in section 2.8. The expression levels of MmAQP genes under various environmental stressors were standardized and visualized using pheatmap package in R.

2.10 Statistical analysis

Statistical analyses were performed using IBM SPSS Statistics 25 (IBM Corp., US). To evaluate statistical differences, the expression levels of MmAQP genes were tested using one-way analysis of variance with Tukey's test. *P* values less than 0.05 were considered to be statistically significant.

3 Results

3.1 Identification of AQPs in nine bivalve species

Nineteen potential AQPs were screened out from the genome of hard clam through BLASTP analysis. Sixteen of the nineteen potential AQPs comprised typical MIP domains. Moreover, seven AQPs were filtered out because their MWs were much smaller than those of other known AQPs. Therefore, nine AQPs were identified in the genome of hard clam (MmAQPs). Additionally, we identified 13 AQPs in *C. gigas*, 15 AQPs in *C. virginica*, 7 AQPs in *P. fucata*, 10 AQPs in *A. purpuratus*, 9 AQPs in *C. farreri*, 11 AQPs in *P. yessoensis*, 9 AQPs in *M. philippinarum*, and 12 AQPs in *S. constricta*.

3.2 Phylogenetic analysis and subfamily classification of AQPs in different bivalves

To classify MmAQPs, an unrooted phylogenetic tree was constructed based on the AQPs from the hard clam and three model organisms, including *H. sapiens*, *D. rerio*, and *C. elegans* (Figure 1A). The tree consisted of four distinct clades, representing four subfamilies. MmAQPs and their homologues in model organisms were clustered on the same branch. Hence, MmAQPs could be classified into three subfamilies: AQP1-like (MmAQP1_1, MmAQP1_2, MmAQP4, MmAQP5_1, and MmAQP5_2), AQP3-like (MmAQP3), and AQP8-like (MmAQP8_1, MmAQP8_2, and MmAQP8_3). A lineage-specific expansion was observed in AQP8-like subfamily in hard clams. However, AQP11-like subfamily members were not identified in the genome of hard clams.

Another phylogenetic tree was constructed based on 95 AQPs that were identified in nine bivalves to investigate their evolutionary relationships (Figure 1B). The AQPs belonging to different subfamilies identified from different bivalve species clustered together to form four major branches on the phylogenetic tree. The AQP1-like subfamily members accounted for the largest proportion of all bivalve AQPs (55.79%), whereas AQP-11 like subfamily members accounted for the smallest proportion (8.42%). Each bivalve species had only one AQP-11 like member, except for *C. virginica* (2), *C. farreri* (0), and hard clam (0). MmAQP1_1 and MmAQP1_2 clustered most closely with ScAQP1_2, which was consistent with the evolutionary relationship between the two species. Similarly, MmAQP3 clustered closely with ScAQP10_3. MmAQP4, MmAQP5_1 and MmAQP5_2 clustered together with most of the bivalve AQP4. As opposed to that in the other bivalves, the AQP8-like subfamily has undergone expansion in *C. gigas* and *C. virginica*. The AQP4 had more than three copies in bivalves, except for *P. fucata* and hard clam. The AQP3-like subfamily had the largest number of members in *S. constricta*, and AQP5 was the most abundant (five copies) in *C. virginica* compared to that in other bivalves.

3.3 Physicochemical properties of MmAQPs

As shown in Table 1, the predicted MWs of MmAQPs ranged from 24.79 to 52.59 kDa, encoding a maximum of 234 amino acids and minimum of 505 amino acids. The pI of MmAQPs ranged from 7.7 to 7.7. The GRAVY values were between 0.349 and 0.806, suggesting that MmAQPs are hydrophobic proteins. All MmAQPs were located on the cell membrane and contained 6 transmembrane α-helices structure, except MmAQP8_2, which contained 12 transmembrane α-helices. In general, the physicochemical properties of MmAQPs were found to be consistent with those of other known AQPs.

3.4 Chromosomal distribution, gene duplication and collinearity of MmAQPs

Nine MmAQP genes were unevenly distributed on four chromosomes in hard clam (Figure 2A). The MmAQPs clustered on the same branch of the phylogenetic tree were located adjacent on the same chromosome. MmAQP4 and two MmAQP5 genes were located on chr4. Three MmAQP8 genes were located on chr9. MmAQP3 was distributed on chr10, and two MmAQP1 genes were observed on chr18. Through a gene duplication analysis using MCScanX software, we identified 3,962 pairs of tandemly-duplicated genes in *M. mercenaria* genome, including two

10.3389/fmars.2023.1138074

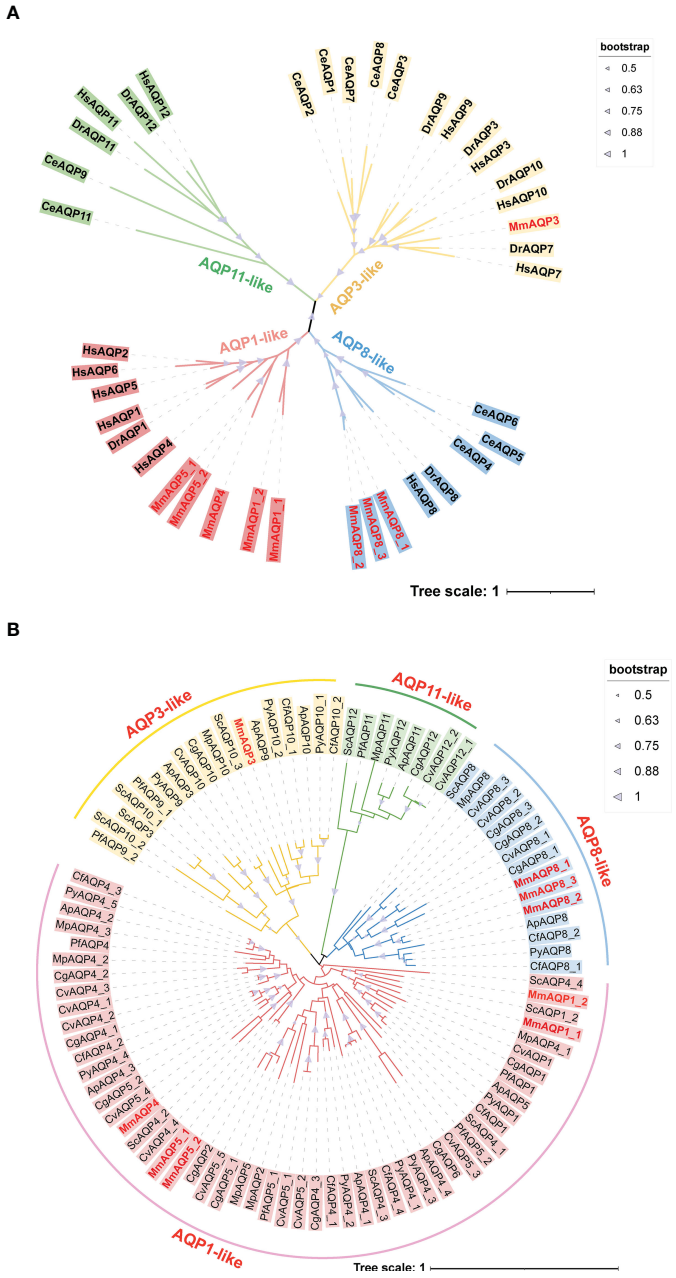

FIGURE 1
Phylogenetic analysis of MmAQPs and other known AQPs in three model organisms **(A)**, and the AQPs identified in nine bivalves **(B)**. The species names are abbreviated as follows, *H. sapiens*, Hs; *D. rerio*, Dr; *C. elegans*, Ce; *C. gigas*, Cg; *C. virginica*, Cv; *P. fucata*, Pf; *A. purpuratus*, Ap; *C. farreri*, Cf; *P. yessoensis*, Py; *M. philippinarum*, Mp; and *S. constricta*, Sc. AQP3-like, AQP1-like, AQP8-like, and AQP11-like subfamily members are marked in yellow, pink, blue, and green, respectively. The MmAQPs are highlighted in red. The bootstrap values greater than 50 are marked with purple triangles.

MmAQP5 genes and three MmAQP8 genes distributed on chr4 and chr9, respectively. Additionally, we detected 135 pairs of collinear genes in *M. mercenaria* genome, among which no MmAQPs were found (Figure 2B).

3.5 Gene structures of MmAQPs

The gene lengths and exon-intron structures varied greatly among different MmAQP genes (Figure 3). Apart from MmAQP8_2, each MmAQP gene had 3–5 exons. Although the gene lengths of MmAQP5_1 and MmAQP5_2 were different, they exhibited similar gene structures (consisting of three exons and three introns). The CD-Search analysis revealed that each MmAQP had 1–2 conserved MIP domains. Motif analysis showed that motifs 3, 10, 4, and 1, and motifs 5, 6, and 2 were highly conserved among different MmAQPs. Motif 8 was only present in MmAQ8. The similar motifs distribution was observed among the MmAQPs belonging to the same subfamily (Figure 3).

TABLE 1 Physicochemical properties of MmAQPs.

Protein name	MWs (kDa)	pI	GRAVY	Number of transmembrane α-helix	Subcellular localization
MmAQP1_1	24.79	6.81	0.661	6	plasma membrane
MmAQP1_2	26.50	7.7	0.493	6	plasma membrane
MmAQP3	31.44	6.53	0.349	6	plasma membrane
MmAQP4	32.58	5.58	0.354	6	plasma membrane
MmAQP5_1	32.43	6.06	0.358	6	plasma membrane
MmAQP5_2	32.51	5.78	0.358	6	plasma membrane
MmAQP8_1	28.56	5.7	0.706	6	plasma membrane
MmAQP8_2	52.59	6.11	0.806	12	plasma membrane
MmAQP8_3	27.85	6.19	0.728	6	plasma membrane

MWs, molecular weights; pI, isoelectric points; GRAVY, grand averages of hydropathicity.

3.6 Amino acid composition, secondary and tertiary structures of MmAQP proteins

As shown in Figure 4A, two highly-conserved NPA motifs were observed in each MmAQP. The composition of the secondary structural unit of each MmAQP exhibited high similarity (Figure S1). The α-helices and random coil structures were the most abundant (32.65–45.51% and 30.89–41.63%, respectively) secondary structural units in MmAQPs, while β-turns accounted for the smallest proportion (2.33–4.75%). Notably, each secondary structural unit accounted for almost the same proportion of the tandemly-duplicated MmAQP5_1 and MmAQP5_2. The 3D homology modeling of each MmAQP was performed using SWISS-MODEL. The crystal structure of the *Bos taurus* AQP1 (PDBID: 1J4N) was found to be the best structural template for MmAQP1_1 and MmAQP1_2. The *H. sapiens* AQP10 (PDBID: 6F7H) was the most suitable template for MmAQP3. The *Rattus norvegicus* AQP4 (PDBID: 2ZZ9) was selected as the template for MmAQP4. The *H. sapiens* AQP5 (PDBID: 5C5X), and *Anabas testudineus* AQP (PDBID: 7W7S) were the two best templates for the two MmAQP5, and three MmAQP8, respectively. Different MmAQPs that were modeled homologically with the same template showed almost identical 3D structures (Figure 4B). All MmAQPs displayed six typical transmembrane domains and a water-transporting pore.

3.7 Synteny analysis of AQP genes between hard clam and other bivalves

Four bivalve species with different taxonomic statuses, including *P. yessoensis* (Autobranchia, Pectinidae), *C. gigas* (Autobranchia, Ostreida), *C. sinensis* (Autobranchia, Venerida, Veneridae, *Cyclina*), and *A. marissinica* (Autobranchia, Venerida, Vesicomyidae, *Archivesica*) were selected to perform synteny analyses with *M. mercenaria* (Autobranchia, Venerida, Veneridae, *Mercenaria*). A total of 130 and 123 collinear gene pairs were detected between *M. mercenaria* and *P. yessoensis* and *M. mercenaria* and *C. gigas*, respectively; however, no ortholog of MmAQPs was identified in the genomes of *P. yessoensis* and *C. gigas* (Figure 5A). The syntenic conservation was observed between *M. mercenaria* and *C. sinensis* as well as *M. mercenaria* and *A. marissinica*. Three orthologs of MmAQPs were detected in the genome of *C. sinensis*, which were collinear with MmAQP4, MmAQP8_3, and MmAQP1_1. Similarly, the orthologs of MmAQP5_1, MmAQP4, and MmAQP8_1 was identified in the genome of *A. marissinica* (Figure 5B).

3.8 Tissue expression profiles of MmAQP genes

The transcriptional profiles of MmAQP genes were characterized in nine tissues to determine their spatial expression patterns. The AQP genes showed tissue-specific expression in hard clams. Most of the MmAQP genes were expressed in the foot and hepatopancreas tissues. MmAQP1_1 was the only gene that was highly expressed in the gills, and MmAQP1_2 was specifically expressed in the foot. MmAQP4 gene expression was detected in the foot and adductor muscles.The tandemly-duplicated MmAQP8_2 and MmAQP8_3 genes showed almost identical expression levels in different tissues (Figure 6).

3.9 Expression patterns of MmAQP genes under environmental stress

We further investigated the variations in gene expression of MmAQPs in the gills of hard clams under various environmental stressors. Upon exposure to severe hyposalinity (5 psu) for 10 days, the expression of MmAQP1_1 and MmAQP5_2 was significantly upregulated, and that of MmAQP3 was significantly downregulated (P <0.05). The expression of these three MmAQP genes was not significantly different between the S15 group and the control groups. The expression levels of MmAQP5_1 and MmAQP8_2 reached the highest after 10 days of moderate hyposalinity stress. Moreover, the expression of MmAQP4 and MmAQP3 were

10.3389/fmars.2023.1138074

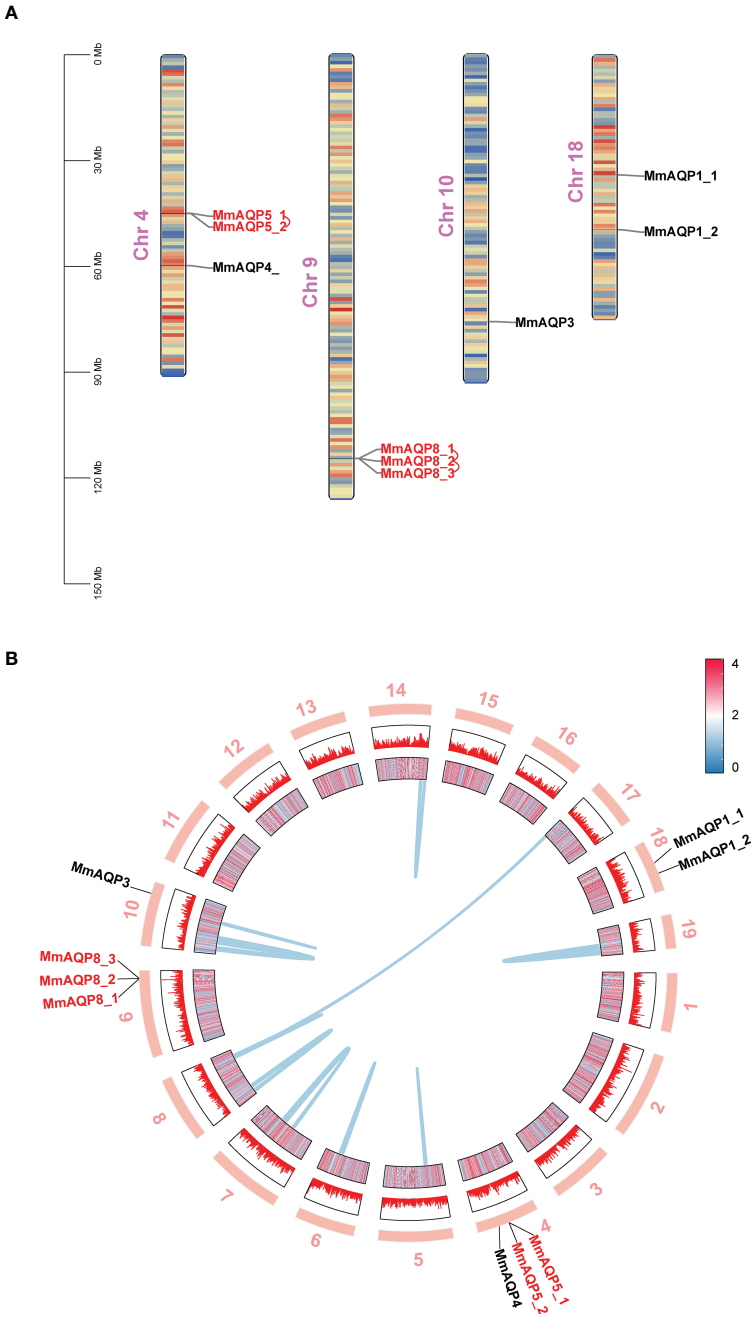

FIGURE 2
Chromosomal distribution, gene duplication and collinearity of MmAQPs. **(A)** Chromosome location of MmAQP genes. Tandemly-duplicated MmAQP genes are marked in red. **(B)** Collinear gene pairs on different chromosomes. The outer circle represents 19 chromosomes in hard clams. The inner circle represents the gene density of each chromosome. Red represents high, and blue represents low. The collinear gene pairs are linked by blue lines.

significantly upregulated, and MmAQP8_1 was significantly downregulated in the S40 group (Figure 7).

During air exposure stress, the expression levels of MmAQP1_1, MmAQP4, and MmAQP_3 were significantly downregulated on the 8th day and remained at low levels until the 16th day. The expression patterns of tandemly-duplicated MmAQP5_1 and MmAQP5_2 was almost identical in each group; both were downregulated to the lowest level on the 16th day. The expression levels of tandemly-duplicated MmAQP8_2 and MmAQP8_3 was continuously upregulated during air exposure stress (Figure 7).

MmAQP1_1 expression was significantly induced under heat stress (P <0.05), but remained at the control level under hypoxia and combined heat and hypoxia stress. The highest expression levels of tandemly-duplicated MmAQP5_1 and MmAQP5_2 was observed in the C_02 group. MmAQP4 expression was significantly downregulated, whereas three tandemly-duplicated MmAQP8 genes were significantly upregulated under combined heat and

10.3389/fmars.2023.1138074

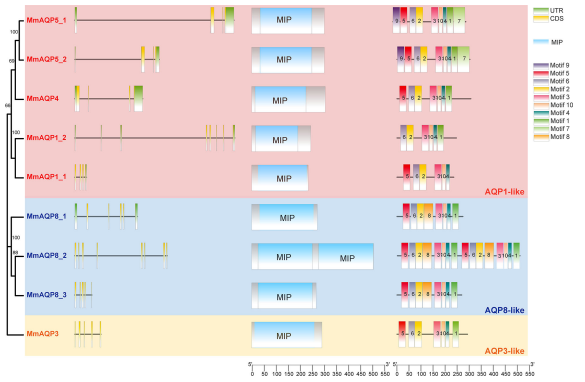

FIGURE 3
Phylogenetic tree, exon-intron structures, conserved domains and motifs of MmAQPs. On the left side of the diagram, green boxes, black lines, and yellow boxes represent untranslated regions (UTRs), introns, and exons, respectively. In the middle, blue boxes represent the MIP domains. On the right, 10 boxes of different colors represent different motifs. The AQP1-like, AQP8-like, and AQP3-like subfamilies are marked with pink, blue, and yellow, respectively.

hypoxia stress (P <0.05). Unlike that of the other MmAQP genes, MmAQP3 expression was inhibited under heat, hypoxia, and combined stress (Figure 7). Additionally, we did not detect the MmAQP1_2 expression in any group, likely because it was specifically expressed in the feet of hard clams (Figure 6).

4 Discussion

AQPs are members of the major intrinsic protein superfamily that mediate the specific permeation of water and other small solutes across the cell membrane (Hara-Chikuma and Verkman, 2006). The structures and functions of AQPs have been thoroughly studied in humans and other animal models, such as mice and zebra fish, uncovering their important roles in osmoregulation and metabolic homeostasis maintenance (Saparov et al., 2007). Euryhaline bivalves showed extraordinary osmoregulation ability and have evolved a wide range of salinity adaptation. However, knowledge of AQP gene family remains limited in bivalves. To fill this gap, we investigated the genome-wide identification, gene and protein structures, evolutionary relationships, and expression profiles of AQP gene family members in hard clams. This study provides a comprehensive understanding of AQPs in bivalves and highlights their roles in osmoregulation and stress responses.

The number of AQP genes is highly diverse among different groups of animals (Agre, 2004). The number of bivalve AQPs was similar to that in mammals but much less than that in fish (Cao and Shi, 2019). Oysters (*C. gigas* and *C. virginica*) had the highest number of AQPs (13 and 15, respectively), whereas clams (*M. philippinarum* and *M. mercenaria*) had the lowest (9), suggesting that the number of AQPs is more consistent among bivalve species with close phylogenetic relationships. A previous study identified more than 20 AQPs from the genome of oyster using BLASTP method (Jia and Liu, 2022). Our study combined BLASTP and hmmsearch, and filtered out the short AQPs to strictly identify the

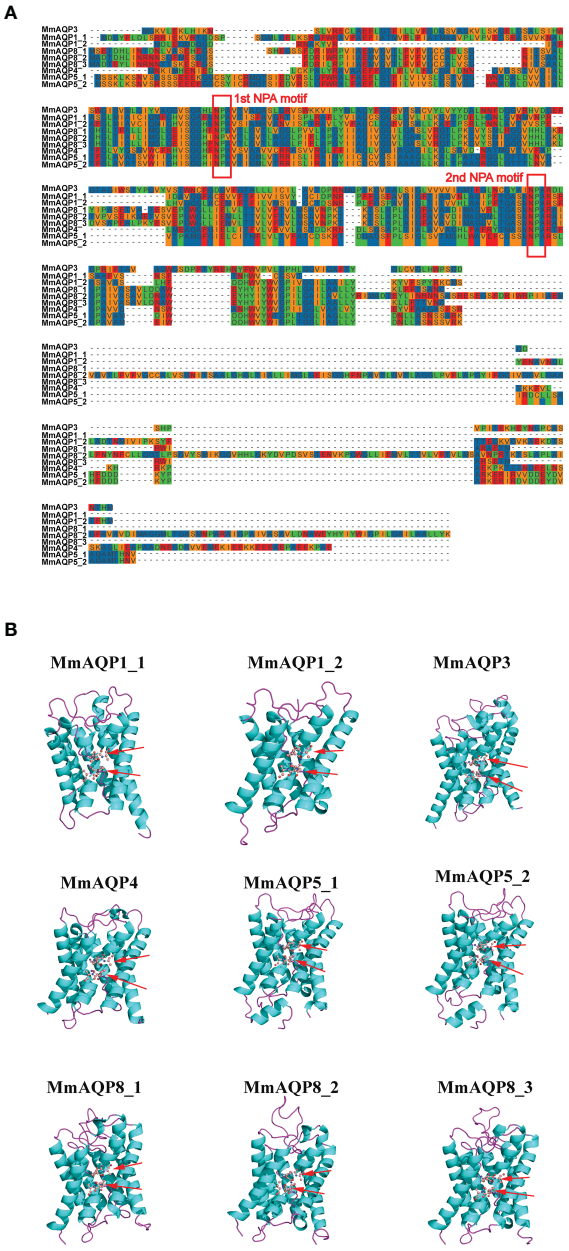

FIGURE 4
Amino acid composition and tertiary structures of MmAQPs. **(A)** Multiple sequence alignment of MmAQPs to detect the conserved NPA motifs. The two NPA motifs in each MmAQP are marked with red rectangles. **(B)** Homology modelling of the 3D structures of MmAQPs. Six transmembrane α-helices in each MmAQP are labeled with cyan, and the linker loops are labeled with purple. The NPA motifs are marked with red arrows.

AQP gene family members in bivalves. Structurally, although the overall primary sequences of the AQPs were not well conserved in different animals (approximately 30% identity), all MmAQPs exhibited the conserved structural characteristics, including six or twelve transmembrane α-helices, one MIP domain, and two NPA motifs. Based on phylogenetic analysis, MmAQPs could be classified into three subfamilies: AQP1-like, AQP3-like, and AQP8-like. The same classification of AQPs was observed in *C. gigas* and *C. virginica*. Only one AQP3-like AQP was identified in

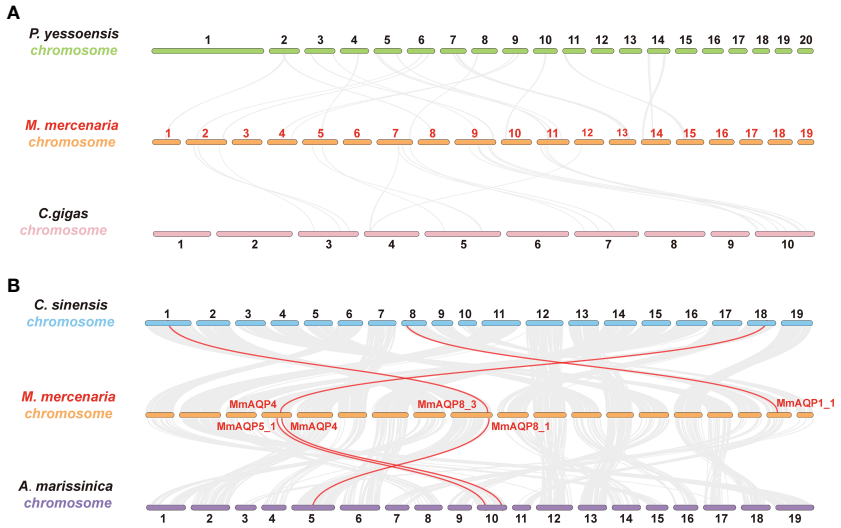

FIGURE 5
Synteny analysis to detect the orthologs of MmAQPs in the geome of *P. yessoensis* and *C. gigas* **(A)**, as well as *C. sinensis* and *A. marissinica* **(B)**. Grey lines in the background represent the collinear gene pairs between the two genomes. The orthologous AQP gene pairs are linked by red lines.

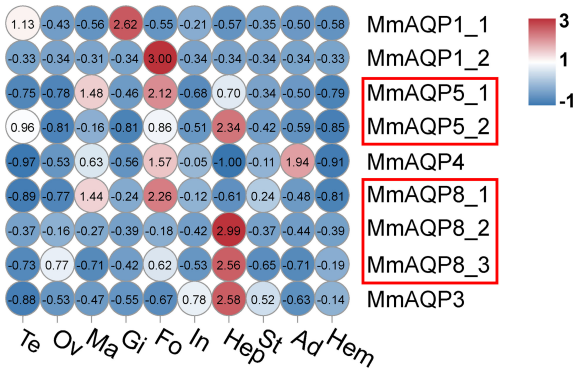

FIGURE 6
Heatmap analysis of MmAQP genes in different tissues. The name of each tissue is abbreviated as follows: Te, testis; Ov, ovary; Ma, mantle; Gi, gill; Fo, foot; In, intestine; Hep, hepatopancreas; St, stomach; Ad, adductor muscle; and Hem, hemolymph. Red indicates a high level of gene expression, and blue indicates low expression. The tandemly-duplicated genes are marked with red rectangles.

hard clams, which was far less than that in other animal models. This indicates that AQP7, AQP9, and AQP10 may have undergone gene loss during evolution, resulting in a weakened function of glycerol and urea penetration in hard clams. Similarly, AQP10 was found to be lost or turned into a non-functional pseudogene in mice (Morinaga et al., 2002), and chickens (Isokpehi et al., 2009). The presence of AQP11-like subfamily members in molluscs remains debatable (Colgan and Santos, 2018). In this study, we did not identify any AQP11-like member in the genome of hard clam, possibly because AQP11 and AQP12 were distinguished on the basis of their NPA structures and showed low sequence identities with other AQPs.

Compared with that in other bivalves, AQP8-like subfamily has undergone a considerable lineage-specific expansion in hard clams. The expansion of the AQP8-like subfamily was also observed in *H. discus hannai* (Jia et al., 2022), and *C. gigas* (Jia and Liu, 2022). The expansion of the AQP8-like subfamily in hard clam may have been related to the evolutionary process of adaptation to dynamic environments. In this study, the expression patterns of three tandemly-duplicated MmAQP8 genes showed high similarity under heat, hypoxia, and air exposure stress, reflexing their functional conservation in resistance to these stressors. Tandem duplication is a powerful driving force for evolutionary novelty (Chen et al., 2013). Tandemly-duplicated genes may obtain new functions through neofunctionalization and sub-functionalization (Sémon and Wolfe, 2007). In hard clam, we observed that three tandemly-duplicated MmAQP8 showed significant differences in gene expressions under salinity stress. MmAQP8_3 expression was specifically downregulated upon exposure to severe hyposalinity stress, whereas the expression levels of MmAQP8_1 and MmAQP8_2 remained at the control level. When the hard clams were exposed to moderate hyposalinity stress, the expression of MmAQP8_1 and MmAQP8_2 was specifically upregulated, whereas MmAQP8_3 was downregulated. Moreover, the expression of MmAQP8_1 and MmAQP8_3 was significantly inhibited under hypersalinity stress, whereas MmAQP8_2 did not change. These results indicate that MmAQP8 genes are more sensitive to salinity stress compared to heat, hypoxia, and air exposure stress. Tandem duplication events may acclerate the functional divergence of AQP8 genes in hard clams. Additionally, synteny analyses were performed to detect the orthologs of MmAQPs in different bivalves to further understand the origin and evolution of MmAQPs. No orthologous AQP gene pairs were detected among the different chromosomes in hard clams. This may have been because only a few whole-genome duplication events occurred in molluscs during

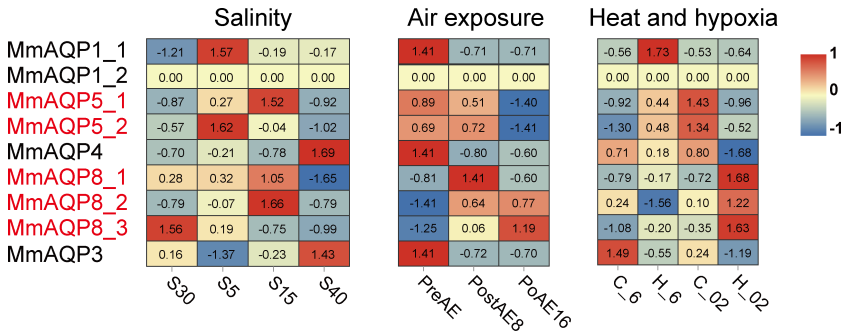

FIGURE 7
Heatmap analysis of MmAQP genes in response to salinity, air exposure, and heat and hypoxia stress. Red indicates a high level of gene expression, and blue indicates low expression. The tandemly-duplicated genes are marked in red.

evolution (Liu et al., 2021). Additionally, low collinearity in the gene arrangements and no orthologous AQP gene pairs were observed between *P. yessoensis* and hard clam as well as *C. gigas* and hard clam. This indicates that the evolution and diversification of AQP genes occurred independently in Autobranchia, the common ancestor of *P. yessoensis*, *C. gigas*, and hard clam. The orthologs of MmAQP4, MmAQP8_3, and MmAQP1_1 were detected in the genome of *C. sinensis*, which belongs to the same family (Veneridae) with hard clams. Moreover, the orthologs of MmAQP5_1, MmAQP4, and MmAQP8_1 were detected in the genome of *A. marissinica*, which belongs to same order (Venerida) with hard clams but different families (Vesicomyidae). These results indicates that the AQP4 and AQP8 genes in bivalves are highly orthologous at the order level.

An assessment of the gene expression patterns provided insights into the possible physiological roles of MmAQPs. The AQP genes showed tissue-specific expression in hard clams. Almost no MmAQP gene was expressed in the testes, ovaries, mantles, intestines, stomachs, adductor muscles, or hemolymph under suitable living conditions. Consistent with this result, inactive AQPs gene expression was also observed in most of the tissues of *S. constricta* (Ruan et al., 2022), and nile tilapia (Ni et al., 2022). MmAQP5_2, MmAQP8_2, MmAQP8_3, and MmAQP3 were highly expressed in the hepatopancreas, and the expression levels of MmAQP1_2, MmAQP5_1, and MmAQP8_1 were highest in the foot, suggesting that these MmAQPs play an important role in maintaining the basic physiological processes in the hepatopancreas and foot. AQPs are closely related to environmental adaptation in broader phyla (Finn et al., 2014). We further investigated the variations in the gene expression of MmAQP under various environmental stressors. MmAQP genes belonging to the same subfamily showed diverse expression patterns under salinity stress. Six MmAQP genes specifically responded to hyposalinity stress, among which four were significantly upregulated and two were downregulated. MmAQP4 and MmAQP3 showed the highest expression levels under hypersalinity, whereas MmAQP8_1 and MmAQP8_3 showed the lowest. Under salinity stress, the downregulation of MmAQP genes expressions resulted in a widespread reduction in water permeability. This regulation was vital to maintain and rebuilt the osmotic gradient between the gill cells and hemolymph in hard clams. Consistent with this result, the expression levels of three AQP genes in *C. gigas* decreased to protect against water currents and cell swelling under hyposalinity stress (Meng et al., 2013). Additionally, our previous study reported that ammonia was significantly accumulated in the gills of hard clams after 5 days of hypersalinity exposure (Zhou et al., 2023). Therefore, the significant upregulation of MmAQP3 expression under hypersalinity stress may be closely related to its specific function in ammonia transport.

The roles of AQPs in drought resistance have mainly been reported in plants (Zhang et al., 2021). Except for three MmAQP8 genes, the gene expressions of the remaining MmAQPs were significantly inhibited after air exposure, implying that MmAQPs also function to maintain the intracellular water contents during drought stress. Decreased expression of AQPs can enhance anti-apoptotic responses and affect the cell apoptosis rate in mammals (Jablonski et al., 2004; Jablonski et al., 2007). The stress resistance role of inhibitor of apoptosis has been highlighted in hard clams (Song et al., 2021). Hence, we speculate that the AQP-related anti-apoptotic responses may be activated in hard clams during air exposure stress. Additionally, hypoxia has been reported to alter the gene expressions of AQPs in the rat astrocytes (Yamamoto et al., 2001). In hard clams, two MmAQP5 genes were highly expressed under hypoxia stress and three MmAQP8 genes were significantly upregulated under the combined stress of heat and hypoxia. Oxidative stress and the accumulation of reactive oxygen species (ROS) in the gills are common physiological changes in bivalves upon exposure to heat and hypoxia stress (Chen et al., 2007). The enhancement of antioxidant enzyme activity and gene expression is vital for bivalves to resist environmental stress (Freitas et al., 2017). Human AQP8 has been reported to regulate the diffusion of H_2O_2 across cell membranes (Bienert et al., 2007). Results of this study imply that the overexpression of the three MmAQP8 genes under air exposure and the combined stress of heat and hypoxia were important responses to eliminate excess intracellular ROS in hard clams. Our previous metabolomics studies have reported that environmental stress can cause alterations in various metabolic processes in hard clams, including osmoregulation, lipid metabolism, ROS generation, ammonia transport, and membranes stabilization (Zhou et al., 2022; Zhou et al., 2023). These metabolic alterations were highly related to the roles of human AQPs (Hara-Chikuma and Verkman, 2006; Bienert et al., 2007; Maeda et al., 2008; Ishibashi et al., 2011;

Tamma et al., 2018). Therefore, the diverse MmAQPs may play critical and non-redundant roles in maintaining the metabolic homeostasis in hard clams under environmental stress. Functional experiments, such as the gene knockdown or overexpression of MmAQPs, will further be conducted to investigate the osmoregulation and stress resistance roles of MmAQPs.

5 Conclusions

In the present study, nine MmAQPs were identified in the genome of *M. mercenaria*, which were classified into AQP1-like, AQP3-like, and AQP8-like subfamilies. Structurally, MmAQPs showed typical characteristics of AQPs, including transmembrane α-helices, MIP domains, and NPA motifs. A lineage-specific expansion of AQP8-like subfamily and gene loss of AQP3-like subfamily was observed in hard clams. Three orthologs of MmAQPs were detected in the genome of *C. sinensis* and *A. marissinica*, suggesting that AQP4 and AQP8 genes were highly orthologous in the order Venerida. Tissue expression profiles showed that MmAQP genes were highly expressed in the foot and hepatopancreas. Three tandemly-duplicated MmAQP8 genes showed different expression sensitivity to different environmental stressors. The gene expression patterns of three MmAQP8 were similar under heat, hypoxia, and air exposure stress, but differed greatly under salinity stress. Tandem duplication events may acclerate the functional divergence of MmAQP8 genes. Under salinity and air exposure stress, several MmAQP genes in gills were significantly downregulated to reduce the water permeability and maintain the osmotic equilibrium. Other MmAQP genes were significantly upregulated to promote the transport of ammonia and ROS, and activate the anti-apoptotic responses to resist hypersalinity, heat, hypoxia, and air exposure stress. This study provides a comprehensive understanding of AQP gene family in hard clams and is of great significance for further studies to explore the AQPs-related stress resistance mechanisms in bivalves.

Data availability statement

The original contributions presented in the study are included in the article/Supplementary Material. Further inquiries can be directed to the corresponding authors.

Author contributions

CZ: Investigation, data curation, methodology, writing – original draft. Z-SL: Data curation, writing – review & editing. YS: Methodology, investigation. JF: Methodology, investigation. ZH: Methodology. M-JY: Methodology. PS: Investigation, Data curation. Y-RL: Investigation. Y-JG: Investigation, methodology. TZ, HS: Conceptualization, supervision, funding acquisition, writing – review & editing. All authors contributed to the article and approved the submitted version.

Funding

This research was supported by Tianjin science and technology commission project (20YFZCSN00240), Tianjin Agricultural Committee Project (202103010), the earmarked fund for CARS (CARS-49), Shandong Province Agricultural Major Applied Technology Innovation Project (Grant No. SF1405303301), the Key Research and Development Program of Guangxi Province (Grant No. 2021AB34014), Taishan Industrial Leading Talents Project (Grant No. LJNY201704, Recipient: TZ), the 'Double Hundred' Blue Industry Leader Team of Yantai (Recipient: TZ), the Creative Team Project of the Laboratory for Marine Ecology and Environmental Science, Qingdao Pilot National Laboratory for Marine Science and Technology (Grant No. LMEES-CTSP-2018-1), the Young Elite Scientists Sponsorship Program by CAST (2021QNRC001), and the Youth Innovation Promotion Association CAS. The funders had no role in the study design, data collection and analysis, decision to publish, or preparation of the manuscript.

Acknowledgments

The authors acknowledge the Oceanographic Data Center, IOCAS for providing assistance of bioinformatics analyses.

Conflict of interest

The authors declare that the research was conducted in the absence of any commercial or financial relationships that could be construed as a potential conflict of interest.

Publisher's note

Supplementary material

The Supplementary Material for this article can be found online at: https://www.frontiersin.org/articles/10.3389/fmars.2023.1138074/full#supplementary-material

SUPPLEMENTARY FIGURE 1
The composition of the secondary structural unit of MmAQPs.

References

Agre, P. (2004). Aquaporin water channels (Nobel lecture). *Angew. Chem. Int. Ed. Engl.* 43, 4278–4290. doi: 10.1002/anie.200460804

Arnold, K., Bordoli, L., Kopp, J., and Schwede, T. (2006). The SWISS-MODEL workspace: A web-based environment for protein structure homology modelling. *Bioinformatics* 22, 195–201. doi: 10.1093/bioinformatics/bti770

Bailey, T. L., Johnson, J., Grant, C. E., and Noble, W. S. (2015). The MEME suite. *Nucleic Acids Res.* 43, W39–W49. doi: 10.1093/nar/gkv416

Benga, G. (2012). The first discovered water channel protein, later called aquaporin 1: molecular characteristics, functions and medical implications. *Mol. Aspects Med.* 33, 518–534. doi: 10.1016/j.mam.2012.06.001

Berger, V. J., and Kharazova, A. (1997). "Mechanisms of salinity adaptations in marine molluscs," in *Interactions and adaptation strategies of marine organisms* (Springer), 115–126.

Bienert, G. P., Møller, A. L., Kristiansen, K. A., Schulz, A., Møller, I. M., Schjoerring, J. K., et al. (2007). Specific aquaporins facilitate the diffusion of hydrogen peroxide across membranes. *J. Biol. Chem.* 282, 1183–1192. doi: 10.1074/jbc.M603761200

Buchfink, B., Xie, C., and Huson, D. H. (2015). Fast and sensitive protein alignment using DIAMOND. *Nat. Methods* 12, 59–60. doi: 10.1038/nmeth.3176

Cao, J., and Shi, F. (2019). Comparative analysis of the aquaporin gene family in 12 fish species. *Animals* 9, 233. doi: 10.3390/ani9050233

Chen, C., Chen, H., Zhang, Y., Thomas, H. R., Frank, M. H., He, Y., et al. (2020). TBtools: an integrative toolkit developed for interactive analyses of big biological data. *Mol. Plant* 13, 1194–1202. doi: 10.1016/j.molp.2020.06.009

Chen, S., Krinsky, B. H., and Long, M. (2013). New genes as drivers of phenotypic evolution. *Nat. Rev. Genet.* 14, 645–660. doi: 10.1038/nrg3521

Chen, M., Yang, H., Delaporte, M., and Zhao, S. (2007). Immune condition of *Chlamys farreri* in response to acute temperature challenge. *Aquaculture* 271, 479–487. doi: 10.1016/j.aquaculture.2007.04.051

Colgan, D., and Santos, R. (2018). A phylogenetic classification of gastropod aquaporins. *Mar. Genomics* 38, 59–65. doi: 10.1016/j.margen.2017.12.002

Denker, B. M., Smith, B. L., Kuhajda, F. P., and Agre, P. (1988). Identification, purification, and partial characterization of a novel Mr 28,000 integral membrane protein from erythrocytes and renal tubules. *J. Biol. Chem.* 263, 15634–15642. doi: 10.1016/S0021-9258(19)37635-5

Dong, C., Chen, L., Feng, J., Xu, J., Mahboob, S., Al-Ghanim, K., et al. (2016). Genome wide identification, phylogeny, and expression of aquaporin genes in common carp (*Cyprinus carpio*). *PloS One* 11, e0166160. doi: 10.1371/journal.pone.0166160

Finn, R. N., and Cerda, J. (2015). Evolution and functional diversity of aquaporins. *Biol. Bull.* 229, 6–23. doi: 10.1086/BBLv229n1p6

Finn, R. N., Chauvigné, F., Hlidberg, J. B., Cutler, C. P., and Cerdà, J. (2014). The lineage-specific evolution of aquaporin gene clusters facilitated tetrapod terrestrial adaptation. *PloS One* 9, e113686. doi: 10.1371/journal.pone.0113686

Freitas, R., De Marchi, L., Bastos, M., Moreira, A., Velez, C., Chiesa, S., et al. (2017). Effects of seawater acidification and salinity alterations on metabolic, osmoregulation and oxidative stress markers in *Mytilus galloprovincialis*. *Ecol. Indic.* 79, 54–62. doi: 10.1016/j.ecolind.2017.04.003

Gonen, T., and Walz, T. (2006). The structure of aquaporins. *Q. Rev. Biophys.* 39, 361–396. doi: 10.1017/S0033583506004458

Groszmann, M., Osborn, H. L., and Evans, J. R. (2017). Carbon dioxide and water transport through plant aquaporins. *Plant Cell Environ.* 40, 938–961. doi: 10.1111/pce.12844

Hara-Chikuma, M., and Verkman, A. (2006). Physiological roles of glycerol-transporting aquaporins: the aquaglyceroporins. *Cell Mol. Life Sci.* 63, 1386–1392. doi: 10.1007/s00018-006-6028-4

Heymann, J. B., and Engel, A. (1999). Aquaporins: phylogeny, structure, and physiology of water channels. *News Physiol. Sci.* 14, 187–193. doi: 10.1152/physiologyonline.1999.14.5.187

Hosoi, M., Shinzato, C., Takagi, M., Hosoi-Tanabe, S., Sawada, H., Terasawa, E., et al. (2007). Taurine transporter from the giant pacific oyster *Crassostrea gigas*: function and expression in response to hyper-and hypo-osmotic stress. *Fisheries Sci.* 73, 385–394. doi: 10.1111/j.1444-2906.2007.01346.x

Hu, Z., Feng, J., Song, H., Zhou, C., Yu, Z., Yang, M., et al. (2022a). Mechanisms of heat and hypoxia defense in hard clam: Insights from transcriptome analysis. *Aquaculture* 549, 737792. doi: 10.1016/j.aquaculture.2021.737792

Hu, Z., Song, H., Feng, J., Zhou, C., Yang, M.-J., Shi, P., et al. (2022b). Massive heat shock protein 70 genes expansion and transcriptional signatures uncover hard clam adaptations to heat and hypoxia. *Front. Mar. Sci.* 9. doi: 10.3389/fmars.2022.898669

Ishibashi, K., Hara, S., and Kondo, S. (2009). Aquaporin water channels in mammals. *Clin. Exp. Nephrol.* 13, 107–117. doi: 10.1007/s10157-008-0118-6

Ishibashi, K., Kondo, S., Hara, S., and Morishita, Y. (2011). The evolutionary aspects of aquaporin family. *Am. J. Physiol. Regul. Integr. Comp. Physiol.* 300, R566–R576. doi: 10.1152/ajpregu.90464.2008

Isokpehi, R. D., Rajnarayanan, R. V., Jeffries, C. D., Oyeleye, T. O., and Cohly, H. H. (2009). Integrative sequence and tissue expression profiling of chicken and mammalian aquaporins. *BMC Genomics* 10, 1–12. doi: 10.1186/1471-2164-10-S2-S7

Jablonski, E. M., Mattocks, M. A., Sokolov, E., Koniaris, L. G., Hughes, F. M. Jr, Fausto, N., et al. (2007). Decreased aquaporin expression leads to increased resistance to apoptosis in hepatocellular carcinoma. *Cancer Lett.* 250, 36–46. doi: 10.1016/j.canlet.2006.09.013

Jablonski, E. M., Webb, A. N., McConnell, N. A., Riley, M. C., and Hughes, F. M. Jr. (2004). Plasma membrane aquaporin activity can affect the rate of apoptosis but is inhibited after apoptotic volume decrease. *Am. J. Physiol. Cell Physiol.* 286, C975–C985. doi: 10.1152/ajpcell.00180.2003

Jia, Y., and Liu, X. (2022). Diversification of the aquaporin family in geographical isolated oyster species promote the adaptability to dynamic environments. *BMC Genomics* 23, 1–20. doi: 10.1186/s12864-022-08445-4

Jia, Y., Xu, F., and Liu, X. (2022). Duplication and subsequent functional diversification of aquaporin family in pacific abalone *Haliotis discus hannai*. *Mol. Phylogenet. Evol.* 168, 107392. doi: 10.1016/j.ympev.2022.107392

Koprivnikar, J., and Poulin, R. (2009). Effects of temperature, salinity, and water level on the emergence of marine cercariae. *J. Parasitol. Res.* 105, 957–965. doi: 10.1007/s00436-009-1477-y

Krane, C. M., and Goldstein, D. L. (2007). Comparative functional analysis of aquaporins/glyceroporins in mammals and anurans. *Mamm. Genome.* 18, 452–462. doi: 10.1007/s00335-007-9041-5

Liu, C., Ren, Y., Li, Z., Hu, Q., Yin, L., Wang, H., et al. (2021). Giant African snail genomes provide insights into molluscan whole-genome duplication and aquatic–terrestrial transition. *Mol. Ecol. Resour.* 21, 478–494. doi: 10.1111/1755-0998.13261

Maeda, N., Funahashi, T., and Shimomura, I. (2008). Metabolic impact of adipose and hepatic glycerol channels aquaporin 7 and aquaporin 9. *Nat. Clin. Pract. Endoc.* 4, 627–634. doi: 10.1038/ncpendmet0980

Marchler-Bauer, A., Derbyshire, M. K., Gonzales, N. R., Lu, S., Chitsaz, F., Geer, L. Y., et al. (2015). CDD: NCBI's conserved domain database. *Nucleic Acids Res.* 43, D222–D226. doi: 10.1093/nar/gku1221

Meng, J., Zhu, Q., Zhang, L., Li, C., Li, L., She, Z., et al. (2013). Genome and transcriptome analyses provide insight into the euryhaline adaptation mechanism of *Crassostrea gigas*. *PloS One* 8, e58563. doi: 10.1371/journal.pone.0058563

Morinaga, T., Nakakoshi, M., Hirao, A., Imai, M., and Ishibashi, K. (2002). Mouse aquaporin 10 gene (AQP10) is a pseudogene. *Biochem. Biophys. Res. Commun.* 294, 630–634. doi: 10.1016/S0006-291X(02)00536-3

Ni, P., Zhao, X., and Liang, Y. (2022). Genome-wide identification and expression analysis of the aquaporin gene family reveals the role in the salinity adaptability in Niletilapia (*Oreochromis niloticus*). *Genes Genom.* 4(12), 1457–1469. doi: 10.1007/s13258-022-01324-y

Pieńkowska, J. R., Kosicka, E., Wojtkowska, M., Kmita, H., and Lesicki, A. (2014). Molecular identification of first putative aquaporins in snails. *J. Membr. Biol.* 247, 239–252. doi: 10.1007/s00232-014-9629-0

Preston, G. M., Carroll, T. P., Guggino, W. B., and Agre, P. (1992). Appearance of water channels in xenopus oocytes expressing red cell CHIP28 protein. *Science* 256, 385–387. doi: 10.1126/science.256.5055.385

Ruan, W., Dong, Y., Lin, Z., and He, L. (2022). Molecular characterization of aquaporins genes from the razor clam *Sinonovacula constricta* and their potential role in salinity tolerance. *Fishes* 7, 69. doi: 10.3390/fishes7020069

Saparov, S. M., Liu, K., Agre, P., and Pohl, P. (2007). Fast and selective ammonia transport by aquaporin-8. *J. Biol. Chem.* 282, 5296–5301. doi: 10.1074/jbc.M609343200

Sémon, M., and Wolfe, K. H. (2007). Consequences of genome duplication. *Curr. Opin. Genet. Dev.* 17, 505–512. doi: 10.1016/j.gde.2007.09.007

Sokolov, E. P., and Sokolova, I. M. (2019). Compatible osmolytes modulate mitochondrial function in a marine osmoconformer *Crassostrea gigas* (Thunber). *Mitochondrion* 45, 29–37. doi: 10.1016/j.mito.2018.02.002

Song, H., Guo, X., Sun, L., Wang, Q., Han, F., Wang, H., et al. (2021). The hard clam genome reveals massive expansion and diversification of inhibitors of apoptosis in bivalvia. *BMC Biol.* 19, 1–20. doi: 10.1186/s12915-020-00943-9

Soto, G., Alleva, K., Amodeo, G., Muschietti, J., and Ayub, N. D. (2012). New insight into the evolution of aquaporins from flowering plants and vertebrates: orthologous identification and functional transfer is possible. *Gene* 503, 165–176. doi: 10.1016/j.gene.2012.04.021

Tamma, G., Valenti, G., Grossini, E., Donnini, S., Marino, A., Marinelli, R. A., et al. (2018). Aquaporin membrane channels in oxidative stress, cell signaling, and aging: recent advances and research trends. *Oxid. Med. Cell. Longev.* doi: 10.1155/2018/1501847

Tamura, K., Stecher, G., and Kumar, S. (2021). MEGA11: molecular evolutionary genetics analysis version 11. *Mol. Biol. Evol.* 38, 3022–3027. doi: 10.1093/molbev/msab120

Törnroth-Horsefield, S., Wang, Y., Hedfalk, K., Johanson, U., Karlsson, M., Tajkhorshid, E., et al. (2006). Structural mechanism of plant aquaporin gating. *Nature* 439, 688–694. doi: 10.1038/nature04316

Wang, S., Hou, R., Bao, Z., Du, H., He, Y., Su, H., et al. (2013). Transcriptome sequencing of zhikong scallop (*Chlamys farreri*) and comparative transcriptomic analysis with yesso scallop (*Patinopecten yessoensis*). *PloS One* 8, e63927. doi: 10.1371/journal.pone.0063927

Wang, Y., Tang, H., DeBarry, J. D., Tan, X., Li, J., Wang, X., et al. (2012). MCScanX: a toolkit for detection and evolutionary analysis of gene synteny and collinearity. *Nucleic Acids Res.* 40, e49–e49. doi: 10.1093/nar/gkr1293

Wang, X., Wang, S., Li, C., Chen, K., Qin, J. G., Chen, L., et al. (2015). Molecular pathway and gene responses of the pacific white shrimp *Litopenaeus vannamei* to acute low salinity stress. *J. Shellfish Res.* 34, 1037–1048. doi: 10.2983/035.034.0330

Yamamoto, N., Yoneda, K., Asai, K., Sobue, K., Tada, T., Fujita, Y., et al. (2001). Alterations in the expression of the AQP family in cultured rat astrocytes during hypoxia and reoxygenation. *Mol. Brain Rec.* 90, 26–38. doi: 10.1016/S0169-328X(01)00064-X

Zhang, G., Yu, Z., da Silva, J. A. T., and Wen, D. (2021). Identification of aquaporin members in *Acacia auriculiformis* and functional characterization of AaPIP1-2 involved in drought stress. *Environ. Exp. Bot.* 185, 104425. doi: 10.1016/j.envexpbot.2021.104425

Zhou, C., Song, H., Feng, J., Hu, Z., Yang, M., Shi, P., et al. (2022). Metabolomics and biochemical assays reveal the metabolic responses to hypo-salinity stress and osmoregulatory role of cAMP-PKA pathway in *Mercenaria mercenaria*. *Comput. Struct. Biotechnol. J.* 20, 4110–4121. doi: 10.1016/j.csbj.2022.08.004

Zhou, C., Xu, L., Song, H., Feng, J., Hu, Z., Yang, M., et al. (2023). Examination of theregulation of energy metabolism, antioxidant response, and ammonia detoxification inhard clam, *Mercenaria mercenaria*, under hypersalinity stress. *Aquaculture* 563, 738916. doi: 10.1016/j.aquaculture.2022.738916

Frontiers in Marine Science

Explores ocean-based solutions for emerging global challenges

The third most-cited marine and freshwater biology journal, advancing our understanding of marine systems and addressing global challenges including overfishing, pollution, and climate change.

Discover the latest Research Topics

See more →

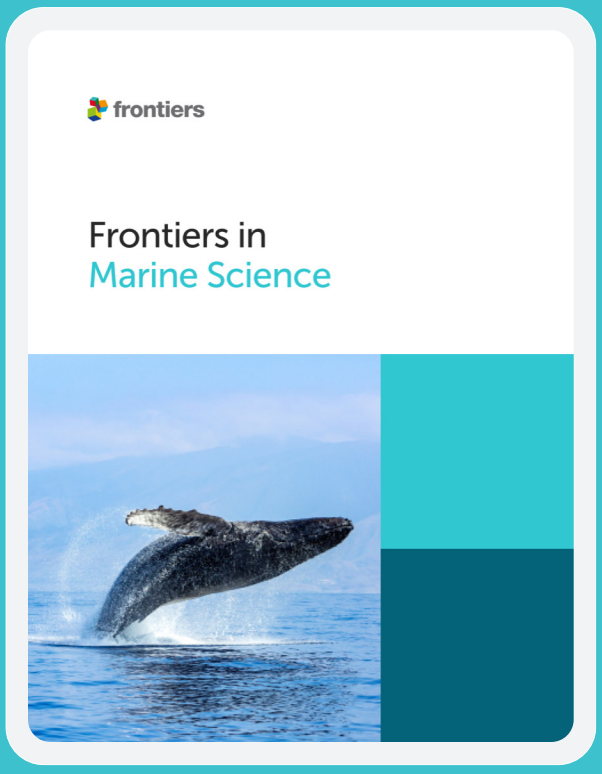

Frontiers

Avenue du Tribunal-Fédéral 34
1005 Lausanne, Switzerland
frontiersin.org

Contact us

+41 (0)21 510 17 00
frontiersin.org/about/contact